




UNIVERSITE PARIS.DIDEROT (Paris 7)
SORBONNE PARIS CITE

ED: 474, Frontières du Vivant

Laboratoire d'Océanographie et du Climat
LOCEAN

UNIVERSITY OF TASMANIA
Institute of Marine and Antarctic Studies

Quantitative Marine Science Program

Living in a fluid-dynamical landscape: how do marine predators respond to turbulence?

Submitted in partial fulfilment of the requirements for the degree of Doctor of Philosophy in Marine Science
May 2016

ALICE DELLA PENNA, M.Sc.

Supervisors:
Francesco D'OVIDIO
Christophe GUINET
Silvia DE MONTE
Craig JOHNSON
Thomas TRULL
Simon WOTHERSPOON

Defended in Paris 13/05/2016

Jury
Guido BOFFETTA
Yan ROPERT-COUDERT
Pascal RIVIERE
Guillaume LAPEYRE
Francesco D'OVIDIO
Christophe GUINET
Silvia DE MONTE
Craig JOHNSON

Authority of access statement

The publishers of the papers comprising Chapters II.1, II.2 and Appendix A and B hold the copyright for that content, and access to the material should be sought from the respective journals.

The remaining non published content of the thesis may be made available for loan and limited copying and communication in accordance with the Copyright Act 1968.

Paris 13/05/2016

Declaration of authorship

I, Alice Della Penna, declare that this thesis titled, 'Living in a fluid dynamical landscape: how do marine predators respond to turbulence?' and the work presented in it are my own. I confirm that:

- This work was done wholly or mainly while in candidature for a research degree at this University.
- Where any part of this thesis has previously been submitted for a degree or any other qualification at this University or any other institution, this has been clearly stated.
- Where I have consulted the published work of others, this is always clearly attributed.
- Where I have quoted from the work of others, the source is always given. With the exception of such quotations, this thesis is entirely my own work.
  I have acknowledged all main sources of help.
- Where the thesis is based on work done by myself jointly with others, I have made clear exactly what was done by others and what I have contributed myself.

Paris 13/05/2016

Abstract

Marine top predators play a fundamental role in maintaining the structure and functioning of healthy marine ecosystems. In the last decades the development of bio-logging (i.e. deployment of autonomous recording tags on free-living animals) has radically changed the study of top predators and their interactions with their environment. Combinations of sensors measuring position (Argos and GPS), environmental properties (water temperature, light) and proxies for foraging behavior (accelerometers) have enabled relating migrations of large fish, marine mammals, sea turtles and seabirds to basin scale patterns of ocean currents, temperature, and productivity. However, what influences marine predators' movement at smaller spatial and temporal scales, such as the ones they experience during their foraging trips, is still largely unknown. This project analyses the interaction between marine top predators (elephant seals and macaroni penguins) and sub-mesoscale (few days-months, 10-100 km) ocean dynamics. This is achieved by combining in-situ observations, bio-logging data, remote-sensing, ecological modelling and a Lagrangian approach (i.e. based on the tracking of water parcels). The study is conducted in the sub-Antarctic region around the Kerguelen Plateau (Indian Sector of the Southern Ocean). This sector of the Southern Ocean provides a useful natural laboratory for this work in that (i) several marine predators species have large colonies on the island, (ii) the area is located in a highly dynamical ocean regime dominated by the Antarctic Circumpolar Current, (iii) the trophic web in the area is relatively simple and (iv) production is dominated by iron limitation, making it possible to disentangle physical and ecological effects.

First, I examine whether the mechanical effect of mesoscale currents on the trajectories of large fast-swimming marine predators is significant. I find that, in spite of what is often assumed, foraging marine predators are transported by the horizontal ocean dynamics for a non-negligible part of their foraging trip, exhibiting a 'quasi-planktonic' behaviour. This phenomenon is more likely to occur on sub-meso and mesoscale fronts that are favourable for animal foraging.

Secondly, I focus on how mesoscale turbulence affects the distribution of ocean productivity by combining a Lagrangian approach with previous biogeochemical and ecological knowledge of the region. A novel result is that waters that have been recently ($\sim$ 20 days) in contact with the Kerguelen plateau (which is assumed to be the major source of iron of the region) are more likely to manifest a system dominated by large diatoms. I parametrise and spatialise a simple model describing phytoplankton community structure in the area to predict which dynamical niches are more favourable for high concentrations of diatoms. This result is important because qualitative assessment of the regional food web shows that the growth of fish larvae and crustaceans (that occupy

a large fraction of top predators' diet) benefit from phytoplankton communities dominated by large diatoms. The findings of this project support and complement previous studies about the role of mesoscale dynamics on marine life and open challenging questions about an "end-to-end" approach to bio-logging observations and ecosystem-based conservation management.

Acknowledgements

During these years I received a great amount of help, support and inspiration by a great number of people. I hope not to forget anyone in this long list.

First of all, my supervisors, all the six (!) of them. Thanks for accepting to work in such a big, interdisciplinary and international team. Thanks for your different ways to help me, your complementary points of view and for the patience that sharing a student with other five people requires. I have learnt a lot from all you. I would like to thank **Francesco d'Ovidio** for constantly guiding my work, sharing ideas and suggestions, answering all my questions (including the very stupid ones, yes I think you have really heard the worst ones), encouraging my independence and supporting every aspect of my project. **Christophe Guinet** for the extreme enthusiasm for our work together, the science and career suggestions and the organisation of always stimulating and productive meetings. **Silvia De Monte**, for her precious feedback and the pleasant discussions about all my work, her help in saving my calculus skills from extinction and the accurate corrections of everything I wrote. **Tom Trull**, for always challenging any idea (his, mine or anyone else), the fun and extremely instructive discussions and for giving me the possibility of spending some time at sea (finally experiencing the mesoscale eddies!). **Craig Johnson**, for the interesting discussions, the corrections of my extremely long sentences in English, all the last minute help and accepting to join a very different project that I hope he enjoyed. **Simon Wotherspoon**, for helping me with all the QMS coursework, sharing his code (and coding skills) with me and finding a solution for most of the problems I encountered in front of a computer.

I would like to thank the FdV directors **David Tareste** and **Samuel Bottani** for their support in my cotutelle project, **Sofie Leon** and **Elodie Kaslikowski** for their quick replies and in general the very pleasant and energising atmosphere of the 'Frontiers du Vivant' doctoral school. I would like to thank **Tamara Milosevic** for getting me involved with some fun and stimulating teaching at the CRI and being a great example of time management.

I would like to thank **Pascal Riviere** and **Guillaume Lapeyre** for being part of my thesis committee and providing me with valuable advice.

During these 3 (and half) years I have been lucky enough to experience three great research institutions: LOCEAN in Paris, CEBC in Chize' and IMAS in Hobart. In all of these very different environments I always felt welcomed and supported and I learnt a lot. I would like to thank the administrative staff in LOCEAN for being incredibly patient with my incomplete and hard to decipher paperwork and **Dany Thomas**, for

having a happy smile and a solution for any problem even on very difficult Monday mornings. I am grateful to all the researchers, research engineers and PhD students of LOCEAN, in particular all the members of the PEPS team. I would like to thank **Jean Baptiste Sallée**, for his encouraging and enriching comments on my work and for sharing some of his knowledge of the vertical dynamics of the Southern Ocean with me and **Cedric Cotte'** for his comments on my work. I would also like to thank the 'marine predators' team in Chize' for the very productive interactions during my visits, in particular **Yves Lebras, Thomas Jaud, Cecile Bon, Charly Bost, Yves Cherel, Jade Vacquet Garcia** (especially for the intensive lessons of statistics) and **Baptiste Picard**. It would be hard to enlist all the people I had good discussions with in Hobart: I'm really grateful to **Phil Boyd**, for his phytoplankton expertise (and for providing me with a bicycle during all my visits), **Marion Fourquez**, **Mark Hindell** and his team, the participants of the "biogeochemistry" journal club (organised by **Kristen Karsh**), all the DASHers for their vibrant and stimulating discussions (and in particular **Stuart Corney, Rob Johnson, Tom Remenyi** and **Mike Summer** who organised it) and **Andreas Klocker** and **Clothilde Langlais** for their submesoscale interesting discussions. I am especially grateful to **Mary-Anne Lea**, for helping me with the revisions of my first paper and for the many interesting discussions. I would also like to thank **Melanie Grenier** for the instructive (and fun) collaboration and **Philippe Koubbi** for his enthusiasm about our work together and his valuable comments. I would also like to thank **Di Davies** and **Abe Passmore** for their patience and their teachings in biogeochemistry, lab practise and "survival on a ship" and **Francesco Nencioli** for his support for the use of SPASSO. Finally I would like to thank **Martin Marzloff** for his suggestions and enthusiasm about ecological modelling and **Andrew Davidson** for sharing papers and comments with me.

I would also like to thank **Peter Gaube** and **Patrice Klein** for making me feel so welcome during my visits in Seattle and Brest respectively. Both visits turned out to be an extremely motivating time of my PhD and broadened my perspectives.

I would also like to thank all the friends I have met during this very dynamic part of my life and the ones that were there before and stayed (and here my language coherence will be completely lost).

First of all I would like to thank all the great flat/house mates I have had. **Fulvio**, il mio cuoco preferito, il piu' grande denigratore della RER B e il mio "fratello adottivo". Se al liceo qualcuno mi avesse detto quanto mi sarei divertita a vivere nella tua stessa casa...avrei traslocato subito: grazie! E grazie a **Becky** per le sue sempre brillanti idee su mostre da vedere/ristoranti da provare/ libri da leggere/film da vedere e per le lunghissime chiacchierate. Grazie anche per aver corretto il mio inglese (e il mio

italiano). **Juan Carlos**, I still expect to find you at unlikely times of the night in the kitchen making a sandwich. I would like to thank **Christine** (Crawford) for having me in her house for a year, sharing recipes, science and travel tips and excursions into the Tasmanian life.

Je veudrais aussi remercier le groupe "Apero post-boulot au LOCEAN": **Martin, Laurent, Casimir, Alice S., Loriane, Laurène, Vera, Anthony, Sarah B., Sarah N., Swen, Victor, Jean-Baptiste, Clement, Cedric, Karine, Joan (and Ari!), Marion** etc. and all the IMAS friendly community of PhD students and post-docs (and here I will surely forget someone): **Julie (fluffy!), Sally, Pearse, Michel, Kevin, Roxy, Lucho, Marion, Andreas, Aurelie, Eva, Xavier, Claudio, Sandra, Giulia, Matilde, Amelia, Ben, Jaimie, Andrea, Nathalie, Ale, Manu, Mauro, Clara, Matthieu (and Clemence!), Seb, Joan, Lavy, Gabi, Ana, Vero, Eric, Pam, Elena, Hanne, Tom, Molly, Mana, Thibaut, Christine, Axel, Delphi, Malcom, Ziya, Hugo, Jan, Viviane, Leo, Melanie, Romain**. It is a long list and I am sure I must have forgotten someone!

A special thanks goes to **Sara L.** (I even don't know in which language I should thank you), who has been part of both my Tasmanian and Parisian life, sharing chocolate, tea, science and life advice and being simply a great friend (and helping me not to forget anybody in the acknowledgments).

Another very special thanks goes to ...il mio **gruppo italiano** a Hobart! Grazie soprattutto a Paola per avermi coinvolta in questo progetto bellissimo e grazie a tutto il gruppo di bravissime poliglotte, ma soprattutto amiche.

I would also like to thank all the friends that made these years pleasant (even if sometimes I wasn't pleasant at all) and fun. **Ophelie** and **Raphael** for all the French-languange support, for their game nights, cups of tea and parties in the French countryside, **Sara** and **Marjorie**, for the lovely weekends across France (and Europe). **Alice C.**, per essere stata un grande esempio per me, per le conversazioni che passano dall'oceanografia all'ornitologia, passando per lingue e viaggi e per avermi sempre fatta sentire la benvenuta nella sua bella casa a Chize'. **Irene**, grazie per avermi ascoltata, fatta ridere (ma tanto!), sostenuta per questi anni. Grazie per le avventure Lionesi e Parigine, per le lunghe passeggiate e per i racconti da pet-sitter che mi fanno ancora ridere dopo cento volte che li ho ascoltati. Vorrei anche ringraziare **Pietro** per i bei momenti passati insieme, per il sostegno, per i viaggi in giro per l'Europa e per avermi convinta a usare Python. Le **"tonne"**, perche' dopo 5 anni di universita', 4 anni di dottorato mi sembra che non sia cambiato niente. **Isa**, perche' ogni tazza di te', email, lettera o cartolina riesce a sorprendermi anche dopo anni di amicizia. Grazie a **Corrado** per le chiacchierate torinesi, per i consigli per il futuro (e per avermi convinta a viaggiare negli USA).

Finally, I would like to thank **John** for being my most motivated supporter, travel companion, bushwalking buddy, housemate, etc. I look forward to future adventures together.

Contents

List of Figures

List of Tables

A mamma e papa'

Part I

Introduction

Research context and challenges

Predators occupying high trophic levels in marine habitats play a fundamental role in maintaining the structure and functioning of healthy marine ecosystems [Camphuysen, 2006, Estes et al., 2011, Sala, 2006]. Recent observations in the marine [Myers et al., 2007, Heithaus et al., 2008, Frank et al., 2007, Estes et al., 1998, Baum and Worm, 2009] environment (as well as terrestrial [Ripple and Beschta, 2007, Sala, 2006] and freshwater [Carpenter et al., 1985] ones) suggest that presence and abundance of top predators trigger top-down effects. Top-down effects can heavily affect ecological communities at all trophic levels down to phytoplankton [Worm and Myers, 2003, Frank et al., 2005].[1] Another reason behind the interest of studying top marine predators lies in a complementary ecological mechanism: the bottom-up effect. Since top predators occupy by definition the apex levels of the trophic web, natural or human induced perturbations occurring at any of the underlying trophic webs and in the physical habitat is likely to affect them. Therefore top predators are considered to act as *integrators* of the trophic web [Camphuysen, 2006] and have been identified as ideal sentinel species to monitor the health of ecosystems [Fossi et al., 2012, Burger and Gochfeld, 2004].

In the last decades the development of bio-logging (i.e. deployment of autonomous recording tags on free-living animals [Ropert-Coudert and Wilson, 2005]) has radically changed the study of top predators, which are often large marine animals, and their surrounding environment [Boyd et al., 2004, Ropert-Coudert and Wilson, 2005]. Combinations of sensors measuring position (Argos and GPS), environmental properties (i.e. water temperature and light) and proxies for foraging behavior (i.e. stomach temperature sensors [Weimerskirch, 2007] and accelerometers [Viviant et al., 2010, Gallon et al., 2012]), have been attached to more than 500 marine species [Ropert-Coudert et al., 2009, Block et al., 2002] in order to address matters such as:

- key habitats location (i.e. foraging and breeding grounds) [Dragon et al., 2012b, Dragon et al., 2012a, Le Boeuf et al., 2000, Block et al., 2011, Bestley et al., 2009, Carlson et al., 2010, Bost et al., 1997, Block et al., 2002]
- analysis of the relationship between marine animals and oceanographic features [Bailleul et al., 2010a, Cotté et al., 2011, Dragon et al., 2010, De Monte et al., 2012, Cotté et al., 2007, Guinet et al., 2001, Biuw et al., 2007, Hays et al., 2001, Kai et al., 2009a, Block et al., 2011]

[1] A striking example was observed in the Northwest Atlantic Ocean where the decline of large sharks resulted in a drastic increase of cownose rays and the loss of bay scallop populations, an important ecological and economical resource for the region [Myers et al., 2007, Heithaus et al., 2008].

- investigation of animal navigation capabilities [Åkesson and Alerstam, 1998, Flemming et al., 2006]
- biotic and abiotic monitoring of the marine environment (especially in remote oceanic regions) [Charrassin et al., 2008, Roquet et al., 2009, Padman et al., 2010].

In my thesis work, I focused in particular on the foraging aspects, for several reasons. On one hand most marine predators' movements at sea aim at seeking and eating their prey, therefore the knowledge of their foraging behaviour is key for their understanding and conservation. On the other hand, foraging can be seen as a trophic interaction and can be used to analyse and monitor not only marine predators themselves but also their prey. This is very important because most of marine predators' prey (often fish, cephalopods or small crustaceans) are often difficult to study directly.

When approaching foraging ecology, a major difference between the marine and terrestrial environment lies in the fact that marine animals move, feed and make decisions in an inherently more dynamic environment. In the open ocean physical, chemical and biological conditions change at spatial and temporal scales comparable with the ones of animal movement itself. In particular foraging trips of far-ranging marine mammals and seabirds have durations between a few days and a few months, corresponding to the oceanic submesoscale and mesoscale (days-months, 1-100 km, see Figure 1).

Meso and submesoscales (from now on (sub-)mesoscale in the text) are characterized by strong gradients in physical and biological properties. Eddies, fronts and meanders are typical (sub-)mesoscale physical structures: they regulate horizontal and vertical transport of passive and quasi-conservative tracers like sea surface temperature (SST), nutrients or chlorophyll a (Chl) [Mahadevan and Campbell, 2002]. (Sub-)mesoscale variability distributes water properties so that it is not unlikely to observe the same differences in water properties within tenths of kms and over an entire oceanic basins. The effect of (sub-)mesoscale structuring of tracers creates a highly dynamical and heterogeneous landscape that can be readily seen from remote-sensing observations of the ocean surface. Figures 2 b) and c) display an example of a patchy distribution of surface chlorophyll and the rapid change that occurs in one week in time. The range of the chlorophyll values in Figure 2 b) and c) is the same as the one in Figure 2 a) that represents an average over the spring and summer of the years 2010 and 2011. Almost the same range of values that can describe the variability over all the Southern Ocean can be found in typical mesoscale distances.

Beside their role in structuring horizontal transport, eddies and fronts have been observed to be regions of enhanced vertical movements [McGillicuddy et al., 1998, Gaube et al., 2013, Mahadevan et al., 2012, Klein and Lapeyre, 2009a, Lévy et al., 2012b, Rosso

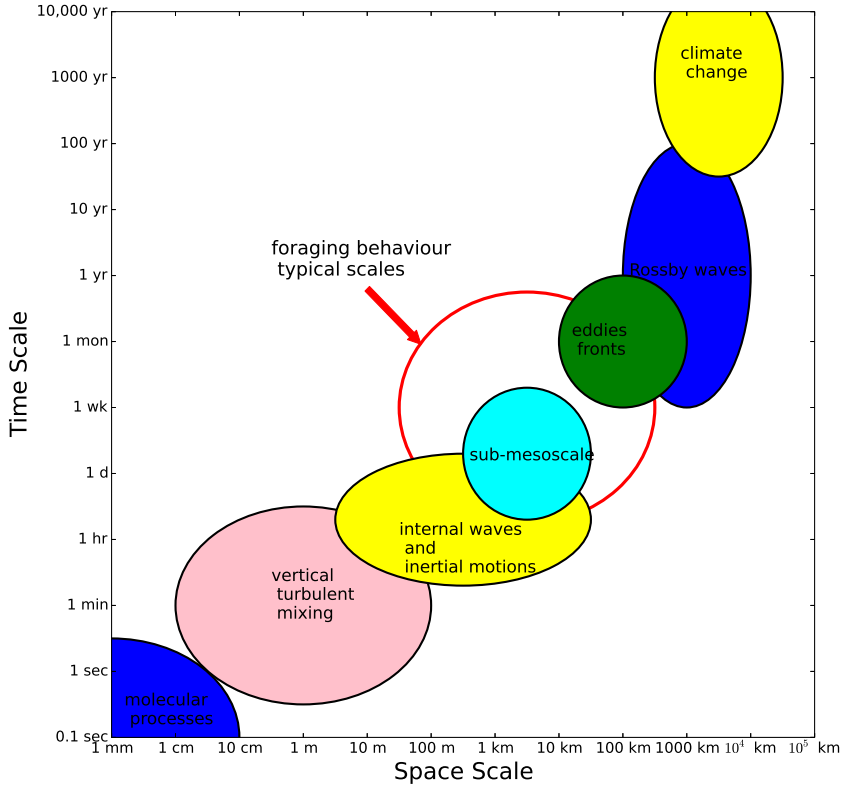

FIGURE 1: Typical spatial and temporal scales in oceanographic processes (adapted from Ref.[Chelton, 2001]). Top marine predators foraging behaviours correspond to scales (highlighted in red in the figure) from hours-few meters (punctual hunting behaviour) to few weeks and months-10-100 kms (lengths foraging trips). The corresponding oceanographic scales are the sub and mesoscale, that are well known also for being key spatial and temporal scales for phytoplankton bloom cycles.

et al., 2014] that may cause upward displacements of nutrients from deep reservoirs to nutrient-depleted surface waters. The upwelling of nutrients enhanced by (sub-)mesoscale activity makes regions with intense horizontal dynamics particularly rich in terms of primary production.

The patchy distribution of chlorophyll observed by satellite is a typical example of how the (sub-)mesoscale skeleton influences the distribution of biomass and community structure of drifting marine life as phytoplankton [Strass et al., 2002, Lévy et al., 2012b, Abraham, 1998, Martin, 2003, Lehahn et al., 2007, d'Ovidio et al., 2010], bacteria [Baltar et al., 2010a], zoo-plankton [Labat et al., 2009] and micro-nekton [Sabarros et al., 2009].

More surprisingly, large marine top predators like fishes [Godø et al., 2012], pinnipeds [Bailleul et al., 2010b], whales [Cotté et al., 2011], squid [Waluda et al., 2001a], sea turtles [Polovina et al., 2006] and sea-birds [Cotté et al., 2007, Kai et al., 2009a, De Monte

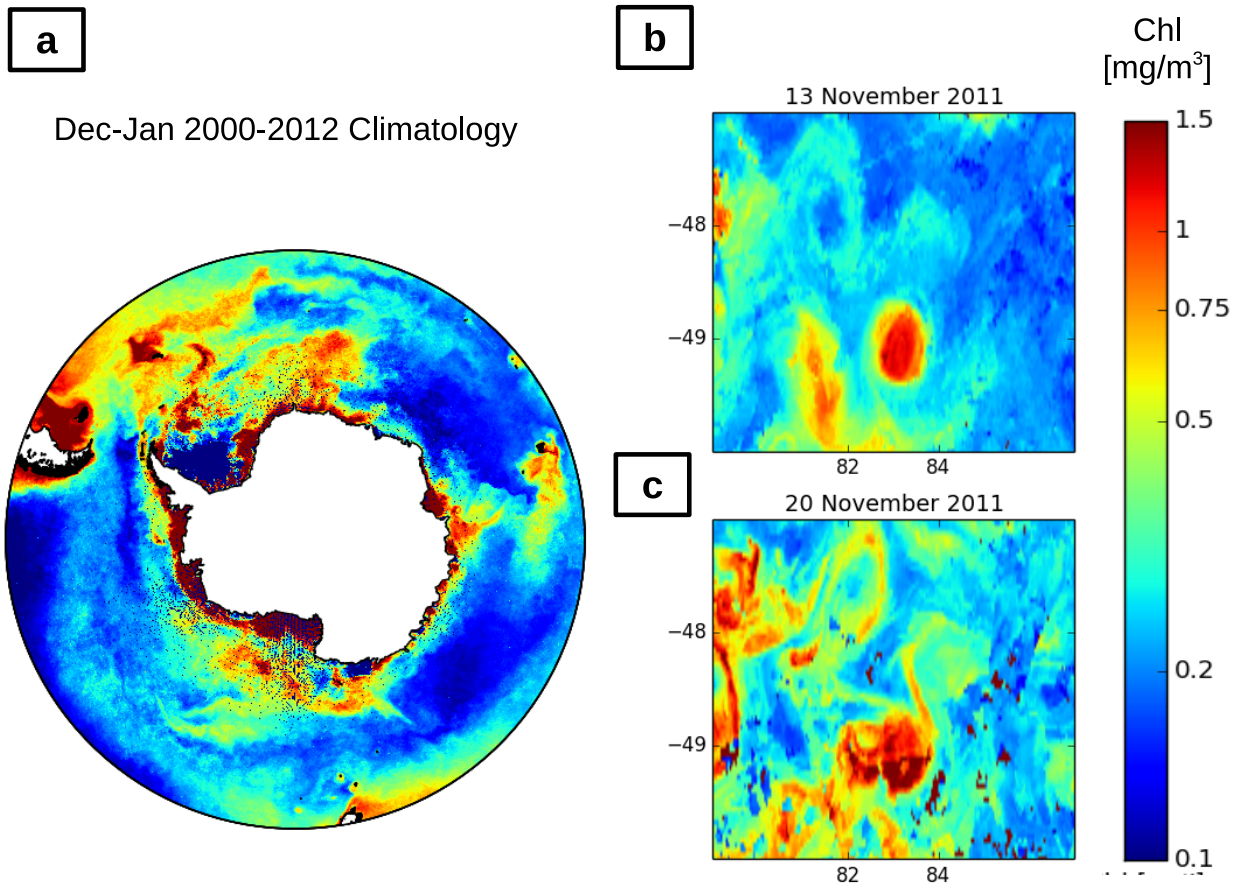

FIGURE 2: Primary production as seen from space: a) sea surface chlorophyll climatology of the Southern Ocean for the months of December and January (spring-summer) from 2000 to 2012. b) and c) Daily sea surface chlorophyll images for a region of Indian Sector for two days in November 2011 with a two week interval. Data from GlobColour (http://hermes.acri.fr/) and CLS (http://www.cls.fr/en/) experimental regional product.

et al., 2012, Nel et al., 2001] have been observed to co-localize with (sub)mesoscale structures like eddies and fronts. However, the mechanism behind this co-localisation, an interplay of ocean physics and ecological dynamics, is still challenging to understand. Possible mechanisms include bottom-up effects where horizontal and vertical dynamics make fronts and eddies oases of enhanced productivity and planktonic convergence, the potentially more favourable conditions that gradients in contrasting water masses create and energetically efficient swimming and searching behaviour. In spite of the growing number of observations of this phenomenon, these questions are all still unanswered.

Current technologies and theoretical tools to address them are finally available. First of all, bio-logging data have increased in reliability, space and time resolution [Ropert-Coudert and Wilson, 2004], variety of sensors [Ropert-Coudert and Wilson, 2005] and consequently use [Ropert-Coudert et al., 2009, Evans et al., 2013]. In particular, after almost

exclusively large scale studies that focused on basin scale migrations [Block et al., 2011], the increase in spatial and temporal resolution of tracking data allows presently to retrieve almost errorless (i.e. with an error of the same order of the size of the animal, and far smaller than the spatial resolution of the (sub)mesoscales) information about animal locations. This spatio-temporal resolution is ideal for sub and mesoscale studies. Secondly, accuracy and availability of remote sensing information have increased [Rio et al., 2007, Cracknell, 2007]. The knowledge of appropriate resolution horizontal velocity field, sea surface temperature, chlorophyll concentration and its optical re-analyses [Brewin et al., 2011] is fundamental to reconstruct the heterogeneous and dynamical mesoscale landscape top marine predators explore during their foraging trips. Third, methods borrowed from theoretical physics [Aurell et al., 1997, Boffetta et al., 2001, Shadden et al., 2005] have been translated into robust Lagrangian techniques that allow to extract further information from remote-sensing to locate fronts [Hernández-Carrasco, , d'Ovidio et al., 2009] and eddy cores [Okubo, 1970, Weiss, 1991], but also to combine remotely sensed data with in-situ observations [Nencioli et al., 2011].

Objectives and structure of this thesis

The aim of this thesis is to investigate how mesoscale ocean dynamics influences the foraging behavior of top marine predators. In order to disentangle the dynamics and ecological complexity of the effects of oceanic currents on marine predators, this thesis addresses the following questions:

1. Does (sub-)mesoscale turbulence directly affect top predators? How can we evaluate the role of direct mechanical transport on top marine predators in respect to their swimming capabilities?

2. How does (sub-)mesoscale turbulence structure the dynamical and contrasted *"seascape"* that top predators navigate?

The first question is addressed in the first part of this thesis corresponding to Chapters 1 and 2. Chapter 1 challenges the common view that fast swimming predators are not directly affected by oceanic currents. The study is conducted by combining animal tracking of southern elephant seals, satellite and oceanographic data in a diagnostic that quantifies the variability of currents influence the horizontal movements of elephant seals. Chapter 2 combines the observation that the effect of currents on diving top predators is variable and related to foraging behaviour with remote sensing and animal tracking data

in order to study the foraging trips of Macaroni penguins from the Crozet archipelago (North-West of the main study region described in Section I).

The second question is addressed in the second part of my thesis. The last two chapters aim at describing the mesoscale landscape explored by Kerguelen's marine top predators in terms of primary production and phytoplankton biogeography. Part II's chapter 1 combines different remote sensing products, in-situ data and a very simple modelling approach into a dynamical biogeography of dominant phytoplanktonic type. In part II's chapter 2 the complexity of the model is increased to take into account of a more complex ecological dynamics. Together Chapters 1 and 2 describe the complexity of the ecological patterns Kerguelen marine predators encounter and respond to during their foraging trips.

The Kerguelen region natural laboratory

The Kerguelen region is located in the Indian Sector of the Southern Ocean (see Fig. 3) where the Kerguelen Plateau, a Northwest-Southeast shallow ($\sim$ 500 m) seafloor feature, represents a major topographic obstacle for the Antarctic Circumpolar Current (ACC). The zonal fronts of the ACC create the most intense oceanic current in the world (130-140 Sv, 1 $Sv = 10^6\, m^3/s$) and strongly interact with the shallow bathymetry creating a highly dynamical eddy field East from the Kerguelen Plateau [Roquet et al., 2009, Pollard et al., 2002, Orsi et al., 1995].

The Kerguelen region presents one of the largest natural phytoplankton bloom of the Southern Ocean ($\sim$ 1000 km [Mongin et al., 2008]), that is well known for being High Nutrient Low Chlorophyll (HNLC). Several studies suggest that Kerguelen's bloom is likely to be triggered by the advection of waters from the plateau that are rich in iron [Mongin et al., 2009, d'Ovidio et al., 2015], a key factor in controlling primary production, phytoplankton community structure and CO_2 uptake in HNLC regions [Blain et al., 2001, De Baar et al., 2005, De Baar et al., 1995, Martin, 1990, Blain et al., 2007, Blain et al., 2008, Boyd et al., 2007, Boyd et al., 2012a]. However, other mechanisms, such as vertical water movements induced by the intense (sub-)mesoscale activity [Rosso et al., 2014], grazing [Smetacek et al., 2004] and silicate limitation [Sullivan et al., 1993], have been observed to play an important role in regulating and structuring blooms in the Southern Ocean.

The complex spatial and temporal distribution of iron and different physical conditions structure the phytoplanktonic community in a mosaic of different groups. Biogeochemical research voyages highlighted that different types of diatoms tend to dominate the

bloom [Blain et al., 2008, Armand et al., 2008] on the plateau and in the inter-frontal open ocean region East of Kerguelen. This intense production supports a relatively simple ecological web that include variety of meso-zooplankton such as copepods, salps, amphipods and euphausiids [Carlotti et al., 2015, Bocher et al., 2001] and mesopelagic fish, dominated by myctophids [Pakhomov et al., 1996]. Myctophids have been suggested to play a key role in the ice-free regions of the Southern Ocean, being the main prey of many of the top predators colonies of the Kerguelen and Heard archipelagos that include southern elephant seals, fur seals, gentoo and king penguins that have been the object of bio-logging studies [Hindell et al., 2011, Koz, 1995, Lea et al., 2006, Lea et al., 2008, Deagle et al., 2007, Cherel et al., 2008].

In spite of the remoteness and the difficult operational conditions, the physical, biogeochemical and ecological interest of the Kerguelen area justified interdisciplinary research voyages, a yearly monitored station, KERFIX, [Jeandel et al., 1998], remote-sensing regional products (developed by Collective Localisation Satellite - CLS (http://www.cls.fr/en/) and at least two decades of studies of demography [Guinet et al., 1992, Guinet et al., 1999, Slip and Burton, 1999, Campagna and Lewis, 1992] and animal tracking [Bailleul et al., 2007, Dragon et al., 2010, d'Ovidio et al., 2013, Guinet et al., 2014] of large animals having colonies on the Kerguelen and Heard archipelagos. Yet, the information about this region is highly inhomogeneous: for practical operational reasons research voyages have been focused on the Kerguelen plateau itself and on the nearby region and the cloud coverage interferes with the detection of SST and Chl from remote sensing. However, the increased use of floating drifters [d'Ovidio et al., 2015], autonomous bio-profilers [Boss and Pegau, 2001] and instrumented animals [Roquet et al., 2009] is largely improving the data coverage in this remote region.

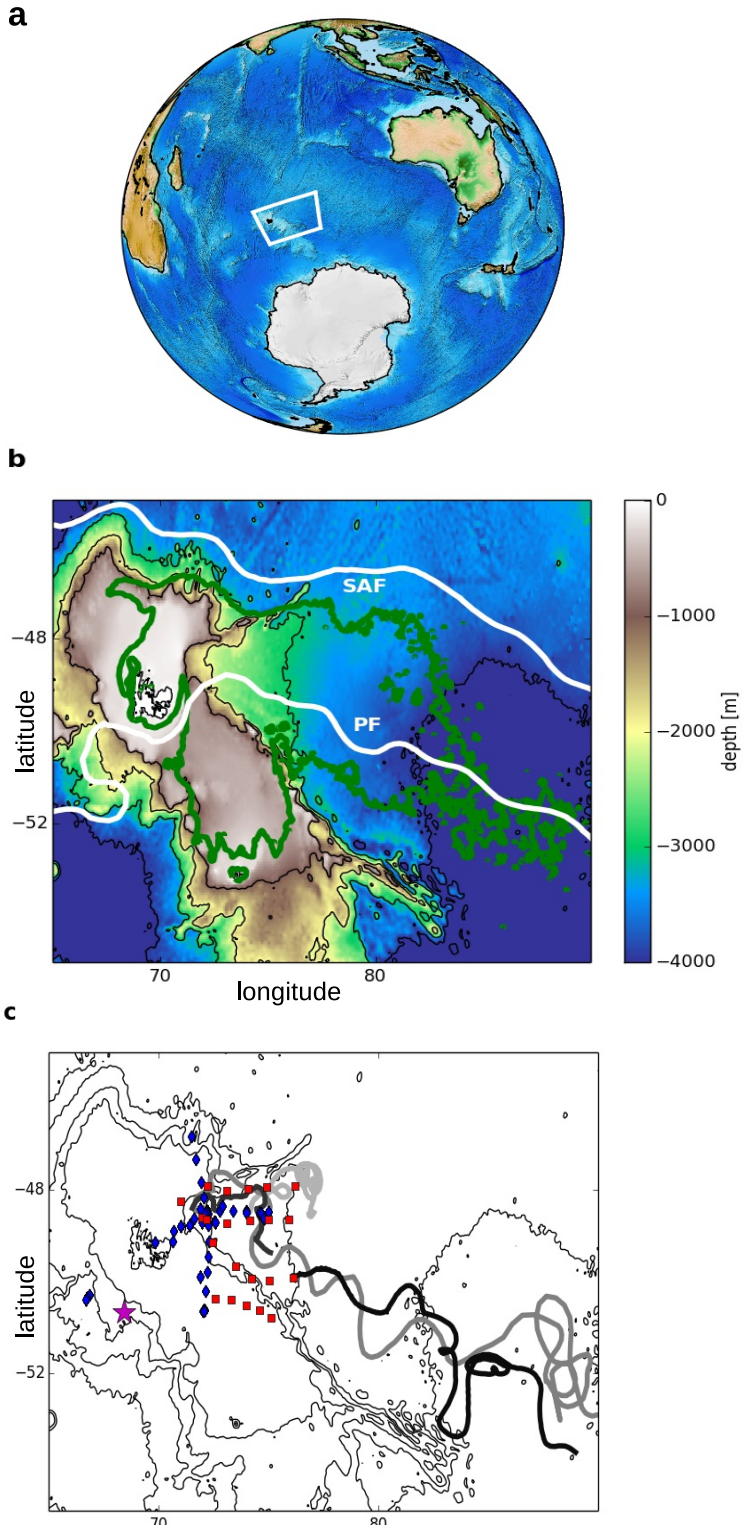

FIGURE 3: The Kerguelen region is located in the Indian Sector of the Southern Ocean (a). The shallow bathymetry of the Kerguelen Plateau (b) interacts with the Antarctic Circumpolar Current Fronts (white, SAF = Sub-Antarctic Front, PF = Polar Front) triggering one of the largest blooms of the Southern Ocean (green contour, corresponding to $Chl = 0.35\mu g/L$). (c) The Kerguelen region has been the subject of interdisciplinary field programs (blue diamonds = KEOPS2 stations (2011), red squares = ANR-Mycto 3D stations (2014), grey lines = trajectories of autonomous bio-profilers deployed between 2011 and 2014).)

Part II

Marine top predators in a dynamical environment

Co-localization between marine top predators and sub and mesoscale features like eddies and fronts has been observed for several species [Bost et al., 2009] including squids [Waluda et al., 2001b], whales [Cotté et al., 2011], king penguins [Cotté et al., 2007], sea turtles [Polovina et al., 2006], frigatebirds [Kai et al., 2009b, De Monte et al., 2012], southern elephant seals [Bailleul et al., 2010b, Campagna et al., 2006], northern fur seals [Nordstrom et al., 2012], mola mola [Sims et al., 2009], manta rays [Jaine et al., 2012] and albatross [Nel et al., 2001, Hyrenbach et al., 2002].

In spite of the growing amount of observations of this phenomenon, the responsible mechanisms are still unknown. Most authors have interpreted the co-localization as a consequence of the *bottom-up effect*. Submesoscale fronts and mesoscale eddies have been observed to be associated with vertical water movements [Klein et al., 2005] that models and observations suggest may lift deep and nutrients-enriched water masses to the euphotic layer enhancing primary production [Mahadevan et al., 2012, Lévy et al., 2012a, McGillicuddy et al., 1998, Bakun, 2006, Klein et al., 2005]. Such an increased production is estimated to be able to support the high concentrations of zooplankton [Labat et al., 2009] and micronekton [Sabarros et al., 2009] that have been measured within (sub-)mesoscale structures. As a result, according to this theory, fronts and eddies would become hotspots of marine life and attract higher trophic marine organisms [Godø et al., 2012, Boero, 2014]. However, eddy peripheries and fronts are also dynamically attractive structures for horizontal ocean circulation. Therefore passive (or almost-passive) tracers like Surface Chlorophyll [Lehahn et al., 2007], Sea Surface Temperature [Mahadevan and Campbell, 2002] and drifting buoys [Nencioli et al., 2011] are preferentially advected to fronts and eddy peripheries by the horizontal velocity field. Indeed, another possible mechanism to explain colocalization of fronts and marine animals could be concentration and retention of planktonic organisms within (sub)mesoscale structures. Both these hypotheses are based on the assumption that marine top predators actively search and are able to locate (sub)mesoscale structures responding to either prey density or to cues associated with the structures themselves (for example gradients in temperature). To my knowledge no study has explored the possibility that marine top predators may actually be advected to fronts and eddy edges by mesoscale oceanic currents.

Marine top predators are in most cases large marine animals and they are referred to as *nekton* -free swimming organisms – as they are capable of swimming speeds that can be one order of magnitude larger than typical ocean currents. In contrast, *plankton* – literally “drifter” and “wanderer” - refers to organisms who are largely advected by the surrounding waters. Coherently with these definitions, the direct mechanical effect of currents on trajectories is considered negligible for fast swimming nektonic organisms, such as pinnipeds and tuna fish, and dominant for planktonic ones. An important consequence of this assumption is that the classification of marine predators behaviors

from movement patterns is typically performed by borrowing approaches from terrestrial ecology, where changes in the physical landscape occur in time scales that are much slower than the typical lifetime of organisms. For example, a common method to identify intensive foraging behaviour consists in studying the sinuosity of animal trajectories. According to Optimal Foraging Theory (OFT) [Hengeveld, 2007] the optimal movement pattern for an animal searching for a patchly distributed resource consists in small scale movement search clusters (called Area Restricted Search) - corresponding to intensive search and foraging- separated by large scale displacements- corresponding to research for favourable foraging grounds. Therefore, regions of interests for foraging predators are selected by identifying bouts of trajectories with particularly high sinuosity. In a flowing medium considering the effect of currents negligible may be misleading as trajectories' shapes could be deformed by oceanic currents. This assumption may be especially difficult when marine animals are moving in highly dynamical oceanographic structures such as fronts. The scheme displayed in Fig. 4 shows how stirring may stretch a convoluted trajectory, typical of ARS behaviour, into a total displacement characterized by long scale movements that may suggest that the animal is not engaging in ARS but is instead ranging long distances to look for favourable grounds.

However, the distinction between plankton and nekton is qualitative and depends largely on the scale of movement of interest. Theoretical and experimental studies have quantified the active propulsion of phytoplankton, zooplankton, jellyfish and fish larvae and how it affects their spatial distribution [Leis, 2006, Durham et al., 2013, Seuront et al., 2004, Vandromme et al., 2010, Fossette et al., 2015]. By contrast, the effect of oceanic currents on nektonic organisms has received relatively little attention. To my knowledge, horizontal currents have been shown only to significantly affect sea-turtles, one of the slowest nekton [Gaspar et al., 2006, Girard et al., 2006, Luschi et al., 2003]. Comparisons with satellite altimetry and synthetic water parcels advection in numerical models have suggested no direct effects of oceanic currents on fast swimmers like elephant seals and whale sharks [Bailleul et al., 2010b, Sleeman et al., 2010]. However, Campagna et al.[Campagna et al., 2006] present an example of elephant seals whose long trajectories ($> 500\,km$) closely resemble that of a drifter released almost simultaneously in their proximity.

Chapter 1, "Quasi-planktonic behavior of foraging top marine predators", explicitly addresses the issue of investigating the direct mechanical effect of currents on a fast swimming top predator of the Southern Ocean, the Southern Elephant Seal (*Mirounga leonina*, see Figure 5 a)). In this study we combine the use of high resolution bio-logging (GPS trajectories and accelerometry), satellite altimetry, in-situ oceanographical data (ADCP and drifting buoys) and a Lagrangian approach to define a novel diagnostic

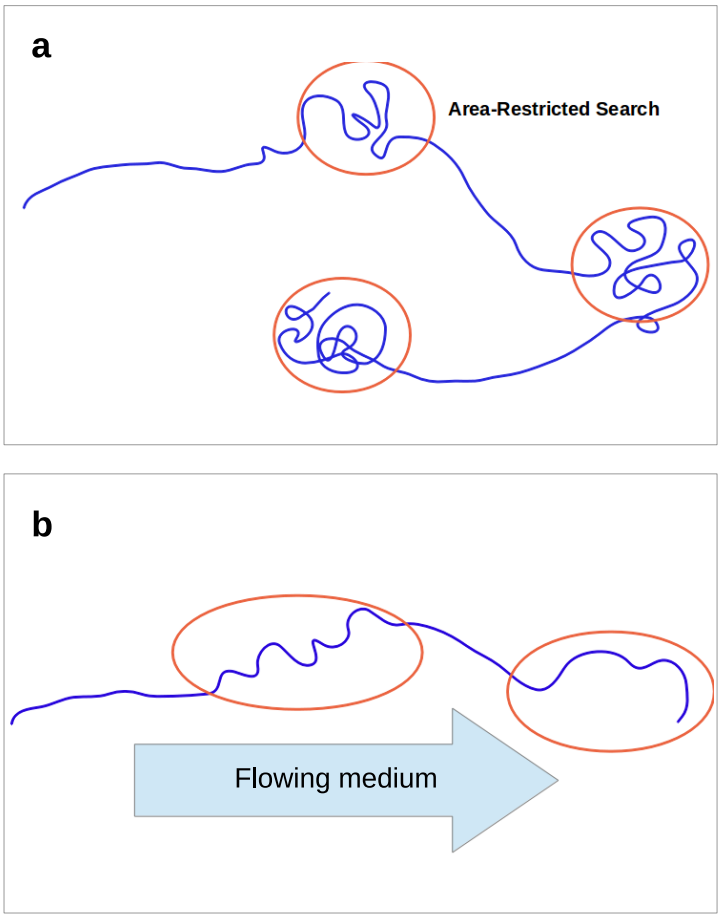

FIGURE 4: Typical search trajectories (a) are characterized by clusters of short-scale movements (ARS) and long displacements. However, if this pattern is embedded into a moving medium (b) the resulting trajectory is deformed affecting the correct identification of ARS.

to quantify the similarity between actual animals' trajectories and simulated ones. We find that the studied elephant seals trajectories are characterized by horizontally "quasi-planktonic" bouts where the animals are horizontally drifting. These bouts correspond to an increased foraging effort, indicating that during the quasi-planktonic condition energy is allocated for diving and chasing, rather than in horizontal active displacement. This result suggests another possible mechanism behind the co-localization of marine top predators and (sub)mesoscale structures. The latters, may not just affect the prey distribution (through bottom-up or concentration-retention mechanisms), but also directly entrain horizontal displacements of marine top predators themselves.

Chapter 2, "Influence of oceanographic structures on foraging strategies: Macaroni penguins at Crozet Islands ", is the result of a collaboration with Cecile Bon, a PhD student

FIGURE 5: Southern elephant seals (a) and Macaroni penguins (b) are top marine predators of the Southern Ocean and have colonies on several sub-Antarctic islands including Kerguelen and Crozet. Photographs by Sara Labrousse (IPEV109).

in ecology who is working on foraging strategies of seabirds. The goal of this work is to compare for the first time the trajectories of foraging Macaroni penguins (*Eudyptes chrysolophus*, see Figure 5 b) with mesoscale oceanographic features. My contribution consists in handling the remote-sensing products used in this study (altimetry, Sea Surface Temperature and Chlorophyll) and their Lagrangian re-analyses and contributing to the tracks analysis. We find that the analyzed individuals -incubation stage males of Macaroni penguins- target the (sub)mesoscale fronts surrounding the Sub-Antarctic Front and reduce their horizontal swimming when encountering fronts and eddies. As a result their horizontal displacement is largely affected by oceanic currents especially in the central phase of their foraging trip that is estimated to be the one of more intensive foraging. The results of this study confirm that the "quasi-planktonic" trajectory bouts are not a specific behaviour associated with elephant seals, but that they are likely to be generally observed in diving marine top predators.

The results of Chapter 1 and Chapter 2 suggest that diving marine top predators may exhibit horizontally "quasi-planktonic" behaviors when intensively foraging. During "quasi-planktonic" phases of foraging trajectories, marine top predators are likely to be entrained by attractive features of the horizontal (sub-)mesoscale dynamics: eddies and fronts. Therefore, the performance of methods that relate movement patterns to animal behaviours could be improved if they were applied to a "processed trajectory" where the offset of the background currents is filtered out.

Chapter 1

Quasi-planktonic behavior of foraging top marine predators

This chapter has been published as *Quasi-planktonic behaviour of foraging top marine predators* by A. Della Penna, S. De Monte, E. Kestenare, C. Guinet and F. d'Ovidio in *Scientific reports*, 2015.

Abstract

Monitoring marine top predators is fundamental for assessing the health and functioning of open ocean ecosystems. Although recently tracking observations have substantially increased, factors determining the horizontal exploration of the ocean by marine predators are still largely unknown, especially at the scale of behavioral switches (1-100 km, days-weeks). It is commonly assumed that the influence of water movement can be neglected for animals capable of swimming faster than the current. Here, we challenge this assumption by combining the use of biologging (GPS and accelerometry), satellite altimetry and in-situ oceanographic data (ADCP and drifting buoys) to investigate the effect of the mesoscale ocean dynamics on a marine predator, the southern elephant seal. A Lagrangian approach reveals that trajectories of elephant seals are characterized by quasi-planktonic bouts where the animals are horizontally drifting. These bouts correspond to periods of increased foraging effort, indicating that in the quasi-planktonic conditions energy is allocated to diving and chasing, rather than in horizontal search of favourable grounds. These results suggest that mesoscale features like eddies and fronts may act as a focal points for trophic interactions not only by bottom-up modulation of nutrient injection, but also by directly entraining horizontal displacements of the upper trophic levels.

Introduction

Marine top predators play a key role in maintaining the health of open ocean ecosystems and their monitoring is fundamental for assessing the quality of the marine environment, in particular in the wake of a changing climate [Camphuysen, 2006, Estes et al., 2011]. Over the last two decades marine top predators have been the subject of numerous tracking programs [Hussey et al., 2015, Block et al., 2002] aimed at identifying key habitats, e.g. foraging and breeding grounds [Dragon et al., 2012b, Dragon et al., 2012a, Le Boeuf et al., 2000, Block et al., 2011, Bestley et al., 2009, Carlson et al., 2010, Bost et al., 1997] , studying their relationship with oceanographic features [Bailleul et al., 2010a, Cotté et al., 2011, Dragon et al., 2010, De Monte et al., 2012, Cotté et al., 2007, Guinet et al., 2001, Biuw et al., 2007, Hays et al., 2001, Kai et al., 2009a], investigating their navigation capabilities [Åkesson and Alerstam, 1998, Flemming et al., 2006] and gathering information about their biotic and abiotic environment, notably on remote oceanic regions [Charrassin et al., 2008, Roquet et al., 2009, Padman et al., 2010, McMahon et al., 2005]. The temporal and spatial resolution of these studies is rapidly improving, enabling the observation of not only large scale migrations, but also the fine scale ($\sim 1\,km$) features of foraging trips. This increasing spatiotemporal resolution and the use of accelerometers makes it now possible for the first time to investigate the behaviors that underpin the observed patterns of displacement, and to relate these patterns to the physical properties of the turbulent environment that marine predators experience.

Large predatory fish, marine mammals and swimming seabirds are classified as *nekton* - free-swimming animals - because they are able to swim at a speed that is several times larger than the strongest currents of the open ocean. In contrast, *plankton* - literally meaning “wanderer” or “drifter” - refers to organisms that are passively transported, typically because they have no autonomous capacity of motion, or this is too weak to overcome transport. Consistently with such a view, the mechanical effect of currents on the trajectories of marine predators is often neglected and the classification of their behaviors is typically performed by borrowing approaches from terrestrial ecology, where animal search for food occurs on a faster timescale than the temporal variability of the landscape.

However, both the “nekton” and “plankton” labels are used in a qualitative sense, as most drifting organisms have some propulsion capabilities, and the currents affect any free swimming organism by shifting its frame of reference. Although the swimming capabilities of planktonic organisms have received quite a lot of attention [Durham et al., 2013, Seuront et al., 2004, Vandromme et al., 2010, Fossette et al., 2015], only few studies have tackled explicitly the question of the extent to which ocean currents can

determine the trajectories of large marine animals and have concluded that this effect can be generally neglected. Indeed, the fact that nektonic animals are able to overcome oceanic currents does not imply that their movement is not directly influenced. To our knowledge, horizontal currents have only been shown to offset the trajectories of sea-turtles, which not surprisingly are among the slowest nekton [Gaspar et al., 2006, Girard et al., 2006, Luschi et al., 2003]. Similarly, Lea et al.[Lea et al., 2009] identified a relationship between fur seal pups swimming speed and wind speeds during their initial dispersal in extreme wind events. Instead, the need for correcting tracked trajectories of fast swimmers, such as elephant seals or whale sharks, has been ruled out by comparison with satellite altimetry [Bailleul et al., 2010b] and synthetic water parcels advected in numerical models [Sleeman et al., 2010].

Interestingly however, Campagna et al.[Campagna et al., 2006] present a striking example of elephant seals whose long trajectories ($> 500\,km$) closely resemble that of a drifter released almost simultaneously in their proximity. Is this example merely anecdotal or should the common assumption be revised? This question is important in marine ecology because the assumption that a swimming behavior is not directly affected by the ocean currents stands at the core of the analysis of search behavior of fast swimming animals - the majority of tagged species. This assumption has enabled this field of research to borrow techniques from terrestrial ecology, and notably the classification of animal behavior based on the sinuosity of trajectories for the identification of foraging grounds. On the other hand, if currents had sizable effects on the displacement of a marine predator, then ocean circulation features - like eddies and fronts - may play an important role in structuring the ecosystem not only bottom-up, but at multiple levels of the food chain. Besides, being hotspots of primary production, they would entrain top marine consumers, and thus concentrate in the same locations different organisms and their trophic interactions.

Here, we aim at assessing the impact of ocean currents on one of the fastest marine predators for which high-resolution tracking is available: the southern elephant seal. Using a novel biologger, we analyse simultaneous tracking (GPS - Global Positioning System) and behavioral data (accelerometry) from female southern elephant seals, *Mirounga leonina*, from the Kerguelen Islands (Indian Sector of the Southern Ocean, see Figure 1.1). Southern elephant seals are a model species to address our research aims. During their long-range foraging trips, these animals encounter different oceanic regimes, and in particular highly energetic features emerging between the Polar and the Sub-Antarctic fronts. Their size allows them to carry with minimal disturbance large bio-loggers with long-lasting batteries and multiple detectors, among which accelerometers that can provide a direct estimation of capture attempts independently of the trajectory analysis.

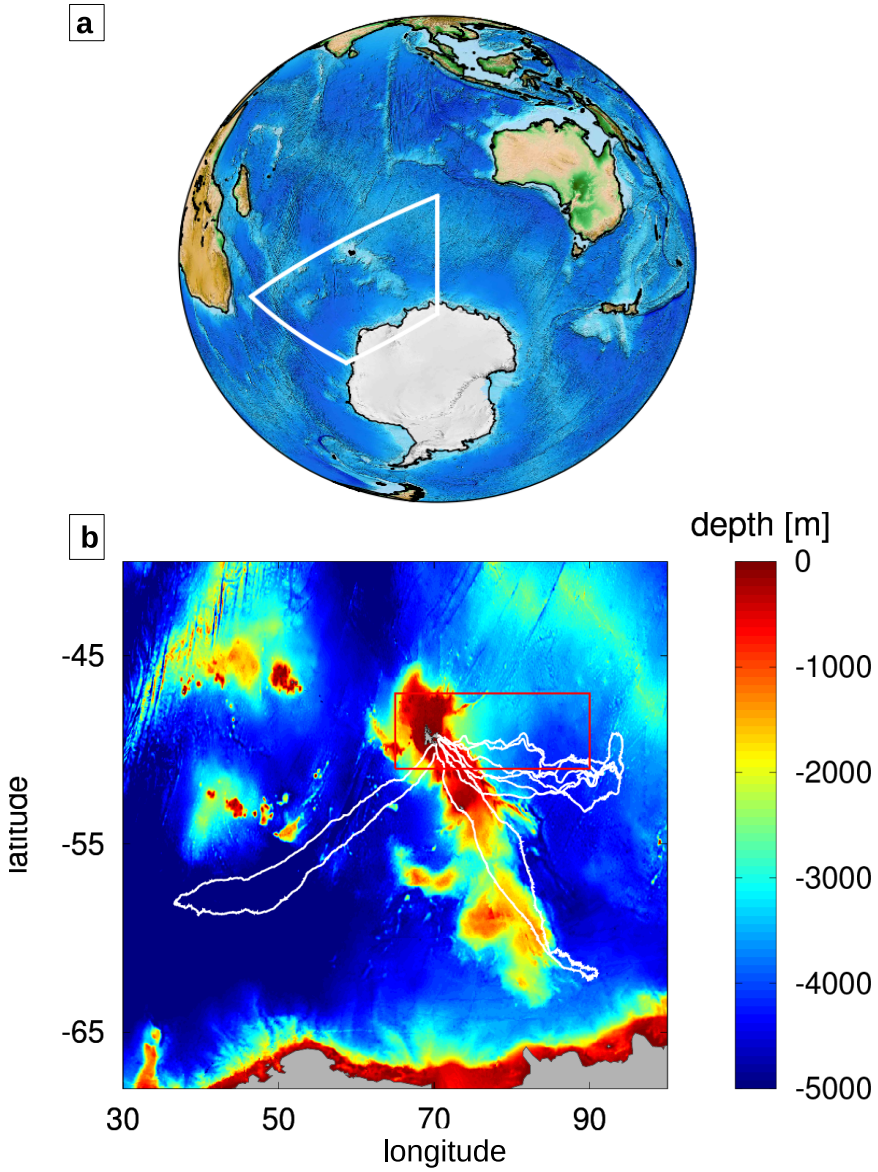

FIGURE 1.1: The data employed in this study refer to the Kerguelen region (white polygon), in the Indian Sector of the Southern Ocean (a). (b) The trajectories of the tagged elephant seals (white) overlapped with the bathymetry of the region. The red rectangle identifies the sub-region containing the trajectories of the drifting floats released during the KEOPS II campaign. Bathymetric data from ETOPO2 Global 2-Minute Gridded Elevation Data Volume E1 [U.S. Department of Commerce, National Oceanic and Atmospheric Administration, National Geophysical Data Center, 2001. 2-minute Gridded Global Relief Data (ETOPO2), access:8/30/2001]

The Kerguelen sub-population, the second largest in the world, is the subject of an on-going decadal study in terms of demography [Guinet et al., 1992, Guinet et al., 1999] and animal tracking [Bailleul et al., 2007, Dragon et al., 2010, d'Ovidio et al., 2013].

Our study focuses on the scale at which switches in the patterns of foraging behavior of marine predators are observed ($\sim 10km$). In terms of ocean physics, this is the (sub-)

mesoscale. This scale is also referred to as *ocean weather* because of the presence of eddies and frontal systems [Belkin et al., 2009, Shadden et al., 2005, Shadden, 2005] similar to meteorological systems. Such dynamical structures shape the distribution of chemico-physical tracers such as Sea Surface Temperature [Mahadevan and Campbell, 2002], biotic fields like Chlorophyll concentration [Strass et al., 2002, Lévy et al., 2012b, Abraham, 1998, Martin, 2003, Lehahn et al., 2007] and community composition [d'Ovidio et al., 2010]. Furthermore, mesoscale turbulence is a major determinant of the distribution of consumers as zooplankton [Labat et al., 2009] and micronekton [Sabarros et al., 2009]. Top predators such as whales [Cotté et al., 2011], squid [Waluda et al., 2001a], king penguins [Cotté et al., 2007], sea-turtles [Polovina et al., 2006], frigatebirds [Kai et al., 2009a, De Monte et al., 2012], elephant seals [Bailleul et al., 2010b], fur seals [Nordstrom et al., 2012, Sterling et al., 2014] and albatrosses [Nel et al., 2001] have been observed to co-localise with mesoscale structures but how much these animals actively track these features and how much they are entrained by them is part of the open question which we address here. In this study we find that, in contrast to what is often assumed, all the analyzed trajectories are characterized by bouts that are largely dominated by the currents advection and we develop a Lagrangian method to quantify the contribution of horizontal oceanic currents to an animal trajectory.

Method

The elephant seals tracking dataset employed in this study consists of five post- breeding foraging trips collected between October 2010 and January 2012 (see Figure 1.1). The elephant seals were tagged with GPS transmitters with a space-time resolution of 50 m and 20 minutes respectively. All animals in this study were cared for in accordance with the IPEV ethical and Polar Environment Committees guidelines. The experimental biologging protocol was approved by the IPEV ethical and Polar Environment Committees. A total of more than 20000 km and 300 days data were recorded, from single trips of 72 to 85 days in duration. The tracking data were filtered by removing the locations that would have implied seals velocities larger than $2.8\,m/s$ according to the algorithm described in References [Dragon et al., 2010, Dragon et al., 2012b]. Seal velocities larger than this threshold are unrealistic and likely to be due to GPS errors. Individual seals were also equipped with accelerometers to detect rapid head movements that characterize prey capture attempts. Accelerometers allow the identification of prey captures with an accuracy of more than 80% [Viviant et al., 2010, Gallon et al., 2012, Dragon et al., 2012b, Guinet et al., 2014]. However, due to limited battery power, for the three longest trajectories we were only able to measure the rate of prey capture for the first part of the foraging trip (about half of the round trip, or $\sim$ 2000 km). Both GPS transmitters

and accelerometers have been observed not to interfere with marine mammal behavior [McMahon et al., 2008, Wilson and McMahon, 2006, Gallon et al., 2012]. Following References [Gaspar et al., 2006, Girard et al., 2006], we define *tracking velocity* the velocity estimated by differentiating in time the GPS positions and *heading velocity* the tracking velocity minus the estimated velocity of the ocean currents. In practice, the tracking velocity corresponds to the speed of the animal in a fixed frame of reference, and the heading velocity to the component relative to the moving water parcel the animal belongs to.

Geostrophic currents were quantified through an altimetry multi-satellite global product (Delayed Time Maps of Absolute Dynamic Heights (DT-MADT)) developed by CNES/-CLS Aviso (http://www.aviso.oceanobs.com). This product has temporal and spatial resolution of respectively 1 week and 1/3 ° [Handbook, 2010]. Regional versions of the product, one of which is corrected with wind-induced Ekman component at 15m (the depth of the SVP - Surface Velocity Program- drifters' drogue), have been also used. A comparison between the Lagrangian diagnostic introduced in this study -the Quasi-Planktonicity Index, see later- computed using different remote sensing products is shown in the Supplementary Information. Although the findings of this study do not depend on the choice of specific altimetric products, the presented results are obtained by using geostrophic products, that better refer to the typical diving depths of elephant seals, as detailed in the discussion.

The altimetry-derived velocity field was used to evaluate the heading velocity [Girard et al., 2006] and to compute the synthetic trajectories of virtual drifters. Simulated trajectories have been obtained by integrating the velocity field through a 4th order Runge-Kutta algorithm and allowed to compute two Lagrangian diagnostics: the Quasi-Planktonicity Index (QPI) -which we introduce in this paper- and the finite-size Lyapunov exponent (FSLE). This exponent is obtained by measuring the backward-in-time divergence of initially nearby particles and it is commonly used as an indicator of frontal activity and stirring intensity. Indeed, highest dominant FSLE values are associated to formerly distant water masses, whose confluence creates a transport front [d'Ovidio et al., 2009, d'Ovidio et al., 2004]. Fronts identified as maxima (ridges) of FSLEs have a convergent dynamics transverse to them, so that passive particles - like plankton or drifting buoys - in their neighbourhood are attracted to the front and then advected along it. Following Ref. [Haller and Yuan, 2000] we refer to these fronts as attractive Lagrangian Coherent Structures.

The Lagrangian features of elephant seal trajectories were compared with those of 47 WOCE-SVP drifters (GDP – http://www.aoml.noaa.gov/phod/dac/index.php) released during the multidisciplinary cruise KEOPS 2 (November 2011). The cruise and the

release of the drifters took place in a sector of the region explored by the elephant seals trajectories and during the same season when trajectories were recorded [Zhou et al., 2014]. Some examples of drifters trajectories are shown in the Supplementary Information (Fig. 1.6).

Because elephant seals are diving predators [Hindell et al., 1991], we used more than 20 casts (see Supplementary Information for more details) of two RD Instrument 300 kHz lowered acoustic Doppler current profilers (LADCP, also from the KEOPS2 cruise) to relate the horizontal currents integrated over the average diving depth (500 m, [Guinet et al., 2014]) with those of the upper layer (here approximated at 50 m) that we infer from altimetry.

Multivariate statistical analyses were performed using linear mixed effect models ("lmer" function in the R package [Laird et al., 1982]) to relate the number of prey capture attempts -response variable (fitted with a Poisson distribution) - , to the standardised (centered and scaled) frontal activity (FSLE) and QPI - explanatory variables. Individual seal identity was included as a random effect to account for the individual variability.

Results

The comparison between the heading velocity of elephant seals and the accelerometry data (see Figure 1.2) along trajectories shows that when foraging more intensively (with attempt capture rate deviation from the average larger than its standard deviation), the tracking velocity of the elephant seals is close to the geostrophic current measured in the same location (i.e. the heading velocity is small). As displayed in Figure 1.2, 85% of the intensive foraging locations correspond to heading velocities below $2km/h$ and a significant ($p - value < 0.01$) negative correlation of -0.34 suggest a relation between heading velocity and foraging behavior.

Do the low values of heading velocity imply that elephant seals in intensive foraging activity are "locked" to a specific water parcel and horizontally transported within?

By only considering heading velocities, it is not possible to answer this question as the small values that the heading velocities have in these cases could lead to a large trajectory difference when integrated in time.

Therefore, in order to quantitatively associate horizontal passive movement to a predator's trajectory, we compare the animal's trajectory to that of real buoys and of virtual particles purely displaced by advection, obtained by integrating altimetry-derived

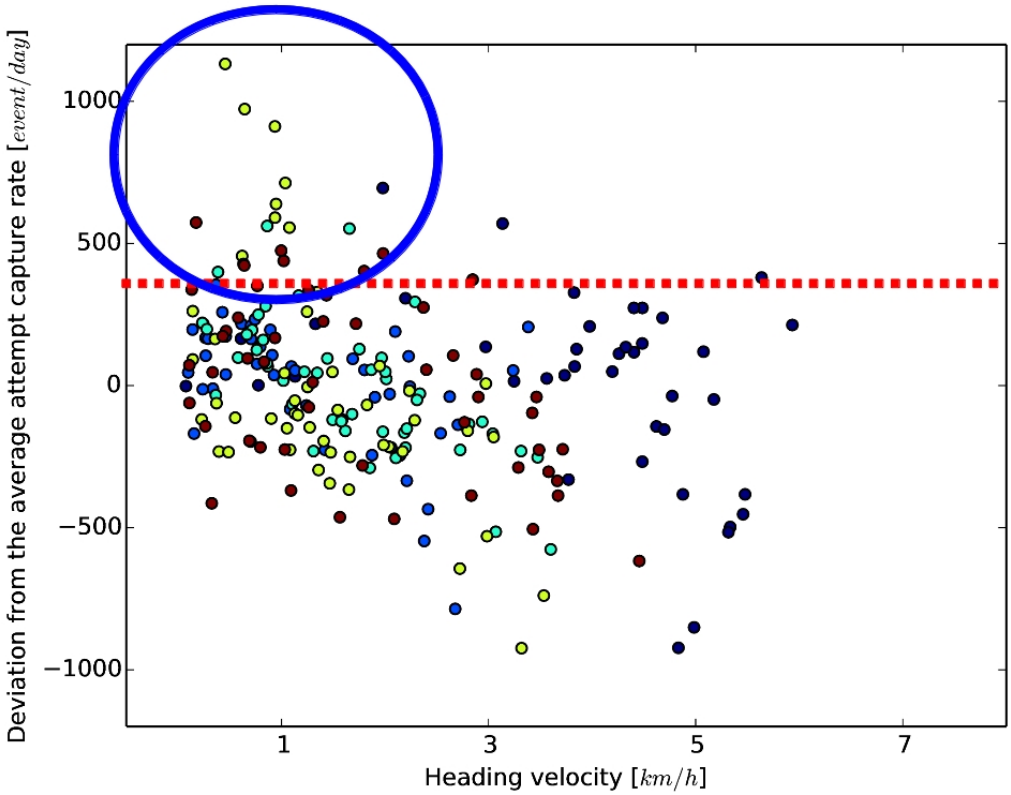

FIGURE 1.2: Deviations from the individually-averaged attempt capture rate for different values of heading velocities. Different colors correspond to different individuals. 85% of attempt capture rate of intensive foraging (deviations larger than 300 event/day, above the red dashed line) correspond to heading velocity below $2\,km/h$ (blue circle).

currents in time. To this aim, we define a new Lagrangian diagnostic: the Quasi-Planktonicity Index (QPI). For each day along an elephant seals' trajectory, we initialize a synthetic passive tracer in a disk centered around the current animal's location and we simulate the motion of the particles contained within the disk forward in time for 4 days. We define as *shadow trajectory* the synthetic trajectory closest to the path the elephant seal actually takes in the following 4 days (see SI for the details about the definition of the distance and its computation). The value of the QPI is the mean distance between the observed and the shadow trajectories. In other words, the QPI measures the offset over a four day period between the animal trajectory and the trajectory of a virtual drifter released next to it at the starting position over a four day period.

Figure 1.3 displays two examples of the computation of the QPI along two different sectors of the same trajectory (in blue). The red patches represent the disk of initialized trajectories and their size takes into account of the uncertainty on the initial condition due to the error induced by altimetry resolution. The shadows trajectories are represented in red: in case a), corresponding to a QPI = 7.8 km, the shadow trajectory closely resembles that of elephant seal, whereas in case b), referring to a QPI = 46.1 km, the

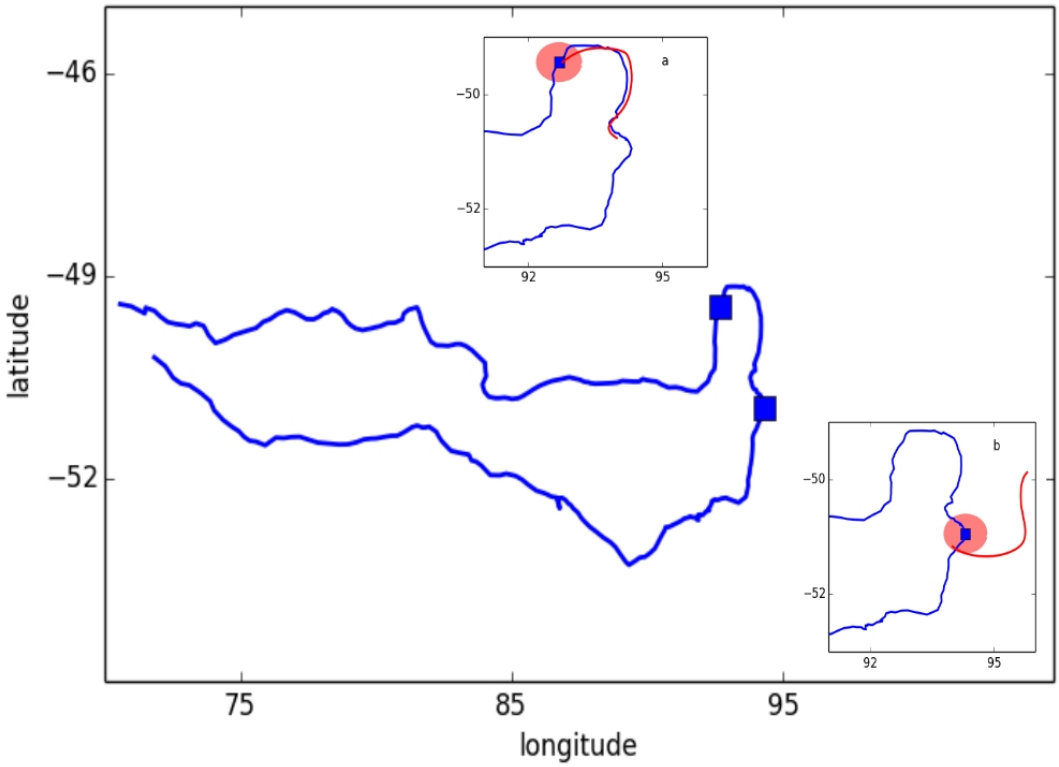

FIGURE 1.3: Two examples of computation of the QPI (Quasi-Planktonicity Index) along the same individual's trajectory (blue line). Disks of simulated trajectories (red disks) are initialised around two locations along the trajectory of the elephant seal (blue squares). The simulated trajectories are the result of the only effect of the currents and the one that minimizes the distance from the elephant seal's one is used to compute the QPI. The QPI corresponds to the average distance between this trajectory (red lines) and the elephant seal's. In case (a) ($QPI = 7.8km$) the two trajectories resemble each other whereas in case (b) ($QPI = 46.1km$) they diverge.

trajectory of the elephant seal appears strongly uncorrelated with that of the simulated tracer.

Cases such as that illustrated in Fig. 1.3 a) account for on average more than 30% of the time along a foraging trajectory. The values of the QPI in these bouts are compatible with the trajectory being generated by passive advection. This is confirmed when we compare them to the values obtained by applying the same diagnostic to SVP (real) drifter trajectories. Figure 1.4 shows the distribution of the QPI computed for elephant seals and for 47 SVP drifters. The considerable overlap between the two distributions suggests that values of the QPI below the 20 km threshold refer to bouts of elephant seals' trajectories where the animals display horizontally passive, quasi-planktonic behavior. This result does not change quantitatively if different altimetry products are used, as detailed in the Supplementary Information, and even when the movement of SVP drifters

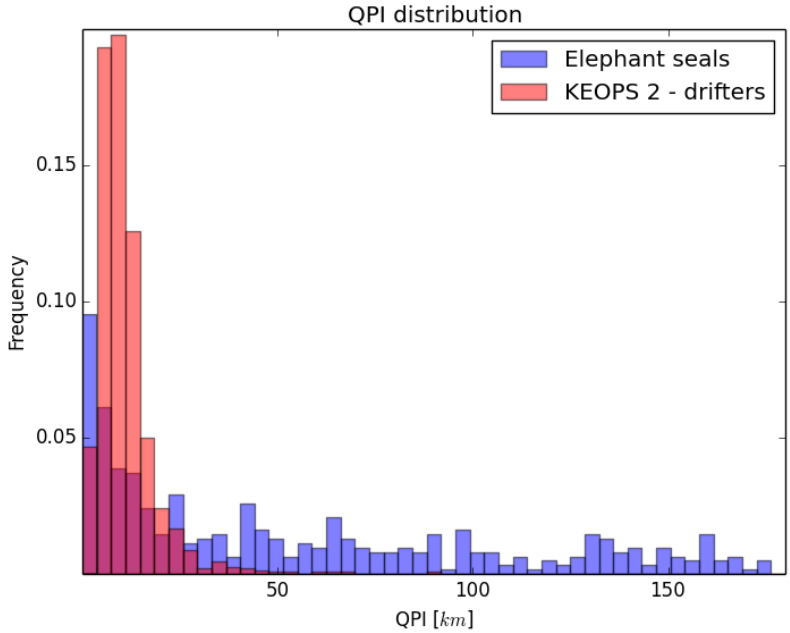

FIGURE 1.4: Normalized distribution of values of QPI for buoyant drifters (red) and elephant seals (blue). The extent of the drifters' distribution suggests that values of QPI below the 20 km threshold refer to bouts of elephant seals' trajectories where they are considerably affected by the horizontal currents.

are corrected for the wind-induced Ekman component, that affect the movement of SVP drifters.

When the trajectories are strongly affected by the horizontal dynamics, physical forcing acts as a major driver in the exploration of the horizontal space. As a consequence, animals are expected to be found more often on attractive transport structures induced by horizontal stirring. Attractive Lagrangian Coherent Structures (LCSs) can be identified by remote sensing as ridges of Finite-Size Lyapunov Exponent (FSLE) [d'Ovidio et al., 2004]. A multivariate analysis through a linear mixed effects model (see Methods) reveals highly significant ($p-values < 0.001$) correlations between FSLE, the QPI and the rate of attempted prey capture (see Table SI1). These results indicate that on transport fronts the tracked elephant seals are passively advected to a higher degree (they have smaller QPI) and forage more intensively.

Figure 1.5 shows a typical example of this correlation. The gray-scale image in the background refers to the FSLE (the lighter the color, the stronger the transport-induced front). The points along the elephant seal's trajectory are colored according to the QPI (Figure 1.5 a) and the attempt capture rate (Figure 1.5b). As the capture rate increases, the QPI decreases (note that the color scales are reversed), meaning that the trajectory is more affected by the currents. This situation occurs in regions of high FSLE, indicating

transport fronts, whereas outside of fronts there are no recognizable patterns in either of the two behavioral diagnostics.

These results are obtained by assuming that the geostrophic currents are representative of the ones experienced by diving elephant seals. This assumption is checked by using vertical profiles of horizontal velocities from ADCP: the correlation between the zonal and meridional components of the velocities at 50 m depth and the integral between 50 m and 500 m is significant in both cases with values over 0.7 (r = 0.7 and r = 0.9 for the zonal and the meridional components of the velocity field - $p-values < 0.01$), indicating that the surface currents provide reliable information on the horizontal advective drift experienced by the animals during their diving.

Discussion

The results of this study challenge the common assumption that fast swimming predators have horizontal displacements that are substantially independent of surface currents. Moreover, the distortion of the trajectory caused by horizontal transport appears to occur prominently where foraging is most intense, stressing the importance of taking water movement into account when analyzing animal displacements at the scale of tens of kms. Determining the correct repartition of efforts between active displacement and passive plankton-like behavior is a central requirement for the application to marine mammals of general frameworks such as Optimal Foraging Theory [Hengeveld, 2007]. Such a theory, based on the hypothesis that animals invest a limited amount of energy between foraging-inefficient displacement and targeted local search for food, suggests that the optimal trajectory is composed by an alternation of long exploratory bouts and of clusters of localized movement known as area-restricted search (ARS). If a searcher's movement is embedded in a flowing medium, however, its trajectory is deformed by the currents. Moreover, such a deformation is not uniform, since it occurs to a different extent, depending on the animal's propulsion relative to the surrounding water. Instead of being characterized by short and localized displacements, hence, the intensive search in the vertical direction produces horizontal trajectories that are closer to the flow-induced movement of the animal's frame of reference, and can therefore being considerably stretched out. The Quasi-Planktonicity Index introduced in our study provides a criterion to measure the degree to which the trajectory of a tracked animal is the outcome of advection by the physical flow. The corresponding partition of elephant seals foraging trips supports the conclusion that would be drawn by optimal foraging theory: animals feed more intensively when their horizontal displacements are more passive.

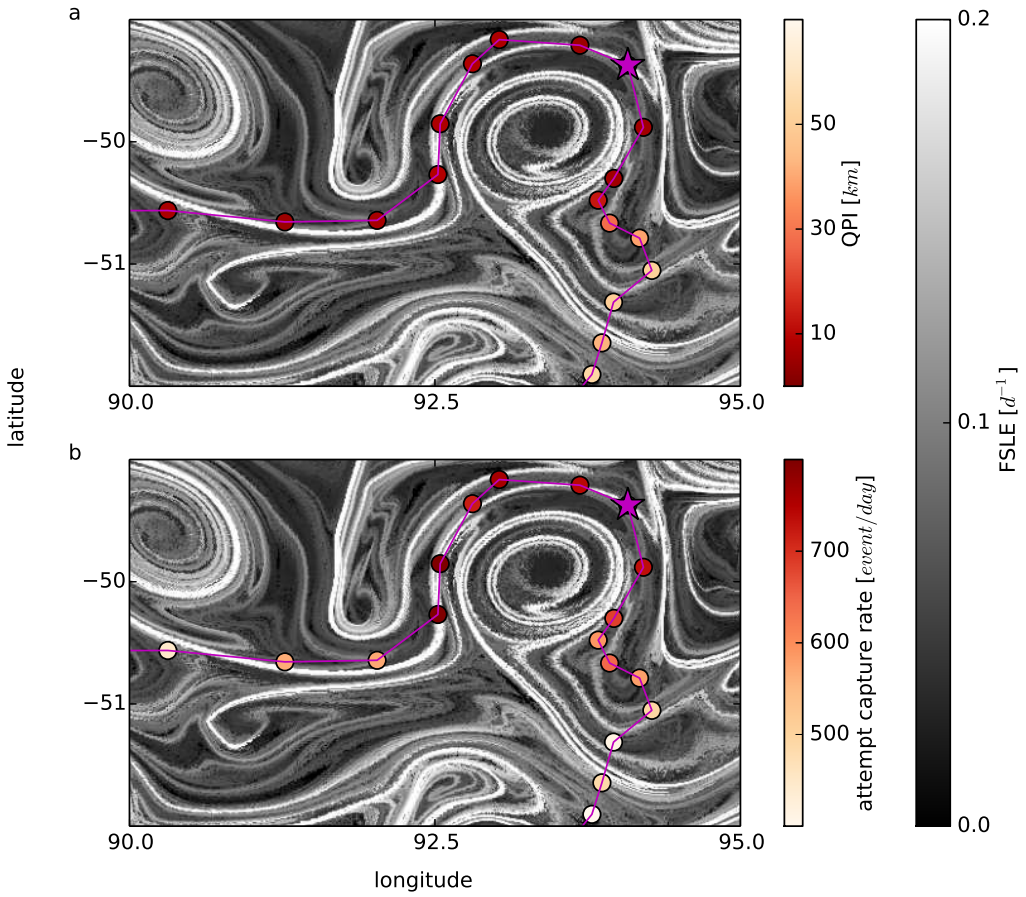

FIGURE 1.5: Fronts, identified as FSLE ridges (gray scale background image in both (a) and (b), computed the day corresponding to the location marked as a purple star(02/12/2011)) correspond on average to lower QPI values (a) and higher attempt capture rates (b). Note that the colorscales are reversed to better highlight that lower QPI correspond to higher attempt capture rates. In most cases locations with low QPI correspond to high capture rate. However, cases excepting this trend (in this example the locations of longitude between $90 - 92.5°$) suggest that elephant seals could present a quasi-planktonic behaviour in response to physical clue usually, but not always, associated to rich foraging grounds.

Our results suggest that ARS algorithms used to detect intensive foraging areas of elephant seals may be misleading in the ocean, if the trajectories are not corrected for the effect of the currents. Indeed, in contrast to the terrestrial environment, ARS in the open ocean produce displacements that are localised in the reference frame of the water parcel which contains the animal, hence trajectories that are shadowed by passive drifters. Especially in energetic regions, like frontal systems, quasi-planktonic horizontal displacements may be comparable in length to the bouts resulting from active propulsion. Correcting the trajectories for the effect of the currents is expected to improve the sensitivity in detecting and classifying behaviours, and in particular those

related to foraging activity. In this regard, we note that recent work by Cotté et al. [Cotté et al., 2015] highlights a strong association between transport fronts and the Kerguelen elephant seals' displacements, but surprisingly not with intensive foraging locations. A possible reason may be that the state space model approach used in that work was applied to the absolute displacement of the animals and not the one corrected for the effect of currents.

The partitioning of elephant seals foraging trips into quasi-planktonic bouts and active horizontal displacements supports optimal foraging theory: the possibility of exploring new foraging grounds is traded off for intensive foraging, which entails focusing on the local resources. This horizontal pattern is consistent with elephant seal diving behavior. When foraging intensively, elephant seals generally increase their diving angles and both the horizontal and vertical sinuosity of the local displacements [Dragon et al., 2012b]. As a consequence, when diving they reduce their active horizontal movements (Lebras,Y., personal communication), so that their change results in a horizontal displacement movement that is largely determined by the currents. Note also that because of the increased diving effort in foraging regions, the "quasi-planktonic" horizontal bouts do not necessarily corresponds to periods of reduced energy consumption. Energy is invested more in short- range activity (deep diving and hunting) rather than in large-scale horizontal displacement (commuting).

We choose to use the term "quasi-planktonic" to refer to cases where a nektonic animal's behavior, in our case intensive foraging, results in an increased vertical movement and a reduced horizontal displacements. This behavioral change makes the horizontal trajectory largely affected by oceanic currents.

In this study, we assume that the velocity field of geostrophic currents inferred from altimetry accounts for the horizontal displacement of the water surrounding the elephant seals. If this is probably a good assumption close to the surface, it may only explain part of the animals' behaviour, since elephant seals however move considerably in the vertical direction as well. They dive to an average depth of 300-500 m (and up to 2000 m) [Guinet et al., 2014] and spend more than 60% of their lifetime below 100 m depths [McIntyre et al., 2010]. If geostrophic velocities are considered to be representative of the mixed layer [Dong et al., 2008], their ability to quantify horizontal displacements at depth is not the same in different regions of the ocean. In the Southern Ocean, where the mixed layer is considerably deep ($\sim 100\,m$ [Sallée et al., 2010]), the vertical distribution of horizontal velocities suggests that geostrophic velocity can reliably represent that of the whole water column [Wunsch, 1997, Vivier et al., 2014]. We checked that this was the case in the region of our study by analyzing Acoustic Doppler Current Profiler (ADCP) velocities from the KEOPS 2 campaign and the results confirmed that the zonal

and meridional components of the horizontal velocities at 50 m depth are significantly related to the integral between 50 m and 500 m.

The "quasi-planktonic" nature of intensive foraging bouts implies that transport structures can entrain animal trajectories. This observation agrees with the increasing number of studies on tracked marine predators, showing that they tend to co-occur with thermal and transport fronts [Bost et al., 2009]. The common explanation for the localization of top predators over fronts is the bottom-up structuring effect of these transport features due to the local enrichment in nutrients entailed by vertical sub-mesoscale circulation [Lévy et al., 2012a]. The consequent boost in the biomass of lower trophic levels is believed to attract free-swimming predators over fronts. Our results indicate that a second, top-down mechanism may also exist, by which frontal structures directly entrain the trajectories of actively foraging predators. Passive advection towards attractive frontal regions may cause an increased localization of predators in those areas, in spite of the relatively small portion of the ocean surface they occupy. It is still an open question whether this mechanism is sufficient to ensure an efficient identification of putative nutrient-rich spots, or if the observed distributions also require the guidance of a cue. A question however remains, on the existence of a cue able to initially guide predators towards the putative nutrient-rich spots, that represent a minority of the ocean extension. Some species of seabirds have been observed to respond to chemical cues of compound dimethyl sulfide (DMS), that accumulates in the air above productive ocean areas [Nevitt et al., 1995, Nevitt and Bonadonna, 2005], but relatively little is known about potential physical or chemical cues followed by swimming predators. An alternative hypothesis is that seals moving within a global foraging area modify their behavior according to prey density, which is influenced by (sub-)mesoscale oceanographic structures. With our data it is not possible to address directly this question. However, we observed cases in which elephant seals exhibit quasi-planktonic behaviors without foraging intensively, suggesting that they may be not reacting to the density prey as a cue.

Conclusions

The term *planktonic* has been traditionally reserved to the lower levels of the trophic chain. However, we have shown that top predators, in spite of being capable of large scale active swimming, can also display a (horizontal) planktonic behavior, that we have called quasi-planktonic. This behavior is associated with intensive foraging, where elephant seals displace mostly in the vertical direction, so that the horizontal displacements follow their moving frame of reference. The entrainment by currents of nekton, as well as of

plankton, suggests a mechanism which focuses trophic interactions on physical features which have an attractive dynamics transverse to them, - like eddies and fronts – in alternative (or in addition) to bottom up effects expected by nutrients injections and concentration [Godø et al., 2012, Boero, 2014, Lévy et al., 2012a, McGillicuddy et al., 2007].

Understanding how the behavior of individual predators is modulated by structures that vary on the spatiotemporal scale of tens of kilometers and of days - the (sub) mesoscale - is an essential step in linking marine predators ethology to conservation ecology, and lies at the heart of predicting large-scale patterns of displacement and the response of marine predators to climate change[Di Lorenzo and Ohman, 2013, Hoegh-Guldberg and Bruno, 2010, Fraser and Hofmann, 2003, Lea et al., 2006].

Acknowledgments

The altimeter products were produced by Ssalto/Duacs and distributed by Aviso with support from Cnes. The authors would also like to acknowledge AVISO/CLS and the Global Drifter Program/NOAA/AOML, Miami, Florida both the Drifter Operations Center and Data Assembly Centers and Météofrance for arranging drifter deployments and data assembly, quality control and distribution of the data. This study is part the national research program no. 109, H. Weimerskirch and the observatory Mammifères Explorateurs du Milieu Océanique (MEMO SOERE CTD 02) supported by the French Polar Institute (Institut Paul Emile Victor,IPEV), the ANR: MyctO-3D-MAP,SVSE 7 2011 and the CNES-TOSCA program (Éléphants de mer océanographes and ALTIMECO). CG and ADP thank respectively the Total Foundation and the Fondation Bettencourt-Schueller (through the program Frontières du Vivant) for their financial support. SDM acknowledges support of the CNRS-PSL Eco-Evo-Devo program "Pépinière Interdisciplinaire". The authors wish to thank the Kerguelen fieldworkers (in particular N.El Shaby, J-B. Pons and G.Bessigneul), Y. Lebras, C.Cotté, J. Garcia-Vaquet, B. Picard, T. Trull, A.C. Dragon and R. Bell. The authors wish also to thank M.A. Lea for helping reviewing the paper.

Authors contribution

ADP: designed the experiment, performed the research, analysed the data and wrote the paper. SDM: designed the experiment, performed the research,wrote the paper. EK: analysed the data. CG: designed the experiment, performed the research, wrote the

paper. FD: designed the experiment,performed the research, analysed the data, wrote the paper

Supplementary information

Details about the Quasi-Planktonicity Index algorithm

The QPI compares a section of a seal's trajectory with the movement of a numerical passive tracer that is determined only by the horizontal currents. In the ideal case of a perfectly determined velocity field, if a trajectory is purely passive, the numerical passive tracer should perfectly match the real trajectories. However, in reality there are two sources of error that have to be dealt with:

- **an uncertainty on the initial condition of the velocity field:** the spatial resolution of altimetry is considered to be comparable to its grid spacing, i.e., $1/3°$, hence when we initialize a numerical drifter we may actually initialize it with a mismatch of $1/3°$ in respect to the velocity field,
- **an underestimation of the horizontal velocities:** altimetry observations are taken along satellite tracks and are then interpolated together for providing a gridded product. The interpolation procedure smooths the signal and may underestimate real velocities, resulting in our case into a *delay* of the simulated trajectories which lag behind real ones and in turn, into a spurious mismatch during the comparison.
- **ageostrophic components:** by definition, ageostrophic components of the velocity fields do not appear as a signal on the Sea Surface Height and therefore cannot be observed by satellite altimetry.

The algorithm to compute the QPI aims at mitigating the effect of these sources of error. To compute QPI, we perform the following steps:

1. sample the elephant seal's trajectory $\mathbf{X(t)} = (X(t), Y(t))$ with a 6-hours frequency.
2. for each day t_0 we initialize around the location $\mathbf{X}(t_0)$ a set of j initial conditions $\mathbf{x_j}(t_0) = (x_j(t_0), y_j(t_0))$. They represent the initial conditions of a set of synthetic trajectories $D_r(\mathbf{X}(t_0)) = \{\mathbf{x}(t) : |\mathbf{x}(t_0) - \mathbf{X}(t_0)| < r\}$ where r indicates the radius of the disk.
3. advect the initial conditions for a time $t_{max} = N + t_{buffer}$.

4. for each elephant seal's locations between t_0 and $t_0 + N$: $\mathbf{X}(t_0), \mathbf{X}(t_1)...\mathbf{X}(t_N)$ compute the *pseudo-distance* (from now on distance):

$$\Delta(\mathbf{X}(t_0), \mathbf{x_j}; N) = \min_{i \in [0, t_{max}]} (dist(\mathbf{X}(t_0), \mathbf{x}(t_i)) \tag{1.1}$$

   where *dist* refers to en Eulerian distance computed on the non-regular latitude-longitude grid.

5. compute the QPI as the mean distance between the closest simulated trajectory (shadow trajectory) and the real one

$$QPI(\mathbf{X}(t_0); N, r) = \frac{1}{N} \min_{j \in D} \left(\sum_{i=t_0}^{t_0+N} \Delta(\mathbf{X}(t_i), \mathbf{x_j}) \right). \tag{1.2}$$

This algorithm limits the effect of the uncertainty on the initial location of the altimetric velocity in respect to the location of the real trajectory (that for the case of elephant seals and SVP drifters we consider with no error, given the high resolution of GPS tracks), by advecting an ensemble of numerical trajectories whose radius r is chosen in relation to the resolution of the altimetry data: in this study we used $r = 0.3°$.

To compensate for a lag in the simulated trajectory we introduce the pseudo-distance defined in step 4 instead of an Eulerian step-by-step distance. Indeed, even if a simulated and a measured trajectory are very close, if the velocity field is underestimated, the Eulerian distance would increase and we would not identify a low value of the diagnostic. Therefore, we advect the simulated trajectory for a t_{max} that is not just equal to the number of steps we use for the comparison (N), but we introduce a buffer (in this study $buffer = 4\ days$), so that we make sure that we are compensating for all the effects of the delay. We then ensure that for each position of the real trajectory, the distance is computed with the closest point of the simulated trajectory, and not the point that corresponds to the same instant.

Finally, we addressed the presence of possible ageostrophic components by validating the QPI (i.e., computing it for SVP drifters) also adding to satellite-derived currents the Ekman components derived by wind re-analysis. Figure SI 1.9 displays the distributions of the QPI computed for SVP drifters using different altimetry products. Even if by using a regional Ekman-corrected altimetry the simulated trajectories have Lagrangian properties that are more similar to the SVP ones, as detailed in Ref [d'Ovidio et al., 2015], the changes in the QPI distribution does not change qualitatively the result.

When computing this algorithm, there are few parameters that can be tuned. If r is constrained by the resolution of the velocity field, the choice of N is relatively flexible

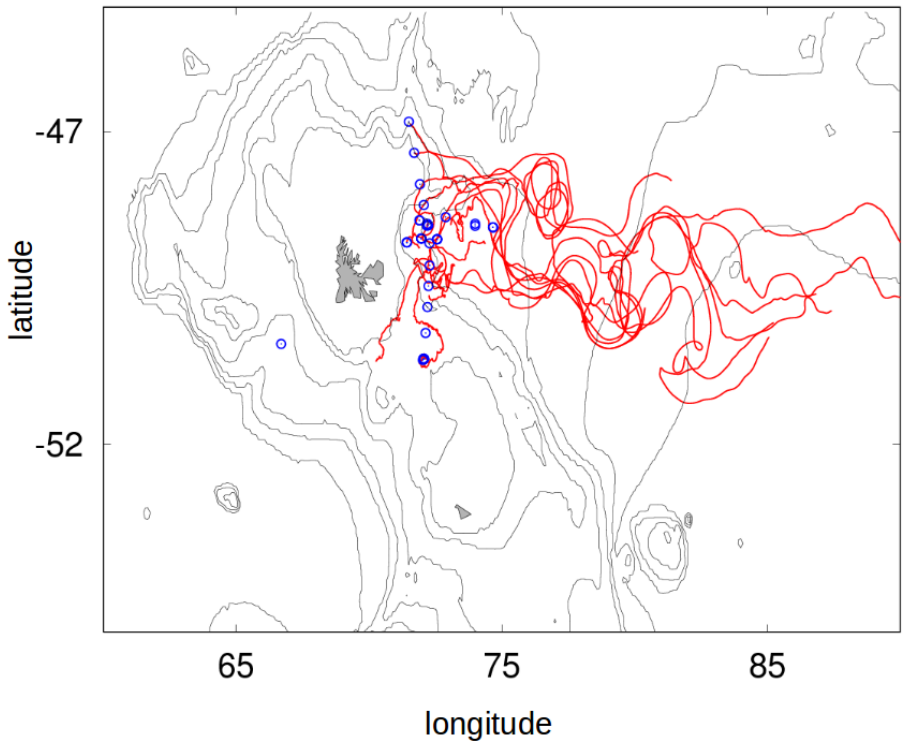

FIGURE 1.6: Distribution of in-situ physics measurements used in this study. The blue dots represent the location of the ADCP casts and the red lines the trajectories of some of the drifting buoys.

Variables	Estimate	Error	z-value	p-value
QPI	-0.258	0.004	-72.50	$< 2 \cdot 10^{-16}$
FSLE	0.015	0.003	5.46	$4.71 \cdot 10^{-8}$

TABLE 1.1: **Linear Mixed Effect Model relating** *attempt capture* $\sim QPI + FSLE + (1|ID)$. The variability between individuals is taken into account by considering the ID as a random effect. Both explanatory variables are significantly related to the attempt capture rate, yet the QPI appear to have a stronger effect.

and it is related to the scale of the patterns we want to identify. As in this study we are interested in labelling bouts of trajectories with a resolution high enough to distinguish behavioral switches between extensive and intensive foraging (typically of of few days) we used a value of $N = 4\ days = 16\ steps$. The QPI can be computed with different frequencies: in this study we sampled the trajectories every 6 hours, but when comparing the QPI with the attempt capture rate, we used a daily resolution to integrate for the effects of the day-night cycle of the attempt capture rate.

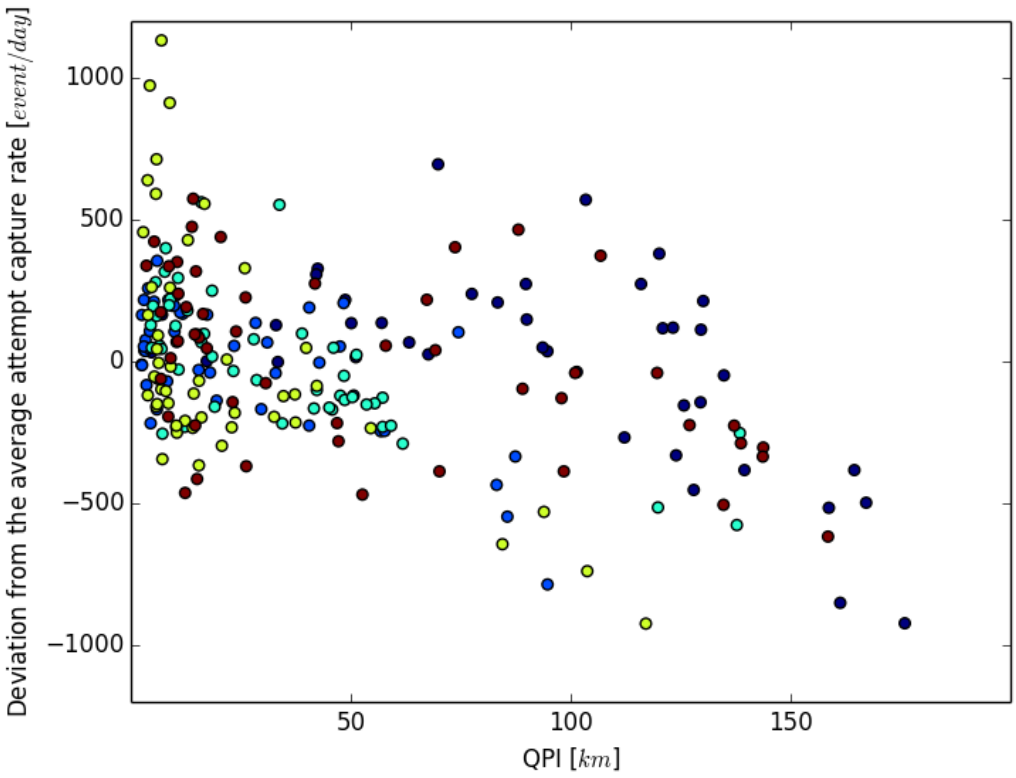

FIGURE 1.7: The QPI and deviation from the individually-averaged capture rates. Different colors refer to different individuals.

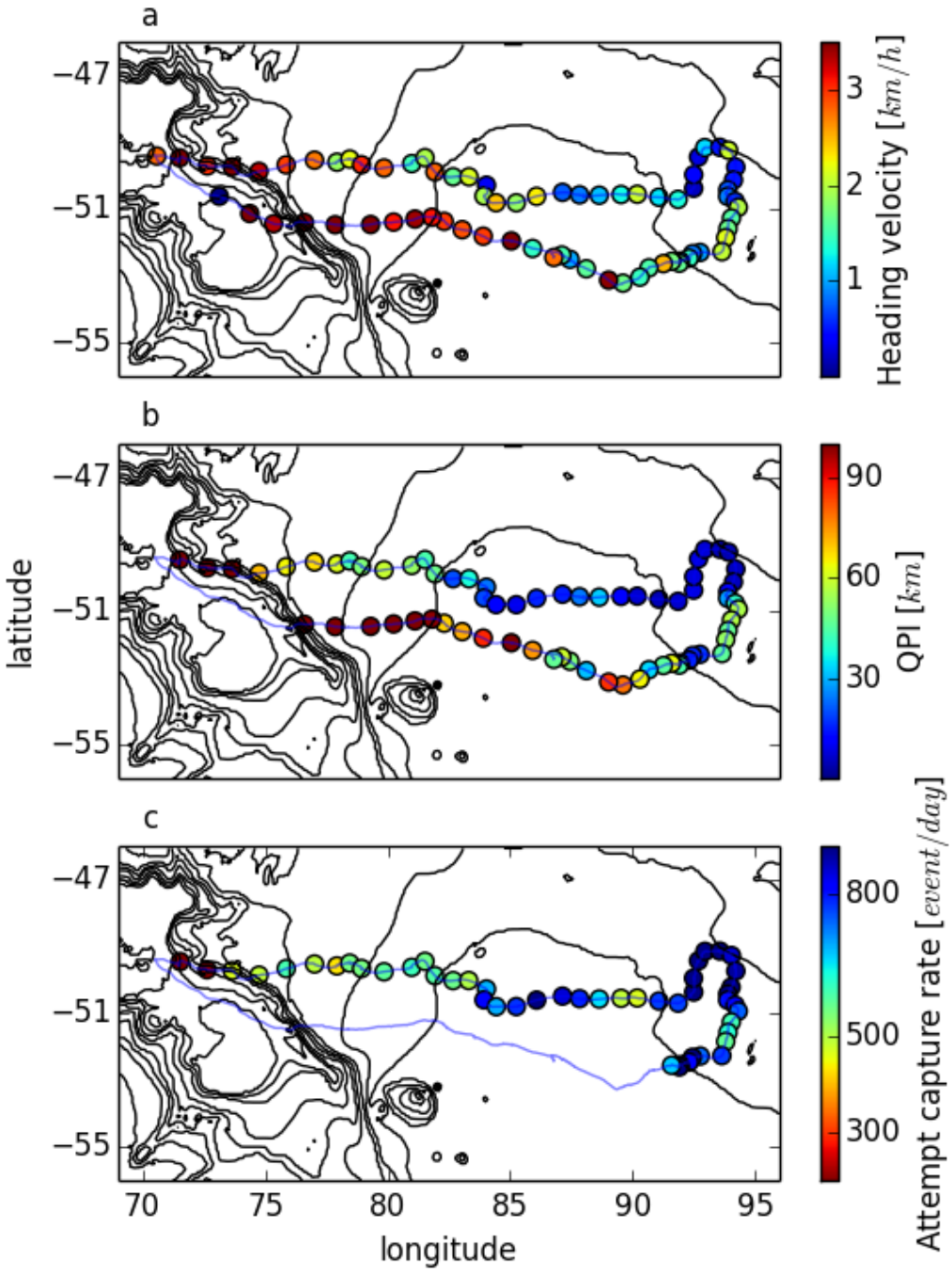

FIGURE 1.8: Example of computation of heading velocity (a), QPI (b) and attempt capture rate measurements (c) along an elephant seal's trajectory. Note that the colorscale in (c) is reversed. The patterns along this and the other trajectories of the attempt capture rate, heading velocity and the QPI include, in agreement with previous observations [Horsburgh et al., 2008] of their foraging habit, an inbound and an outbound phase of the trajectory, with a lower attempt capture rate and high QPI, with an intensive foraging and low QPI phase in between.

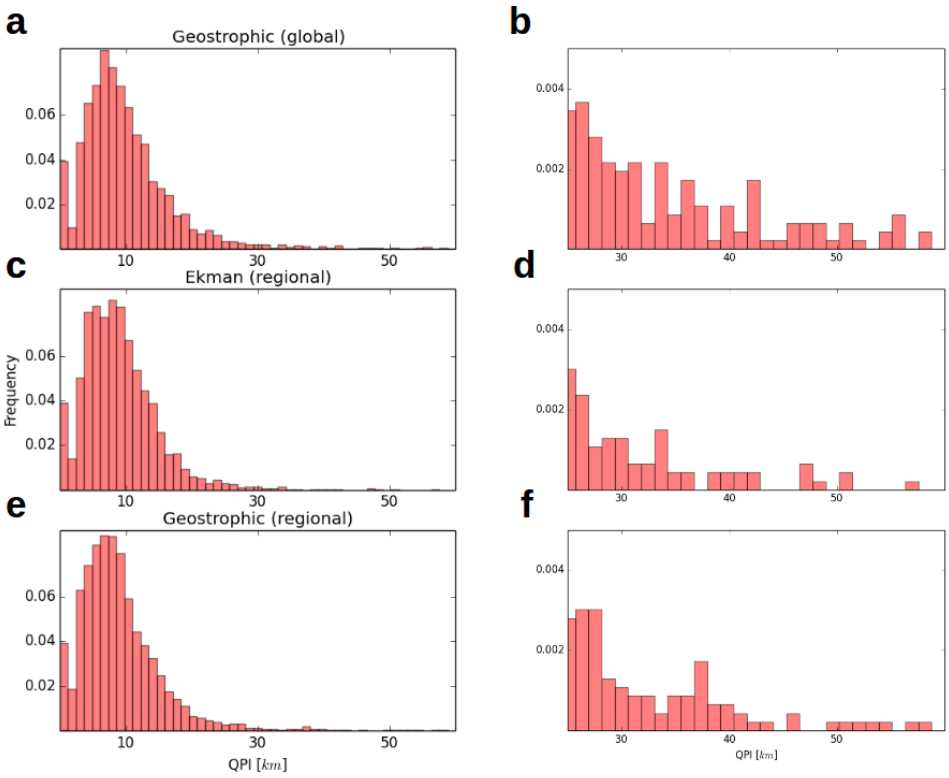

FIGURE 1.9: Distributions of the QPI for SVP (real) drifters computed using different altimetry products: a) geostrophic global product, c) Ekman-corrected regional product and e) geostrophic regional product. Using different products does not alter significantly the shape and the extent of the distribution, yet differences in the distributions can be observed in the tails, as displayed in b), d) and f).

Chapter 2

Influence of oceanographic structures on foraging strategies: Macaroni penguins at Crozet Islands

This chapter has been published as *Influence of oceanographic structures on foraging strategies: Macaroni penguins at Crozet Islands* by C. Bon, A. Della Penna, F. d'Ovidio, J.Y.P. Arnould, T. Poupart and C-A. Bost in *Movement ecology*, 2015.

Abstract

Background

In the open ocean, eddies and associated structures (fronts, filaments) have strong influences on the foraging activities of top-predators through the enhancement and the distribution of marine productivity, zooplankton and fish communities. Investigating how central place foragers, such as penguins, find and use these physical structures is crucial to better understanding their at-sea distribution. In the present study, we compared the travel heading and speed of the world's most abundant penguin, the Macaroni penguin (*Eudyptes chrysolophus*), with the distribution of surface physical structures (large-scale fronts, eddies and filaments).

Results

The study was performed during December 2012 in the Crozet Archipelago ($46.42°S; 51.86°E$), South Indian Ocean. Six males at incubation stage were equipped with GPS loggers to get their trajectories. We used Eulerian and Lagrangian methods to locate large-scale fronts, mesoscale eddies (10–100 km) and part of the sub-mesoscale structures ($<$ 10 km, filaments) at the surface of the ocean. By comparing the positions of birds and these structures, we show that Macaroni penguins: i) target the sub Antarctic Front; ii) increase their foraging activity within a highly dynamic area, composed of eddy fields and filamentary structures; and iii) travel in the same direction as the predominant currents.

Conclusions

We show that penguins adjust their travel speed and movement during their whole trips in relation with the oceanographic structures visited. At a large scale, we hypothesize that Macaroni penguins target the sub Antarctic Front to find profitable patches of their main prey. At finer scale, Macaroni penguin may adopt a horizontal drifting behavior in strong currents, which could be a way to minimize costs of displacement.

Background

In the open ocean, the distribution and abundance of marine organisms is related to physical processes at different spatial and temporal scales [Hunt et al., 1999]. Many studies have provided evidence of strong relationships between the foraging movements of top-predators and the distribution of mesoscale (10–100 km), predictable oceanographic structures such as large fronts and eddies (e.g.[Tew Kai and Marsac, 2010, Bost et al., 1997, Tynan, 1997]). Recently, the relationships between marine top predators and sub-mesoscale ($<$ 10 km) features (e.g. filamentary structures) have also received growing interest and have triggered the development of new Eulerian (observations at a given time, in the "non-moving" frame of reference of the bathymetry) and Lagrangian diagnostics (from the frame of reference of flowing water particle). Lagrangian diagnostics enable the analysis of the temporal and spatial variability of oceanographic features to identify physical structures like eddies, fronts, and part of the filament variability. Such structures have been shown to affect the distribution and growth of phytoplankton because their lateral and vertical transport properties influence the supply and retention of nutrients in the euphotic layer from deeper waters [Lévy et al., 2012a, d'Ovidio et al., 2010]. Correspondingly, such aggregations of primary production can influence food web

dynamics due to their profitability for all species from grazers to top predators [Hunt et al., 1999, Bradshaw et al., 2004, Cotté et al., 2011]. Indeed, it has been shown that several top predators use eddies (e.g. [Bailleul et al., 2010b, Cotté et al., 2007]), currents and associated filaments to forage (e.g.[Cotté et al., 2011, Lowther et al., 2014]). Relatively, few studies have focused on penguins [Lowther et al., 2014, Cotté et al., 2007] despite their key role in marine food webs [Brooke, 2004]. These non-flying, diving predators are highly constrained in their foraging range because of their low travelling speed and high cost of transport. It might be expected, therefore, that oceanic penguins should target sub-meso and mesocale structures during their at-sea activities to maximise their foraging efficiency [Cotté et al., 2007]. Consequently, we investigated the at-sea foraging movements of the Macaroni penguin (*Eudyptes chrysolophus*) in a highly dynamic marine environment: the waters around the Crozet Archipelago in the South Indian Ocean. The Macaroni penguin is a pelagic predator, diving within the mixed layer to mean depths of 50 m (up to 163 m, [Green et al., 1998a]) to capture crustaceans and myctophid fish [Pichegru et al., 2011, Cherel et al., 2008, V.Ridoux, 1995]. The species exhibits large flexibility in its foraging range, exploiting frontal structures or the shelf area according to the breeding requirements [Barlow and Croxall, 2002, Thiebot et al., 2011]. While the world population is currently decreasing [Reid and Croxall, 2001, Crossin et al., 2013], it is still the most abundant penguin species and the largest marine biomass consumer among seabirds [Brooke, 2004]. The Crozet Archipelago is a breeding stronghold for the species [Crossin et al., 2013]. Our aim was to identify how Macaroni penguins use oceanic structures to forage at different spatial scales, from large-scale (front) to meso- (eddies) and sub-mesoscale filamental structures [Kai et al., 2009b]. We attempted to answer the following questions: i) do Macaroni penguins adjust their spatial movements with the regional circulation of currents?; and ii) how do they adjust their foraging behavior within meso- and sub-mesoscale structures? We address these questions by investigating the relationships between the spatial behavior of penguins and: i) the presence of persistent, large-scale frontal structures; ii) the occurrence of eddies and filamentary structures; and iii) the adjustment of their travel speed with the encountered currents. We hypothesize that penguins would target these structures, reducing travel speed within eddies and filamentary structures to foraging intensively, as such behaviors should be advantageous with respect to travel costs.

Results

After their foraging trips (18 ± 2 days), all the instrumented penguins were recaptured upon returning to their colony having increased their body mass (subsequently, all pairs successfully fledged their chicks). Data from one GPS were lost due to technical failure

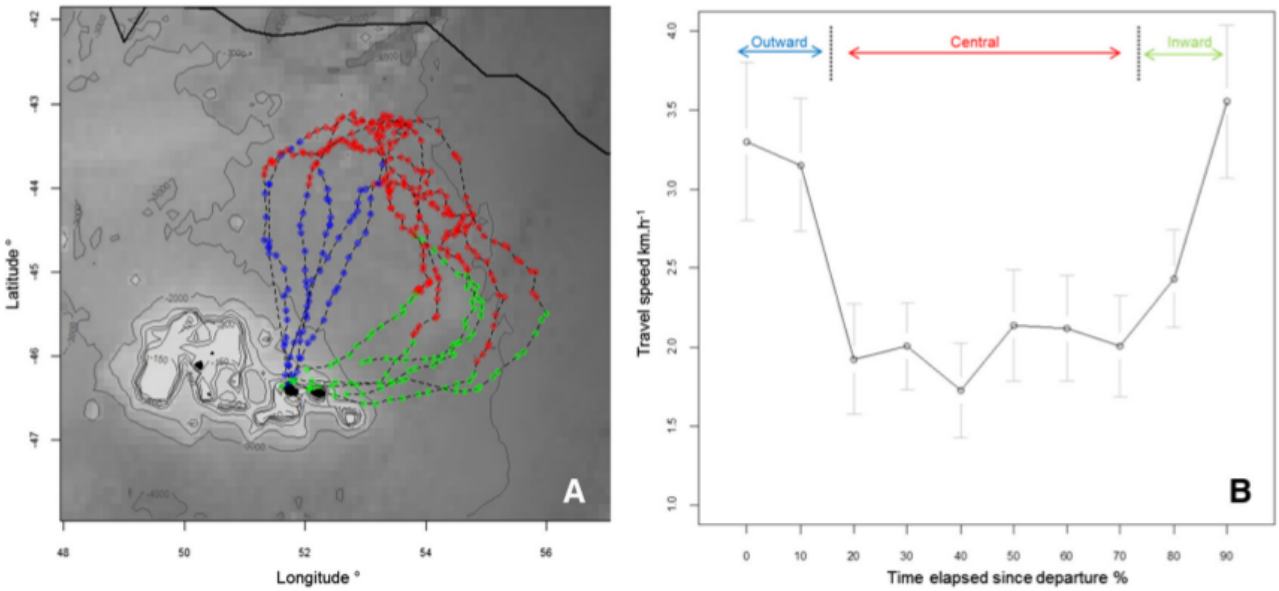

FIGURE 2.1: Trips and travel speed of six incubating macaroni penguins presented on a bathymetry map around the Crozet islands. a) The three phases defined by the variation in heading velocity are represented in distinct colours: outward: blue, central: red, inward: green. Black line: Sub-Antarctic Front. b) The travel speed was averaged for each 10% of time elapsed since the departure of travel. Arrows indicate separation of the trip in three phases.

and thus six tracks were analyzed in the present study. Individuals performed long clockwise looping trips, heading north towards the SAF, up to 388 km in a region encompassing positive and negative eddies, before returning to the colony (Fig. 2.1). The central phase of their trips were longer (435.7 ± 69.9 km; 9.66 ± 1.35 d) than the outward (280.8 ± 38.9 km; 3.80 ± 0.47 d) and inward phases (237.6 ± 72.8 km; 9.66 ± 1.35 d, Kruskal- Wallis test on duration: $\chi^2 = 11.94$, df $= 2$, $p < 0.01$, Table 2.1). The distance travelled every 6 h was on average 15.2 ± 12.7 km. The travel speed was significantly lower within the central phase (outward: $3.57 \pm 1.25 km/h$, central: $1.93 \pm 1.05 km/h$, inward: $3.30/pm1.30 km/h$, Kruskal-Wallis test: $\chi^2 = 103.97$, df $= 2$, $p < 0.0001$, Table 2.1, Fig. 2.1 b). There was a gradient in SST encountered by penguins during their trip from $\sim 4°$ at the colony to $8°$ at the lowest latitudes visited ($\sim 43° S$, Fig. 2.2 a). The SST was highly positively correlated with the current speed. This suggests that the warmer waters encountered by penguins located at the lowest latitudes were also in the strongest currents visited (Spearman correlation test: 7068809, $R^2 = 0.40$, $p < 0.001$).

Penguin and mesoscale eddies

During the central phase of their trips, Macaroni penguins foraged at the edge of two large eddies, situated in the vicinity of the SAF (Fig. 2.2 b). These two eddies were located to the south of a large eddy field which was not used by the birds. Overall, 63

% of the locations associated with an eddy were within the central phase whereas 11 and 26 % were within the outward and inward phases, respectively (Table 2.2). This indicates that the main eddy activity was observed within the central phase where the penguins had reduced swimming speed. Indeed, the degree of association with eddies was 37 % in the central phase, 17 % in the outward phase and 38 % in the inward phase (Table 2.2). Examination of time spent within eddies (successive locations in an eddy) indicates penguins spent more time within eddies in the central phase (43 ± 25 h, 11 cases) than in the transit phases (25 ± 10 h, 10 cases, Mann-Withney: U =81.5, P = 0.066). The retention parameter was small for eddies in the central phase (9.7 ± 15 d, n = 60 locations) since 80 % of water parcels had been recirculating within the eddy for less than 8 d. In transit phases, the re- tention parameter of eddies was significantly higher (16 ± 15 d, n = 32 locations, Mann-Withney test: U =658, P = 0.013). Finally, the three mixed models built for each phase indicated that penguins significantly slowed down when they were inside eddies in the inward phase, contrary to that observed in the two other phases (Table 2.3 models M1, M2,M3, Fig. 3a).

Penguin movements and filaments

Filaments identified by the FSLE method were present over the whole area prospected by the penguins (Fig. 2.2 c). At the trip scale, we observed high inter-individual variation in the level of association with filaments ($n_{locs\,within\,filaments}/n_{locstotal}$) (from 5.6 to 35.9 %). Across all trips, 66.7 % of the locations associated with filaments were located within the central phase of the foraging trip where penguins reduced travel speed (20.8 and 12.5 % in outward and inward phases, respectively, Table 2.2. The degree of association was significantly higher in the central phase since 27.6 % of locations were within filaments. In the two others phases, the number of locations within filaments were significantly lower (Kruskal-Wallis test: χ^2= 6.976, df = 2, $p < 0.05$, Table 2.2. FSLE values of the filaments were significantly higher at the central phase ($0.20 \pm 0.05 d^{-1}$) than at the outward ($0.15 \pm 0.04 d^{-1}$) and inward ($0.12 \pm 0.02 d^{-1}$) phases (Kruskal-Wallis test: χ^2 = 18.603, df = 2, $p < 0.001$). Once individuals were inside the filaments, they slowed down more when FSLE values were higher (Table 2.3 model M4, Fig. 2.3 b).

Penguin movements and currents

At the whole-trip scale, at-sea movements of individuals seem to be strongly modified by the currents encountered. Firstly, travel speed was negatively correlated with the current speed indicating that penguins decelerated when they encountered stronger currents (Table 2.3 model M5). Indeed, during the outward phase, the current speed was generally

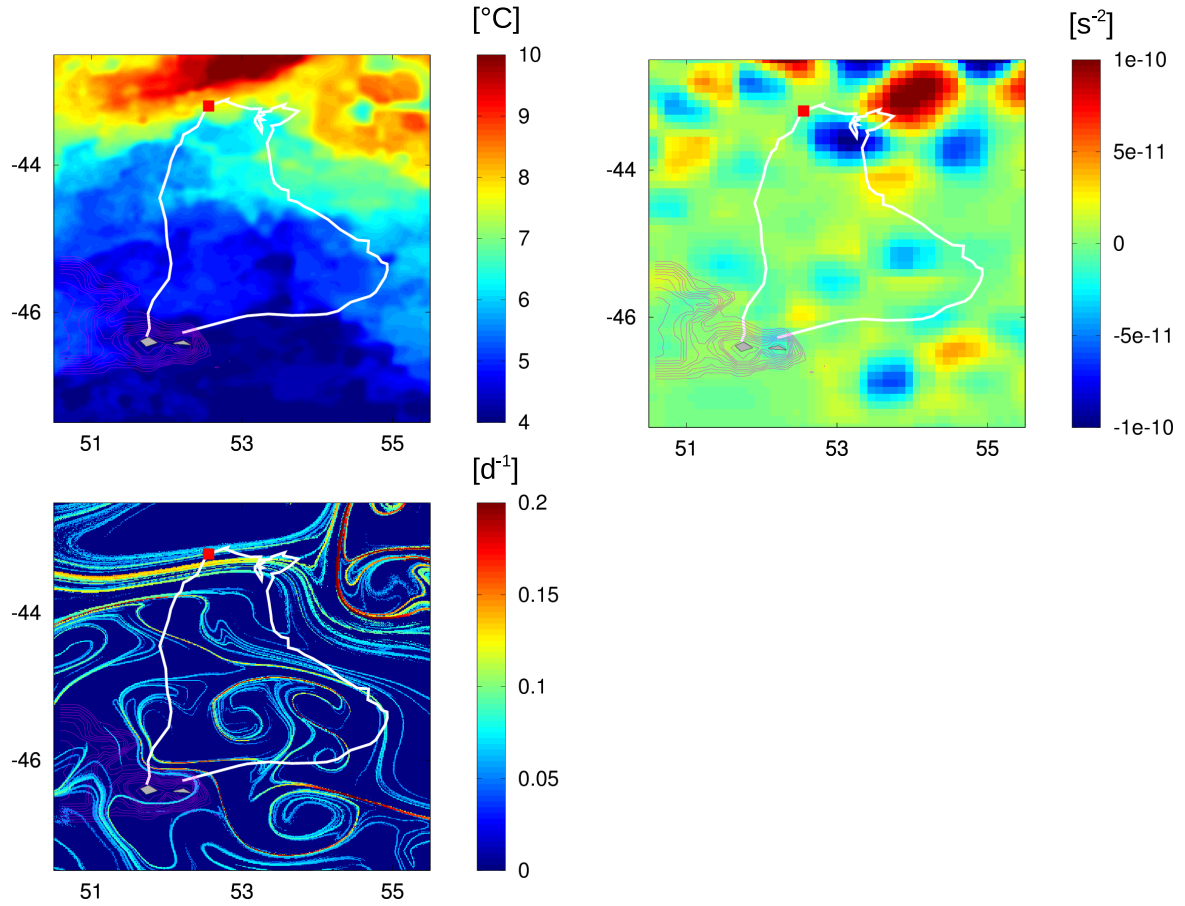

FIGURE 2.2: The positions of one bird overlaid on oceanographic features. a) Map of Sea Surface Temperature ($°C$). b) Okubo-Weiss parameter: eddy cores are characterised by negative values. c) Finite-size Lyapunov exponents ($\delta_0 = 0.01°, \delta_f = 0.6°$):larger values indicate stronger transport barriers.

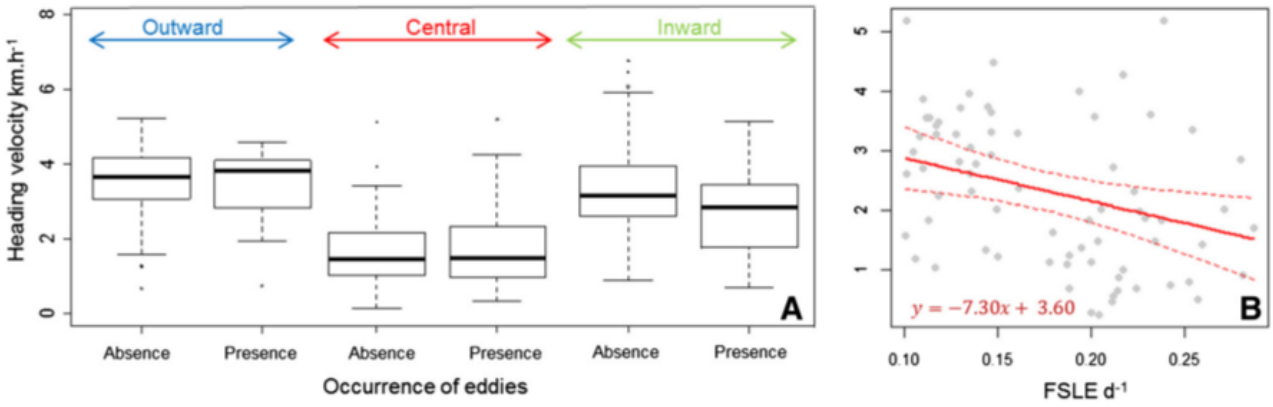

FIGURE 2.3: Heading velocities related to eddies and filament characteristics. a) Distribution of heading velocity inside or outside eddies within each trip phase. Arrows indicate trip phases. b) Heading velocity in relation to the FSLE values within filaments ($FSLE > 0.1d^{-1}$). Red line is the regression line resulting from the M4 model. Dashed lines indicate 95% confidence intervals of predictions.

TABLE 2.1: Main characteristics of foraging trips of six Macaroni penguins. (n= number of gps locations).

Trip phase	Duration (j)	Travel speed (km/h)	Heading velocity (km/h)	Current speed (km/h)	Animal direction (°)	Current direction (°)
Outward n=86	3.8 ± 0.5	3.6 ± 1.3	3.5 ± 1.3	0.2 ± 0.2	11.4 ± 22.4	61.4 ± 97.8
Central n=233	9.7 ± 1.4	1.9 ± 1.1	1.7 ± 0.9	0.9 ±0.4	141.4 ± 68.8	118.1 ± 37.9
Inward n=96	3.8 ± 1.1	3.3 ± 1.3	3.2 ± 1.3	0.3 ± 0.1	233.2 ± 45.0	246.3 ± 101.0

TABLE 2.2: Distribution of eddies and filaments within trips of six macaroni penguins.

		Eddies		Filaments	
Trip phase	n(locs averaged on individuals)	Distribution of eddy locations % - n_{locs}	Degree of association %-n_{locs}	Distribution of filaments % - n_{locs}	Degree of association % - n_{locs}
Outward	14 ± 4	11% - 15	17% -3 ± 1	20.8 % - 22	21.7 % -3 ± 1.0
Central	38 ± 5	63% - 87	37 % -15 ± 6	66.7 % - 61	27.6 % - 9.6 ± 6.0
Inward	16 ± 4	26% - 36	38% - 6 ± 3	12.5% - 10	12.5% - 2.0 ± 1.0

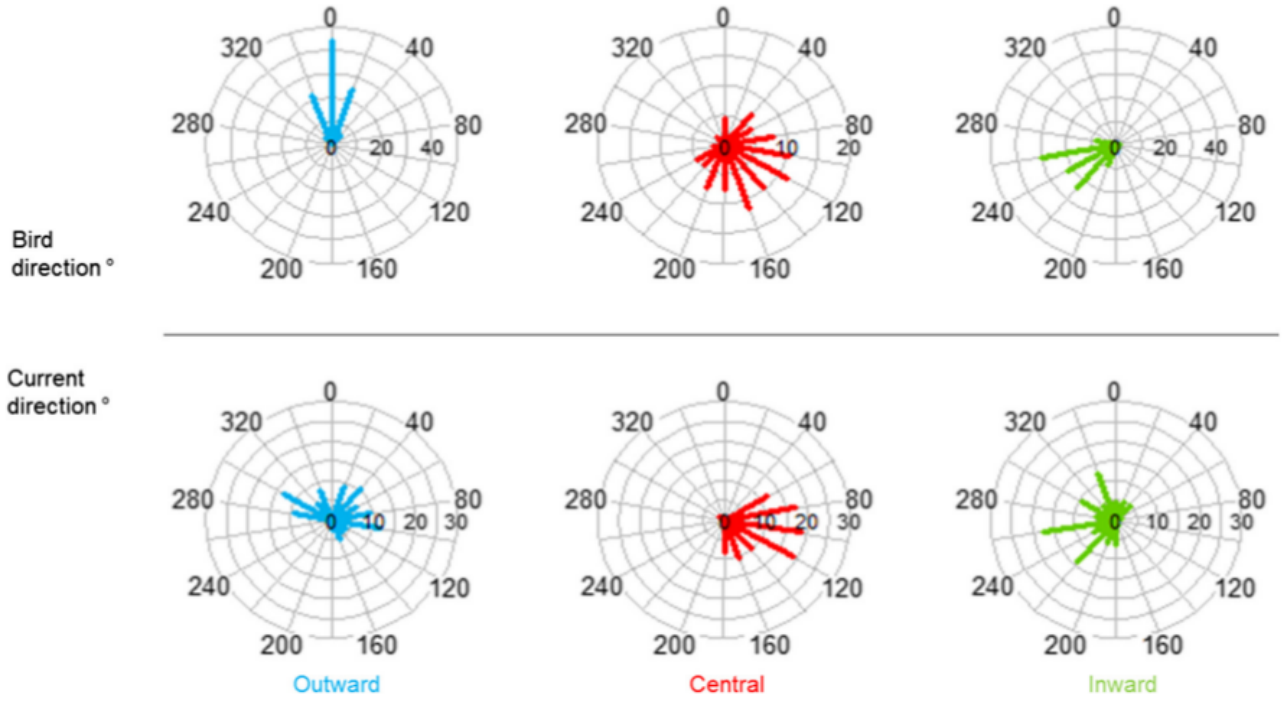

FIGURE 2.4: Angular deviations in the headings of penguins and ocean currents within each phase of trips. The proportion (%) of deviations between the direction of travel of ocean currents and the tracked penguins, computed at the resolution of 20°.

low and no clear relationship was observed between the penguins and direction of the current (Table 2.1, Fig. 2.4). In the central phase, penguins shifted toward a south-eastern direction ($141.40 \pm 68.78°$) with a travelling speed significantly lower than during the two other trip phases (Kruskal-Wallis test: $\chi^2 = 103.9734$, df $= 2$, $p < 0.001$). At that time the currents were significantly faster than during the two other phases (Kruskal-Wallis test: $\chi^2 = 169.90$, df $= 2$, $p < 0.001$), up to $1.6km/h$, and mainly oriented in the same direction as the penguins' headings ($118.10 \pm 37.86°$, Fig. 2.4. A strong correlation between the directions of the penguins and currents were also found (circular Pearson test: 5. 78, $R^2 = 0.40$, $p < 0.001$). A substantial proportion (25.3 %) of heading velocities was $< 1km/h$ indicating displacement close to that of the current speed suggesting a possible drifting behavior by the birds. During the inward phase, the penguins moved quickly back to the colony and their paths were mostly orientated south-westerly (Fig. 2.4). The weak currents were also oriented south-westerly and positively correlated with the penguins' main direction (circular Pearson test:4.55, $R^2 = 0.50$, $p < 0.001$).

TABLE 2.3: Influence of the occurrence of eddies, filaments and current speed on heading velocity. Linear mixed models were independently built with individual bird included as a random effect (n=6) for each explanatory variable. Responses variables are heading velocity (HV) and travel velocity (TV). The Okubo-Weiss parameter is a binary factor coding for the occurrence of eddies (0: absence, 1: presence). Current speed and FSLE are continuous variables. Only FSLE values $> 0.1d^{-1}$ were selected to test for the influence of filaments on HV when penguins were within a filament. Significant coefficients (mean ± se) are in bol. P= $p - value$, NS= non-significant. $\Delta AICNull$ shows the AIC deviation from AIC of the null model.

HV ~ OW$_{category}$	**Intercept**	**Presence of eddy**	**P$_{intercept}$/P$_{variabile}$**	**ΔAICNull**
M1 - Outward phase	3.57 ± 0.20	0.14 ± 0.40	$< 0.0001/NS$	+1.87
M2 - Central phase	1.62 ± 0.11	0.12 ± 0.16	$< 0.0001/NS$	+3.30
M3 - Inward phase	3.43 ± 0.25	-0.635 ± 0.29	$< 0.0001/ < 0.05$	-2.14
HV ~ FSLE(> 0.1)	**Intercept**	**FSLE(> 0.1)**	**P$_{intercept}$/P$_{variabile}$**	**ΔAICNull**
M4 - Whole trip	3.60 ± 0.51	-7.29 ± 2.78	$< 0.001/ < 0.05$	-6.40
TV ~ Current speed	**Intercept**	**Current speed**	**P$_{intercept}$/P$_{variabile}$**	**ΔAICNull**
M5 - Whole trip	3.51 ± 0.19	-1.51 ± 0.24	$< 0.001/ < 0.001$	-27.38

Discussion

The salient findings of this study can be summarized as follows. Firstly, tracked Macaroni penguins performed long looping trips north of Crozet towards a predictable large-scale frontal structure, the SAF. The similarity in their swimming direction strongly suggests a common use of oceanographic features. Secondly, during the central phase of their trip, the penguins slowed down and foraged inside large eddies, following a northeast flow. Overall, in accordance with our assumptions, the penguins adjusted their travel speed and movement throughout their trips in relation to the oceanographic structures visited.

Use of large-scale circulation around the Crozet Archipelago

The foraging movements of Macaroni penguins toward the SAF demonstrate these diving predators use predictable, large-scale physical feature in agreement with our first assumption. This is consistent with the highest mean seabird species richness and diversity in the South Indian Ocean having been reported at the SAF [Abrams, 1985]. This diversity and abundance is driven by the high concentration of chlorophyll-a and macrozooplankton within the SAF, resulting from increased water column stability and availability of nutrients [Venables et al., 2007]. Recent in situ oceanographic sampling and remote sensing data [Pollard et al., 2007a] have shown that a predictable phytoplankton bloom occurs north of Crozet [Sanial et al., 2014a] each year in early September. North of Crozet, the SAF deviation creates a closed area with long residence time which allows dissolved iron from land or sediments of the Crozet plateau to fertilize the water during winter. These conditions enhance the development of the phytoplankton bloom [Pollard

et al., 2002, Planquette et al., 2007] which reaches a peak in late October i.e. during the period before the at-sea sojourns of incubating males tracked in our study. During this time, Macaroni penguins mainly feed on euphausiids, (primarily *Euphausia valentini* and *Thysanoessa macrura*), amphipods (*Themisto gaudichaudii*) and myctophid fish (*Krefftichthys anderssoni spp.*) [Cherel et al., 2008, V.Ridoux, 1995], which have been found in high concentrations within the PFZ [Pakhomov and McQuaid, 1996, Pakhomov and Froneman, 1999a, Koubbi, 1993].

Foraging behavior in meso- and sub-mesoscale structures

At a fine scale, individuals modified their swimming behavior when entering meso- (eddies) and sub-mesoscale (filaments) structures. In agreement with other diving predators [Bailleul et al., 2010b, Cotté et al., 2007, Cotté et al., 2015], Macaroni penguins slowed down, suggesting they undertook more intensive foraging activity, during this phase characterized by an important eddy field. The greater relative abundance of young eddies in this phase compared to the two other phases confirms that the central phase is located in a branch of the SAF characterized by an important mixing activity [Kostianoy et al., 2003]. Numerous studies have shown that several trophic levels of organism can aggregated within eddies [Riandey et al., 2005, Landry et al., 2008] and, through a cascading effect, many predators could benefit from this [Cotté et al., 2007, Cotté et al., 2015, De Monte et al., 2012]. In addition, in this study, penguins showed no difference in heading velocity within and outside of eddies in the central phase, whereas currents were stronger and filamentary activity higher than in the other phases. We suggest that the prey field was extended at the spatial scale of the branch of the SAF and this hypothesis is coherent with the spatial structure of the annual phytoplankton bloom [Pollard et al., 2007b]. While it is reasonable to assume that local variations of prey density exist at finer scale, at the sub-mesoscale, the sampled distance between locations (tens of km) was too large to detect variations in heading velocity responding to such prey distributions. During outward and inward phases, penguins did not respond in the same way to the presence of eddies. Eddies were not visited in the outward phase since no changes of heading velocity were observed. However, a significant slow-down was shown in the inward phase within an eddy. As suggested by Cotté et al. [Cotté et al., 2015], all eddies are not used and it would depend on their life-time and history. In our study, eddies in transit phases presented a retention time significantly higher than in the central phase. As eddy cores present a relatively poorly mixing environment [d'Ovidio et al., 2013], they retain nutrients and thus probably enhance biological productivity and prey aggregation. The weak currents inside the eddy cores may also explain the reduced travelling speed of individuals as they foraged inside these structures. Thus,

the behavioral changes observed in the eddy during the inward phase could indicate that the eddy is profitable. Concerning the sub-mesoscale activity, the central phase was also the area where the filamentary structure was the highest, confirming the dynamic character of the area. This is to be expected as filaments are mostly formed from eddy-eddy interactions [Lapeyre and Klein, 2006b]. Furthermore, once individuals were inside filaments, they slowed down more as the horizontal stirring increased. This is consistent with the trapping characteristics of these structures retaining chlorophyll and thus attracting species in the upper trophic levels [d'Ovidio et al., 2010, Lévy, 2008]. However, no difference was detected in swimming behavior inside and outside the filaments, in contrast to that observed with eddies. This may be due to several factors. Firstly, crustaceans and fish are mobile in comparison to the phytoplankton patches which are transported by currents, which could induce a more dispersed spatial distribution outside the filaments. Secondly, these transport barriers are mostly located at eddy edges [d'Ovidio et al., 2013]. Thus, Macaroni penguins may have responded to the productivity associated with eddy characteristics and not to the filament properties (i.e. at a finer scale). Finally, any adjustment of movements by penguins to filament characteristics may not have been detected due to the spatial resolution of the datasets used (i.e. altimetry data at 0.33° and 1 week, GPS locations limited to 6 h intervals, tens of km).

Currents

Throughout the different phases of their foraging trips, Macaroni penguins exhibited marked shifts in their travel speed in relation to the current directions encountered. The heading velocities (HV) were generally much greater than the fastest encountered currents ($> 0.8 km/h$). However, in areas where currents were fastest, 30 % of trip segments were associated with an HV of less than $1 km/h$. This indicates a travel speed close to the current speed which strongly suggests individuals were drifting horizontally. In marine predators, surface drift behaviors have been explained as a consequence of different processes. Firstly, current speeds may be similar to the swimming ability of the studied species. This results from the current's influence on the animals' trajectories [Gaspar et al., 2006]. Secondly, drift behavior could occur at night in daytime foragers resting during multi-day trips [Barlow and Croxall, 2002]. Thirdly, horizontal drift behaviors could be indicative of an increase in vertical foraging activity. Finally, the maximum swimming speed of Macaroni penguins (up to $10 km/h$ [Brown, 1987]) is high compared to the current speed. Hence, the low HV observed at the central phase of the foraging trips in the present study could correspond to an increase in diving activity resulting in passive horizontal movement (drift). Association with the local currents

could be a good way to minimize transports costs. Indeed, from the start of the breeding cycle until the creching phase, males have to endure two extended fasting periods. The first lasts $\sim$ 35 d (i.e. from the arrival of the birds at the colony until their departure after the first long incubation period) and the second occurs at the end of their first post-incubating trip until the end of brooding (i.e. $\sim$ 35 days [Williams and Croxall, 1991, Stahl et al., 1985]). Thus, during their first post-incubation trip, males are highly energetically constrained as they have to restore their body condition and acquire enough reserves to prepare for the next fasting event. Consequently, individuals would gain significant energetic advantages by adopting behaviors that avoided swimming against currents. Our results support this hypothesis. Such behavior has been observed in other oceanic penguins (e.g. king penguins *Aptenodytes patagonicus*, Magellanic penguins *Spheniscus magellanicus*) at a time when they also need to quickly progress to favorable foraging areas [Cotté et al., 2007, Rey et al., 2010].

Conclusions

This work confirms the high dependence of Macaroni penguins on large-scale frontal zones such as the SAF in the Crozet area, a key breeding area for the species. This is the first demonstration of such strong dependence to the SAF for the Crozet Macaroni population. In addition, our study highlighted the role of currents and eddy activity on the foraging behavior of a diving predator. In future studies, the adjustment of movement behavior to filaments should be tackled at a finer scale with a more precise overlap between predator movements and the location of frontal structures. Investigating diving success in these structures would be also of special interest. Furthermore, analysis of whether the drift behavior is actually associated with more intensive foraging should be undertaken, potentially using 3D movement data. Finally, it would also be important to know if such behavior is exhibited during other periods where penguins are subjected to other major energetic constraints such the creche phase or pre-moulting period [Green et al., 2009].

Methods

The study was carried out at the Jardin Japonais colony, Possession Island ($46°21'S, 51°43'$ E), Crozet Archipelago (hereafter, referred to as Crozet). The archipelago lies on the Crozet Plateau (45–47° S, 49–51° E) (150 km of width, less than 500 m deep) and at the northern extent of the eastward flowing Antarctic Circumpolar Current (ACC) [Pollard et al., 2007b]. The Crozet Plateau deflects one of the current's major branches, the sub

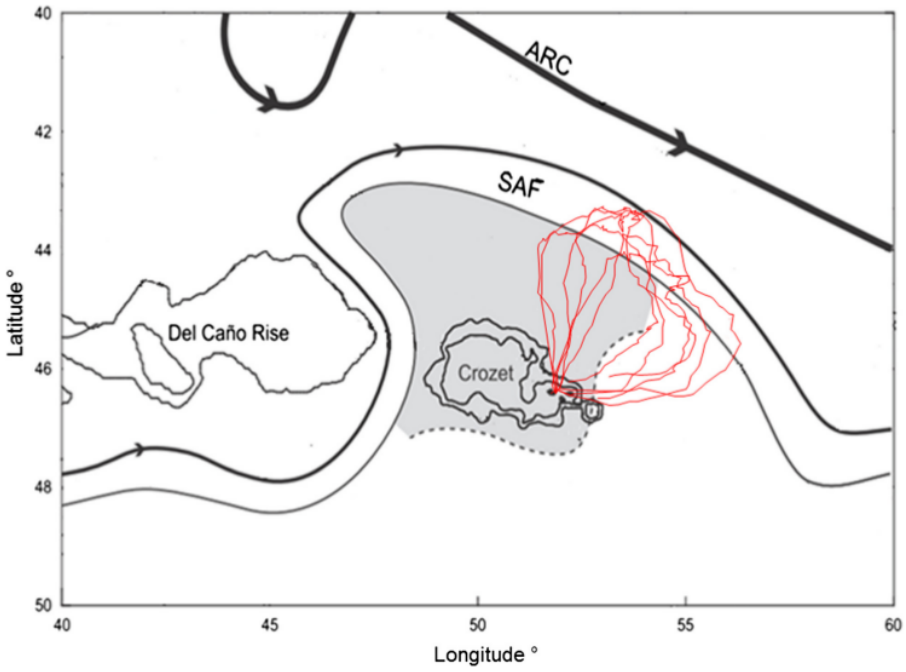

FIGURE 2.5: Map of oceanographic fronts taken from Pollard and Read (2001, [Pollard and Read, 2001]). Macaroni trips (red) are shown in red. SAF = Sub-Antarctic Front. ARC = Agulhas Return Current.

Antarctic Front (SAF), to the south of the Del Caño Rise before flowing northward under the influence of the local bathymetry. North of the plateau, it turns eastward under the influence of the Agulhas Return Current and the SubTropical Front [Pollard et al., 2007b] . The SAF is associated with strong eastward currents, located between 42 and 43° S, whereas a weak circulation dominates between the Crozet shelf and 44° S [Sanial et al., 2014a] (Fig. 2.5, [Pollard and Read, 2001]). During the 2012 Austral summer, a total of 7 adult breeding males (incubation stage) were captured (20–21 November) before the departure for their first long trip. The penguins were instrumented with a GPS logger (Fastloc 2, Sirtrack, Havelock North, N.Z.) when leaving their colony. The devices were programmed to record location every 15 min. Each logger was attached to the lower dorsal feathers along the central mid-line, to minimize drag effects [Bannasch et al., 1994], with instantaneous cyanoacrylate glue (Loctite 401 Prism, Instant Adhesive, Hempstead, Hertfordshire, HP2 4RQ UK) and waterproof tape (Tesa 4651, Tesa Tape, Quickborn str 24, Hamburg 20253, Germany), and further secured by two cables ties. The duration of the instrumentation procedure lasted <15 min. All the birds were recaptured upon their return to the colony and the equipment removed.

Oceanographic data

Altimetry maps were obtained from the CNES/CLS AVISO website [Handbook, 2010] with spatial and temporal resolutions of 0.33° and 1 week, respectively [Le Traon et al.,

1998]. Altimetry was used to compute the velocity of horizontal currents and to identify sub- and mesoscale physical structures. The currents' velocities were compared with the velocity of penguins, called travelling velocity (TV), determined from GPS tracking, by computing the heading velocity (HV) [Girard et al., 2006], which is defined as:$v_{(heading)} = v_{(tracking)} - v_{(currents)}$. To identify sub- and mesoscale structures, we used Eulerian and Lagrangian diagnostics: the Okubo-Weiss (OW) parameter to identify eddies, the Finite Size Lyapunov Exponent (FSLE) to identify filaments, and the Retention Parameter (RP) to quantify for how long the water parcels within an eddy have been recirculating. The Okubo-Weiss parameter OW [d'Ovidio et al., 2013, Weiss, 1991] is defined as:

$$W = sn^2 + ss^2 - \omega^2 \tag{2.1}$$

where sn and ss are the normal and shear components of strain and ω is the relative vorticity of the flow. The sign of this parameter locates eddies as regions with negative OW parameters (vorticity is dominant) and background as oceanic regions of small negative and positive OW pa- rameters (strain is dominant, absence of eddies). Following Bailleul et al. [Bailleul et al., 2010b], we used the $W_o = 0.2\sigma_w$ (σ_w is the standard deviation of W in the whole domain) threshold to separate vorticity-dominated ($W < -W_O$, presence of eddy) regions from strain-dominated regions ($W \geq W_O$, absence of eddy) and the background field ($|W| \leq W_O$). The Finite Size Lyapunov Exponents (FSLE) method provides a direct measure of the amount of local stirring by mesoscale currents. It can be used to identify transport barriers along which water parcels are stretched into elongated structures (hereafter, termed filaments), typically in the region between eddies [Lapeyre and Klein, 2006b]. The FSLE computes the backward-in-time divergence (i.e. convergence) of particles initially in close proximity to each other and is commonly used as an indicator of frontal activity and stirring intensity [d'Ovidio et al., 2004]. It is computed as:

$$\lambda(x, t, \delta_0, \delta_f) = \frac{1}{\tau} log \frac{\delta_f}{\delta_0} \tag{2.2}$$

Where δ_0 represents the initial separation of water parcels, and τ the time taken for the water parcels to reach a separation δ_f . For the present study, the parameters used for the calculation were $\delta_f = 0.6$ degrees, $\delta_0 = 0.01$ degrees and τ had a maximum limit of 100 days. Highest FSLE values are associated to formerly distant water masses, whose confluence creates a transport front [d'Ovidio et al., 2004]. Here, we used $FSLE > 0.1d^{-1}$ as indicators of the presence of a transport front. FLSE ridges can represent the edges of mesoscale eddies but also the convoluted boundaries of sub-mesoscale filaments. The Retention Parameter (RP) computes the backward trajectories of simulated water parcels from negative OW regions (i.e. eddies) and measures for how long each water parcel

has been within the same OW negative patch. This quantity corresponds to the time the water has been recirculating within the eddy [d'Ovidio et al., 2013]. The SAF was identified as the 8 ° C sea surface isotherm during the period corresponding to the measured trajectories (22/11/2012-11/12/2012) [Orsi et al., 1995, Park et al., 1993]. Sea Surface Temperature (SST) was obtained from the G1SST (Global 1-km Sea Surface Temperature) Level 4 product from GHRSST (Group for High Resolution Sea Surface Temperature [ghr,]). In addition, to provide context for primary production in the regions explored by the tracked penguins, we used sea-surface chlorophyll-a concentration data from GlobColour [glo,] with a daily average resolution of 9 km^2.

Track analysis

A speed filter was applied on locations to delete speed data higher than 10 km/h, which is the maximum travel speed previously recorded by Macaroni penguins [Brown, 1987]. The temporal resolution of the oceanographic data limited us to subsample the tracks at four points per day. Therefore, we chose to keep locations closest to 04:00 h, 10:00 h, 16:00 h and 22:00 h (local time) which provided a 24 h cycle divided into 4 × 6 h periods. It has been shown that penguins decrease their horizontal movements when increasing their foraging activity, especially during the central phase of their trip [Bost et al., 1997, Pütz et al., 1999]. Thus, trips were split into three phases according to the smoothed relation between the heading velocity and the elapsed time relative to the departure. First, the outward phase, indicating the journey between the island and the central phase, was defined as the initial contiguous period where the smoothed heading velocities were higher than the average heading velocity during the whole trip ($2.2 \pm 1.4 km/h$, Table 2.1). Second, the central phase was defined as the period where the heading velocities were below the mean heading velocity. Finally, the inward phase, from the central phase to the colony, corresponded to an increase of the heading velocity. In addition, as Macaroni penguins forage less at night [Green et al., 1998a, Croxall et al., 1993], we excluded from the analyses the velocities between 22:00 and 03:00 which, respectively, correspond to local dusk and dawn [sun,]. Directions of penguins and currents they experienced (varying from 0 to 360 °) were then computed or each location using the Great Circle distance (bearing function, "geosphere" package). The distribution of sub-mesoscale structures were investigated in two ways. Firstly, we looked at "the distribution of eddies within each trip phase" computed as $\frac{n_{locs-eddies}(in\,trip\,phase)}{n_{locs-eddies}(on\,the\,whole\,trip)} * 100$ for each trip respectively. $n_{loc-eddies}$ indicates the number of locations within an eddy. Secondly, we looked at the "degree of association with eddies" computed as $\frac{n_{locs-eddies}}{n_{locs}(in\,trip\,phase)} * 100$, for each trip trip phase respectively. Same ratios were computed for investigating filaments distributions.

Statistical analysis

All analyses were conducted in the R statistical environment [r$_s$,]. We used circular statistics ("circular" package) to determine the average bearing of currents and animals within each phase and assess the correlations between currents and animal directions. A Mann–Whitney U test ("stats" package) was used to compare the behavior of penguins within and outside of eddies or filaments. Following these descriptive analyses, different linear mixed effects models (lme function, "nlme" package) were constructed. For all models, individuals were included as a random effect as each location within individuals was not independent. The autocorrelation of residuals was tested (acf function) and consequently an autoregressive term of order 1 (coAR1) was included. The best model was selected using the Akaike criterion (AIC [Burnham and Anderson, 2004]). Firstly, to investigate the response behavior to occurrence of eddies within each trip phase, three mixed models (one by trip phase, called M1, M2, M3) were built with the heading velocity as response variable and the factor "occurrence of eddies" (explanatory binary variable: absence or presence). Secondly, another model was built to link the variation of heading speed to the occurrence of frontal structures (explanatory binary variable: absence or presence). This model (not presented) had an AIC higher than the null model and the weak number of filaments within the outward and inward phases prevented us from building one model per trip phase. Thus, we looked at the relation of heading velocity (response variable) with the FSLE values (explanatory variable) when penguins were inside filaments ($FSLE > 0.1$, model called M4). Finally, we tested the influence of currents (explanatory variable) on the travelling speed (response variable, model called M5). The different studied parameters are presented as Mean ± Standard Deviation (SD) whereas coefficients of models are presented as Mean ± SE (Standard Error). AIC deviations of tested models from the null models are shown. Results were considered significant at $P < 0.05$.

Authors contributions

CB analysed the trajectories, performed the statistical analysis and drafted the manuscript. AD handled the oceanographic products, created the oceanographic maps and assisted with the analyses. FO helped in obtaining oceanographic products, helped design the study and to draft the manuscript. JA provided devices, participated in discussion of the results and helped to draft the manuscript. TP participated in the field work and data processing. CAB conceived of the study, helped develop the design, coordinated the study and helped to draft the manuscript. All authors read and approved the final manuscript.

Acknowledgements

The authors sincerely thank T. Powolny and all fieldworkers who helped with data collection. The present work was supported financially and logistically by the Institut Polaire Français Paul Emile Victor (IPEV, Program No. 394, leader C.A. Bost) and the Terres Australes et Antarctiques Françaises (TAAF) and the EU-BEST penguins project N° 07.032700/2012/634945/SUB/B2. CB's work was funded by a grant of the Région Poitou–Charentes and by the Conseil Général des Deux Sèvres. The altimeter products were produced by Ssalto/Duacs and distributed by Aviso with support from Cnes. Chlorophyll images were obtained by the GLOBCOLOUR project. We are especially indebted to L.G. Halsey for improving the English and helpful comments to the manuscript.

Part III

Mesoscale and submesoscale turbulence and ecological dynamics shape the biological landscape marine predators explore

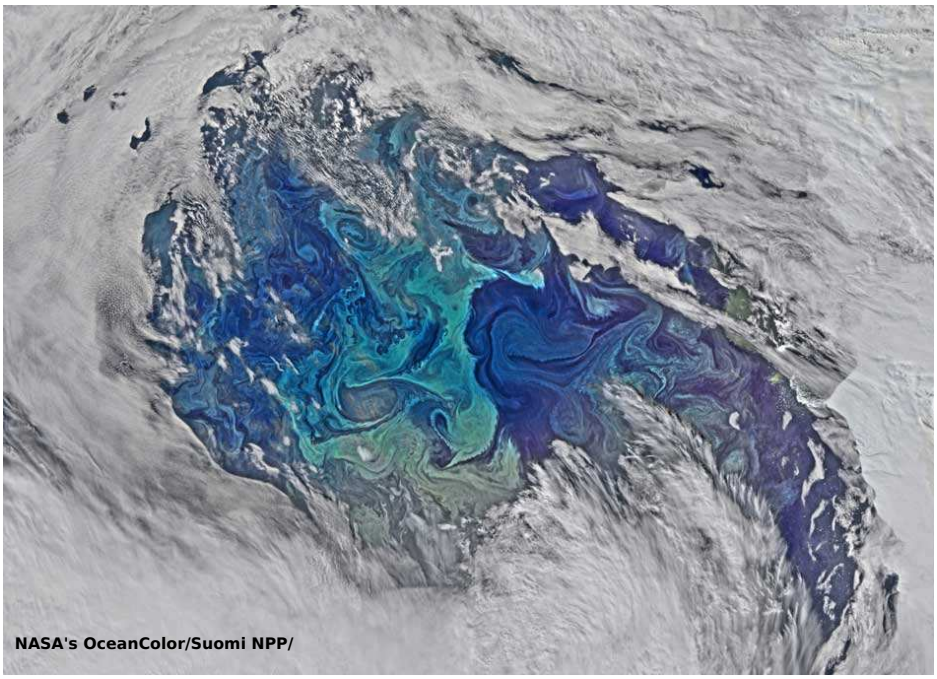

An important response of marine predators to (sub-)mesoscale ocean dynamics is related to how the latter structures the spatial distribution of their prey, determining which open ocean areas potentially provide richer foraging grounds. In this section I present my results on how stirring and ecological dynamics affect the habitat of marine predators in the $\sim$ 1000km pelagic region east of Kerguelen which hosts an important phytoplanktonic bloom and which is the foraging ground of several magafauna species.

The Southern Ocean is characterised by two highly contrasted trophic webs: the so-called "trophic chain of giants" and the microbial foodweb (Figure 2.6) [Smetacek et al., 2004, Cushing, 1989, Irigoien et al., 2002]. A major driver of which of the two trophic webs is dominant in specific areas is the availability of iron. As mentioned in the introduction of this thesis, the Kerguelen region is a particularly productive region contrasting with the general High Nutrient Low Chlorophyll (HNLC) nature of the Southern Ocean that is generally iron-limited [Boyd et al., 2007, De Baar et al., 2005]. The microbial foodweb is typical of oligotrophic regions where small phytoplankton ($\sim< 10\mu m$) dominate the phytoplanktonic community. Zooplankton like salps, characterised by short generation times and efficient grazing for low chlorophyll and small phytoplankton, constitute the dominant zooplanktonic group in such environments [Zeldis et al., 1996]. By contrast, in iron enriched waters, for example near the sea-ice interface and in the wake of sub-Antarctic islands, large diatoms bloom and support the development of crustaceans (mainly krill in Antarctic waters and amphipods in areas around Kerguelen) and fish larvae. Because salps tend to be "clogged" by large or abundant phytoplankton, whereas crustaceans can regulate their feeding but need high abundance of phytoplankton to grow, crustaceans (often in assemblages with micronekton larvae) and salps tend to occupy very distinctive niches [Pakhomov et al., 2002, Loeb et al., 1997, Ducklow et al., 2007]. Crustaceans and fish larvae play a pivotal role in the Southern Ocean ecosystems, representing a large proportion of the diet of large marine predators and constitute an important trophic link between diatom dominated communities of primary producers and large marine predators [Takahashi et al., 2003, Moline et al., 2004, Reid and Croxall, 2001].

This classification of contrasted trophic webs is qualitatively defined as they are not always mutually exclusive. Some marine predators indeed feed on salps [Catry et al., 2004, Cruz et al., 2001], salps and diatom abundances have been occasionally observed to correlate [Zeldis et al., 1996], and coexistence of copepods and salps has been reported (in parasitic behaviour [Perissinotto and Pakhomov, 1997]). However, the distinction between the "trophic chain of giants" and microbial foodweb generally well describes trends in Southern Ocean marine ecosystems [Irigoien et al., 2002].

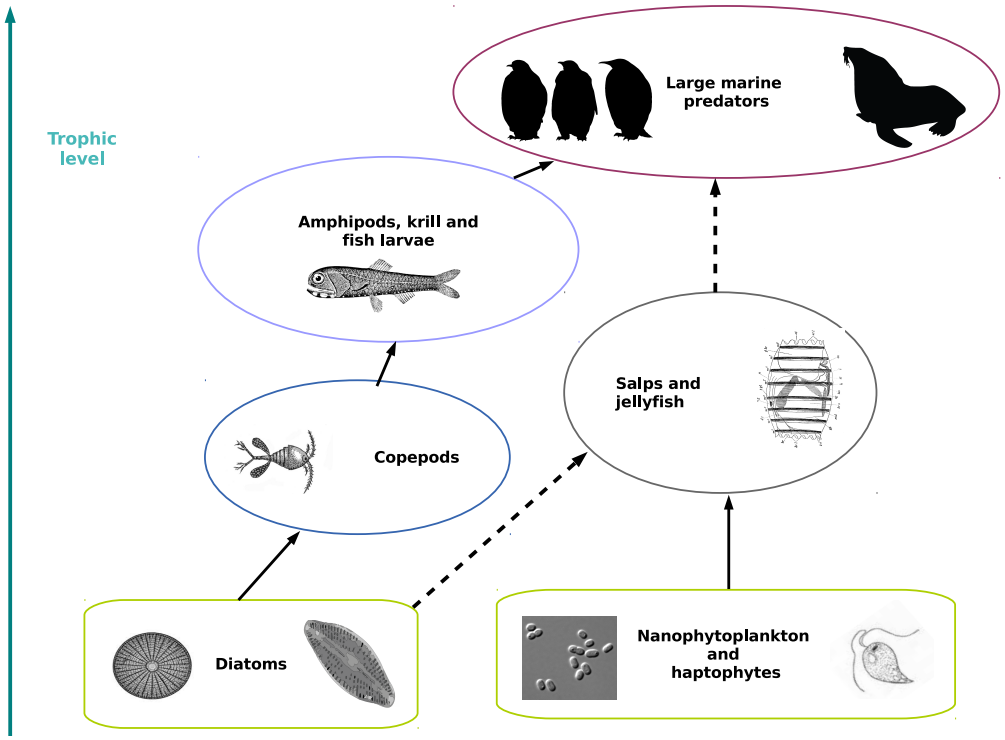

FIGURE 2.6: Qualitative scheme of the foodweb structure around Kerguelen. Solid line represents trophic links that we expect to be dominant in respect to dashed ones. In this thesis, we assume that favourable waters for large marine predators are the ones that experience diatom blooms.

In this thesis, I use information on phytoplanktonic communities (that is available from in-situ observations and remote sensing) as an indicator for which of the two contrasted trophic webs may dominate a water parcels and therefore to identify which regions around Kerguelen are likely to be more favourable for large marine predators. Kerguelen's large marine mammals (e.g. fur seals, southern elephant seals [Connan et al., 2007, Cherel et al., 2008]) and seabirds [Guinet et al., 1996, Raclot et al., 1998] populations have been observed to feed on fish [Cherel et al., 2008], small crustaceans [Bocher et al., 2001] and squid [Cherel and Weimerskirch, 1995]. Therefore we expect them to rely on the "trophic chain of giants" and have a preference for foraging in waters that have hosted a diatom bloom.

First, in Chapter 1 I discuss how horizontal transport affects the spatial distribution of favourable conditions for diatoms growth and dominance. The effects of iron on the spatial distribution of phytoplankton abundance has been the subject or recent studies that related iron enriched waters from the Kerguelen Plateau (where resuspension of sediments caused by the shallow bathymetry fertilises water parcels), with the distribution of the Kerguelen chlorophyll plume (one of the largest ones of the Southern Ocean). First, a study performed in preparation of the KEOPS2 (Kerguelen Ocean and Plateau compared Study 2) voyage defined a Lagrangian diagnostic, the "water age"

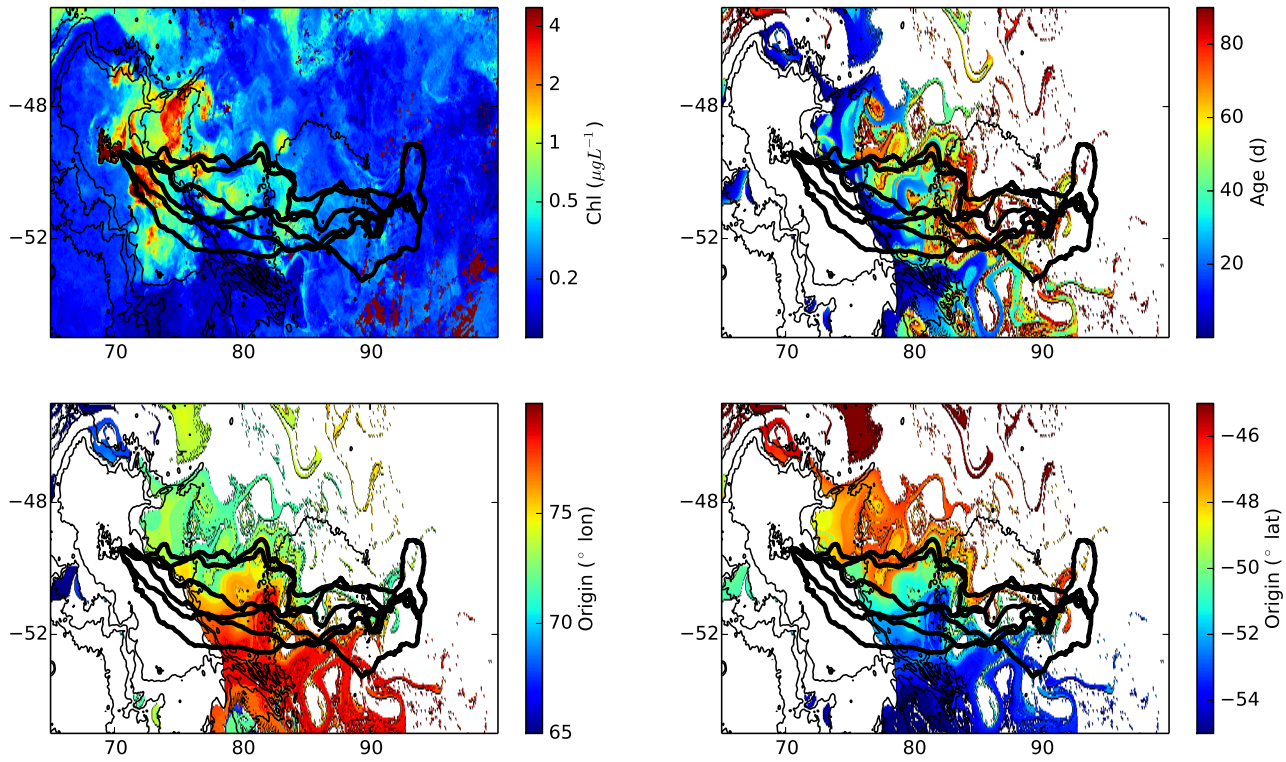

FIGURE 2.7: During their foraging trips elephant seals encounter contrasted biological regimes. In this example three foraging elephant seals (their trajectories are in black) cross the iron enriched phytoplankton plume (remotely sensed chlorophyll concentration a)) and water parcels having different origins and "water age" (water age, b) and origin (c) and d)).

that quantifies how long before a water parcel has been in contact with the Plateau. Considering that the plateau is a source of iron and that iron is slowly depleted by the water parcel due to scavenging, the water "age" diagnostic is a proxy of a (relative) iron concentration in the surface waters around Kerguelen. This diagnostic, along with the "water origin" that quantifies where on the Plateau the water parcel was enriched, can be used to predict, similarly to what Mongin and co-authors [Mongin et al., 2009] had done before, the extent and the shape of the Kerguelen chlorophyll plume that can be detected from space [d'Ovidio et al., 2015]. Then, the same diagnostics have been used to interpret the in-situ measurements from four Bio-Argo profilers that were deployed during KEOPS2 and MYCTO-3D, another research voyage in the region that occurred in January 2014 [Grenier et al., 2015]. For reasons of brevity, the papers containing these results are not part of the thesis but they can be found in Appendixes A and B. However, the main results of these works that are relevant to this thesis are:

1. The spatial patterns in "water age" (days since having left the plateau) and "water origin" (last contact position over the plateau) (Figure 2.7 b) and c)) that can be inferred from the altimetry-derived velocity field capture the same dynamical structures as the same diagnostics computed using the trajectories of 200 Surface Velocity Program (SVP) that transited in the study region.

2. Water parcels that have been in contact with the Plateau present a considerable overlap with the chlorophyll plume that can be observed in ocean color images.

3. Locations of high chlorophyll concentration correspond in particular to water parcels that have recently ($\sim 20 - 30$ days) left the Plateau (in particular its Northern part).

Chapter 1 uses the definition of "water age" to sketch a biogeographical description of dynamical niches favourable to diatoms, based on the hypothesis that such group is more likely to dominate the phytoplanktonic community in iron-enriched water parcels. I first combine in-situ pigment sampling and PHYSAT, an optical re-analysis that allows to estimate phytoplanktonic dominance from ocean color images [Alvain et al., 2008, Alvain et al., 2005], with a Lagrangian approach. This data analysis establishes a relationship between conditions favourable to diatom occurrence and dominance on the one side, and iron transport, through the "water age" diagnostic. The observed patterns of diatom dominance are then compared to those obtained by advecting a simple "threshold" model for the ecosystem response to iron availability (illustrated in Figure 2.8, green line).

Then, in Chapter 2 we explore the possibility that the Kerguelen phytoplankton ecosystem may allow bistability between alternative states exhibiting large diatoms or nanoplankton dominance. In contrast to systems whose state variables respond smoothly to external forcings, bistable systems may show some "inertia" (sometimes referred as hysteresis) over certain ranges of conditions – the "original" stable state - and respond strongly when conditions approach certain levels, without any tendency to return to the previous state as the forcing changes -"secondary" stable state [Scheffer et al., 2001]. As a consequence, according to the history of the system, different states may be stable for the same condition in the forcing. Bistable systems have been observed in a variety of ecological contexts in marine environments [Van Nes et al., 2007, Steneck et al., 2002, Ling and Johnson, 2009, Nyström et al., 2000, Marzloff et al., 2011] and have been the object of theoretical studies [Lenton, 2013, Scheffer et al., 2001] and applied studies [Marzloff et al., 2011, Petraitis and Dudgeon, 2004]. In the model described in Chapter 2 water parcels with the same iron content may present both a diatom-dominated or a nanoplankton-dominated community, depending, other than on iron concentration, on

the initial inoculum of the phytoplankton assemblage. I analyse under which circumstances this may happen and how it qualitatively affects shifts in trophic webs up to top predators.

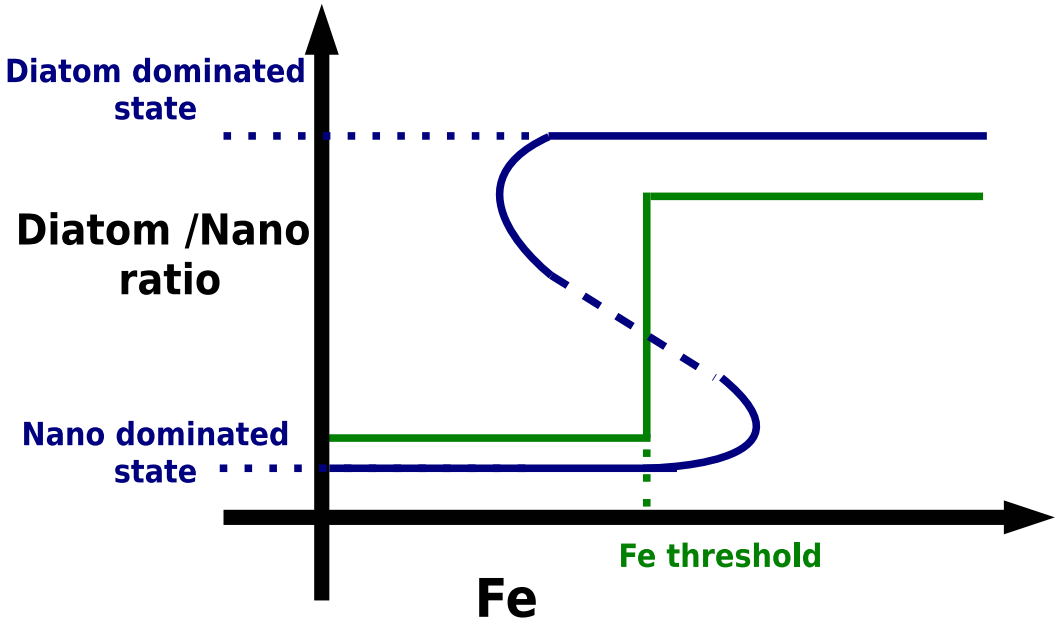

FIGURE 2.8: Response functions for phytoplankton community structure in relation to iron concentrations. The "threshold" approach discussed in Chapter 1 is represented in green and the bistable state permitting one is represented in blue. The blue curve shows how for the same value of iron two possible states with difference in phytoplankton dominance are possible.

Chapter 1

Mesoscale variability of diatom favourable conditions in the East Kerguelen region (Southern Ocean)

This chapter will be submitted soon to *Journal of Biogeography* as *Mesoscale variability of diatom favourable conditions in the East Kerguelen region (Southern Ocean)* by A. Della Penna, S. Wotherspoon, T. Trull, S. De Monte, C. Johnson, F. d'Ovidio.

Abstract

A major goal of biogeographical studies is to identify areas within which a characteristic ecosystem is expected to occur. In the case of phytoplanktonic communities this knowledge is key to distinguish regions that may be characterised by different biogeochemical processes, to design efficient sampling strategies, and to recognize hotspots of ecological activity. High temporal and spatial variability in ocean physics at meso and submeso scales (1-100 km, few days to months) can strongly influence the dynamics of phytoplankton blooms. Such coupling between physics and ecology makes investigating phytoplankton biogeography challenging, especially in remote regions like the Southern Ocean where in-situ observations are sparse. Here we use multi-satellite observations (color of the ocean, the PHYSAT re-analysis, and altimetry), in-situ pigment sampling and a Lagrangian approach to study the spatial variability of favourable conditions for large diatoms and their dominance over other phytoplanktonic types in the iron-enriched

plume east of the Kerguelen Plateau (Indian Sector of the Southern Ocean). We find that, even though diatoms are observed ubiquitously in this region, water parcels that have recently left the Kerguelen Plateau tend to show higher concentrations of in-situ measured fucoxanthin (the secondary photosynthetic pigment associated with diatoms). Spatial differences in favourability for diatom growth within the plume is also reflected in the dominance of diatoms inferred from remote sensing. Here we combine this result with biogeochemical hypotheses and consideration of competition among phytoplankton guilds to develop a simple "threshold" model. Even if it performs poorly at predicting phytoplankton dominance at specific locations, the model successfully capture the extent and the spatial structure of diatom dominance in region East of Kerguelen.

Introduction

One of the main goals of biogeography is to identify regions where specific ecosystems may be expected to occur [Longhurst, 2010] . For phytoplankton communities this knowledge is key [Longhurst, 2010, Oliver and Irwin, 2008] for distinguishing regions characterised by different biogeochemical processes [Dutkiewicz et al., 2009, Follows et al., 2007, Falkowski et al., 1998, Allen et al., 2005, Watson et al., 1991, Trull et al., 2014], designing efficient sampling strategies, recognizing hotspots of ecological activity [De Monte et al., 2013] and predict primary production's response to a changing climate [Barton et al., 2013]. Furthermore, differences in phytoplankton community composition act through a bottom-up effect to determining community structure and the magnitude of secondary production of mid-trophic levels and ultimately of top predators. This 'bottom-up' mechanism, as distinct from top-down effects where grazing and predation (and in some cases fisheries) control the state of the ecosystem, have been observed frequently in marine ecosystems [Frederiksen et al., 2006, Hunt and McKinnell, 2006]. In the Southern Ocean in particular, contrasting phytoplankton communities are observed to sustain different ecosystem structures up to higher trophic levels including top-predators [Moline et al., 2004, Kopczynska, 1992].

In the open ocean, defining biogeographical provinces is challenging even when summarizing phytoplankton diversity in terms of functional groups (for example by using pigments as distinguishing functional traits). Defining the boundaries of open ocean bioprovinces requires disentangling several physical and biogeochemical factors including the physical properties of water masses, dispersal, predation, and competition for macro and micro-nutrients [Follows et al., 2007]. These factors interact in the open ocean, and are themselves characterised by high temporal and spatial variability. Typical phytoplanktonic patchiness extends on temporal and spatial scales (days-months,1-100 kms)

that overlap with ocean sub- and meso-scale phenomena such as fronts and eddies. These structures produce a contrasted and highly dynamical sea landscape that underpins the distribution of planktonic organisms by both shaping their niche and advecting them [Lévy, 2008, Lehahn et al., 2007, d'Ovidio et al., 2010].

The goal of this study is to combine remote-sensing (ocean color and altimetry information) with in-situ data of pigment concentrations and a Lagrangian approach to sketch a biogeography of areas of ocean favourable for dominance by large diatoms in the iron-limited system to the east of the Kerguelen Plateau.

The Kerguelen region is located in the Indian Sector of the Southern Ocean (Fig. 2.1 a), that is recognised as the largest High Nutrient Low Chlorophyll (HNLC) region in the world [Boyd et al., 2012a]. Kerguelen Island and Heard Island arise from a large ($\sim$ 60, 000 km2, referring to the 1000 m bathymetric line, [Mongin et al., 2009], see Fig. 2.1 b) plateau that is thought to act as a major source of iron, the main limiting factor for primary production in the Southern Ocean [Boyd et al., 2012a, De Baar et al., 2005, Boyd et al., 2007]. An annual phytoplankton bloom that extends for more than 250, 000 km^2 [d'Ovidio et al., 2015] downstream with chlorophyll concentrations up to 10 times that of surrounding waters [Trull et al., 2014] is attributed to sediment resuspension from the Kerguelen plateau [Blain et al., 2001, Zhang et al., 2008, Van Der Merwe et al., 2015] . The Kerguelen bloom is one of the most studied examples of natural iron fertilisation and has been the subject of several interdisciplinary field studies [Blain et al., 2001, d'Ovidio et al., 2015, Blain et al., 2008, Blain et al., 2007]. The shape and extension of the Kerguelen bloom is known to be strongly related to the circulation patterns [Trull et al., 2014, Mongin et al., 2009, d'Ovidio et al., 2015, Grenier et al., 2015], which are mainly determined by the Antarctic Circumpolar Current (ACC) fronts and the intense mesoscale activity originating from frontal instabilities and their interaction with the shallow bathymetry of the plateau [d'Ovidio et al., 2015, Park et al., 2008]. The community structure of the Kerguelen bloom has been studied during ship-based oceanographic campaigns, which have focused on differentiating diatoms types [Armand et al., 2008, Quéguiner, 2013, Lasbleiz et al., 2014] and on pigment and size analyses [Trull et al., 2014, Uitz et al., 2009]. However, even though this region is the focus of active research compared with other regions of the Southern Ocean, because it is based on in-situ observations, the dataset for community structure and dominance in the region is sparse relative to the magnitude of the plume feature and clustered in the proximity of the plateau. Relatively little is known about phytoplankton community structure in the plume area away from the Kerguelen Plateau despite that it is recognised as a region of high primary production and an important habitat for top marine predators [Guinet et al., 2014, Guinet et al., 2001].

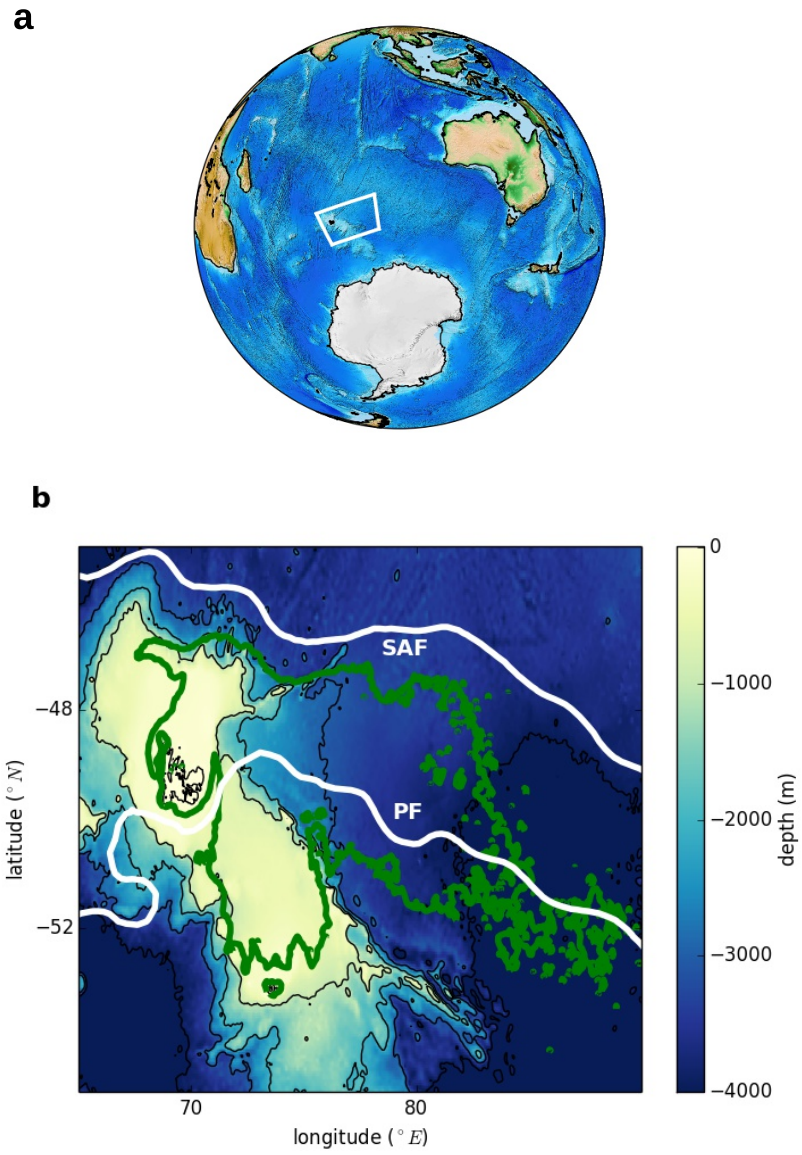

FIGURE 1.1: a) Location of the study region in the Indian Sector of the Southern Ocean. b) Bathymetry (colorscale and black lines), overlapped with the location of the Polar (PF) and Sub-Antarctic (SAF) fronts (white), and climatological extension of the chlorophyll plume (green). The shape of the chlorophyll plume is computed by putting a threshold (0.35 μ g/L) on the ocean color climatology for surface chlorophyll (calculated over spring and summer 2011-2012).

Methods

In this study we first related in-situ data (collected during KEOPS2 [Lasbleiz et al., 2014]) describing spatial variability in fucoxanthin (the secondary pigment associated with diatoms) to the Lagrangian properties of water parcels, following d'Ovidio and co-authors [d'Ovidio et al., 2015]. Lagrangian properties were computed using horizontal velocities inferred from altimetry. Secondly, we use the PHYSAT ocean color re-analysis to study whether the same Lagrangian properties might be related to diatom dominance over other phytoplankton types. For this analysis we focused on the month of December (the month with the most PHYSAT observations available) and we used data from December 2007 to 2010. We then combined these results with ecological considerations to develop a simple "threshold model" to test whether iron enrichment can explain the spatial distribution of the probability of observing diatoms as the dominant phytoplankton type in the region. Finally, in the discussion we use Mixed Layer Depth monthly climatologies to investigate the role of seasonal changes in MLD in influencing the phytoplanktonic community. This dataset was provided by J-B. Sallee [Sallée et al., 2010] and has been computed using temperature and salinity from ARGO floats.

In-situ observations

The in-situ observations used in this study were collected during the KEOPS2 cruise (November 2011) [Lasbleiz et al., 2014]. Biomarker pigments were analysed on seawater samples on a total of 30 stations. In our study we extracted the 23 off-plateau measurements (where "off-plateau" is defined as corresponding to a bathymetry deeper than 700 m) and we studied the distribution of fucoxanthin, the typical secondary pigment of diatoms [Vidussi et al., 2001]. Fucoxanthin concentrations are commonly [Hirata et al., 2011, Vidussi et al., 2001, Lasbleiz et al., 2014] used as a diagnostic for diatom presence. During the field program, pigments were collected at several depths (up to 2000 m), but since this study is focused on horizontal spatial variability, we only considered the samples collected close to the surface (between 40 and 90 m depending on the station).

Remote sensing and Lagrangian approach

Remote sensing products were used for two main objectives. First, altimetry was used to estimate the spatial distribution of horizontal currents and, consequently, to integrate the trajectories of different water parcels. Second, the PHYSAT ocean color re-analysis was used to extract observations of dominant phytoplankton types (DPT) in the study region.

To compute water parcels' trajectories we used geostrophic currents from an altimetry multi-satellite global product (Delayed Time Maps of Absolute Dynamic Heights (DT-MADT)) devel-oped by CNES/CLS Aviso [1]. The global product has spatiotemporal resolution of 1/3° and one week respectively. Two regional versions of the product have been developed by CLS with the support of CNES and are available for years from 2007 to 2014 : the geostrophic product only takes into account altimetric currents; the "Ekman-corrected" one (computed by combining altimetry with information from drifting buoys trajectories), taking into account the wind-induced Ekman component of the currents (which can dominate the first 15 m [Roach et al., 2015] of the euphotic layer). Both regional products are distributed as daily maps with 1/8° spatial resolution. For the comparison with in situ measures of fucoxanthin concentrations we computed the Lagrangian diagnostics using geostrophic currents since they are usually representative of the mixed layer, which in the region of study can be between 50 and 200 m [Sallée et al., 2010, Vivier et al., 2014]. For the comparison with remotely sensed PHYSAT re-analysis we used the "Ekman-corrected" product, which we expect to be more representative of the first 15 m.

Following previous works [d'Ovidio et al., 2015, Sanial et al., 2014a] we interpolated the velocity field and integrated it with a Runge-Kutta 4th order scheme (time step = 6 hours) to compute water parcels trajectories. Water parcels' trajectories were used to compute the "water age", which describes the time since a specific water parcel has been in contact with the Kerguelen Plateau. The plateau is considered to be a source of iron, which is the limiting nutrient of phytoplankton in the region. "Younger" water parcels (i.e. those more recently in contact with the plateau) are considered to be favourable for diatoms and high chlorophyll concentration. "Older" water parcels, instead, are likely to be iron depleted and therefore less likely to sustain phytoplankton (and in particular diatom) growth. "Water age" has been used by d'Ovidio and co-authors [d'Ovidio et al., 2015] to predict, after Mongin and co-authors [Mongin et al., 2009], the extent of the Kerguelen plume and to design an adaptive sampling scheme during KEOPS2 that followed the spatial structure of the plume. These assumptions are consistent with Grenier and co-authors [Grenier et al., 2015] who showed that autonomous profiler observations of particularly high chlorophyll concentrations corresponded to "young" water parcels. For each 20 x 20 km pixel of the domain (latitudes = $[-55°, -45°]$, longitudes = $[65°, 90°]$), we backtracked the occupying water parcels to compute the water age. We produced daily maps of water age for years 2007-2010. Water parcels that never came in contact with the plateau (defined as the 700 m isobath) were considered to have an age of 90 d corresponding to the maximum backward advection time.

[1] http://www.aviso.oceanobs.com

To assess diatom dominance in the region of study we used PHYSAT [Alvain et al., 2005, Alvain et al., 2008] images for the years 2007 through 2010 (the the period for which PHYSAT and Ekman corrected velocities are available). The PHYSAT [2] algorithm filters out the signature of the chlorophyll-a concentration from the remotely detected water reflectance spectra. (The remotely detected spectrum used is from SeaWifs 9 km resolution, but without the correction suggested by [Johnson et al., 2013] to more accurately quantify the Chl signal associated with diatoms). The obtained spectra are compared to a large in-situ database of secondary pigments that are specific for six different phytoplankton types (DPT): nanoeukaryotes, *Prochlorococcus*, *Synechococcus*, diatoms, *Phaeocystis*, and coccolithophores. A phytoplankton type is considered dominant if the contribution of the characteristic pigment (i.e. fucoxanthin for diatoms) to the signal is larger than 60%. As a consequence, for some pixels it is not possible to assign a DPT and they are labelled as "non-classified". There are also missing values related to cloud coverage, since the ocean color signal is an optical signal it is obscured by clouds. In the region of interest between the years 2007 and 2010, considering interpolated daily images of 20 km pixels (see the next section for details of the re-sampling), only 0.7% of the pixels are classified.

Statistical methods and maps comparison

Statistical analyses were undertaken using the R package (version 3.1.1). To compare the in-situ concentrations of fucoxanthin with the "water age" we used Pearson's correlation.

To quantify and evaluate the relationship between the threshold model and the PHYSAT observations we resampled PHYSAT observations and model outputs (i.e. age of a water parcel, proxy for iron content and expected dominant type) on a 20 km grid to limit the effect of spatial correlations in the model. Since the main focus of this study is diatoms, the original PHYSAT information was converted to a binary map showing diatom-dominance / non-diatom dominance. Because of the sparsity of the PHYSAT dataset data from 2007 to 2010 were pooled to enable pixel by pixel day by day comparisons between the model outputs and the PHYSAT observations. The comparison was performed using Generalized Additive Models (GAM). The R package "mgcv" which employs multiple generalized cross-validation (MGCV) was used to fit GAMs to examine the non-linear response of the dominance of diatoms in the PHYSAT image to the age of water parcels. To evaluate the performance of the GAM fit we used the area under the curve (AUC) of the Receiver Operating Characteristic (ROC) [Fawcett, 2004]. To compute the ROC the same GAM model was combined with different thresholds to predict whether the pixels related to a specific water age were dominated

[2] http://log.univ-littoral.fr/Physat - license (IDDN.FR.001.330003.000.S.P.2012.000.30300)

by diatoms or not. The results of these predictions were represented as a curve describing true positive rate versus false positive rate; the AUC is the area under this curve and equals 0.5 in the case of a null random model (i.e. the rate of true positives is the same as that of false positives for all the thresholds).

To identify the optimal threshold for the "threshold" model, we choose the one that maximised two versions the Jaccard index of similarity [Jaccard, 1912] in comparing the 'model daily maps' with the 'PHYSAT daily maps' and the 'probability of observing diatom dominance map' computed using the model and PHYSAT respectively This diagnostic quantifies the similarity between two sets of data (in this case, the binary probability of observing diatom dominance using PHYSAT versus the threshold model). It ranges between 0 and 1, where 1 corresponds to a perfect match. For the case of the comparison between two binary vectors, we computed it according to the formula:

$$J = \frac{M_{11} + M_{00}}{M_{11} + M_{00} + M_{01} + M_{10}} \tag{1.1}$$

where M_{11} and M_{00} correspond to the total number of cases when both PHYSAT and the threshold model attributed diatom (M_{11}) or non-diatom (M_{00}) to a pixel and M_{01} and M_{10} correspond to the cases when they attributed different dominance. For the case of the probability comparison, we used the formula:

$$J(physat, threshold) = \frac{\sum_i min(physat_i, threshold_i)}{\sum_i max(physat_i, threshold_i)} \tag{1.2}$$

where *physat* and *threshold* represent two vectors corresponding to the pixels of the probability maps and i represents their length.

Results

Identification of niches for diatom dominance

The spatial variability in the amount of fucoxanthin measured at the KEOPS2 stations (dots in Figure 1.2 a) spans one order of magnitude, indicating big differences in diatom concentration on the scale of few hundreds of kms. Its distribution does not display any clear gradient, and that cannot be related directly with the geographical distance from the Kerguelen Plateau.The east-west transect presents a minimum fucoxanthin concentration around 72-73 ° E and an increase towards the stations farther from the plateau. A similar structure can be found in the North-South transect, suggesting

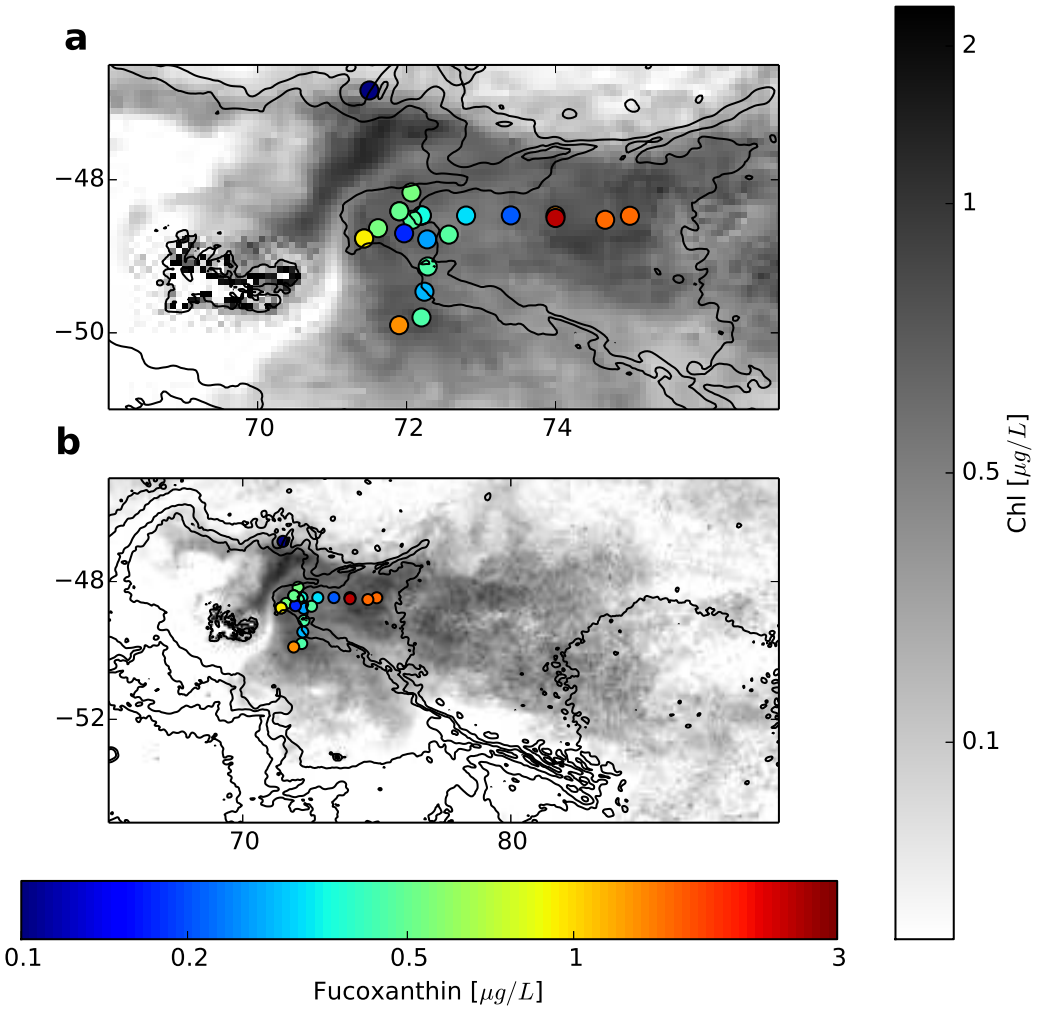

FIGURE 1.2: (a) Spatial distribution of fucoxanthin (at 40 - 90 m) measured during KEOPS2 (colored dots) overlapped with a November 2011 climatology of chlorophyll concentration measured from remote sensing (grey scale). (b) The same quantities showing the extent of the Kerguelen plume.

that there is a specific area that is less diatom-favourable than the surroundings. A climatology of the distribution of chlorophyll in November, shown in the backgrounds of Figures 1.2 a) and b), suggests that spatial variability in fucoxanthin concentrations may not be simply recapitulate a typical recurring plume structure.

Biogeochemical studies [d'Ovidio et al., 2015, Grenier et al., 2015] -after [Mongin et al., 2009, Sanial et al., 2014a]- suggest that the ecological success of diatom East of Kerguelen may be related to the "water age", i.e. the time since water was in contact with the plateau, and this is supported by our analysis (Figure 1.3, Pearson's $corr = -0.66$, $p - value = 5 * 10^{-4}$).

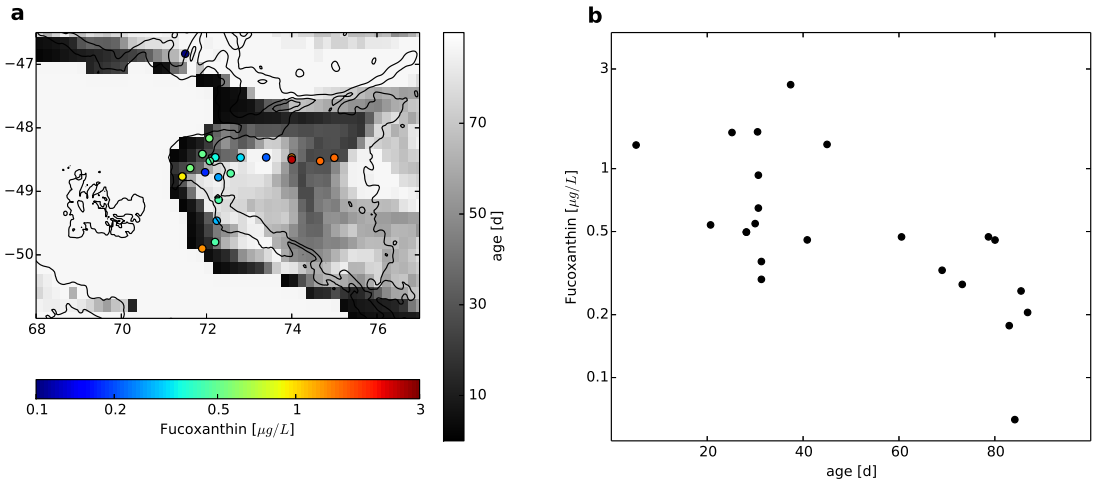

FIGURE 1.3: (a) Spatial distribution of fucoxanthin (colored dots) overlapped with a November 2011 climatology of water age (estimated using Lagrangian analysis) suggesting that fucoxanthin concentrations decline with the time since water was in contact with the plateau. This negative trend is displayed (b) ($corr = -0.66, P = 5 \cdot 10^{-4}$).

Water age as an environmental driver of dominance

Water parcels characterized by small values of water age appear to be particularly favourable for diatoms. To describe how the relative abundance of diatoms is reflected in whether diatoms dominate the phytoplankton community in different regions, and to expand coverage to the full extent of the Kerguelen plume, we relate PHYSAT observations with water age. The best fitting GAM model is:

$$odds(diatom\ dominance) \sim -0.31 + s(age) \tag{1.3}$$

were s(age) is the GAM smooth function ($P < 2 * 10^{-16}$) that best fits the data (Figure 1.4). For the first 30 days the trend is the expected one; the odds of observing diatoms as the dominant phytoplankton decrease as the age of the related water parcel increases. However, after the first month of advection, the odds increase between 40 and 60 days, and then decrease again. The AUC of the ROC for this model is 0.61, suggesting that, in spite of being statistically significant, the GAM fit may not be sufficiently accurate to predict diatom-dominance from the ages of water parcels with a level of certainty that is useful. This model allows however to test against satellite observations coarse-grained predictions of diatom dominance, based on projections of the model in the Kerguelen plume, where no in situ data are available.

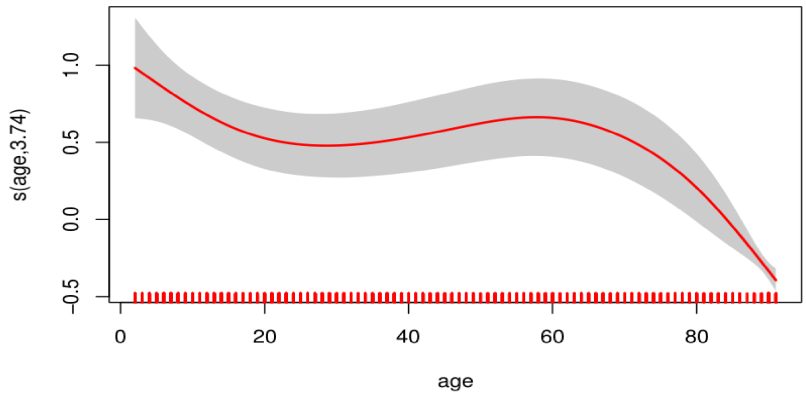

FIGURE 1.4: Smooth function for the GAM statistical model showing the relation between the log(odds) of observing diatom dominance and age of the water parcel. The grey bands indicate the upper and lower 95%-confidence limits.

Reconstructing biogeography from ecology and transport

A further elaboration of this approach is to define a simple mechanistic "threshold" model by combining the findings presented above with the biogeochemical hypotheses discussed in [Trull et al., 2014] and [d'Ovidio et al., 2015].

The "threshold model" is based on the assumptions that:

1. **bottom-up ecological effects:** iron is the sole resource determining the success of diatoms, that establish their dominance by competitive exclusion by of other phytoplanktonic types;
2. **ocean dynamics:** the main source of iron is the Kerguelen Plateau; water enriched over the plateau is horizontally advected according to geostrophic currents;
3. **biogeochemistry:** iron's is lost at constant rate during the blooming and the post-blooming seasons, following the equation:

$$dFe/dt = -(k_1 * t_1 + k_2 * t_2) \tag{1.4}$$

where k_1, k_2 represent iron loss rates rates associated with abiotic scavenging and phytoplankton consumption respectively, and are estimated as $k_1 = -0.041 d^{-1}$ and $k_2 = -0.058\, d^{-1}$ [d'Ovidio et al., 2015]. These values are estimated by measuring dissolved iron (i.e. the form of iron that is more likely to be available for phytoplankton growth [Bowie et al., 2014, Quéroué et al., 2015, d'Ovidio et al., 2015]) at stations corresponding to different water ages. These values are also consistent with the estimates of iron export in free-floating traps [Laurenceau et al., 2014].

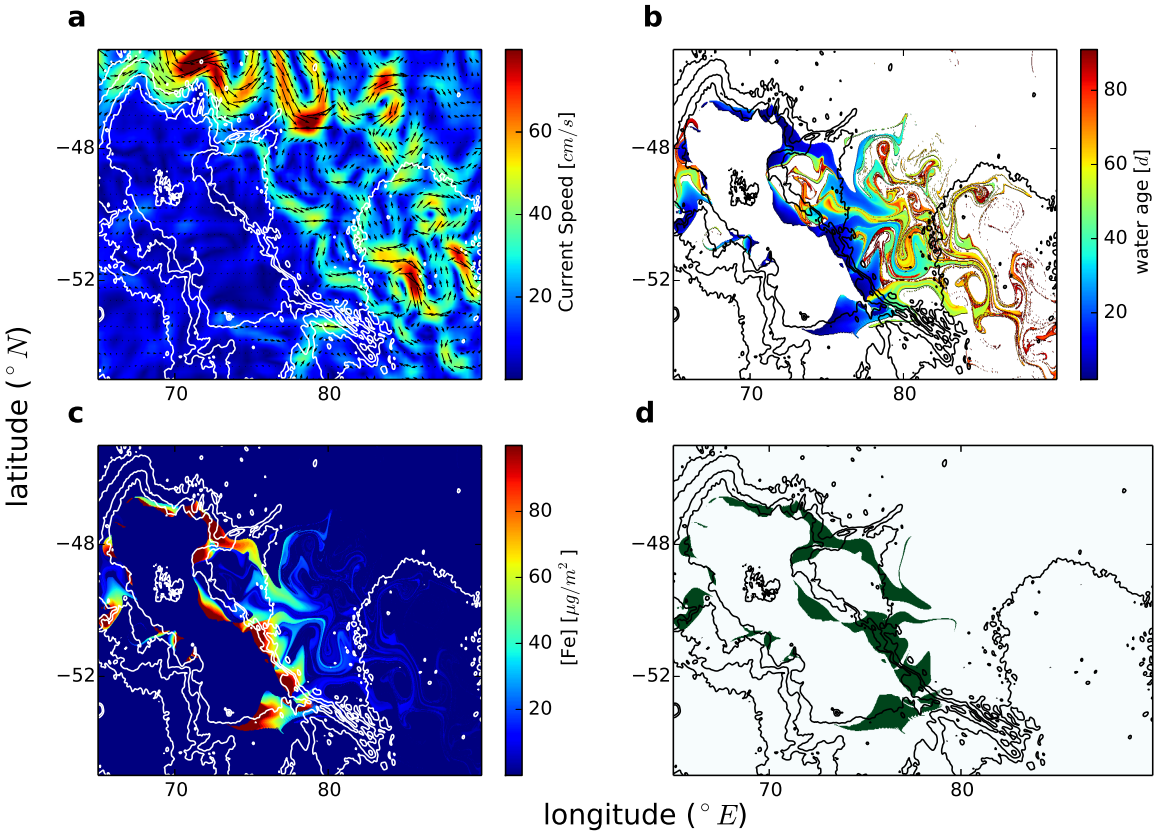

FIGURE 1.5: Conceptual scheme of the threshold model: (a) horizontal velocities derived from altimeter data are (b) integrated to compute water age . Assuming exponential loss, water age is used to calculate (c) a proxy for iron concentration , and iron concentration is then used to identify (d) areas of diatom dominance .

The times t_1 and t_2 represent the time since a specific water parcel left the plateau during the winter and during the blooming season respectively, such that:

$t_1 + t_2 = water\ age.$

Given differential equation 1.4 the quantity of available dissolved iron for a water parcel can be computed as:

$$[Fe] = [Fe_0]\, e^{k_1 * t_1 + k_2 * t_2} \tag{1.5}$$

where $Fe_0 = 150 \mu mol/m^2$ has been estimated in Ref.[d'Ovidio et al., 2015].

4. **top-down ecological effects:** grazing by zoo-plankton is proportional to phyto-plakton growth.

Given hypotheses (1) and (4) this model is expected to capture the dynamics of the beginning of the phytoplankton bloom (months of November and December), but later

in the season other factors such as grazing and silicates limitation gain importance in determining the dominant type [Mosseri et al., 2008, Quéguiner, 2013].

To predict the phytoplankton type dominating a water parcel (represented as a $\sim$ 20 km pixel) we compute its trajectory backward in time by integrating the altimetric velocity field (see Figure 1.5 a), and calculate the age of the water (Figure 1.5 b). Assuming constant iron loss rates [d'Ovidio et al., 2015], this Lagrangian diagnostic is used to quantify a proxy for iron content following equation 1.4 (Figure 1.5 c). Finally, according to the first hypothesis, we consider that diatoms and other types of phytoplankton compete only for iron acquisition. The principle of competitive exclusion [May, 1977, Hardin et al., 1960, Collie et al., 2004] thus predicts that only one type will dominate the community. It is expected that iron stress favours smaller-size phytoplanktonic organisms, that are more efficient at absorbing nutrients. On the contrary, in iron-rich water larger diatoms, who owe their fast growth rate to their opportunistic life strategies, are predicted to dominate the community. Trends that are coherent with this intuitionis approach have been observed both in coastal and open ocean environments limited by silicates [Rousseau et al., 2002, Lochte et al., 1993], and in microcosm experiments [Fernandez et al., 1992]. The model has only one free parameter, that is the threshold in iron concentration that separates the cases when either diatoms or other types win the competition. Depending on such a threshold, the predicted biogeography, hence the map of diatom dominance, can change a lot. We looked at two different sets of observables for the comparison of model and observation. The first is the probability of observing diatoms in a given location, computed as the frequency of occurrence of diatoms across all days when the PHYSAT algorithm provides estimates of the dominant type. The second is the entire dataset of pixel by pixel day by day binary maps. We compared the two sets of observables using the two versions (non-binary and binary respectively) of the Jaccard index in order to chose the value of the threshold for which they are maximal. Using an the probability maps we obtained a value of 2 $\mu mol/m^2$, having J(probability)=0.39. A similar result is obtained by matching the Jaccard binary similarity using the pixel by pixel data from PHYSAT, with a J(binary)=0.36. Comparing the probability of observing diatom dominance based on observations obtained from PHYSAT (Figure1.6 a) with that computed using the threshold model (Figure 1.6 b) indicates that while the model captures the longitudinal extent of the high probability (P $>$ 0.75) of diatom dominance propagating eastward, it does not describe the patch of probabilities $\sim$ 1 located around lon = 85 $^\circ$ identified using PHYSAT. The locations of the intrusion of diatom-poor waters from the south around (78°, $-$52°) indicated from PHYSAT observations are matched by the model, but other inhomogeneities in the distribution of diatoms within the plume indicated from PHYSAT observations tend to be shifted or missing in the model predictions. Finally, the patches West of the plateau and on the

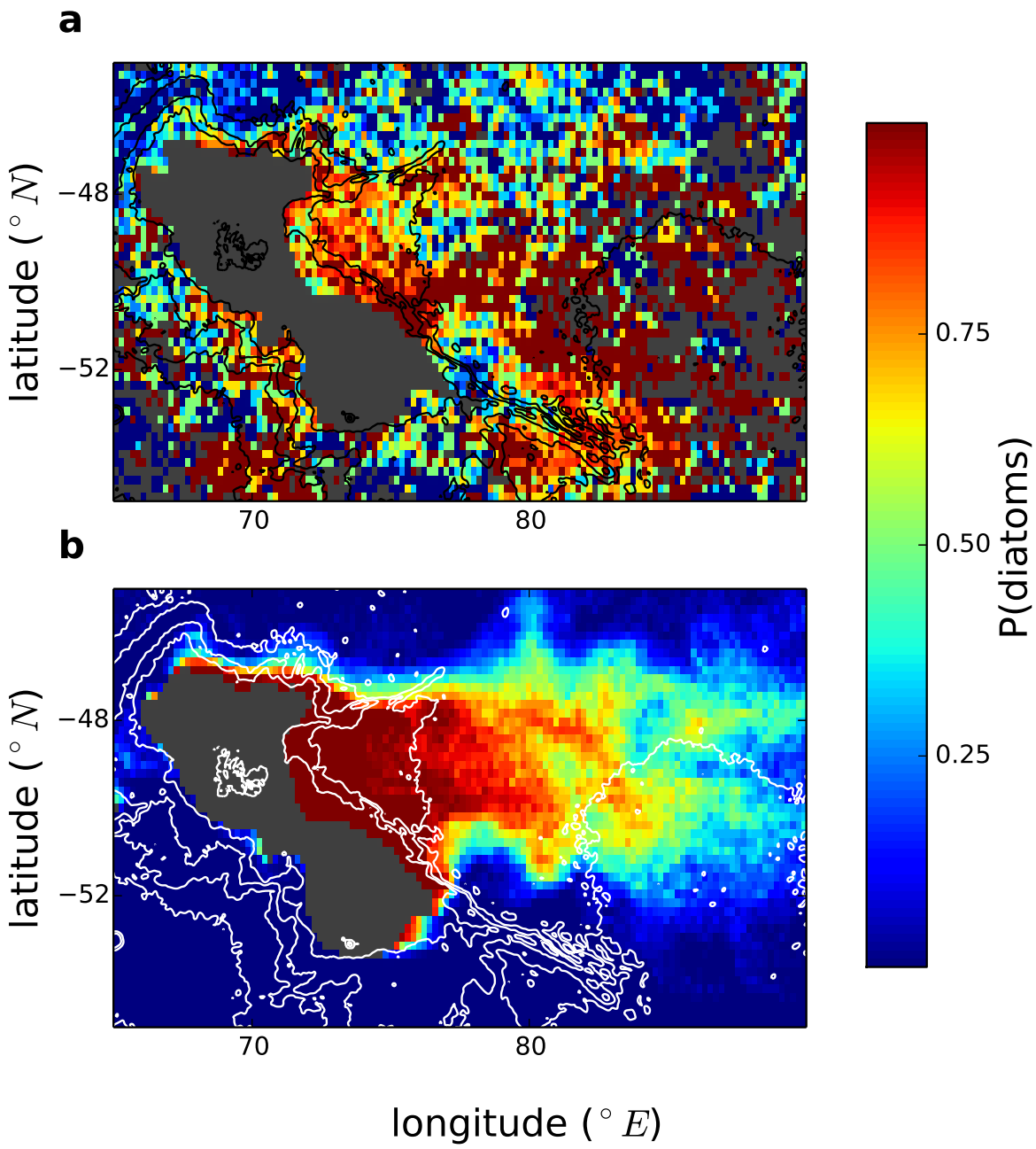

FIGURE 1.6: Probabilities of observing diatoms computed using a) PHYSAT and b) the threshold model.

William's Ridge (80°, −52°) where PHYSAT observations indicate a high probability that diatoms will dominate are not predicted by the model.

Discussion

Our results indicate that, even if during shipboard studies diatoms are observed ubiquitously in the study region, the distribution of areas where they may be expected to dominate the phytoplankton assemblage is patchy. This spatial variability can be interpreted within the framework of Lagrangian approaches applied previously in this area [Mongin et al., 2009, d'Ovidio et al., 2015, Sanial et al., 2014a]. The negative correlation between fucoxanthin concentration measured in situ and water age suggests that iron scavenging and consumption affect the suitability of water parcels for diatom growth. We interpret this pattern to indicate that, because of these processes, the probability of observing diatom dominance over other phytoplankton types decreases with time since a water parcel was in contact with the plateau. On this basis, estimates of the likelihood of diatom dominance can be extended to encompass the full extent of the phytoplankton plume using remotely-sensed observations from PHYSAT [Alvain et al., 2005].

Pixel by pixel day by day analysis using General Additive Models found a significant relationship between diatom dominance indicated from analysis of PHYSAT observations and water 'age'. These results are consistent with previous works that found that meso and sub-mesoscale features affect phytplankton abundance and community structure in models [Bracco et al., 2000, Perruche et al., 2011, Levy et al., 2001, Lévy, 2003] and observations [d'Ovidio et al., 2010, Abraham, 1998] by structuring the distribution of nutrients but also separating competing groups.

However, the shape of the GAM smooth function displayed in Figure 1.4 relating the odds of observing diatom-dominance with the age of water parcels exhibits an unexpected trend. For the first 30 days of backward advection, the odds of observing diatom-dominance decrease with time, consistent with a loss of iron due to abiotic scavenging and phytoplankton consumption. However, after the first month of advection the odds then increase before rapidly decaying to fit the numerous pixels that have never touched the plateau and are largely dominated by non-diatom communities. The peak of odds to observe diatom-dominance around 60-70 days is an unexpected result. Possible explanations include:

1. **Vertical movements induced by sub-mesoscale stirring.** Identifying water parcels of age $>$ 40 d with diatom dominance in PHYSAT – that correspond to pixels responsible for the high probability of observing of diatom dominance for high water ages- reveals a concentration of pixels in the south-east of the domain (Figure 1.7 a). Both analysis of horizontal velocities from altimetry [d'Ovidio et al., 2015] and models [Klocker et al., ress, Rosso et al., 2014] indicate that this region has high kinetic energy (Figure 1.7 b). This highly energetic meso and

sub-mesoscale activity, which enhances vertical stirring, may lift iron-rich waters into the upper layers of the water column, thus introducing a different source of iron than what considered in the threshold model.

2. **Differential initial enrichments due to seasonal changes in the mixed layer depth (MLD).** Since we conducted our analysis for the month of December, water parcels with a 'water age' of two months were enriched during the month of October. Monthly climatologies suggest that in October the MLD on the Kerguelen Plateau varies from 100-250 m, whereas in November and December (i.e. corresponding to water parcels of age < 60 d) the MLD is shallower [Sallée et al., 2010] and thus total iron in the mixed layer would be less than for water > 60 d age. Overlapping the GAM smooth function and MLD (computed at the location where and when water parcels have left the plateau) shows that MLD for water parcels 'younger' than 40 d rarely exceeds ~ 120 m at the location and time of enrichment on the plateau, while the MLD for water parcels of age ~ 60 days tends to be greater. We note however, that to achieve the same iron enrichment at ~ 60 days age as at 10-20 days of water age (inferred from identical log-odds of observing diatoms as the dominant phytoplankton type – see Figure 1.7 c), given exponential loss of iron, enrichment in October would have to be 5 to 10 times larger than that in November and December.

3. **Accumulation of error during advection.** Theoretical and modelling studies [Özgökmen et al., 2000] have shown that (i) the accuracy of simulated trajectories decreases with time, and (ii) that the magnitude of inaccuracy can be highly spatially and temporally variable depending on local sub-meoscale dynamics. Therefore it is not unlikely that after 30 days of advection, a pixel 'mismatch' could appear such that a given level of iron estimated in the model might equate with actual observations but be displaced spatially by one or more pixels. This form of mismatch would affect our analysis, especially for pixels with water ages between 30 and 60 days since these are more likely to be surrounded by pixels with a very different water age, whereas pixels corresponding to water ages > 60 days are likely to be surrounded by other "old" water parcels.

4. **Oversimplified ecological dynamics.** The threshold model neglects ecological interactions other than competition for iron. After a water parcel has been enriched and diatoms have been able to grow, grazing by zooplankton, competition for other nutrients (e.g. limitation by silicates could be relevant [Blain et al., 2001]) and bacterial remineralization of iron may all affect diatom relative abundance. We exclude that our result may be explained by the role of limitation by silicates, as we are focusing on the beginning of the bloom and it would negatively effect diatom

dominance, while we observed unexpected favourable regons. Instead differences in grazing pressure between diatoms and other groups of phytoplankton, more prone to top-down control from grazers, may be a possible mechanism behind the unexpected trend. Another important mechanism that is underestimated in this model is remineralization, that may be able to extend in time the availability of iron for phytoplankton growth.

5. **Limits in resolving community composition.** PHYSAT generically identifies diatoms without distinguishing between different types of diatoms. Queguinier [Quéguiner, 2013] compared observations from natural and artificial iron fertilisation and suggested that there is a succession of different types of diatoms of a large range of sizes that respond differently to silicate limitation and grazing. His analysis suggests that an initial group of diatoms characterised by large size, high growth rates, and rapid onset of limitation by iron and other nutrients dominate the phytoplankton biomass at the beginning of the spring bloom. Later in the summer a second group of much smaller diatoms, characterised by low maximum growth rates but high efficiency of uptake at low nutrient concentrations, and resistance to grazing, increase in biomass to dominate the community. From a Lagrangian perspective, this phenomenon could explain the peak in log-odds (Figures 1.4 and1.7 c) corresponding to "old" water parcels of $\sim$ 60 days age.

While all five mechanisms are possible, we are unable to identify which is the major (or only) one underpinning the phenomenon.

Even though it is statistically significant, it needs to be emphasised that the GAM relationship does not perform particularly well in predicting the PHYSAT observations, as indicated by the AUC value of 0.61. However, the choice of a pixel by pixel comparison is a very strict test, and a simple spatial shift in dominance patterns (e.g. estimates that are spatially displaced by one or a few pixels) would be identified as a fail by this test. Alternatively, this result might indicate that, even if advection of iron eastwards from the plateau is a key mechanism determining biogeochemical provinces in the region in terms of favourability for and dominance by diatoms, water age may not be an efficient predictor of the nature of the phytoplankton community found in a specific water parcel. This is in line with shipboard studies close to and on the plateau itself which indicate that factors other than iron availability, such as upper water stratification [Trull et al., 2014], silicate limitation [Blain et al., 2001], and zooplankton grazing [Laurenceau et al., 2014], may modulate primary production and community composition. These other mechanisms could be tested by conditioning the probability that diatoms dominate at high iron (that is in our case 1) to a different initial condition, or building a more complicated ecological model. The threshold model assumes that planktonic communities are

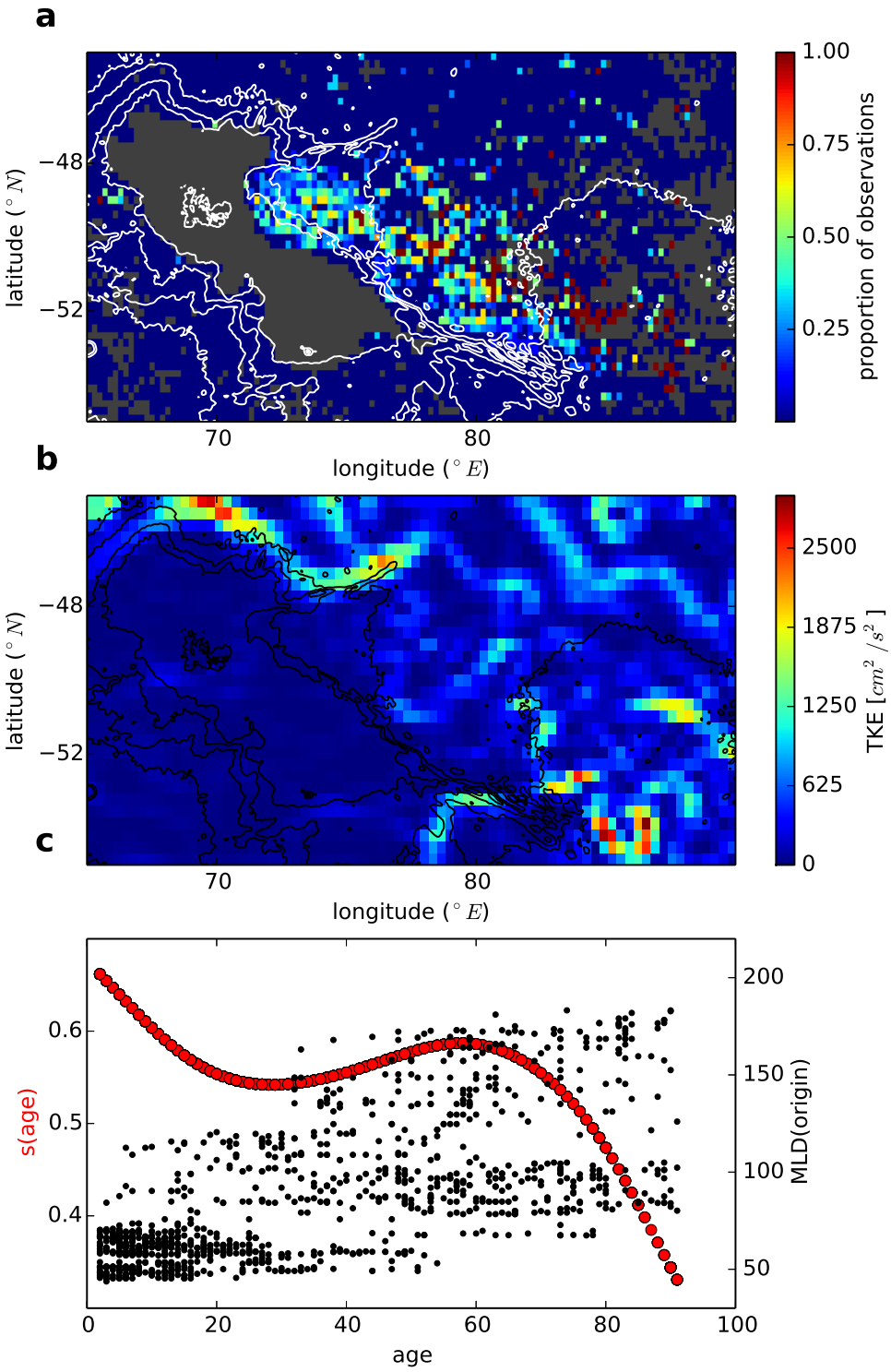

FIGURE 1.7: (a) Proportion of observations from PHYSAT (insert dates) indicating domination by diatoms where water age is >40d. (b) Example of a total kinetic energy (TKE) map for the study region. The region in the South East of the domain that in (a) is characterised by a high proportion of diatom dominated pixels having water age>40d correspond qualitatively to a highly energetic region. c) The GAM smooth function (red dots) compared to the mixed layer depth (MLD) computed at the time and location of each water parcel leaving the plateau.

initially identical when they are on the plateau, so that their dynamics is driven mainly by iron availability after enrichment. However, a different composition of the community, even without subverting the dominance pattern, may lead to different outcomes due to differences in iron scavenging. For instance, a community entirely composed of diatoms will exhaust the available iron faster than one composed by a mixture of diatoms and nanoplankton. Modelling this aspect would require to make the competition model explicit.

Nonetheless, as shown in the comparison of the maps predicting diatom dominance derived from PHYSAT or the threshold model (Figure 1.6), the "threshold" model is successful in capturing the broad extent of the area where diatoms have a high probability of dominating phytoplankton community structure. A final point worthy of consideration is that the optimal threshold for the model is surprisingly low at 2 $\mu mol/m^2$ iron, and there are several possible reasons. First, the iron loss rates measured during KEOPS2 may be overestimates. While these measurements are currently the best available for the region and are of the same order as those estimated by Mongin et al. necessary to reproduce the extent of the chlorophyll plume [Mongin et al., 2009], they are very few in number. Second, we may have underestimated the horizontal velocity field as a result of inaccuracies in the altimetry. Third, we have ignored the potential importance of the composition of the 'initial' community present in a water parcel as it leaves the plateau; it is possible that the ecological dynamics of the planktonic community in water parcels 'inoculated' with a community dominated by large diatoms may manifest inertia to transition to a community dominated by small non-diatom phytoplankton. An intriguing possibility is that the dynamic of the planktonic community in this region is characterised by ecological hysteresis [Begon et al., 1996]. In this scenario, a community initially dominated by large diatoms and subject to declining iron concentrations would transition to domination by other phytoplankton types (e.g. nanophytoplankton) at much lower iron levels than would maintain nanophytoplankton dominance when the initial 'inoculum' was dominated by nanophytoplankton. This mechanism could explain our finding that the model underestimates dominance by diatoms (Figure 1.6), similarly to modelling studies elsewhere in the Southern Ocean in which hydrodynamic biogeochemical models underestimate chlorophyll concentrations [Borrione et al., 2014].

Conclusion

The results of this study are consistent with previous studies in finding that favourable areas for diatom growth appear related to iron supply from the Kerguelen Plateau (i.e. low values of water 'age'). Younger water parcels, recently enriched in iron by contact

with the plateau, correspond to higher fucoxanthin concentrations and are more likely to indicate dominance by diatoms in remotely sensed observations. The "threshold" model combines this result with exponential loss of iron and a threshold to estimate when diatoms are likely to dominate the planktonic community at specific locations. The shape of the statistical relationship between water age and observed dominance, its performance on the pixel by pixel comparison, and the optimal threshold for the threshold model suggest that while iron availability is likely to be an important factor in determining favorability for diatom growth and their dominance over other phytoplankton groups, other mechanisms like grazing and perhaps silicate availability should be considered. However, since information on these kinds of additional ecological processes can be very difficult to obtain, the threshold model remains a useful tool to define approximate biogeographical boundaries of diatom dominance in the Kerguelen bloom.

Chapter 2

Alternative stable states in a model of the ecological dynamics of the Kerguelen phytoplankton community

This chapter will be submitted as *Alternative stable states in a model of the ecological dynamics of the Kerguelen phytoplankton community* by A. Della Penna, S. Wotherspoon, T. Trull, S. De Monte, F. d'Ovidio, C. Johnson.

Abstract

Systems allowing multiple stable states have been the object of several theoretical studies, yet demonstrating their existence in nature and predicting potential phase shifts between states is challenging. Here we analyse the naturally iron-fertilised Kerguelen ecosystem (Indian Sector of the Southern Ocean) as a possible candidate for a bistable system. We develop and parametrise an ecological model to describe the dynamics of the two broad functional groups of phytoplankton in the region (large diatoms and smaller pico- and nano-phytoplankton) and iron, as the main driver for the Kerguelen system. For realistic values of the parameters and across a range of concentrations of available iron, the system demonstrates bistability so that either phytoplankton group can dominate under identical environmental conditions. The ramifications of this dynamic for the upper levels of the trophic web were examined using a qualitative trophic model representing interactions among 10 functional groups of the planktonic system. We find

that, consistent with observations in other regions of the Southern Ocean, phytoplankton communities dominated by large diatoms are likely to support the growth of fish larvae and crustaceans and consequently the development of favourable foraging grounds for fish (myctophids) and top predators, while dominance of nanophytoplankton favours proliferation of salps, ctenophores, and jellyfish which are not favoured prey of fish and top predators.

Introduction

Bistable systems have been observed in a variety of ecological contexts in marine [Van Nes et al., 2007, Steneck et al., 2002, Ling and Johnson, 2009, Nyström et al., 2000, Marzloff et al., 2011, Mumby et al., 2007, Fung et al., 2011, Marzloff et al., 2013] and freshwater [Scheffer and van Nes, 2007] environments. In contrast to systems whose state variables respond smoothly to external forcings, systems that allow multiple stable or persistent states, i.e. discontinuous phase shifts, manifest tipping points in dynamics and inertia or hysteresis over some range of conditions. Hysteresis describes the inability of a system to return an "original" stable state after a forcing has moved the system to a tipping point, and subsequently a new stable state, and the forcing is then relaxed and environmental conditions return to their previous form [Scheffer et al., 2001]. The change from one stable state to another often occurs quickly, over a time-scale that is much shorter than the time scale of persistence of either state [Scheffer et al., 2001], but catastrophic phase shifts may also occur very slowly so that 'tipping' points are difficult to recognise [Hughes et al., 2013]. Systems that allow multiple stable states have been the object of several theoretical studies [Lenton, 2013, Scheffer et al., 2001], yet demonstrating their existence and predicting potential regime shifts is challenging [Marzloff et al., 2011, Petraitis and Dudgeon, 2004]. For example, coral reefs have been observed to quickly transit from a state of coral dominated benthos to a macroalgal dominated one in response to relatively small changes in the environmental conditions [Mumby, 2009]. The alternate states between kelp forests and sea-urchins and calcareous algae dominated seabed in temperate coastal regions is another classical, but more discussed example [Estes and Duggins, 1995, Steneck et al., 2002, Ling et al., 2015].

However, most of the known systems exhibiting multiple stable systems refer to benthic or coastal ecosystems. Very few examples, if any, come from pelagic ecosystems. Because open ocean ecosystems are often located in remote regions characterized by generally harsh conditions, it is difficult to gather the long time series usually necessary to evaluate the possibility of bistable (or multiple) states ecosystems. In addition, open ocean ecosystems are embedded in a complex and dynamical medium that greatly influences

ecological dynamics and which can maintain ecological dynamics well away from any quasi-equilibrium state. Trophic interactions and typical ecological timescales (e.g. the duration of phytoplankton blooms, foraging trips of predators, etc.) overlap with the so-called "ocean weather". The ocean mesoscale and submesoscale (that together refer to phenomena ranging 1-100 km, days to months) are well known to oceanographers to be characterised by strong gradients and highly energetic structures such as eddies and fronts, i.e. the ocean equivalent of weather systems [Chelton et al., 2007]. Disentangling high spatial and temporal variability in the physical system from changes in the ecology is challenging, especially when observations are sparse.

These issues are particularly germane in the remote Southern Ocean, which is characterized by harsh weather and dominated by the turbulent circulation of the Antarctic Circumpolar Current (ACC), the largest current in the world. Observations from the region in the proximity of the Antarctic Peninsula (69.5S, 65W) suggest spatial and/or temporal segregation of alternative states in which large diatoms drive high rates of primary production and supports a zooplankton community dominated by krill, versus a state dominated by small phytoplankton which supports a zooplankton community dominated by salps [Moline et al., 2004, Montes-Hugo et al., 2009,

, Loeb et al., 1997]. Krill plays a pivotal role in transfering biomass from plankton to large marine predators [Loeb et al., 1997] and therefore years and areas when they dominate are likely to be favourable for large predators. Similarly, observations on Prince Edward Island, in the Sub-Antarctic, suggest that locations where euphausiacea dominate the zooplankton community correspond to areas of high primary production of large diatoms, whereas the stations with high concentrations of tunicates correspond to phytoplanktonic communities dominated by pico and nanoplankton [Pakhomov and Froneman, 1999b]. In the waters east of the Kerguelen Islands (Indian Sector of the Southern Ocean), a similar spatial and temporal segregation of distinct zooplankton communities dominated by either crustaceans and fish larvae, or salps, jellyfish, and other gelatinous zooplankton, has been reported by experienced observers (G. Duhamel, personal communication to C. Johnson).

In this study, we analyse the potential for the dynamics of the Kerguelen to manifest as alternative stable states. Most of the Southern Ocean is a High Nutrient Low Chlorophyll region (HNLC) because of scarceness of iron, an essential element for phytoplankton growth [Boyd et al., 2007, De Baar et al., 2005]. The Kerguelen Islands are located at the top of a plateau whose shallow ($\sim$ 1000 m) bathymetry interacts with the dynamical fronts of the ACC re-suspending dissolved iron from deep reservoirs and sediments [Blain et al., 2007, Quéguiner, 2013]. This natural iron enrichment supports one of the largest phytoplankton blooms of the Southern Ocean that extends over the Kerguelen Plateau

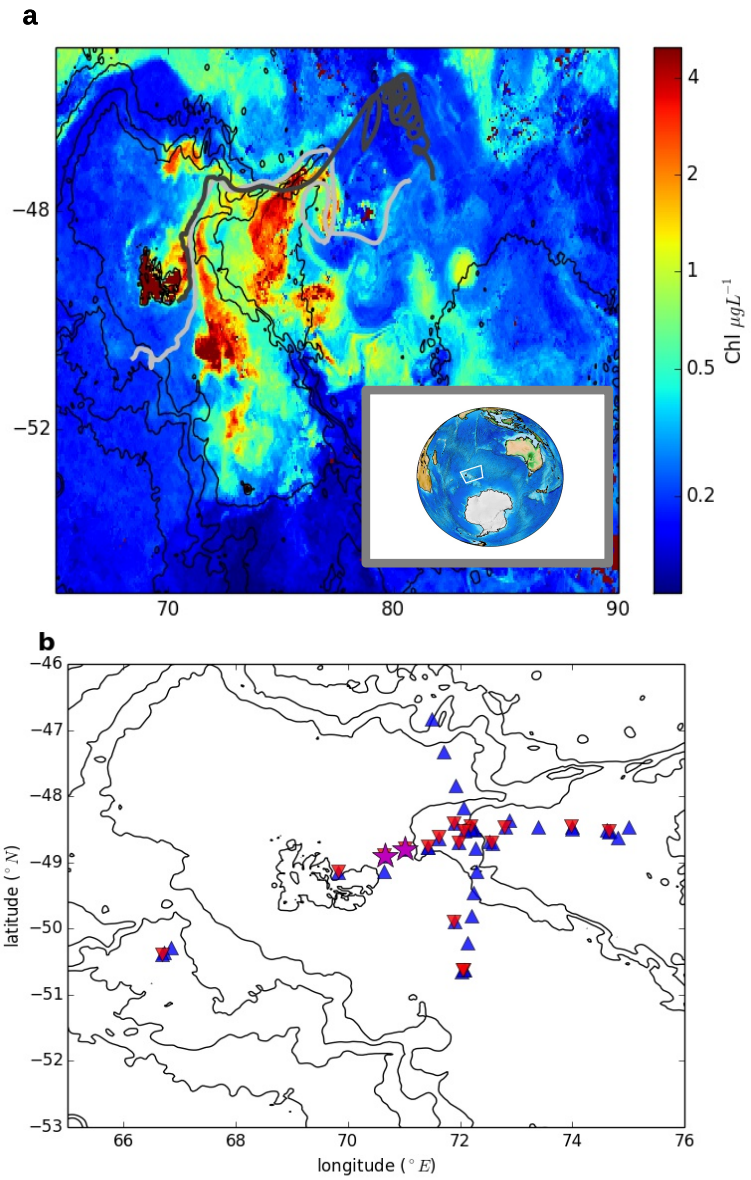

FIGURE 2.1: a) Remotely sensed surface chlorophyll observed during the bloom (11/11/2011) near Kerguelen Island (Indian Sector of the Southern Ocean, see insert). Black contours refer to the bathymetry. Grey lines correspond to the drifters trajectories. b) Most in-situ observations refer to the Kerguelen plateau and its vicinity: blue triangles correspond to sites of pigment samples collection and red reversed triangles to iron measurements. Purple stars represent stations TEW-2 and TEW-3, the stations used to compare spatial patterns.

and downstream in a 1000 km plume [Mongin et al., 2009]. Biogeochemical field programs have found that the Kerguelen bloom is mainly dominated by large diatoms [Armand et al., 2008] that sustain a rich zooplankton community [Carlotti et al., 2015] includingeuphausids and fish larvae, especially of myctophids. These meso- and macro-zooplankton, micronekton, and myctophids constitute the main prey of large fish, marine mammals and seabirds in the region. [Cherel et al., 2010, Goldsworthy et al., 2001, Guinet et al., 1996, Raclot et al., 1998]. Advection of iron enriched waters from the Plateau has been identified as a main driver of the bloom development [Mongin et al., 2009]. Waters that have been recently in contact with the Kerguelen Plateau can contain high concentrations of chlorophyll, indicated both measures in-situ (see Appendix B) and from space (see Appendix A), and their phytoplankton are typically dominated by diatom species, as measured through pigment sampling and estimated from ocean color images as shown in chapter 1. However, while it is well recognized that the relationship between horizontally advected dissolved iron and the community structure of primary producers is also affected by other physical factors including mixed layer depth and upper water column stratification [Trull et al., 2014], relatively few studies have focused on the ecological mechanisms that may affect the phytoplankton community composition of iron enriched waters. The goal of this paper is to evaluate the roles of iron availability, and inter- and intraspecific competition for iron acquisition, in determining the composition of the phytoplankton community in the Kerguelen plume and how the latter affects upper levels of the trophic web. We first implement the knowledge from natural and artificial iron fertilisation experiments into an ecological model describing the interaction between large diatoms, nanoplankton, and iron, and then assess the stability properties of the model for realistic parameter values derived from observations taken on the KEOPS2 (Kerguelen Ocean and Plateau compared Study 2, [d'Ovidio et al., 2015]) field program. To disentangle variability in the ecology and circulation patterns, we adopt a Lagrangian approach and provide a spatial interpretation of the output of the ecological model. We use realistic circulation patterns measured from drifter trajectories to study how conditions on different parts of the plateau are distributed in space by the local mesocale circulation. Finally, we investigate how different phytoplankton communities are likely to affect upper trophic levels by constructing a qualitative model that includes the major functional groups of plankton observed in the region, which we forcing it with different initial communities of primary producers.

Methods

Biogeochemical model structure

We considered two models, one including two phytoplanktonic types and iron (Model a)), and a simplified version of it in which iron is a parameter (Model b)). Both models describe the dynamics of two phytoplankton functional groups (see Figure 2.2), namely large diatoms (P_1), and nanoplankton (and picoplankton-like organisms) (P_2). Both models a) and b) share equations 2.2 for P_1 and P_2:

$$\frac{dP_1}{dt} = [U_1(P_1, P_2, Fe) - \sigma_1]P_1 \tag{2.1}$$

$$\frac{dP_2}{dt} = [U_2(P_1, P_2, Fe) - \sigma_2]P_2 \tag{2.2}$$

where $U_i(P_1, P_2, Fe)$ represent the growth rate for each type (detailed in the next paragraph) and the loss terms σ_i represent senescence, grazing by zooplankton, viral lysis and sinking.

Both groups need iron to perform photosynthesis but, consistent with empirical measurment, their maximum growth rates and iron affinities are different [Arrigo, 2005, Boyd et al., 2015]. Diatoms are adapted for exponential growth and contain a well developed cellular machinery to enable high growth rates when resources densities are high. However, as discussed in Ref. [Boyd et al., 2015, Boyd et al., 2012b], diatoms have lower affinity for iron and limited capacity to access recycled iron. In contrast, nanophytoplankton are modeled as 'survivalists' able to grow when resources are low, investing energy in a cellular machinery that is efficient at resource-acquisition and acquiring recycled iron, but having a relatively limited maximum growth rate when resources are not limiting. We use Michaelis-Menten shaped expressions described by the maximum growth rates $\mu_1 > \mu_2$ and half saturation constants for iron uptake $k_1 > k_2$. The growth rates of each group U_i are not just limited by iron availability, but also by the biomass of competitors from both their own and the other functional group (i.e. capturing both intra- and inter-specific competition):

$$U_i = \mu_i \frac{Fe}{Fe + k_i}(1 - \frac{P_i - \alpha_{ij}P_j}{k_c}). \tag{2.3}$$

The inter-specific competition is weighted by a coefficient α_{ij} (with $i \neq j$) that captures how much the abundance of one type (j) affects the growth of the other (i). k_c represents

the total carrying capacity of phytoplankton in the system. In model a) (see Figure 2.2 a) we consider iron to be a dynamical variable obeying:

$$\frac{dFe}{dt} = \gamma_1(-U_1 + R_1\sigma_1)P_1 + \gamma_2(-U_2 + R_2\sigma_2)P_2 - \lambda Fe. \tag{2.4}$$

This describes that iron concentrations decrease because of phytoplankton consumption (proportional to phytoplankton growth rates and abundances) and abiotic scavenging, as represented by the last term of the equation (iron tends to bind to sinking particles, so the concentration of iron of a water parcel tends to decrease exponentially even if there is no phytoplankton consuming it, as detailed in Ref. [d'Ovidio et al., 2015]). Thus, once water parcels have left the plateau iron concentration can only decrease. However, the decrease rate is limited by the rates of remineralisation of iron (R_1 and R_2) from deceased phytoplankton through the action of heterotrophic bacteria.

Model b) (see Figure 2.2 b) is a simplified version of model a) in which iron concentration is a parameter and kept constant at its initial value (i.e. representing a chemostat environment where iron is constantly replenished). This approximation allows determining the analytical solutions of the system to identify equilibria (which is not possible with model a)) and possible states characterized by the different phytoplankton groups.

Parameters

Table 2.1 summarizes the parameters of models a) and b). When possible, values from the parameters were taken from literature referring to the study region. Results from Sarthou et al. [Sarthou et al., 2008], who investigated the distribution and fate of biogenic iron during the Kerguelen bloom on the plateau during the summer, were used to quantify the iron quota of the two groups. We used results from incubation experiments from Sarthou et al.,2008 [Sarthou et al., 2008] and Brussaard et al., 2008 [Brussaard et al., 2008] for the estimation of σ_i (the combination of grazing, sinking and viral lysis) for both phytoplankton types.

In other cases, we used parameter values that were not measured directly in the study region but elsewhere in the Southern Ocean. This is the case for growth rates and half saturation constants. Results from [Timmermans et al., 2001, Timmermans et al., 2008, Timmermans et al., 2004] show that growth rates and half saturation constants for large diatoms range between $0.20 - 0.62 d^{-1}$ and $0.19 - 1.2 mumol Fe/m^3$ respectively. Since μ_1 is an estimate of the maximum growth rate, we chose to use the upper elements of this range and its associated half saturation constant. To parametrize the growth of P_2 we used data of Price et al., 1994 [Price et al., 1994]from the Equatorial Pacific (another

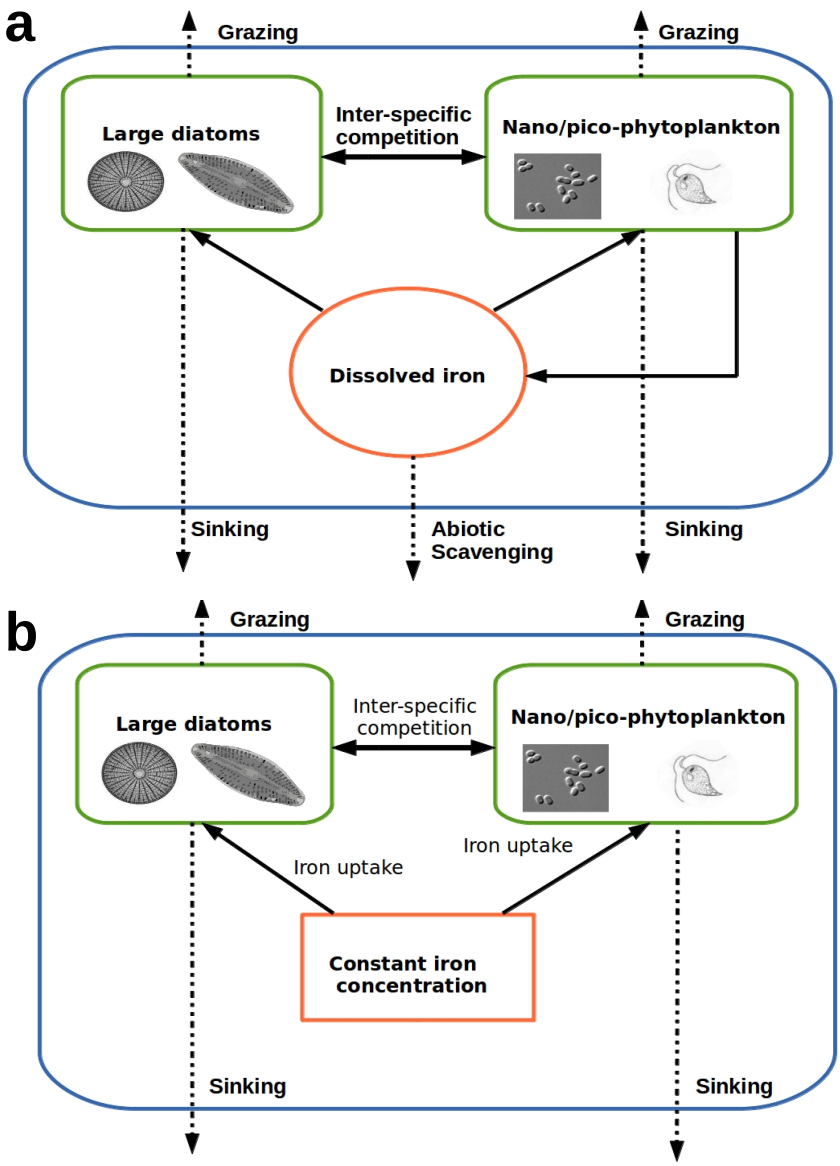

FIGURE 2.2: a) Model a), where iron is a dynamical variable and b) model b), where iron is considered constant, simulating a chemostat environment.

iron limited region), and from Mackey et al. 2015 [Mackey et al., 2015] who studied the response of oceanic species of *Synechoccocus* to iron limitation (although in the North Atlantic). The rate of iron remineralisation for nanoplankton was parametrized after Strzepek et al. [Strzepek et al., 2005], who measured iron regeneration from Synechoccocus during the artificial iron fertilisation experiment FeCycle off the coast of New Zealand [Boyd et al., 2012b]. For the remineralisation rate for diatoms, we argued that it will be very low relative to that for nanoplankton, and estimated it at 0.01% due to rapid sinking of large diatoms out of the euphotic layer.

The parameters most problematic to determine are the inter-specific competition coefficients and total carrying capacity of the system. For the carrying capacity we hypothesise that the total carrying capacity K across both functional groups is constant. Boyd and co-authors [Boyd et al., 2015] observed that biotic iron pools seem to be uniform across high and low-iron pelagic regions containing about $100 - 150 pmol/L$ iron. We use this estimate to calculate k_c by dividing this value for iron quotas (that are between 4-8 mol Fe : mol C) obtaining values of k_c that are of the order of 1 mol C. Since the inter-specific competition coefficients are hard to quantify we identify the range [0-2] that represents different plausible ecological conditions (see Discussion).

In-situ observations of biogeochemical parameters and initial conditions

To estimate the initial conditions for the different versions of the quantitative biogeochemical model we used observations from the KEOPS2 field program. In particular we used dissolved iron as an indicator for bio-available iron, Particulate Organic Carbon (POC) to infer the total biomass, and pigments to indicate initial community composition. To estimate the iron content of water parcels on the plateau we used measurements of dissolved iron. The sampling covered the northern part of the plateau (see reversed red triangles in Figure 2.1 b) with a zonal transect between 70-74 E between the October 20 and November 19 2011. More details about the 3D distribution of iron during the cruise can be found in Ref. [Quéroué et al., 2015]. We used the closest value of iron for initial conditions along the plateau, using values nearest to the surface. We also evaluated the amount of iron available at the beginning of the season, by using the T_{min} and S_{th} methods detailed in Ref. [Trull et al., 2014]. For each station we averaged the values sampled between the surface and the depth of the winter water temperature minimum when a remnant was present, i.e. south of the Polar Front. When the winter minimum remnant was not present we used shallower depths based on an increased in salinity of 0.05 respectively. We considered three possible values for the initial condition for iron: the values obtained using the T_{min} and S_{th} approaches, and that measured at the surface. For iron, we used two values representing "high" and "low" iron concentrations, viz. 1.26 $\mu mol/m^3$ (measured at the TEW-2 station, lon= 70.65 E, lat= 48.88 S; see Fig. 7.1) and 0.19 $\mu mol/m^3$ (measured at the TEW-3 station, lon = 71.02 E , lat = 48.78 S; see Fig. 7.1).

To describe the initial phytoplankton community structure we combined POC and pigments measurements. To make sure that our biomass estimates referred only to phytoplankton we used the size-fractionated POC sampling (see Ref. [Trull et al., 2014]) for fractions below 50 μm (even if considering also the size fraction $> 50\mu m$ and $< 210\mu m$

TABLE 2.1: Parameters used in models a) and b)

Parameter	**Meaning**	**Unit**	**Reference**	**Value**
μ_1	Diatoms' growth rate	d^{-1}	Timmermans et al., 2001	0.62
μ_2	Nanoplankton's growth rate	d^{-1}	Timmermans et al.,2001, Mackey et al., 2015	0.39
k_1	Half saturation for diatoms' iron uptake	$\mu molFe : m^3$	Scharek et al., 1997, Timmermans et al., 2008	1.2
k_2	Half saturation for nanoplankton's iron uptake	$\mu molFe : m^3$	Price et al.,1994	0.03
α_{12}	Inter-specific competition: how nanoplankton affects diatoms	Dimensionless	*Hypothesis*	*[0,2]*
α_{21}	Inter-specific competition: how diatoms affect nanoplankton	Dimensionless	*Hypothesis*	*[0,2]*
k_c	Total carrying capacity of the system	$molC : m^3$	*Hypothesis*	*1*
σ_1	Diatoms' mortality	d^{-1}	Sarthou et al.,2008	0.15
σ_2	Nanoplankton mortality	d^{-1}	Brussaard et al., 2008	0.20
R_1	Remineralisation rate for diatoms	%	*Hypothesis*	*0.01*
R_2	Remineralisation rate for nanoplankton	%	Strzepek et al., 2005	25
γ_1	Iron quota for diatoms	$\mu molFe : molC$	Sarthou et al.,2008	4.4
γ_2	Iron quota for nanoplankton	$\mu molFe : molC$	Sarthou et al.,2008	8
λ	Iron abiotic scavenging rate	d^{-1}	d'Ovidio et al.,2015	0.041

would not change the estimate of more than $0.01\mu M$). We used pigments to evaluate the structure of the phytoplankton community. Different phytoplankton groups are characterised by differences in their pigment composition, as detailed in [Lasbleiz et al., 2014]. As a consequence the concentration of secondary pigments (as chlorophyll is common to all groups) can be used as an indicator of phytoplankton composition. Pigment sampling occurred at 30 stations (see blue triangles in Figure 2.1 b)) encompassing a range of latitudes along the northern part of the plateau. Details about the pigment sampling strategy and an exhaustive discussion of their 3D spatial distribution can be found in Ref. [Lasbleiz et al., 2014]. We estimated the biomassof large diatoms (P_1) by multiplying the POC($< 50\mu m$) by the ratio of fucoxanthin (the secondary pigment associated with diatoms) to the total amount of secondary pigments. Initial conditions on P_2 are computed as the product of POC($< 50\mu m$) and the ratio of all the secondary pigments less fucoxanthin over the total.

For two initial phytoplankton communities, one dominated by diatoms as at TEW-2 and the other by nanophytoplankton, abundances were estimated by multiplying pigment ratios and POC concentration (Table 2.2.

TABLE 2.2: Summary of the initial condition in two KEOPS2 stations presenting contrasting conditions.

station	**Fe**	**POC** $(1-50\mu m)$	**Pigment ratio**	$\mathbf{P_1}$ **Diatoms**	$\mathbf{P_2}$ **Nanopl.**
TEW-2	$1.26\ \mu mol/m^3$	$6.49\cdot 10^3 \mu mol/m^3$	0.88	$5.75\cdot 10^{-3} molC/m^3$	$0.73\cdot 10^{-3} molC/m^3$
TEW-3	$0.19\ \mu mol/m^3$	$9\cdot 10^3 \mu mol/m^3$	0.38	$3.42\cdot 10^{-3} molC/m^3$	$5.58\cdot 10^{-3} molC/m^3$

Realistic spatial patterns from drifters

To describe how phytoplankton communities on the plateau are advected in the open ocean east of Kerguelen, we used trajectories from drifters deployed during the KEOPS2 voyage (see Ref. [d'Ovidio et al., 2015] for more details about the strategy and methodology details). In particular we focused on two trajectories belonging to drifters that were particularly close to stations for which there were observations of pigments, POC, and dissolved iron and that presented contrasting conditions. The trajectories of the selected drifters are shown as grey lines in Figure 2.1 a).

Qualitative modelling

To study how upper levels of the trophic web respond to changes in the community structure of the primary producers we used a qualitative network analysis tool (Qpress library in R, available on https://www.rforge.net/doc/packages/QPress/00Index.html).

This package formally describes a network (in our case the trophic web model) as a qualitative Jacobian matrix where interactions can be positive, negative, or null. Then, a large number (in our case 10000) of random quantitative Jacobian matrices are generated that respect the sign conditions defined in the qualitative matrix. Each matrix is analysed for stability, unstable matrices are discarded, and the stable ones are used to assess the impact of an increase in one compartment (species or group; in our case large diatoms or nanoplankton) on the rest of the network.

Preliminary results

Stability analysis

Model a) has only a single trivial equilibrium because iron can only decrease as a result of uptake by phytoplankton and abiotic scavenging. However, it is useful to identify which phytoplankton functional group is dominant before the system reaches the equilibrium to assess whether large diatoms can bloom. To study this problem, we analyse the stability of model b), which represents a classical example of a system that can solved analytically. Model b) is actually an extension of the Lotka-Volterra model [Begon et al., 1996].

Setting the equilibrium condition:

$$\frac{dP_i}{dt} = 0, i = 1, 2 \tag{2.5}$$

it is possible to find 4 equilibria:

1. $$P_1 = \frac{Fe\mu_1 - Fe\sigma_1 - k_1\sigma_1}{Fe\mu_1}, P_2 = 0 \tag{2.6}$$

   and

2. $$P_1 = 0, P_2 = \frac{Fe\mu_2 - Fe\sigma_2 - k_2\sigma_2}{Fe\mu_2} \tag{2.7}$$

   where one group is driven to extinction ("exclusive" equilibria);

3. the trivial equilibrium $P_1 = P_2 = 0$ and

4.

$$P_1 = \frac{-Fe\mu_1\mu_2 + Fe\mu_1\mu_2\alpha_{12} + Fe\mu_2\sigma_1 + k_1\mu_2\sigma_1 - Fe\alpha_{12}\mu_1\sigma_2 - \sigma_1 k_2\mu_1\sigma_2\alpha_{12}}{Fe\mu_1\mu_2(1-\alpha_{12}\alpha_{21})}, \quad (2.8)$$

$$P_2 = \frac{-Fe\mu_1\mu_2 + Fe\mu_1\mu_2\alpha_{21} - Fe\alpha_{21}\mu_2\sigma_1 - \alpha_{21}k_1\mu_2\sigma_1 + Fe\alpha_{21}\mu_1 - \sigma_1 k_2\mu_1\sigma_2}{Fe\mu_1\mu_2(1-\alpha_{12}\alpha_{21})} \quad (2.9)$$

where the two groups coexist .

We are particularly interested in the case where either exclusive equilibrium can be realized from the same set of parameters but different initial states. This condition can be written as a condition of the eigenvalues of the exclusive equilibria, and can arise if both eigenvalues at both exclusive equilibria are negative. In this circumstance, nanophytoplankton will dominate when:

$$\frac{Fe\mu_2 - Fe\sigma_2 - k_1\sigma_2}{Fe + k_2} > 0 \quad (2.10)$$

$$\frac{-Fe\mu_1\mu_2 + Fe\alpha_{12}\mu_1\mu_2 + Fe\mu_2\sigma_1 + k_1\mu_2\sigma_1 - Fe\alpha_{12}\mu_1\sigma_2 - \alpha_{12}k_2\mu_1\sigma_2}{(Fe + k_1)\mu_2} > 0 \quad (2.11)$$

while an equilibrium of exclusive occupancy by large diatoms occurs when:

$$\frac{Fe\mu_1 - Fe\sigma_1 - k_1\sigma_1}{Fe + k_1} > 0 \quad (2.12)$$

$$\frac{-Fe\mu_1\mu_2 + Fe\alpha_{21}\mu_1\mu_2 - Fe\alpha_{21}\mu_2\sigma_1 - \alpha_{21}k_1\mu_2\sigma_1 + Fe\mu_1\sigma_2 - k_2\mu_1\sigma_2}{(Fe + k_2)\mu_1} > 0 \quad (2.13)$$

Conditions (1) and (3) represent thresholds on the minimum iron availability to support the respective populations. Using the values detailed in table 2.1 the thresholds are: 0.03 $\mu mol/m^3$ for nanoplankton and 0.38 $\mu mol/m^3$ for diatoms. Conditions (2) and (4) relate to the two inter-specific competition coefficients (whose product needs to be larger than one) and iron, shown in Figure 2.3. A dynamic with alternative stable states requires that both α_{12} and α_{21} take a value "above" their respective curve for a given concentration of iron.

An example of a case where bistability occurs is shown in Figure 2.4 where, for a given amount of available iron, the system reaches different stable states dependent on the

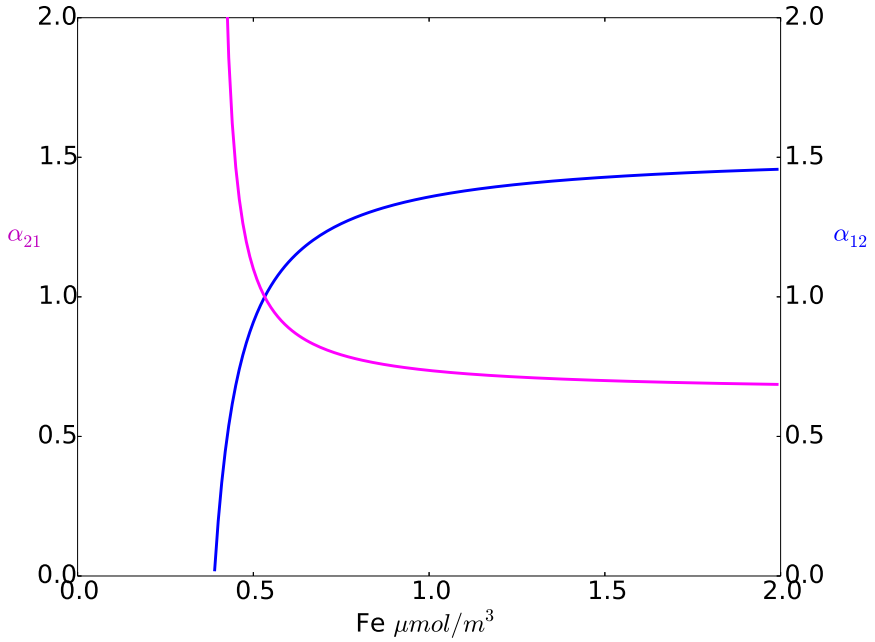

FIGURE 2.3: Results of the stability analysis showing minimum values of α_{12} (the effect of nanoplankton abundance on diatom growth,in blue) and α_{21} (the effect of diatoms abundance on nanoplankton growth, in magenta) and iron in order for alternative stable states to occur depending on iron concentration.

relative abundance of the two functional groups in the initial inoculum of the water parcel. The intersection of the isoclines (green and the red lines), the intersection of each isocline with its associated axis, and the origin represent equilibria (4), (1) and (2), and (3), respectively. The blue line shows the positions of the separatrix, a 1-dimensional space defining an unstable equilibrium that divides the phase space into two regions that develop into the two different equilibria, i.e. domination by one phytoplankton functional group or the other.

For parameter values in the observed range (i.e. Fe at [0-1.2] $\mu mol/m^3$, and P_1, P_2=[0 − 8] $* 10^{-3}$ mol C), alternative stable states under identical environmental conditions can emerge for medium-high values of Fe=[0.7-0.9] $\mu mol/m^3$ providing that values of α_{12} and α_{21} are greater than 1 and that $\alpha_{21} < \alpha_{12}$, while for very high values of iron $\sim$ 1.10-1.20 $\mu mol/m^3$ is suffices that $\alpha_{21} < \alpha_{12}$ and that the product of the coefficients exceeds 1.

Spatial patterns

By combining simulations of model a) and drifter trajectories, we obtain two examples of spatial patterns from drifters that were close to stations TEW2 and TEW3 (stars in Figure 2.1). The station TEW2 is characterised by high concentration of iron ($Fe =$

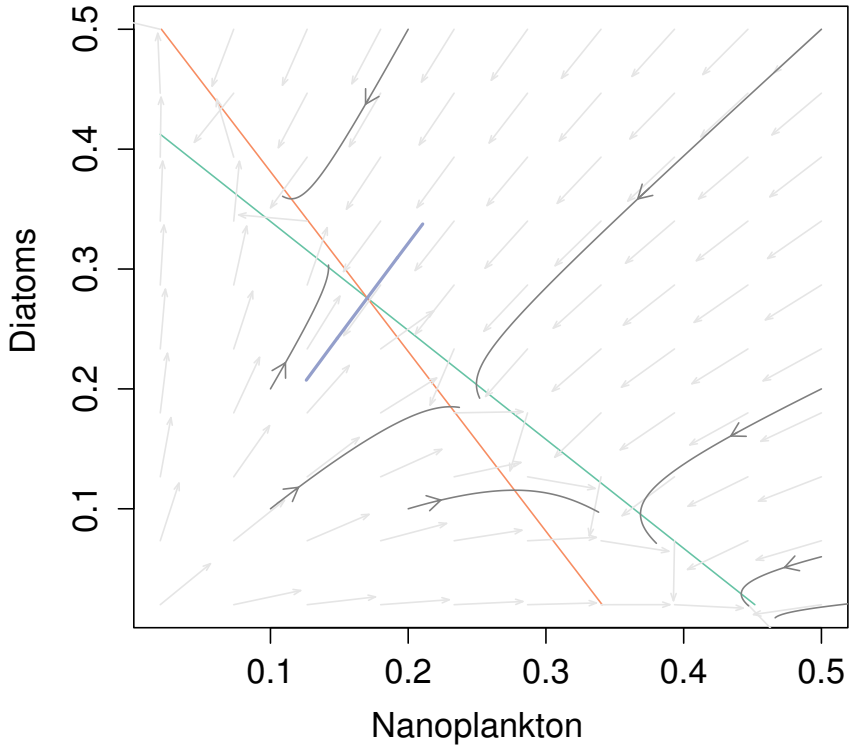

FIGURE 2.4: Phase space of the simplified model (model b, both diatom and nanoplankton abundance is expressed in $molC/m^3$). The red and green line represent the two isoclines of the system. In this example their intersection corresponds to an unstable equilibrium. The blue line represents the separatrix. Initial community compositions on either sides of the separatrix will evolve to different equilibria even for the same amount of iron available. Dark grey: examples of trajectories in the phase space approaching different equilibria depending the initial inoculum.

$1.26\mu mol/m^3$), relatively high biomass ($POC = 6.49 * 10^{-3} mol/m^3$), and dominance by large diatoms. The drifter that was advected from nearby TEW2 spent approximately one week on the plateau (where its horizontal velocity was relatively low) before being advected north -east by a faster current (see Figure 2.5). This water parcel hosted a 2-week diatom bloom which realised a five-fold increase in the biomass of large diatoms. However, nanophytoplankton concentrations also increased, and they became dominant after the first 10 days of the simulation when iron decreases.

In contrast, even though station TEW3 was located relatively close to TEW2, water here was characterised by low iron concentration ($Fe = 0.19\mu mol/m^3$), dominance by nanophytoplankton, and generally very high biomass ($POC = 9 * 10^{-3} mol/m^3$). The trajectory of the related drifter is similar to the one associated with TEW2 as it spent approximately one week on the plateau (see Figure 2.6) before being advected eastwards.

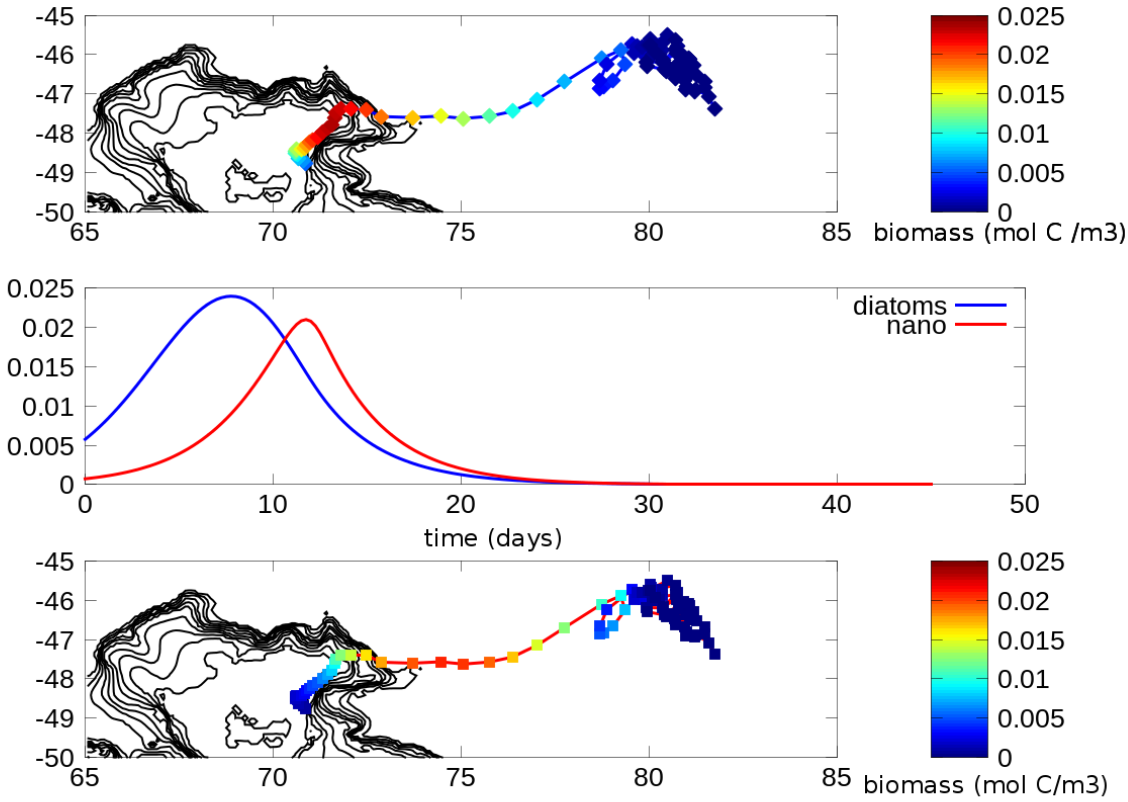

FIGURE 2.5: Trajectory of a drifter transiting in the proximity of station TEW-2 and the ecological dynamics of the corresponding water parcel (central plot of the panel) predicted using model a). Top map: spatial distribution of diatom biomass ($molC$). Bottom: spatial distribution of nanoplankton biomass. ($\alpha_{12} = 1, \alpha_{21} = 1.9$).

However, differences in iron availability (with levels too low to support diatom growth) cause the already low diatom biomass to drop further, while nanophytoplankton doubled in biomass during the first week. The total biomass was close to 0 after the first 2 weeks of simulation.

Bottom-up effects

To assess qualitatively how differences in iron enrichment and the possibility of alternative stable states might affect upper levels of the planktonic trophic web, we describe a minimum plausible trophic web for the study region, representing published results and personal communication with experienced field workers through a mini-workshop involving microbiologists, and phytoplankton and zooplankton ecologists [Smetacek et al., 2004, Pakhomov et al., 1996, Dubischar et al., 2006]. The minimum trophic web, sketched in Figure 2.7, contains two functional groups of phytoplankton, analogous to the ones for models a) and b) and referring to pico- and nano-phytoplankton (compartment 1) and large diatoms (compartment 2). The other elements represent the heterotrophic

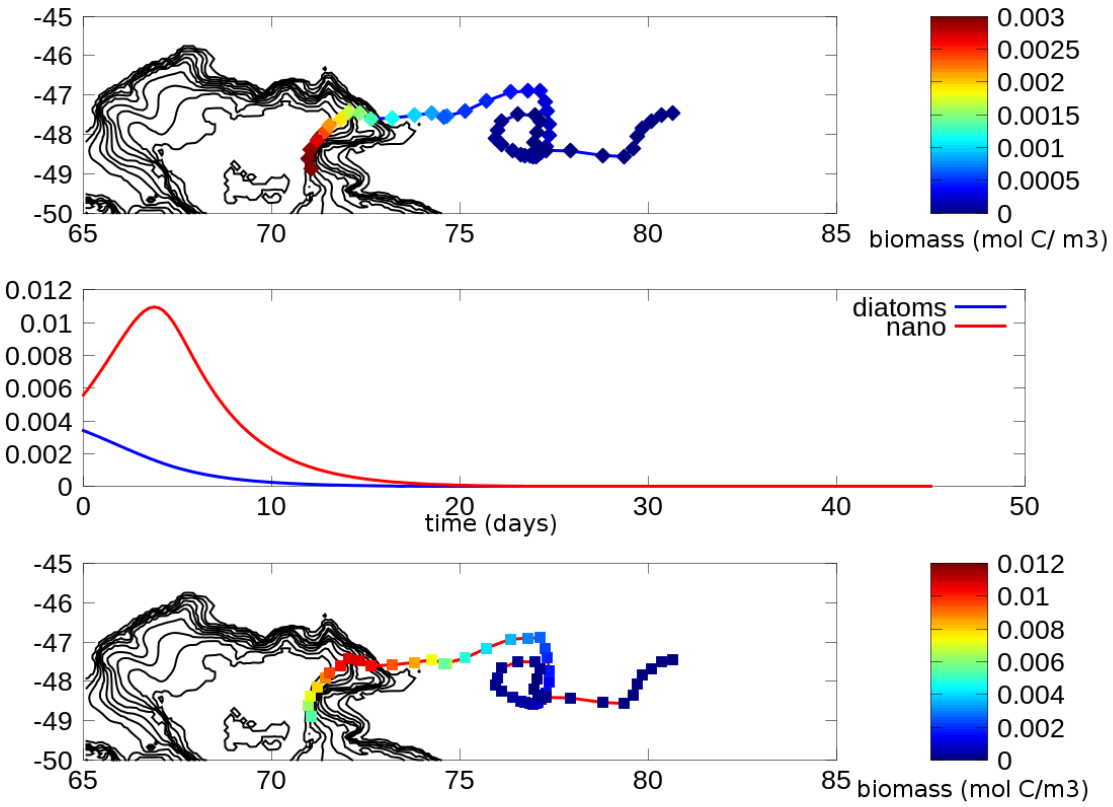

FIGURE 2.6: Trajectory of a drifter transiting in the proximity of station TEW-3 and the ecological dynamics of the corresponding water parcel (central plot of the panel) predicted using model a). Top map: spatial distribution of diatom biomass ($molC$). Bottom: spatial distribution of nanoplankton biomass. ($\alpha_{12} = 1, \alpha_{21} = 1.9$).

bacteria (responsible for the remineralisation of dissolved organic matter [DOM, compartment 3] and ultimately iron) and zooplankton community. Micro-zooplankton (compartments 4 and 5) are differentiated as heterotrophic nanoflagellates (compartment 4) that feed on heterotrophic bacteria and nanophytoplankton, and other micro zooplankton (compartment 5). Both of these compartments and nanophytoplankton constitute the diet of salps (compartment 8; note that this functional group also includes also Appendicularia and Pteropoda as minor components). Meso zooplankton compartments include two types differentiated according to whether they are largely carnivorous (compartment 6) or herbivorous (compartment 7). Compartment 7 includes the large copepod assemblage observed in the Kerguelen region that feeds largely on diatoms, but can, in relatively rare circumstances be carnivorous, and this group constitutes the main food for fish larvae (compartment 10). Other macro zooplankton compartments include larger crustaceans such as amphipods and euphausiids, which are particularly important in the region (compartment 9), and a functional group of other gelatinous zooplankton (compartment 11) that are largely jelly fish and ctenophores which mainly feed on salps and mesozooplankton.

Given the complexity of the system and the sparseness of data to parametrize the numerous interactions, we performed a qualitative analysis (as detailed in the methods). Two types of perturbation were undertaken, one in which biomass of large diatoms was increased, while the other realised an increase in nanophytoplankton biomass. Thus, these perturbations reflect shifts in the dominance of the two phytoplankton functional groups in the system. When large diatoms are increased (Figure 2.8 a), on average the biomass of mesozooplankton, crustaceans, and fish larvae increase while salp biomass declines. Conversely, an increased growth of nanoplankton (see Figure 2.8 b)) positively affects biomass of salps and heterotrophic bacteria (due to a larger remineralisation), while abundances of crustaceans and fish larvae decline in most simulations.

Discussion

An important result is that the simplified biogeochemical model (model b)) allows alternative stable states for realistic conditions provided that the amount of available iron is sufficient for diatoms to grow. Above this threshold, depending on the growth and mortality rates, equally iron-enriched water parcels can be dominated by large diatoms or small nanophytoplankton depending on the inoculum. In model a), where iron is constantly decreasing because there is no mechanism to replenish it, when water parcels leave the plateau containing similar iron concentrations they may display strong contrasts in phytoplankton assemblges.

The alternative stable states found in this case study different from more usual examples from coastal kelp bed [Estes and Duggins, 1995, Steneck et al., 2002, Ling et al., 2015] and coral reef [Mumby, 2009] systems in that the benthic ecosystems exist as persistent quasi-equilibria and can be made to shift between them by forcing, while the Kerguelen phytoplankton-based system is inherently dynamical as iron in the mixed layer is constantly decreasing in time as water is advected away from the Plateau. However, even in this case, the formalism of this bistable system is useful as it shows that iron enriched waters will not necessarily exhibit a large biomass of diatoms.

The threshold for iron levels that can lead to dominance by large diatoms as suggested from the stability analysis, is high compared to the values of dissolved iron (DFe) that have been observed in the field. There are several reasons why this apparent discrepancy may arise:

1. DFe is not an accurate indicator of the bio-available iron. Boyd and co-authors [Boyd et al., 2015] found that the biotically available pool of iron at locations with high and low DFe conditions are comparable (even if the community structure is

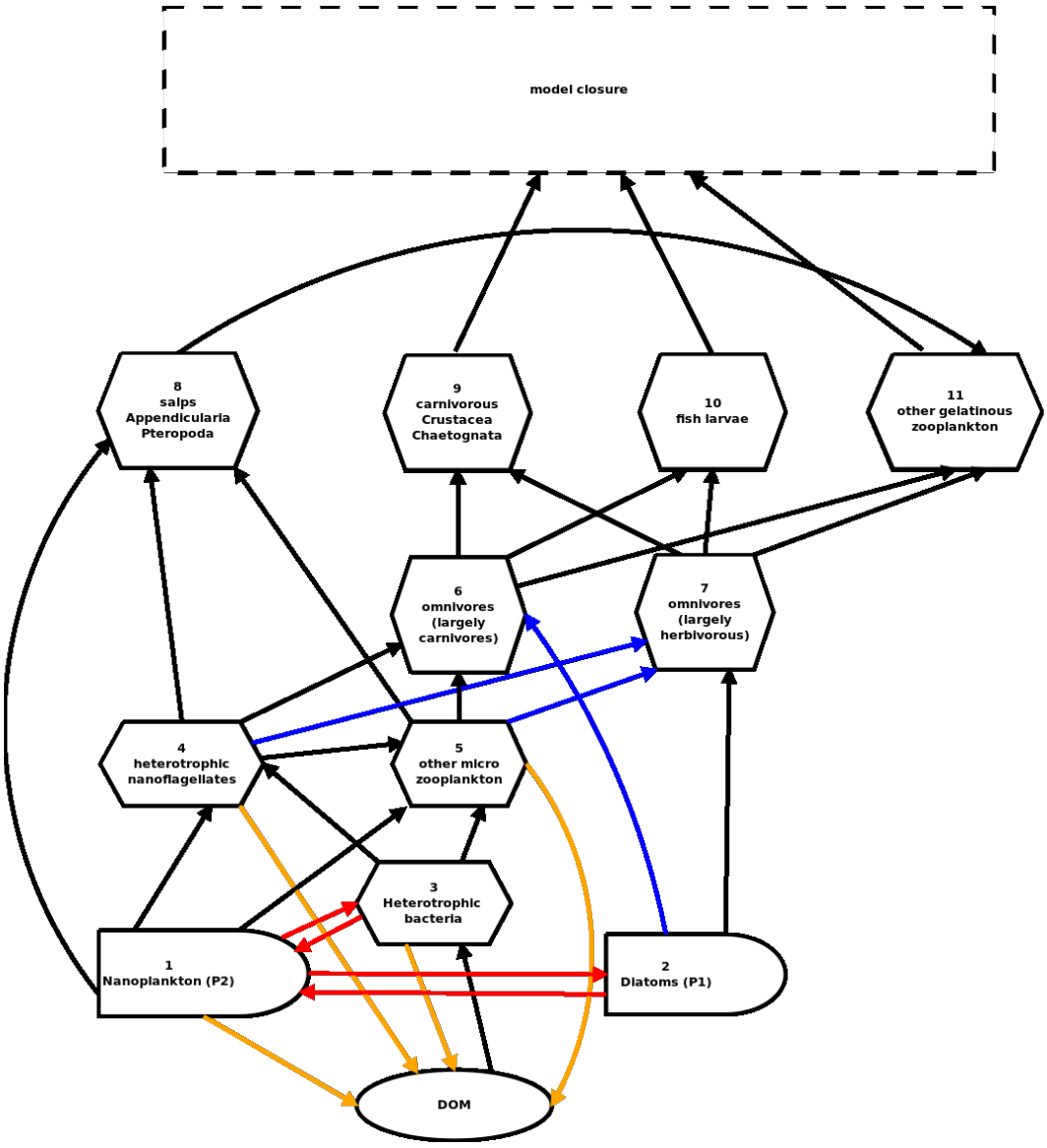

FIGURE 2.7: Scheme of the qualitative trophic web model. Black arrows refer to major trophic pathways, blue arrows reflect minor links that are usually important unless black links are weak because of low prey abundances, red to direct competition for iron acquisition and yellow to pathways that contribute to iron regeneration.

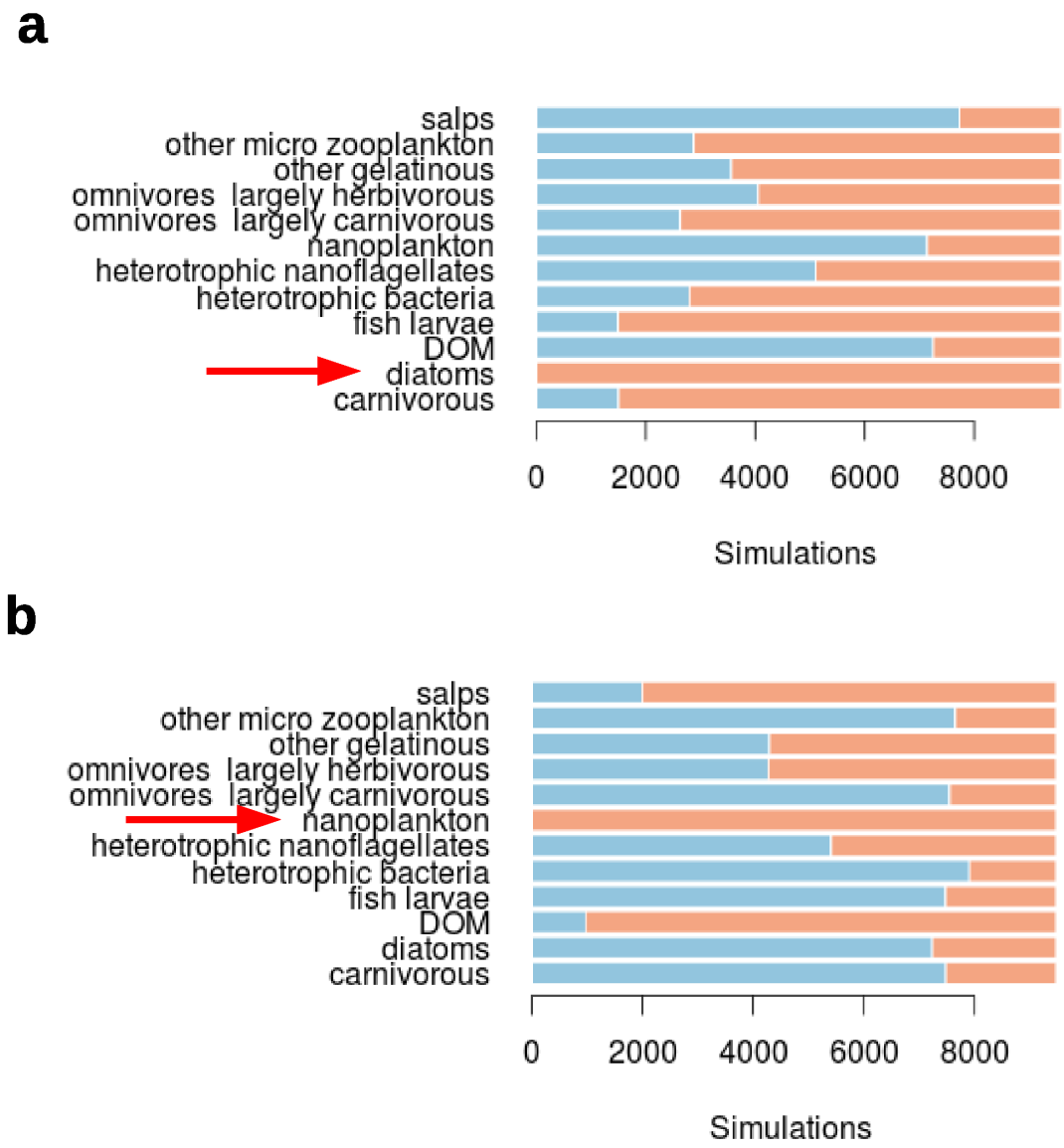

FIGURE 2.8: Perturbation analysis of an ensemble of random quantitative matrices referring to trophic webs as shown in Figure 2.7. Red arrows indicate the compartments where the perturbation is applied (diatoms in case a) and nanoplankton in case b)). Bars indicate the proportion of the simulations having a positive (red) or negative (blue) effect on each compartment.

very different). This result suggests that recycled iron in the mixed layer may be more important than previously thought and therefore that DFe may underestimate the amount of iron that is available in the system.

2. The presence of larger amounts of carbon in the water column releases ligands that are likely to counter abiotic scavenging (P. Boyd, personal communication), so the approximation that the abiotic scavenging coefficient is constant may not be inappropriate.

3. Grazing on nanophytoplankton may be underestimated in the model. Several studies have found that grazing tends to control phytoplankton and in particular weakly silicified diatoms and nanophytoplankton [Smetacek et al., 2004, Dubischar and Bathmann, 1997, Coale et al., 1996]. For higher values of nanophytoplankton mortality, this group would represent a weaker competitor to diatoms, lowering the threshold for diatoms to achieve dominance.

An issue that should be addressed in future studies is whether the interactions described in the models presented in this paper occur in the open ocean at the same rates that were measured during incubation experiments. As discussed in Reference [Boyd et al., 2015] incubation experiments and natural settings present strong differences in environmental conditions, inter-specific competition, and forms of iron present, and so parameters measured from one system may not be relevant to the other.

Generally, the parameters μ_1, μ_2, k_1 and k_2, selected from the literature are consistent with a "size-based" approach. Larger cells have a smaller surface area/volume ratio making them less efficient at nutrient uptake because acquisition is proportional to their surface area, but their need is proportional to their volume. Conversely smaller cells are more efficient at acquiring iron (and dissolved nutrients in general) and so they have a higher iron affinity.

To represent P_2, a broad functional group that is likely to include a diversity of organisms from nano and pico-phytoplankton dominated by cyanobacteria, and possibly including small diatoms, we used empirical measurements made on Synechococcus. This choice is motivated by observations indicating that this group is the dominant phytoplankton type in the region during winter based on PHYSAT [Alvain et al., 2005, Alvain et al., 2008], and from in-situ sampling in biogeochemically similar provinces (such as that of the iron fertilisation experiment FeCycle II off the coast of New Zealand [Boyd et al., 2012b]).

Model a) (and consequently its simplified version, model b), is based on the hypothesis that the growth rate of the two phytoplankton groups is determined mainly by iron.

However, it should be kept in mind that the region tends to become silicate depleted after diatom blooms, but this is not considered explicitly in our models. Silicate limitation would affect diatom growth but not the nanoplankton. It is also possible that for high values of biomass light limitation may occur [Mosseri et al., 2008], which again is not captured directly in the models. However, both models a) and b) can take into account competition for light through the terms for intra- and inter-specific competition. Importantly, given the large difference in the size of the two kinds of organisms, an identical biomass density of nanophytoplankton and diatoms is likely to differentially affect the propagation of light in the water column. While biomass is proportional to the particles' volume, shading is proportional to their surface area. As a consequence, small phytoplankton (P_2) characterised by high surface/volume ratio are likely to have a higher shading and light dispersing effect than an equal amount of large diatoms (P_1) whose surface/volume ratio is smaller [Finkel et al., 2009]. The main condition on inter-specific competition for alternative stable states to occur is that the product of the interspecific competition coefficients must be equal to or larger than 1. For values of Fe, P_1 and P_2 that are typical from empirical observation, both coefficients need to be larger than 1. This situation corresponds to cases where the inter-specific competition is larger than the intra-specific one and where there is little niche differentiation. Given that nutrient uptake and competition for light generally favours small cells, a realistic situation that could produce a dynamic with alternative stable states is where $\alpha_{12} > \alpha_{21}$ and where $\alpha_{21} \approx 1$ and $\alpha_{12} > 1 (\approx 1.5 - 2)$. The preliminary results of the spatial patterns presented in this study are in line with satellite observations of chlorophyll, see Figure 2.1 a). The cases depicted in Figures 2.5 and 2.6 represent the high spatial variability in phytoplankton community structure in the region, both on and off the Plateau. Future work is required to extend this analysis to all the drifters deployed in the area around the plateau, which will make it possible to better characterise the spatial patterns of phytoplankton community structures within the plume. This perspective is particularly interesting in respect to a recurring recirculation structure (discussed more in detail in chapter 1) located approximately at 72E, 42S, where low values of chlorophyll tend to be observed.

Another interesting perspective is to apply our model a) to Lagrangian time-series of observations of chlorophyll and backscattering. The recent deployment of "bio-argo" profilers [Grenier et al., 2015] makes acquiring this information possible (even if it is not possible at the moment to identify the phytoplankton in the community).

The qualitative analysis of the regional trophic web model suggests that contrasting phytoplankton communities are likely to affect upper levels of the trophic web. High abundance of large diatoms sustain fish larvae and meso- and macro-crustaceans, and presumably therefore fish and higher order predators, and thus support the "trophic

chain of giants" [Smetacek et al., 2004]. In contrast, nanophytoplankton dominated communities tend to favor the growth of salps and other gelatinous zooplankton, and support the "microbial" ecosystem [Smetacek et al., 2004]. Future work is required to quantify the interactions between the compartments of this complex model and verify that the findings of the qualitative model occur in the range of the observed rates of interactions and biomasses of different groups. In particular, it would be interesting to quantify if model a) can yield alternative dominance patterns for long enough for macrozooplankton communities to develop while water parcels still maintain their integratity.

Conclusions

The results of this study show that a mechanistic model representing two major functional groups of phytoplankton in the Kerguelen bloom parametrised with realistic values and initialised with observed biomass can show multiple stable states for the same amount of iron. This phenomenon is likely to enhance complexity within the plume of iron-enriched waters leaving the Plateau, adding to the complexity that results from interactions with changes in the vertical structure of the water column and the Lagrangian properties of water parcels as discussed in chapter 1. The qualitative analysis of the regional trophic web model shows that differences in the phytoplanktonic communities, driven by iron availability or stochastic forcing of a bistable ecological dynamic, will affect upper levels of the planktonic trophic webs up to the prey of most of the top predators whose colonies reside on the Kerguelen islands and who embark on significant foraging trips east of the Kerguelen Plateau.

Part IV

Discussion, conclusions and perspectives

Discussion of the key results

Marine predators play a fundamental role in mantaining the function of marine ecosystems and they are sentinels of the their ecosystem health. Their study however presents a challenge due to complexity of their behaviour and of their turbulent pelagic environment. Recently, progress in bio-logging technology, remote sensing and modelling have opened novel possibility of addressing these inter-disciplinary questions. My work has explored how (sub-)mesoscale turbulence structures marine predators habitat by affecting their movement, their foraging behaviour, and the trophic chain they depend on. The (sub)mesoscale is indeed a regime which is expected to have a twofold structuring role on the ecology of top predators: Firstly, through bottom-up effects (because of its impact on lower trophic levels); and secondly, by direct means, because the (sub)mesoscale occurs on temporal scales of days to weeks, which are the same of the behavioral switches of predators. I focused on the case of the Kerguelen region, which is an ideal end-to-end case study because (i) several marine predators species have large colonies on the island, (ii) the area is located in a highly dynamical ocean regime dominated by the Antarctic Circumpolar Current, with strong (sub)mesoscale activity, (iii) the trophic web in the area is relatively simple and (iv) production is dominated by iron limitation, making it possible to disentangle physical and ecological effects. I combined bio-logging, remote sensing, in-situ (samples from ships and autonomous platforms like "bio-argo" profilers) with ecological and Lagrangian modelling to study how (sub)mesoscale features affects movements and foraging behaviours of marine predators from a mechanical and ecological point of view. My work had two main axes: a first one that relates marine predator to the mechanical effect of (sub-)mesoscale turbulence (part II) and a second one where I combined ecology and stirring to describe the "biological" mesoscale landscape explored by Kerguelen's marine predators (part III).

The conclusions of this study can be summarised as:

1. The two species I studied (foraging elephant seals and Macaroni penguins) exhibit "quasi-planktonic" bouts where they horizontally drift together with the water parcel in which they dive for finding their food resource. Locations of quasi-planktonic behaviour statistically correspond to more intense foraging and high frontal activity, suggesting another possible and non-exclusive mechanism to interlace animal trajectories and (sub-)mesoscale fronts apart from bottom-up mechanisms. The results of Chapter 1 and 2 challenge the assumption – until now common among marine ecologists - that the mechanical effect of (sub-)mesoscale currents' on marine predator is negligible. A direct consequence is that models that aim at inferring differences in foraging behaviour from movement patterns are likely to improve

their accuracy if the trajectories are corrected for the effect of the currents. Also, this approach allows to identify qualitatively which sectors along a predator's trajectory are likely to be characterised by intense foraging behaviour, as shown in Chapter 1. The findings presented in Chapter 1 emerge from the specific case study of Kerguelen's elephant seals, but they are confirmed by observations on Macaroni penguins as detailed in Chapter 2. Furthermore, my results are not specifically related to the study region and the same principles and broad findings are likely to be relevant in other highly dynamical regions such as the Gulf Stream, the Kuroshio Current, the Agulhas and the East Australian Current [Cheney et al., 1983, Olson, 1991].

2. The Lagrangian approach "water age", that represents how long before water parcels have been in contact with the Kerguelen Plateau (i.e. before the estimated iron enrichment), positively correlates with diatom-dominance inferred from in-situ pigment sampling and optical re-analysis of ocean color images. This result provides a proxy for favourable conditions for diatom dominance of the phytoplanktonic community that is based on horizontal transport, a variable that is almost synoptically quantified thanks to altimetry. Although this work is focused on the Kerguelen region, the Lagrangian approach is appropriate for application to other iron-limited regions (e.g. the Crozet archipelago, the Galapagos Islands), or even more generally in cases where the distribution of a resource (e.g. nutrients, waters with favourable temperature, etc.) is largely driven by horizontal transport [Coles et al., 2016, Kubryakov et al., 2016].

3. A simple ecological model describing variations in phytoplankton communities in relationship with iron (inferred from altimetry-derived pathways from the plateau) shows that bistable ecological states may occur. This means that, besides being affected by the concentrations of available iron, whose effect is studied in the "threshold model", the initial phytoplankton inoculum that is picked up and advected within a water parcel from the plateau can determine which branch of the trophic web develops. In order to estimate the effect of phytoplankton bistability on the trophic chain, I introduced a qualitative ecological modelling approach, and found that waters hosting a bloom of large diatoms are able to support the growth of crustaceans and fish larvae that constitute a large part of the diet of penguins, seals and large fish. These preliminary results show that iron forcing and inter-specific competition regulate the structure of the base of the Kerguelen trophic web and their effect qualitatively propagate across the trophic web. A preliminary analysis shows that elephant seals' foraging behaviour suggests that particularly profitable foraging areas correspond to water parcels that have been in contact with the Kerguelen plateau approximately 3-4 months before. Figure

2.9 a) shows three simultaneous trajectories of elephant seals that left the colony in the beginning of November 2011, swam and foraged for about 2 months before turning back towards the colony (25th December 2011). Areas characterised by intensive foraging are highlighted in grey, and occurs in the proximity of water parcels of water age around 100-120 days Figure 2.9 b), that are likely to have hosted blooming phytoplankton. While this is a tantalising result, we acknowledge that it is qualitative and preliminary, and that a more systematic analysis of several trajectories would be more conclusive. Also, the relationship is difficult to quantify given that the accuracy on the location of water parcels decreases as time of advection increases [Özgökmen et al., 2000]. However, the result is nonetheless promising and pushes further the findings by Cotte' and co-authors [Cotté et al., 2015] who showed that elephant seals preferred water parcels that had hosted the spring bloom on both their post-moult and post-bloom foraging trips (February-September).

Caveats and limitations

The results of this thesis rely on several assumptions that have been discussed through each chapter. In this section I will detail some of the caveats that underpin this work and that hold interesting implications for future work.

Is seals and penguins behaviour at sea affected by their predators?

In my thesis I assumed that the main driver of the behaviour and movement of marine predators' studied species (Macaroni penguins and southern elephant seals) is foraging. This assumption is based on their definition as "top predators". However, both Macaroni penguins and southern elephant seals are recognised as top predators even though they are known to be prey for other species such as sharks and killer whales [Guinet et al., 1992, Mcmahon et al., 2003, Williams et al., 1990]. Yet, my assumption is supported by demographic studies in different sub-Antarctic islands that showed that predation (and inter-specific competition) represent a second order effect in the survival of elephant seals and penguins that is mainly determined by food availability [Guinet et al., 1999, Mcmahon et al., 2003, Reisinger et al., 2011].

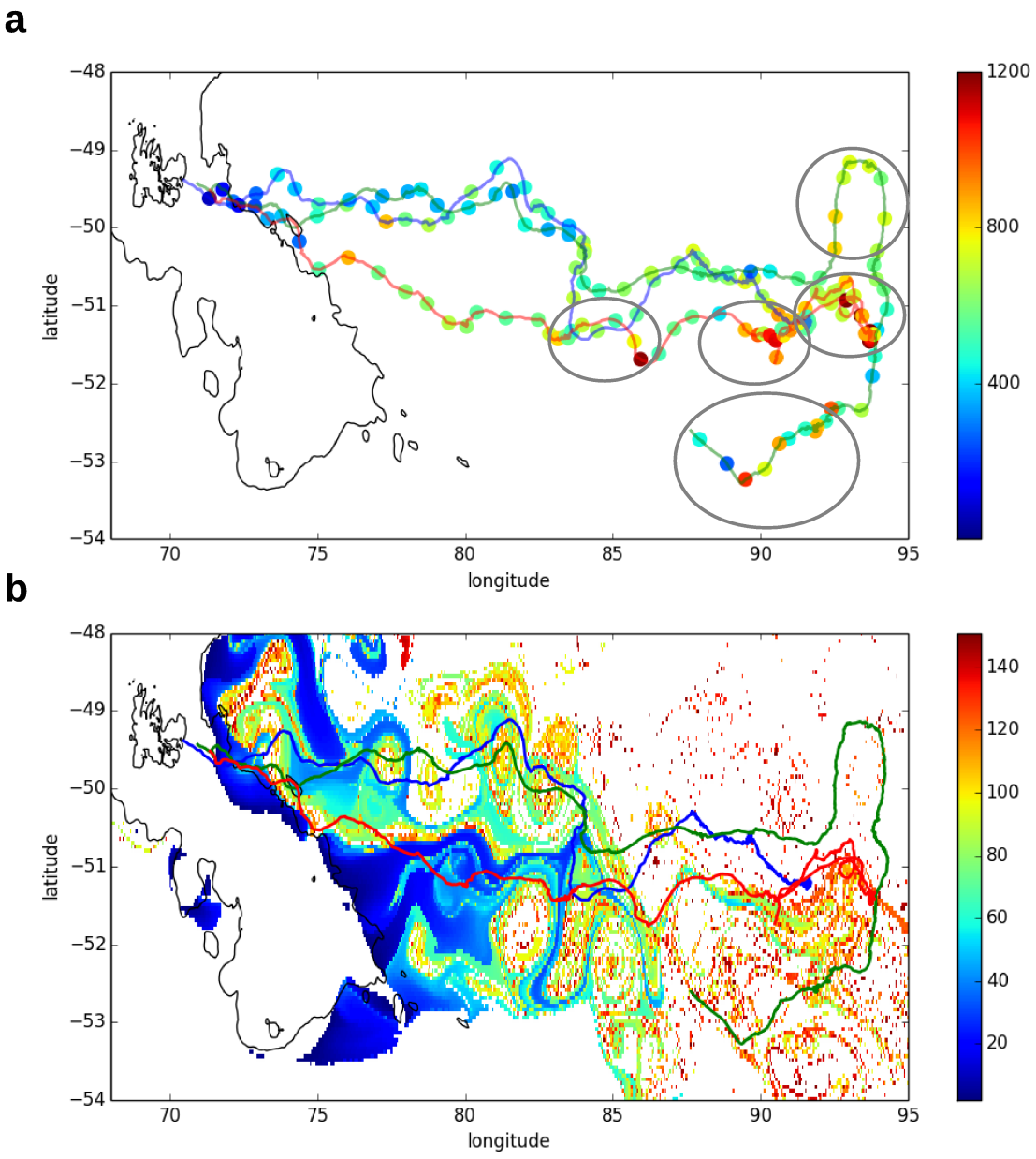

FIGURE 2.9: a) Attempt capture rate (colorbar) along three elephant seals' trajectories (October-December 2011)- grey circles highlight areas of intensive foraging, b) Water age (calculated on the 14/12/2011) overlapped by the same trajectories.

Fit-for-purpose end-to-end modelling

The data used for this project cover the full spectrum of ecosystem dynamics from physics to primary production to marine predators. The expression "end-to-end" usually refers to models that integrate trophic components from primary producers to top predators [Rose et al., 2010, Fulton, 2010] and which accommodate physical dynamics and forcings. Generally these kinds of model aim at representing the entire foodweb and the associated abiotic environment at a variety of scales (see for example OSMOSE [Shin and Cury, 2001], ATLANTIS [Fulton et al., 2011] and SEAPODYM [Lehodey et al., 2008]). In this study foodweb modelling is only used in its last part (chapter 2) to identify qualitative trends in the Kerguelen ecosystem. However, the overall approach in this thesis encompasses the "end-to-end" approach, aiming at integrating different components of the ecological system and their relationship with the dynamical physical environment. In particular, in my study the "end-to-end" approach has been tailored to address specific questions related to a specific scale (the (sub)mesoscale that is described explicitly). An interesting perspective for future work would be to integrate the "end-to-end" analysis described in this thesis with information on physics and trophic interactions in a 3D environment. To pursue this goal a more accurate description of submesoscale processes would be a key point as detailed in the next sessions.

Resolution of pelagic food web dynamics

Given the remoteness of the region, there are relatively few observations of ecological interactions around Kerguelen, especially those concerning the interactions between zooplankton and fish. As a consequence, the foodweb model described in chapter 2 is qualitative, commensurate with the underpinning knowledge base. In contrast, the models involving only interactions among phytoplankton and the iron pool could be parametrised given empirical measurements available from several field programs including KEOPS and KEOPS2 (2005 and 2011). When data from more recent voyages in the area become available, such as the ecological voyage MYCTO-3D (January 2014), HOEBI (January-March 2015) and, for the Southern part of the plateau, Kerguelen-Axis (January-March 2015), it is likely to be possible to test some of the hypotheses described in the discussion session of chapters 1 and 2.

Perspectives

This thesis has approached the challenge of understanding the effect of (sub-)mesoscale turbulence on the movement of marine predators by integrating approaches and datasets

from a variety of disciplines. As a consequence the results of this thesis can be developed in future work from several points of view. This section is focused on some of the perspectives that, in particular, I would like to pursue in future work.

Towards high resolution studies: deep into the submesoscale

This study, coherently with others, identifies (sub-)mesoscale fronts as key regions for marine predators foraging. However, given the resolution of the remote sensing data used in this study, our findings should be considered as "submesoscale permitting" as it refers to the mesoscale and only the upper boundaries of the submesoscale (10-100 km, few days to weeks). This scale corresponds to the daily average behaviour of large predators such elephant seals that cover up to 100 km/d.

A fully submesoscale resolving analysis however should be needed for the recently measured elephant seals trajectories (available in recent bio loggers that are able to have about 1 observation every 20 minutes – and very high frequency accelerometers detecting capture attempts of the order of a second). These very recent observations show that elephant seals foraging in the open ocean exhibit a frantic search beahviour underwater (where they spend 90% of their time, [Hindell et al., 1991]) at the km scale. At this submesoscale elephant seals foraging in the open ocean (mainly females [Guinet et al., 2014, Hindell et al., 2011, O'Toole et al., 2014], as males tend to prefer the Kerguelen or the Antarctic plateaus) encounter a very dynamical environment characterised by strong gradients (represented by filaments) and vertical movements that are on average one order of magnitude larger than the mesoscale ones. Submesoscale fronts and filaments and the associated vertical movements have recently been the object of several modelling studies focusing in particular on their origin (frontogenesis) and their effect on primary production [Lapeyre and Klein, 2006b, Klein and Lapeyre, 2009a, Lévy et al., 2012b, Levy et al., 2001, Lévy et al., 2012a, Rosso et al., 2014, Taylor and Ferrari, 2011a, Perruche et al., 2011]. Modelling studies suggest that submesoscale vertical movements can drive episodic nutrient pulses to the euphotic zone, subduct organic carbon into the ocean's interior and, by reducing local mixing, increase the mean time that photosynthetic organisms can spend in the euphotic zone, enhancing primary production.

If this submesoscale information would be made available for the Kerguelen area and colocalized with elephant seals high resolution trajectories, key ecological questions could addressed.

First of all, by using elephant seals as indicators of their prey, some light could be shed on the distribution of fish in the open ocean, where very little is known about the aggregation mechanisms and biomass hotspots of the intermediate trophic levels. An aspect of my study which I would like to develop in the future is a direct analysis of the prey spatial and temporal distribution and its interaction with the studied predators. This issue is not an unusual problem in models and generally in ecological observations in the open ocean. While animal tracking and satellites observations have made investigations on large animals and phytoplankton spatial distribution possible at relatively high spatial and temporal scale and over a large (in some cases quasi-synoptic) range, observations of fish and zooplankton are mainly the result of shipboard studies. Therefore observations are limited to the location of the ship [Godø et al., 2012, Lebourges-Dhaussy et al., 2014, Béhagle et al., 2015, Luo et al., 2014, Huggett, 2014, Labat et al., 2009, Potier et al., 2014]. In respect to intermediate trophic levels the knowledge of the spatial distribution of submesoscale structures is particularly relevant. Intermediate trophic levels are mainly constituted by zooplankton and micronekton and therefore (i) migrate vertically and (ii) have relatively limited swimming capabilities and are therefore heavily affected by currents. As a consequence they are heavily affected by the vertical velocities that are typical of the submesoscale [Labat et al., 2009].

Another challenge that could be addressed by colocalising submesoscale dynamics to high resolution elephant seals' trajectories is in terms of biophysical process studies. Only very recently data from underwater gliders (i.e. underwater vehicles that exploits small changes in buoyancy and wings to propel themselves forward, see for example Reference [Thomalla et al., 2015]), bio-argo floats (i.e. floats that are equipped with sensors that can measure bio-optical and bio-geochemical properties), ship towed ondulating devices (such as the Triaxus [D'Asaro et al., 2011]) and animal borne sensors have reached the autonomy and the resolution to address submesoscale matters. A recent work by Jaud and co-authors used the information about temperature variability measured by animal borne high resolution sensors to evaluate the 3D high resolution structure of the temperature field deduced from the remotely sensed SST and the efficient-Surface Quasi-Geostrophic theory (eSQG) [Jaud et al., 2016]. This theory, based on the conservation of potential vorticity in the ocean, allows to reconstruct the 3D density and velocity fields at depth given a high resolution description of density field at the surface and a climatology of the vertical stratification [Klein and Lapeyre, 2009a, Lapeyre and Klein, 2006a].

Another promising perspective in respect to the observation of submesoscale phenomena is the one opened by the launch of the SWOT satellite program (Surface Water and

Ocean Topography , 2020). SWOT will be able to map, using a new generation interferometer, the Sea Surface Height with a 1 km resolution providing the first synoptic observations of the oceanic submesoscale circulation.

Decision-making in a flowing environment: perspectives on search strategies in a mesoscale field

A preliminary comparison with the diagnostic, Figure 2.9 b), suggests that intensive foraging occurs in proximity of water parcels with water age around 100-120 days, that are likely to have hosted blooming phytoplankton. This result is qualitative and preliminary. A more systematic analysis of several trajectories would be more conclusive. Also, it may be a hard result to quantify considering that the accuracy on the location of water parcels decreases as time of advection increases [Özgökmen et al., 2000]. However, this result is particularly promising and coherent with the findings by Cotte' and co-authors [Cotté et al., 2015] that showed that elephant seals preferred water parcels that had hosted the spring bloom during their post-moult (and post-bloom) trips (February-September).

The results of this study relate marine predators to physical structures that appear to be favourable for their foraging success such as fronts and mesoscale eddies. But how marine predators find such structures in an highly dynamical and spatially heterogeneous environment? This is a fascinating and challenging question which I would like to address in the future. The results from chapter 1 show an example of an elephant seals displaying a behaviour even before starting foraging intensively 1.5. This observation suggests that elephant seals may follow cues in water parcels to find profitable grounds such as temperature gradients. However it is possible that locations characterised by quasi-planktonic behaviour and low attempt capture rates just before locations of intensive foraging are an artifact due to the resolution of the study. Further studies are necessary to find how far ranging animals are able to sense and find profitable patches.

In this context the theoretical approaches of *search stragegies* are promising. This theoretical framework has been already applied in the study of observed trajectories. For example the Optimal Foraging Theory (mentioned in Part II) describes which search patterns are more efficient for finding a patchy resource [Hengeveld, 2007]. Other examples include the use of First Passage Time as a diagnostic for area restricted search and habitat selection [Fauchald and Tveraa, 2003, Bailleul et al., 2008] and the differentiation of shark vertical movements in an heterogeneous prey field according to their similarity to Brownian motion or Levy flights [Sims et al., 2012].

Another possible approach, based on concepts from the information theory, is the one developed by Vergassola and co-authors [Vergassola et al., 2007]for environments where

the target cues are very sporadic (e.g. odors in air or water). In this approach the search is considered as an acquisition of information on the source location: the strategy consists then in locally maximizing the expected rate of information gain. This approach may be particularly valuable in contexts such as the open ocean where possible cues (such as temperature, chlorophyll, salinity, etc) are likely to be very sporadic.

In the case of pelagic predators, information source may be combination of different variables that a marine animal can sense. Possible candidates include temperature, salinity and their gradients, but also chlorophyll as a a proxy for dimethyl sulfide (DMS) an organic compound is released by some phytoplanktonic types when grazed [Savoca and Nevitt, 2014]. Some species of seabirds have been observed to respond to chemical cues of this substance that cumulates in the air around productive oceanic areas [Nevitt et al., 1995, Nevitt and Bonadonna, 2005]. However, there is very little evidence of the capabilities of detecting DMS in pinnipeds [Kowalewsky et al., 2006].

Future studies are necessary in order to identify which cues can be relevant for different marine predators and in which way they are integrated into search strategies in the open ocean.

Marine conservation at the mesoscale: implications of a changing environment

Another interesting perspective is a novel use of the combination of multi-satellite data, Lagrangian approach and bio-logging in conservation ecology. The open ocean environment represents the largest realm on Earth (99% of the biosphere) [Game et al., 2009] and plays a key role in the global fishery [Game et al., 2009, Pauly et al., 2002], in the carbon cycle [Field et al., 1998] and supports almost all marine life. However, it is also the least protected ecosystem on Earth. This is due to juridical and technical issues. Open ocean ecoregions (i.e. "assemblages of flora, fauna and the supporting geophysical environment contained within distinct but dynamic spatial boundaries" [Vierros et al., 2009]) juridically encompass both national exclusive economic zones (EEZ) and "high seas" -i.e. not part of any country's exclusive economic zone (EEZ), beyond 200 nautical miles from any nation's territory- and therefore present difficulties in their spatial management and enforcement [Hobday and Hartog, 2014]. Only $\sim$ 3% of the marine environment is protected, and of this fraction, high seas protected areas constitute a minority [Game et al., 2009](in 2013, the U.N. Millennium Goal Report states that less than 1% of the high seas are protected).

Also, being a dynamical environment, defining fixed boundaries that are necessary for marine protection policies is challenging. Unlike terrestrial and benthic systems – from

which most management approaches are borrowed- the ecosystems of the open ocean upper layer are only weakly constrained by a bottom topography thousands of meters below. Identifying which of these dynamical features are of relevance for marine organisms, finding the boundaries of the ecoregion in which they evolve, and anticipating their drift in response to scenarios of climate change are therefore issues of primary concern in the definition of open ocean MPAs. The results presented in this thesis aims relate marine predators with physical structures that can be monitored in near-real time. This approach can be integrated in the design of marine protected areas, by combining data from different years that can suggest which are the most likely location of ocean areas that need to be prioritised, but also in dynamical near-real time management as other forms of habitat modelling are [Bailey and Thompson, 2009, Ballard et al., 2012].

This perspective is particularly exciting in respect to the designation through the Convention for the Conservation of Antarctic Marine Living Resources (CCAMLR) of MPAs in priority areas around all the Southern Ocean [cca, 2008]. One of the proposed MPA is located in the study area of this thesis, in the Kerguelen production zone. Possible further development of the studies represented in this work may be a complementary support for the design of the MPA. A similar approach is reported in Appendix C where some of the results of chapter 2 were used to track estimated foraging areas for Macaroni penguins through several years and identify a priority foraging area next to their colony on Crozet Island.

A major challenge for the conservation of open ocean ecosystem is how marine organisms and their interactions will respond to climate change and, consequently, how marine conservation has to adapt to a changing environment. Whereas climate models today produce different scenarios projections for most of the physics of the atmosphere and oceans (even if some mechanisms such as cloud dynamics and soil-related feedbacks are still problematic to predict [Karl and Trenberth, 2003]), very little is known about how marine organisms will respond to a warmer climate, fresher waters and different circulation patterns. The time series of observations for the Southern Ocean from Argo floats and hydrographic surveys indicates a warming and freshening over all the basin [Böning et al., 2008, Gille, 2008], which is likely to cause a shift in the location of fronts of the Antarctic Circumpolar Current (ACC) as shown by Reference [Sallée et al., 2010, Sallée et al., 2008, Lovenduski and Gruber, 2005]. Climate projections suggest a further (although slower) positive change of the Southern Annular Mode (SAM), the main indicator of inter-annual climate variability for the Southern Ocean, [Cai et al., 2005, Mayewski et al., 2009, Miller et al., 2006, Sen Gupta et al., 2009] with a consequent enhancement of westerly winds and an increased equatorial Ekman transport [Sallée et al., 2008]. A major consequence of this shift is a poleward movement of the ACC fronts.

However, there are very few projections of how these changes in the Southern Ocean environment is likely to affect marine predators [Hazen et al., 2013, Doney et al., 2012, Hobday et al., 2015, Robinson et al., 2015]. For the northern hemisphere, Hazen and co-authors [Hazen et al., 2013] have developed predictions using animal tracking information from 23 species in the North Pacific Ocean relating bathymetry, SST, and Chl preferences in species-specific habitat models. They then forced their models with projections for the future state of the North Pacific to identify those species likely to be "loser or winners" given the predicted change. While a similar study is in preparation for the Southern Ocean (M. Hindell, pers. comm.), the spatial trends considered in these works are $>$ 100 km and thus miss the crucial role of submesoscale structures on animal behaviour.

Even if marine organisms are affected by large scale patterns, the dynamics that directly affect their foraging behaviour is at the sub-mesoscale and mesoscale. To fully ascertain the likely consequences of these kinds of changes in the Southern Ocean, complementary information is necessary from study of both the interaction between marine organisms with mesoscale dynamics, and between mesoscale dynamics and basin scale trends. At the moment lack of information at the (sub)mesoscale and of interactions between (sub)mesoscales and large scales is one of the major uncertainties undermining attempts to model interactions among climate change, fisheries, and marine ecosystems [Evans et al., 2015, Hobday et al., 2015].

Appendix A

Appendix A. The biogeochemical structuring role of horizontal stirring: Lagrangian perspectives on iron delivery downstream of the Kerguelen plateau

This appendix is published as *The biogeochemical structuring role of horizontal stirring: Lagrangian perspectives on iron delivery downstream of the Kerguelen plateau* by F. d'Ovidio, A. Della Penna, T. W. Trull, F. Nencioli, M.-I. Pujol, M.-H. Rio, Y.-H. Park, C. Cotte, M.Zhou and S. Blain in *Biogeosciences*, 2015.

Abstract

Field campaigns are instrumental in providing ground truth for understanding and modeling global ocean biogeochemical budgets. A survey however can only inspect a fraction of the global oceans, typically a region 100s km wide for a temporal window of the order of (at most) several weeks. This spatiotemporal domain is also the one in which the mesoscale activity induces through horizontal stirring a strong variability in the biogeochemical tracers, with ephemeral, local contrasts which can easily mask the regional and seasonal gradients. Therefore, whenever local in situ measures are used to infer larger scale budgets one faces the challenge of identifying the mesoscale structuring effect, if not simply to filter it out. In the case of the KEOPS2 investigation of biogeochemical

responses to natural iron fertilization, this problem was tackled by designing an adaptive sampling strategy based on regionally-optimized multisatellite products analyzed in real time by specifically designed Lagrangian diagnostics. This strategy identified the different mesoscale and stirring structures present in the region and tracked the dynamical frontiers among them. It also enabled back-trajectories for the ship sampled stations to be estimated, providing important insights into the timing and pathways of iron supply, which were explored further using model based on first order iron removal. This context was essential for the interpretation of the field results. The mesoscale circulation based strategy was also validated post-cruise by comparing the Lagrangian maps derived from satellite with the patterns of more than one hundred drifters including some adaptively released during KEOPS2 and a subsequent research voyage. The KEOPS2 strategy was adapted to the specific biogeochemical characteristics of the region, but its principles are general and will be useful for future in-situ biogeochemical surveys.

Introduction

The role of iron as key limiting micro-nutrient for large phytoplankton in High Nutrients Low Chlorophyll (HNLC) waters was brought to prominence by Martin in 1990 and motivated a series of bottle incubations experiments. Difficulties in unambiguously interpreting the results of these experiments led to the design and the implementation of more ambitious field studies. They were conducted in regions fertilized artificially or naturally with iron. One of the most striking difference between both types of study is the role played by horizontal transport of iron. Most of the artificial iron fertilization experiments were conducted using specific strategies aimed at minimizing horizontal effects. Some artificial experiments have targeted quasi-isolated eddy cores, so that the water patches which are trapped by the mesoscale circulation are only marginally mixed with the environmental waters on the timescale of the induced bloom. This was the case for the EIFEX, LOHAFEX and SAGE experiments ([Smetacek et al., 2012, Harvey et al., 2011, Martin et al., 2013]) and the FeCycle natural iron response study ([Boyd et al., 2005]). Natural fertilization studies have attempted to target homogeneous regions with weak horizontal transport and mesoscale activity, with the hope that the system could be approximated as a one dimensional water column reactor, with varying degrees of uncertainty for the conclusions (e.g. [Blain et al., 2007, Pollard et al., 2009]).

However, these quasi-isolated or homogeneous regions are not typical or representative of the vast majority of the ocean. In general, water parcels are stirred by the mesoscale field in a non-local way, experiencing the cumulative effects of several mesoscale structures from their iron enrichment event to the moment of the phytoplanktonic bloom.

Horizontal transport does not only modulate the extension of a fertilized region with respect to its sources (e.g. [Mongin et al., 2009]), but may also indirectly affect nutrient concentrations through physical and chemical processes like mixing and scavenging, during the advection of a water parcel. This is evident for iron fertilized waters in the open ocean, which present complex patterns and strong contrasts in satellite images of phytoplankton biomass, reflecting the pathways from the iron sources to the wider ocean coupled with the complexities of biological responses. Thus, for the purposes of quantifying large-scale ecosystem responses to iron inputs, the importance of horizontal transport in redistributing iron-rich waters in complex patterns has become dramatically apparent. The KEOPS2 campaign aimed at addressing the nature of of the response to iron fertilization in deep open ocean waters downstream from the Kerguelen plateau, hence including both the spatial dimension with respect to fertilization and its modulation by the mesoscale circulation. Together with traditional interdisciplinary stations with long occupation time, with some sites repeated to capture the temporal dynamics of the bloom, the campaign needed also to cover enough sites to document the spatial contrasts occurring in the region. These requirements put obviously a strain on the allocation of ship time. The problem was exacerbated by the intrinsic spatiotemporal variability of the phytoplanktonic bloom: the time window allowed for characterizing the region could not be expanded by requesting more days for the campaign, but was upper limited by the duration of the bloom itself. Moreover, a further requirements was that the different sites had to be occupied in the shortest possible time in order to disentangle space from time in the biogeochemical variability.

This paper first presents our efforts to use the prior and real time satellite information to understand bloom dynamics, and thereby define an optimal sampling strategy. In doing so, we examine both Eulerian eddy fields and Lagrangian maps of water mass origins. The paper then validates these initial perspectives on the circulation against drifters released during the KEOPS2 project and a subsequent voyage. It provides an iron supply and removal budget based on the integration of satellite, ship-based and drifter information. It illustrates how the context provided by these circulation perspectives informed the interpretation of the observed ecological states (with reference to other works in this volume). Finally, it offers perspectives for biogeochemical process study planning.

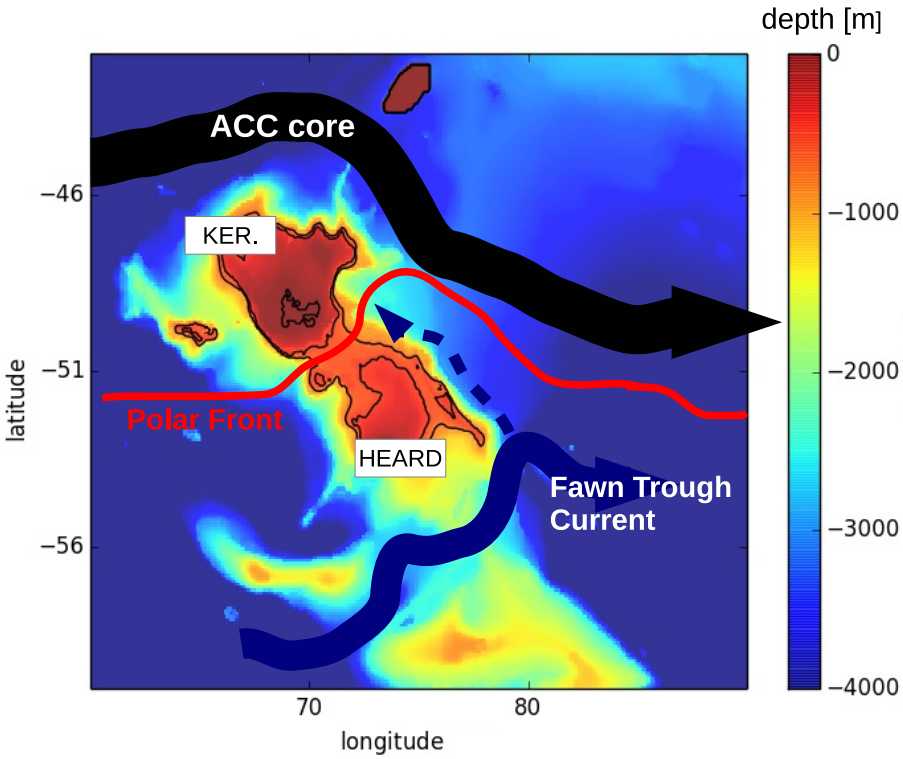

FIGURE A.1: Bathymetry and a sketch of the main current branches. The thick 500 m isobath identifies the Kerguelen and Heard plateaux. The 750 m isobath marks the shelf break.

Data and Methods

Satellite Products

Altimeter and ocean colour products used in this study were specifically produced for the Kerguelen region by Ssalto/Duacs and CLS with support from CNES from mid May 2011 to July 2012. Altimetry maps were generated from Jason-1, Jason-2 and Envisat along-track observations with procedures analogous to those used for AVISO data [Handbook, 2010] . Some of the parameters (i.e. mean dynamic topography, correlation scales and measurements errors) were specifically tuned for the region. These products are based on altimetric measurements at 10 day frequency, and interpolated to provide higher temporal frequency information.

In particular, a high resolution (1/8°) regional Mean Dynamic Topography was computed ([Rio et al., 2012]), applying the same 2-step methodology used for the calculation of the global CNES-CLS09 MDT available at that time ([Rio, 2012]), but with updated input dataset and refined in-situ measurements processing. First, a geoid model based on 1 year of GOCE data was used ([Pail et al., 2011]) together with the CNES-CLS11 Mean Sea Surface ([Schaeffer et al., 2012]) to derive a MDT at spatial scale larger than

125 km. This first guess was then improved by using synthetic mean geostrophic velocities and synthetic mean heights calculated by subtracting the ocean temporal variability measured by altimetry from instantaneous in-situ measurements of the ocean current velocities and dynamic heights. We used velocities from SVP-type drifters available from 1993 to 2011 from the GDP (Global Drifter Program) together with 183,000 velocities from buoys launched during the KEOPS2 sea campaign and spanning the period from 15/10/2011 to 31/05/2012. Ekman currents were subtracted from the buoy velocities. In addition, a significant number of GDP buoys being affected since 2004 by undetected drogue loss, a wind slippage corrective term was removed ([Rio et al., 2012]). Also, a 3 day low pass filter was applied to get rid of the other ageostrophic high frequency currents (stokes drift, inertial oscillations, tidal currents). The dataset of in-situ dynamic heights was calculated using the temperature and salinity profiles from CTD casts (Cora3.2) and Argo floats for the period 1993-2010, together with 75 CTD profiles measured from 15/10/2011 to 19/11/2011 during the KEOPS-2 campaign.

Maps of absolute dynamic topography at a resolution of 1/8° were daily produced in real-time (RT-MADT) by CLS/CNES. Near real-time (NRT-MADT) maps were produced after 6 days by further correcting the real-time products. Only NRT-MADT products are shown in this study.

Geostrophic currents were computed from the maps of absolute dynamic topography by solving the equation for geostrophic equilibrium [Pedlosky, 1987] with centered finite differences. Additionally, wind-induced surface Ekman currents were computed from a 1/8° wind analysis from the European Center for Medium Range Weather Forecasting (ECMWF). These were added to the altimetry-based geostrophic currents to obtain regional maps of total velocity.

Composite maps of surface chlorophyll concentration with a resolution of 1/25° were produced every three days also by CLS/CNES. Each map was constructed by a 10-day weighted mean of MODIS and MERIS measurements. We refer to these as SCHL values and images hereafter.

Eulerian diagnostics

Maps of geostrophic and total velocities have been used to compute the Okubo-Weiss parameter, OW ([Okubo, 1970]; [Weiss and Knobloch, 1989]). OW is defined as

$$OW = s_{sh}^2 + s_{st}^2 - \xi^2, \tag{A.1}$$

where s_{sh} and s_{st} are the shear and strain deformations, and ξ is the vertical component of vorticity, respectively. Thus, OW quantifies the relative importance of deformation with respect to rotation. Negative values of OW can be used to quantify the strength of mesoscale eddies [d'Ovidio et al., 2009, Chelton et al., 2011], since their velocity field is usually dominated by rotation.

In this study, mesoscale eddies have been also identified from satellite velocities using the vector geometry-based eddy detection algorithm developed by [Nencioli et al., 2010]. The method identifies the center of an eddy as a local minimum of velocity within a region characterized by rotating velocity vectors. Eddy boundaries are defined as the outermost closed streamlines across which velocity magnitude is still radially increasing. As in [Liu et al., 2012] and [Amores et al., 2013], the satellite velocity fields have been linearly interpolated to 1/16° resolution to improve the algorithm performance. The method has been applied with parameters $a = 4$ (defining the numbers of grid point across which the rotation of velocity vectors is inspected) and $b = 3$ (defining the dimensions in grid points of the area used to define the minimum of velocity).

Lagrangian and hybrid diagnostics

Several approaches were used to identify the effect of the eddy field on iron redistribution. Altimetry-based Finite Size Lyapunov Exponents (FSLE) were computed with the method proposed by Reference [d'Ovidio et al., 2004] which can be outlined as in the following. In order to construct a map of Lyapunov exponent, at each grid point trajectories are initialized and constructed by integrating in time the velocity field derived from altimetry. The finite-size Lyapunov exponent provides the maximal exponential rate of separation (averaged in time) among trajectories initialized nearby. Calling δ_0 the initial separation, δ a prescribed final the separation and τ the time at which the separation δ is reached, the Lyapunov exponent λ is defined as:

$$\lambda = \frac{1}{\tau} log(\frac{\delta}{\delta_0}). \tag{A.2}$$

Trajectories were derived by applying a Runge-Kutta fourth order scheme with a time step of 6 hours. Velocity fields have been linearly interpolated in both space and time. Initial and final separation distances were set to 0.05° (defining also the resolution of the Lyapunov map) and to 0.6°, respectively. For the real-time analysis during the campaign, only backward integrated FSLE were computed, providing a measure of the intensity of the convergent regions within the surface velocity field.

In practice, the Lyapunov exponent computed backward in time provides the exponential rate at which horizontal stirring has brought at close distance (δ_0) water parcels that were initially located a larger distance (δ) apart. Maxima (ridges) of Lyapunov exponent are used as a way to extract from altimetry data candidates for frontal regions, as a large-scale tracer gradient can be amplified by this mechanism.

The same Runge-Kutta scheme used to compute the backward FSLE was applied to retrieve additional diagnostics fundamental to the real-time analysis. Firstly, the ability of of mesoscale eddy cores to retain water parcels was quantified by backward advection of particles released within regions with negative OW values, and measuring their duration within these regions. In effect this yields an estimate of how long ago a water parcel entered a given an eddy, yielding a retention value expressed in days. Similarly, backward advection was used to identify water parcels originally above the Kerguelen plateau, defined as the region where ocean depths are shallower than 700 m. This was achieved by finding the trajectories of virtual drifters which had touched in the past the 700m isobath, in analogy to the method developed for the underway Crozet experiment ([Sanial et al., 2014a], where a validation of the method with lithogenic radio-isotopes was also performed; see also [Sanial et al., 2014b] in this issue). Particle trajectories have been also used to estimate the origin of water parcels by horizontal transport, finding the position (longitude and latitude) of a particle 30 days before and mapping this information at its current position.

SVP drifters

More than 200 WOCE-SVP drifters have been used to validate the altimetry-based estimation of stirring patterns. 48 drifters have been deployed according to an adaptative strategy during the KEOPS2 campaign and 24 during the MYCTO-3D campaign that took place in the Kerguelen region in January 2014. Furthermore, we collected 120 trajectories measured between 2011 and 2014 in the same region from the Global Drifter Program (GDP – http://www.aoml.noaa.gov/phod/dac/index.php) historical archive. In order to compare the stirring patterns estimated from altimetry, we computed the Lagrangian diagnostics detailed in the previous section using the drifters' measured trajectories instead of the altimetry-derived simulated ones. For each location along a drifter's trajectory we computed how much time before that very drifter had crossed the 700 m bathymetry line ("age of the water parcel") and we recorded at which latitude it left the Kerguelen Plateau ("origin of the water parcel"). For drifters that did not touched the 700m isobath but were close to it (within 100km) we used their closest position. Less than 10 drifters in the study region had left the Plateau more than 90 days earlier: this time exceeds the time extent of the backward computation from altimetry

so we excluded those trajectories from our analysis. In order to perform a visual and quantitative pixel by pixel comparison with the maps computed from altimetry, we averaged the values along the trajectories on 0.25 degrees disks, obtaining climatological maps of the two Lagrangian diagnostics.

Results

Mesoscale activity and stirring patterns

The circulation of the Kerguelen region (see fig. A.1 for the bathymetry and a sketch of its current system) has been the object of many studies in the recent years, and it is now known in great detail (see in particular [Park et al., 2014] and the references therein). When attempting to identify the relation between mesoscale physics and patterns of primary production, standard Eulerian and Lagrangian diagnostics are however quite deceptive. Indeed, there is no obvious association between mesoscale activity and extension of the SCHL plume. Figures A.2 and A.3 show the situation at beginning of the cruise while Fig. A.4 displays the instantaneous and climatological extension of the bloom onset (respectively, 11 November 2011 and mean of November 2000-2010). The ocean color composite depicts a plume of blooming water extending from the Kerguelen-Heard shelf break (72 ° -75 ° E) eastward to 85 ° - 90 °E and contained latitudinally between 47 ° : 53 ° S. This biologically active region is not characterized by anomalous eddy activity: indeed, eddies populate a much larger region, with hotsposts of total kinetic energy located equally inside the plume (e.g., 87 °E 51 ° S) or outside (e.g., 85 ° E 54 ° S). Some of these eddies appear to be strongly retentive, but their location does not indicate the position of the plume. Even more puzzling, the fronts and local transport effect induced by the mesoscale activity has no obvious relation with the plume either. The Lyapunov exponent technique - which is typically used as a proxy of transport fronts [d'Ovidio et al., 2009] - yields an indication of stronger activity off the shelf, but has no clear large-scale latitudinal gradient. Instead, a region with a much larger latitudinal extent than the plume displays intense stirring without suggesting where the seasonal chlorophyll plume may be constrained.

Some improvement in the outlook for understanding and predicting the SCHL pattern emerges when altimetry is used to reconstruct the 30 day longitudinal and latitudinal origin of surface waters (Fig. A.5). The northern flank of the SCHL plume appears to be bounded by the water stream coming from 47S (color coded in orange in fig. A.5 panel b), which interestingly corresponds to the water which peels off from the north-east corner of the shelf break (located at about 72 ° E, 47 ° S). Similarly, the

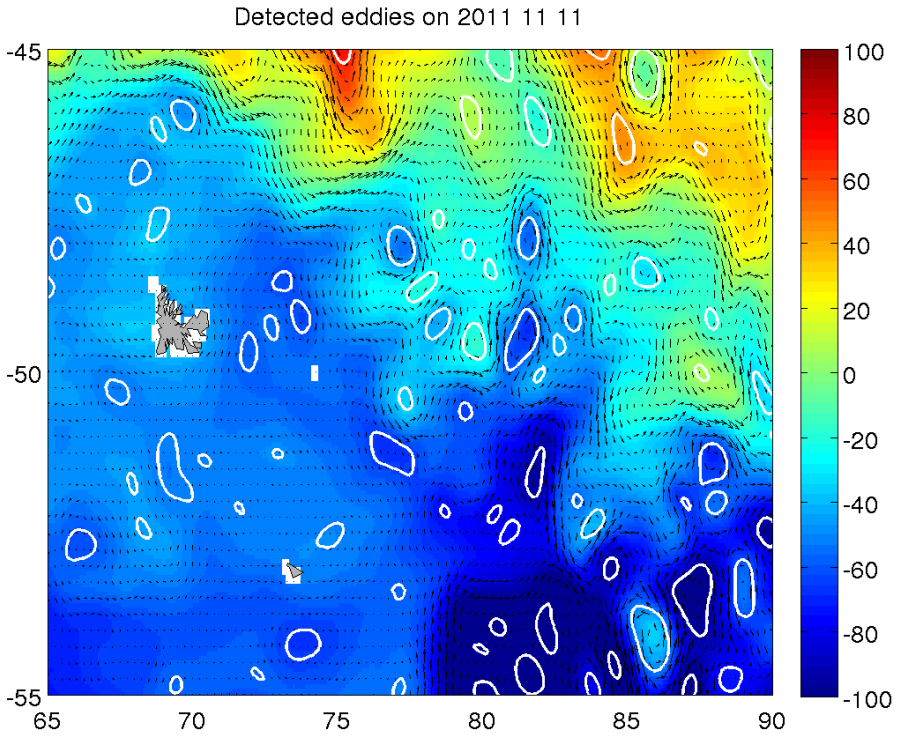

FIGURE A.2: Sea surface height and eddy contours (11 November 2011).

southern flank seems to correspond to the stream which hugs Heard plateau from the south detaching cyclonically around 75 ° E, 72 ° S. This observation in fact is coherent with previous work [Mongin et al., 2009], which has shown that the large-scale pattern of the satellite-derived SCHL plume is determined by the winter-time advection of water emanating from the plateau: in this regard, the two departure points over Kerguelen and Heard plateaux mark the edges which enclose the ACC branch which proceeds eastward after having passed over low bathymetry, and after being enriched in iron. Does this large-scale relation between horizontal advection and shape of the plume extend down to the mesoscale? This is an intriguing question, because it suggests the possibility of reproducing the fine-scale (lobes and filaments) of the SCHL plume by a simple advection scheme based on altimetric velocity. Note that the rationale behind this approach is that horizontal advection preconditions the horizontal spread of iron east of Kerguelen, which then fuels chlorophyll production when restratification increases average light levels. An interesting consequence of this scenario is that this approach permits to estimate from altimetry data the shape of the spring bloom *before* the onset of the bloom, as most of the advection occurs during wintertime. In order to test this possibility, we first developed a new Lagrangian diagnostic, aimed at identifying along backward-in-time trajectories whether a water particle has been in contact with the plateau during its past advective history (see Methods for details). The diagnostic provides both the position (latitude

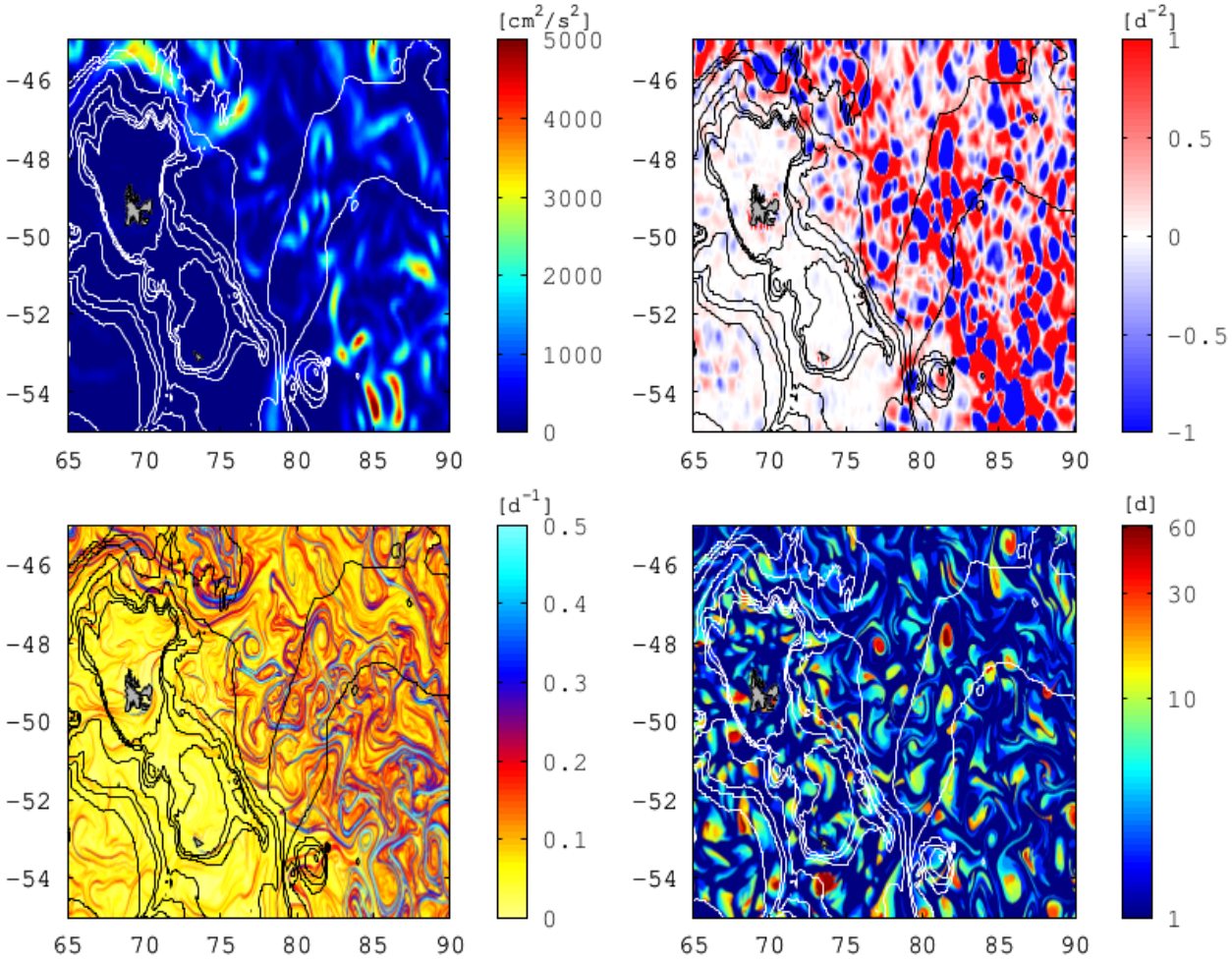

FIGURE A.3: Lagrangian and Eulerian diagnostics derived from satellite altimetry: (top left) total kinetic energy; (top right) Okubo–Weiss parameter; (bottom left) Lyapunov exponents (finite-size); (bottom right) retention parameter. These maps were generated in near-real time for guiding the adaptive sampling strategy of the KEOPS2 cruise.

and longitude) and time of the point at which the water parcels departed from the plateau (Fig. A.6).

These Lagrangian images provide the putative extension of the plume, including the positions of fronts which create contrasts in terms of origin from the shelf break and of time since last contact with the plateau. The temporal information is especially relevant for biogeochemical interpretations, as at a first approximation the dissolved iron concentration can be modeled as decaying exponentially in time due to scavenging [Mongin et al., 2009].

These images were computed starting from winter 2011 and were then updated daily using near-real time altimetry. When the ship headed to the region for measuring pre-bloom conditions, the altimetry-derived calculations were used to forecast the extension

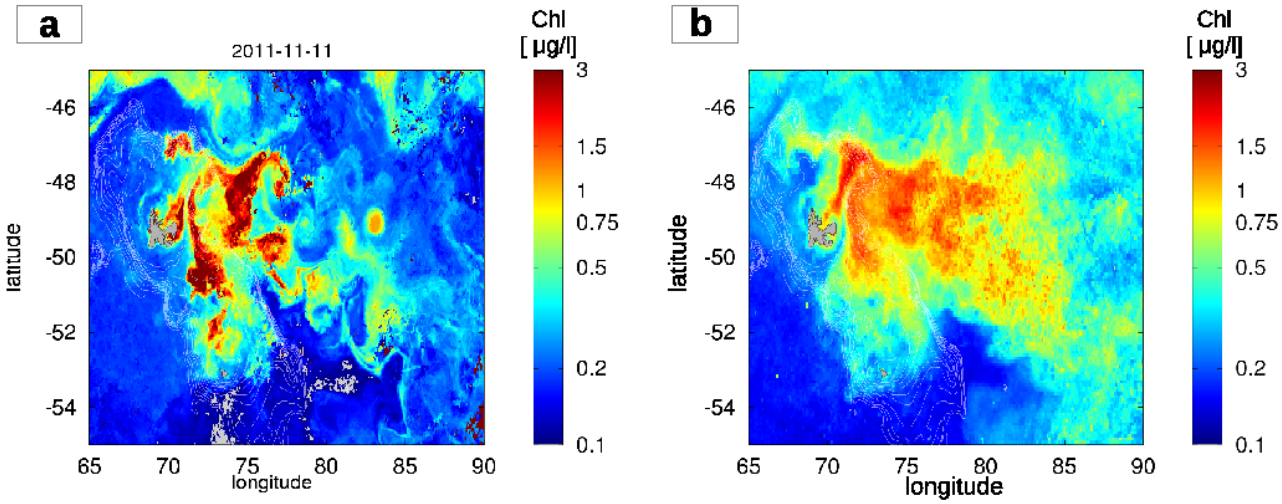

FIGURE A.4: Satellite chlorophyll maps: (a) a snapshot of the situation during the cruise (10 days composite centered on 11 November 2011); (b) November climatology (2000–2011).

of the plume and refine the position of the stations.

Validation

The altimetry-based estimation of the plume has been validated during the cruise with ocean color images of the bloom and post-cruise by analyzing the trajectories of the drifters released during the KEOPS2 and a following cruise two years later (MYCTO-3D-MAP) as well as from historical trajectories of Lagrangian drifters that crossed the region.

Ocean color. The first cloud-free chlorophyll image (fig. A.4a) showing the full extension of the plume was received on the ship the 13th of November 2011 and corresponded to the 11th of November, i.e., after about three weeks from the beginning of the field operations. There was a lot of relief on board by noting the overall good correspondence of the entire plume with the altimetry-based calculation, because the calculation had been used to identify the sampling sites where the bloom was indeed expected to occur.

Table A.1 provides the extension and degree of superposition (congruence) for the altimetry-based forecast and the SCHL plume as seen in ocean color data. In order to define the boundary of the SCHL plume, we used a threshold value of $0.5\mu g/l$, which is a threshold in between typical springtime HNLC values and blooming waters (respectively, around 0.1 and above $1\mu g/l$). Consistently, the extension of the plume obtained with this threshold from ocean color data is approximately the same as the extension of the plume computed by the Lagrangian analysis, setting threshold of three months

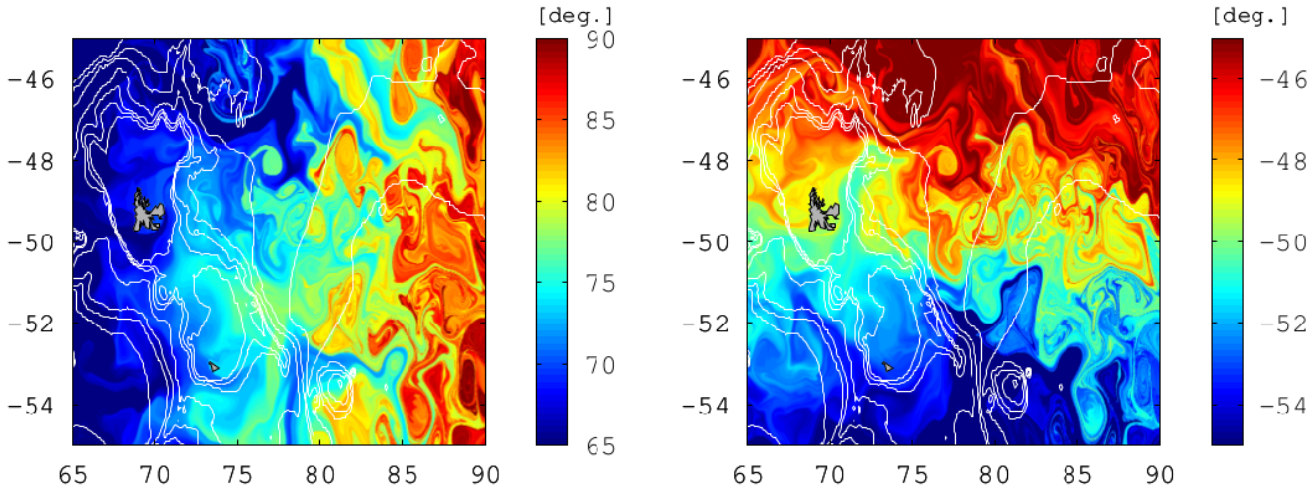

FIGURE A.5: Altimetry-derived 30 day horizontal origin. Left: longitude. Right: latitude.

for the age diagnostic (see Table A.1). Although the objective of the altimetry-based diagnostic is not the prediction of the bloom intensity, note that there is at least a visually qualitative correspondence between "old" water parcels (i.e., the parcels that have left the plateau for comparatively longer times) and low SCHL regions, in particular in the region centered in 73 ° E 49 ° S. This observation suggests that iron removal since leaving the plateau is a more important determinant of spatial iron distributions than variations in iron sources along the shelf break. This does not preclude variations in Fe supply over the plateau, if flow along the shelf break homogenizes the off-plateau supply (as discussed further in section 3.5). This perspective that age since leaving the plateau is a dominant influence on ecosystem responses has become a key tenet of interpretations of the causes of the variations in the magnitudes of the observed mosaic of blooms downstream of the plateau ([Trull et al., 2014, Lasbleiz et al., 2014], this volume) and their associated variations in carbon export ([Planchon et al., 2014, Laurenceau et al., 2014] this volume).

Drifters. In order to validate the altimetry-based estimation of stirring patterns, and in particular the origin from and time since leaving the apparently iron-rich Kerguelen shelf break, 50 SVP Lagrangian drifters were released during the KEOPS2 cruise. An ideal plan would have released the drifters on a regularly spaced linear array which would have followed the shelf break. As this would have consumed too much ship time, drifters have been released instead on transit from one station to another - when approaching the shelf break - or adaptively, when crossing key dynamical features like fronts. In order to palliate to this sub-optimal release scheme, a second opportunistic

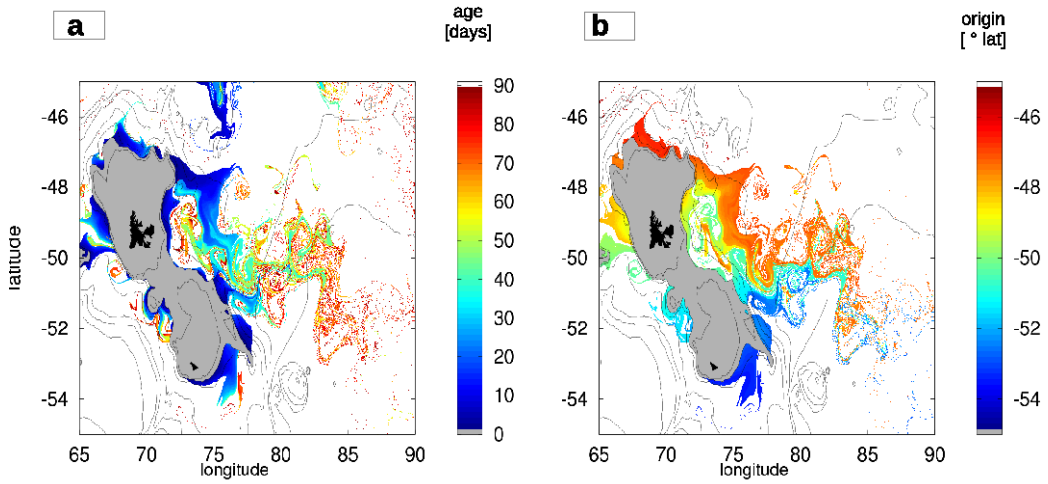

FIGURE A.6: Altimetry-derived estimation of the iron pathways from the plateau to the open ocean: (a) age (days since having left the plateau); (b) latitudinal origin from the plateau.

release experiment was performed by the MYCTO cruise during January-February 2014. This second experiment targeted in particular regions which remained undersampled by the KEOPS2 scheme. Other 2012-2014 SVP historical drifter trajectories were also included in the analysis.

The time since having left the plateau and the latitude of departure from the shelf break also were estimated for each SVP drifter trajectory in analogy with the altimetry-based calculation. Results and comparison are shown in fig. A.7 (first column: altimetry; second row: SVP drifters). As SVP drifters are anchored to a fixed, shallow layer (nominally 15m) under the effect of Ekman drift, the comparison is performed by including in the altimetry-based advection scheme the Ekman component (see Data and Methods). Not surprisingly The SVP plot is much noiser than the altimetry-derived one due to its asynopticity. However, qualitative analogies can be readily seen. In particular, the presence of a "fast lane" stemming from the northern part of the Kerguelen plateau and contouring the Polar front, a recirculation region centered in 74 ° E 49 ° S enclosing older water, and a latitudinal mixing frontier at 85 ° E, where old water parcels encounters are dispersed in thin filaments by strong mesoscale activity. These analogies can be quantified by plotting the ages and origin in scatter plots (fig. A.7,e) and A.7,f)) and noting their compact relationships. We also averaged along the latitude the ages in a band contained between 48S and 50S (fig. A.8). This plot shows that the "age" directly computed from the drifters has a longitudinal dependence of about 5 days per longitude degree, corresponding to a eastward mean drifting speed of 0.15 m/s. On this constant drift local deformations are visible, reflecting the presence of the retentive (hence aging) mesoscale recirculation structures of Figs. A.6 and A.7. In

particular, the drifter-based age has three local maxima centered in 74 ° E, 77 ° E, and 79 ° E. We repeat the same calculation for different altimetry-based products. The regional and global geostrophic products greatly overestimate the retentive effect of the first recirculation region and place its center closer to Kerguelen (in 73 ° E). They both reproduce correctly the mean eastward drift, with the regional product shadowing the drifter-derived calculation closer than the global one - with lower ages, hence stronger and more realistic velocities (black versus green line). Interestingly, the overestimation of the retentive region does not seems to be originated by errors in the geostrophic velocities, but by the fact that drifters also react to Ekman velocities. When Ekman velocities are included into the regional product (blue line), the effect of the retentive region over the age is predicted remarkably well by the satellite product.

		Threshold		Extent plume		Overlap	
		Age (days)	Chl ($\mu g/L$)	Age (km^2)	Chl (km^2)	Extent (km^2)	%
Plume	min	30	1	$1.26 * 10^5$	$1.29 * 10^5$	$3.59 * 10^4$	28
	max	120	0.5	$2.96 * 10^5$	$3.17 * 10^5$	$9.5 * 10^4$	36

TABLE A.1: The table provides the extent and the degree of overlap (congruence) for the altimetry-based forecast – defined through the "water age" diagnostic – and the plume visible from remote-sensed chlorophyll (Chl.). The boundaries of the plume are defined, setting threshold values. The thresholds for the forecasted plumes were chosen to match (within 10 %) the extension of the chlorophyll plume with typical moderate and high values (0.5 and 1 $\mu g L^{-1}$, respectively). The overlap is 36% for the lower chlorophyll threshold (hence for the larger plume) and 28 % for the higher chlorophyll threshold (smaller plume).

Choice of the KEOPS2 stations

A great advantage stemming from the ability of the multisatellite maps to reveal the presence and locations of regions with contrasting origins and histories is that the small scale variability in the age since leaving the plateau can be exploited to examine the large scale contrasts in physical-biological coupling.

Based on the Lagrangian analysis, the chlorophyll plume can be zoned in terms of expected biogeochemical contrasts: a recirculation region; a jet, on the north flank of the Polar Front; a cold water tongue propagating northward along the eastern shelf break; unfertilized, HNLC waters ("reference" case).

For KEOPS2, this perspective was developed in real time. The initial station sampling consisting of a north-south transect to capture latitudinal variations with an east-west transect to examine variations with distance from the plateau, was modified opportunistically to examine the development of a bloom within the "fast lane" jet to the north of the Polar Front, and to cover features evolving in a quasi-langrangian time series

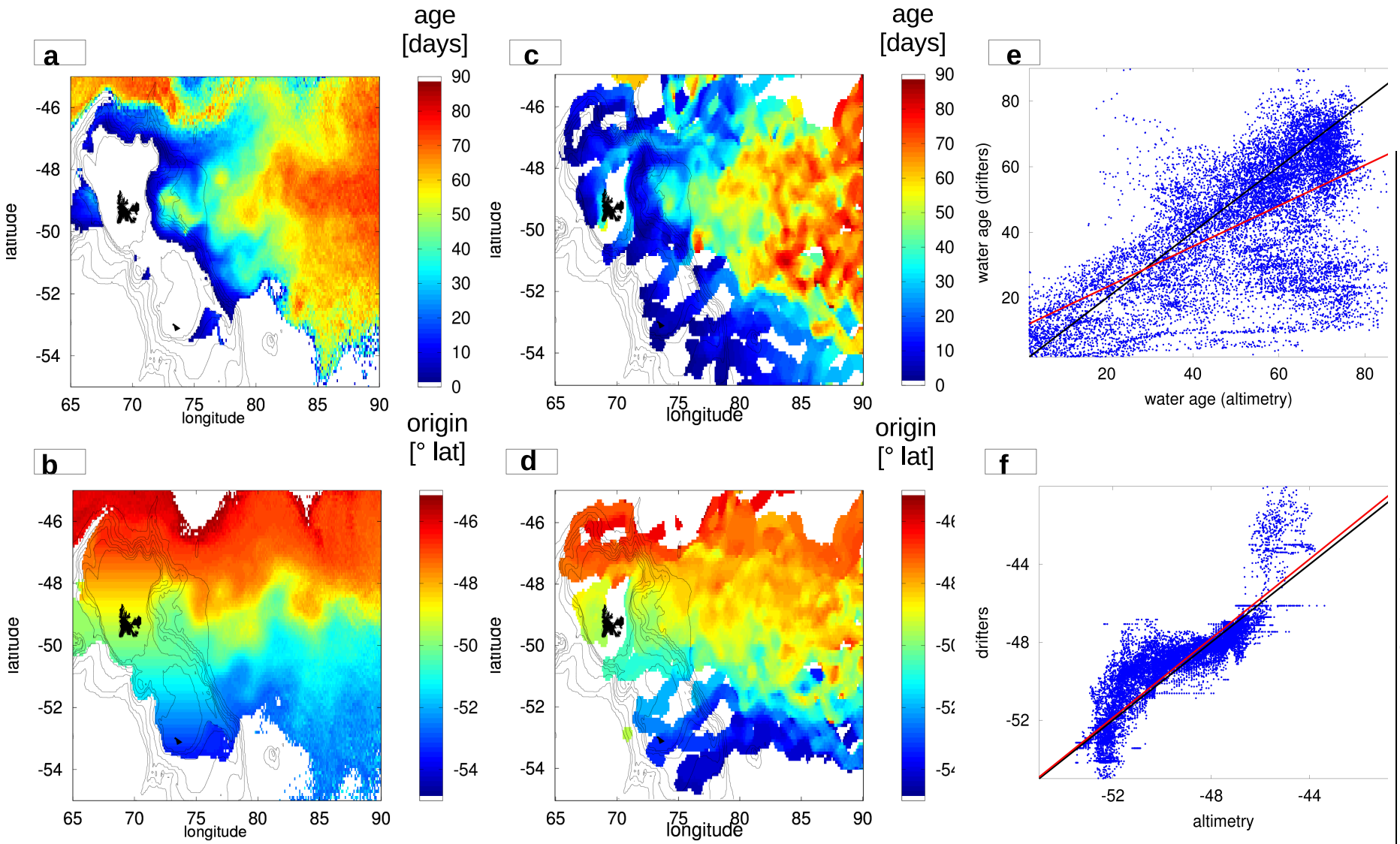

FIGURE A.7: Validation of Lagrangian diagnostics derived from altimetry with the same quantity computed from SVP drifter trajectories. (a–b) Age and origin from the plateau derived from altimetry averaged over spring–summer (October–March) 2001; (c–d) same as (a–b) but derived from trajectories of real SVP drifters deployed during October–November 2011 and January–February 2014. (e–f) Scatter plots of drifter-derived vs. altimetry-derived data for the age and the origin from the plateau, respectively.

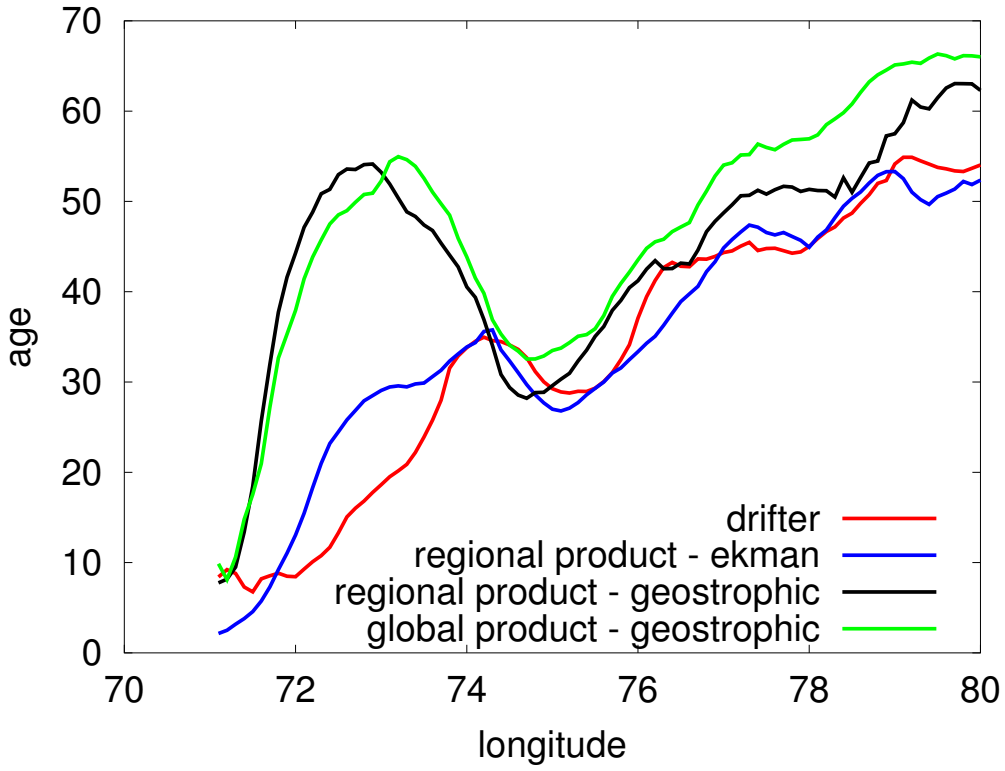

FIGURE A.8: Age from the plateau averaged in latitude along a band $48°S : 50°S$ for different altimetry-based products of surface currents and for SVP drifters. The general trend indicates the mean eastward drift (the age increases with the longitude). Note the local maximum at $72°E : 75°E$ – which indicates a recirculation region – remarkably reproduced by the altimetry regional product which includes Ekman velocities

within the recirculation feature ([Blain et al., 2015], this volume). In addition these perspectives have provided insight with respect to post-voyage analysis and clustering of the results to provide improved insights into the links between iron supply duration and ecosystem responses (e.g. [Lasbleiz et al., 2014, Planchon et al., 2014, Trull et al., 2014], this volume).

Estimation of the mesoscale iron field

Assuming that the iron sources at the shelf break are homogenized by local mixing process and that iron dynamics can be modeled by first order removal, the "age" field can be converted into an iron field (see Appendix). The model has only one free parameter, the scavenging constant λ which relies both on in-situ measurements of DFe concentrations during KEOPS2 and on the determination of τ by satellite altimetry. The stations off the plateau were sorted into two groups, young stations with an estimated age around of 20 days and old stations with an estimated age of around 60 days (Fig. A.9a).

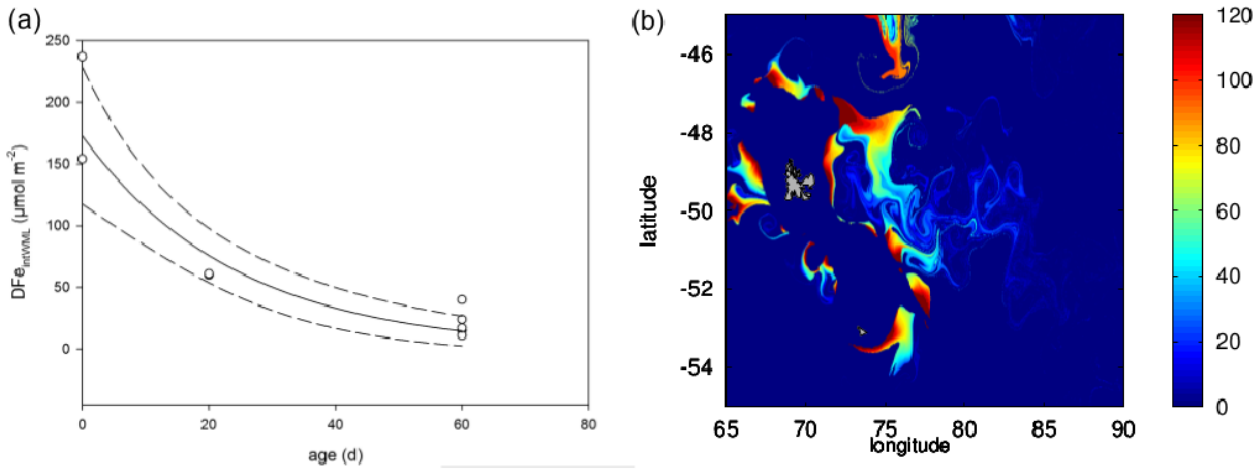

FIGURE A.9: (a) Comparison with in situ iron measurements. (b) Estimation of the iron field ($\mu molm^{-2}$) by merging in situ observations and altimetry-derived age.

We first estimated the removal constant for abiotic conditions (λ_{abio}) using the changes with age of the winter surface mixed layer integrated DFe values. Assuming a first order reaction we derive $\lambda_{abio} = 0.041 \pm 0.006 d^{-1}$ ($r^2 = 0.869$), for those stations located in the northern part of the plateau. Decreasing the age of the young stations to 10 days does not significantly change the estimate of λ_{abio} ($0.038 \pm 0.005 d^{-1}$), but decreases the coefficient of correlation (r^2=0.724). The estimation of the mesoscale iron field is displayed in Fig. A.9b.

We then determined the removal constant λ_{bio} during bloom conditions, from DFe integrated values (0-150m) at the young stations where a large bloom was already well developed at the time of sampling. Combining these values with the integrated values of the source yields $\lambda_{bio} = 0.058 \pm 0.005 d^{-1}$.

Estimation of the exported iron flux

Having estimated Q_{source}, λ and τ, we can estimate the exported flux at any station characterized by its age. For example if $\tau = 20$ days (young water), F_{exp} is in the range $2.6 - 4.3\,10^{-6} mol\,m^{-2} d^{-1}$ and in the range $0.2 - 0.8\,10^{-6} mol\,m^{-2} d^{-1}$ for τ =60 days. Finally, the time scale ts by which this approximation holds is given by the time at which $\lambda t_s << 1$ or $ts << 1/\lambda$. Thus the estimate of the vertical flux is valid for comparison with short term deployment of sediment traps (duration of the deployment of 4-5 days).

Discussion

Biogeochemical field studies are becoming more and more interdisciplinary, so that an increasingly large number of parameters have to be collected and only a very limited number of stations can be occupied during the same day. Nowadays the big challenge of a biogeochemical campaign is how to address this trade off between the biogeochemical analytical resolution and the spatiotemporal coverage with a limited number of multi-disciplinary stations. In-cruise knowledge of the biogeochemical provinces present in a region is therefore an essential information to avoid wasted efforts, for instance sampling multiple times the same conditions. In this regard, remote sensing is an unavoidable tool, because it is the only observation capable of snapshots of regional variability.

The timescales characteristic of a bloom (days to weeks) are also the ones of the (sub)mesoscale and in particular of horizontal stirring. This coupling can create very complex biogeochemical contrasts which evolve in time during the campaign itself. One obvious source of information for mesoscale transport is satellite altimetry. Our study show that this data can be mapped by dedicated diagnostics into biogeochemical regions. The model we developed for the Keops2 cruise may be considered as an attempt to translate altimetric SSH patterns into patterns of primary production, maximizing the spatiotemporal information at the price of any other ones. Indeed, the model provides a pre-condition to the bloom, but does not inform on the intensity (or it does in a qualitative way only) nor on the timing. It is important to notice that this ability to estimate the plume extension at high precision by such a simple model is that the biogeochemical drivers that control the onset of the bloom are relatively simple: high nutrient waters with only one (spring-time) limiting micronutrient; a fixed source of the limiting micronutrient constrained by the topography (the Kerguelen-Heard plateau), possibly homogenized along the shelf by a boundary current, and hence stable in time and space; deep winter convection all over the open ocean region, which dissipate possible nutrient vertical inhomogeneity in the upper layer of the water column. Moreover, the circulation in the region is well captured by altimetry, because there transport is dominated by a barotropic current with a strong geostrophic signal (the ACC). This conditions makes the Kerguelen region as an ideal large scale laboratory for studying fertilization events occurring in the Southern Ocean HNLC systems.

Future developments of the iron dispersion model. It is tempting to extend the altimetry-base model into the vertical for predicting more quantitatively the phytoplanktonic bloom. Indeed, without explicitly accounting for vertical dynamics one may be surprised by the possibility of studying nutrient dynamics at all. However, in the Southern ocean, geostrophic horizontal velocities are typically strongly correlated with the flow within the thick surface layer (of the order of 100m, see [Vivier et al., 2014]). Our

model therefore is a representation of iron transport in the ocean upper layer, whether is it occurring directly in the mixed layer or inside a deeper reservoir which is upwelled by winter-time convection or other vertical processes. The impossibility of resolving in space and time the vertical mechanisms therefore does not hinder the capacity of locating the extension of the iron layer which precondition primary production. On the other hand, the model does not provide any information on the intensity of the bloom and not even on its phenology (i.e., timing). Adding to this model a vertical dynamics, or at least a parameterization, preserving at the same time the fine details directly observed by altimetry, is challenging. The most obvious solution, the use of a three dimensional circulation model, would only maintain the mesoscale dynamics in a statistical sense at best, even when constrained by assimilation. A full three dimensional biogeochemical model would be therefore a natural choice for estimating the regional biogeochemical budgets, but not useful for a (sub)mesoscale adaptive strategy, which requires to track the individual fine scale structures at the best possible precision. For future adaptive sampling, a more promising solution may come from methods which attempt to estimate the vertical dynamics by propagating in the ocean interior surface information (e.g. SSH or SST, [Isern-Fontanet et al., 2008]). This vertical dynamics would require in situ calibration and validation like an array of density casts. This strategy is more complex, costly, and time consuming than the deployment of Lagrangian drifters, and should probably require at least two ships: one for high resolution mapping (for instance with a towed vehicule), the second for traditional in-depth biogeochemical and physical stations (e.g. CTD/rosette).

In terms of future biogeochemical campaigns, it may be instructive to ask which aspects were the most informative, which ones redundant, and which ones should be improved. The most important information for planning the position of the stations was the possibility of sampling waters with contrasted iron concentrations. What would have happened without the Lagrangian model for guiding the adaptive sampling strategy we used? Considering (i) that iron is scavenged during its advection, (ii) that the main source of iron is the Kerguelen plateau, and (iii) that the mean circulation is eastward, it would have been probably tempting to choose the eastward distance from the plateau as a first order proxy of iron scavenging. However, this choice would have been quite misleading due to the presence of mesoscale activity, which creates meandering "high speed lanes" and recirculation features so that locally the relation iron-to-distance may become quite distorted. In particular, we showed that in the few hundreds of km east of Kerguelen (which was the region in the range of the ship) the recirculation region discussed above creates a reservoir of "old" - hence iron-depleted - water in the vicinity of the source, and in turn a locally inverted iron-to-distance relation (i.e., iron locally increasing with distance and not decreasing).

Although the Lagrangian diagnostic discussed here is specific to the Kerguelen situation, the possibility of analyzing multisatellite data with diagnostics based on mechanistic models is a general approach which looks as an appealing companion of multiplatform campaigns. In this study we have performed part of the validation of the diagnostic after the cruise, because the drifters that we used have been released during the campaign. In the case of a multiplatform campaign, a better and safer strategy would be to deploy some of the instruments (like Lagrangian drifters and profilers) before the cruise, in order to have better information on the physical drivers active in the region, integrate in situ information with remote sensing. The possibility of releasing some instruments before the campaign would also avoid the scenario in which a diagnostic is first used for guiding a campaign, and then discovered to perform poorly.

Conclusions

Biogeochemical campaigns are under heavy pressure for resolving the biogeochemical processes at higher precision and for including an increasingly larger number of coupling mechanisms. This need is changing our conceptual view of a biogeochemical process from an approximated zero dimensional or one dimensional water column to a spatial extended system with full three dimensional physical drivers on one side, and complex top-down ecological controls on the other one. This paradigmatic change is blurring the boundaries between biogeochemistry, physics, and ecology, pushing towards end-to-end studies. In this perspective, the use of Lagrangian tools for dynamically zoning a region, mapping in near real time the transport structures present in a region will become even more critical for disentangling the temporal from the spatial biogeochemical variability and for optimally choosing sampling stations in terms of their representativeness.

Further details

Lagrangian modelling of horizontal iron fluxes

Stirring pathways and iron supply

Along a trajectory, the iron content of a water parcel is not affected by transport, because altimetry-derived velocities are almost divergence-free. For a water parcel with coordinate x, y, t, we designate by Q_0 the integrated iron concentration over the plateau and by $\tau(x, y, t)$ the time since when the particle has left the plateau. We assume a first order scavenging process so that the iron content in a given water parcel is given by:

$$Q(x, y, t) = Q_{source} e^{\lambda \tau(x,y,t)}. \tag{A.3}$$

From this equation we see that the spatiotemporal variability of the field Q is completely inherited by the spatiotemporal variability of the field τ. The advantage of rewriting the advection scheme in this form is that the field τ is a purely advective quantity, i.e., it depends only on the velocity field. In physical terms, the field τ can be interpreted as the "age" of the water parcels since leaving the plateau. Calling the time when a particle has left the plateau t_0 (the "birth" of the trajectory), the "age" of that parcel at time t (and hence the length of time for which scavenging has occurred) is $\tau = t - t_0$. In practice, the time t_0 can be found by integrating the velocity field backward in time from x, y, and calculating the time when the backward-in-time trajectory hits the plateau. Note that τ is not defined for particles which do not come from Kerguelen plateau. For these cases, we impose $\tau = \infty$. A map of τ (Fig. A.9 a) provides a snapshot of the stirring pathways east of the Kerguelen plateau. Uncertainties in the estimation of the outflow of water from the plateau, initial iron concentration, scavenging rates, and plume extension can be expected to be large, and it is difficult to make a complete inventory of the major processes that can affect iron dynamics. Nevertheless, we develop here a simple model for estimating the order of magnitude of the flux of iron associated to the Kerguelen plume.

We start by assuming that the iron concentration in the upper layer (0-150m), considered as the winter mixed layer in the plume over the season, is entirely controlled by the off plateau iron flux H and by vertical removal processes Fe_{exp}. Thus, the rate of change of iron content Q (in $molm^{-2}$) can be written:

$$dQ(t)/dt = H - Fe_{exp} \tag{A.4}$$

from which, at equilibrium ($dQ/dt = 0$): $H = F_{exp}$.

We estimated the horizontal iron supply (denoted H in the model described in Methods section 2.5) using altimetry-derived geostrophic surface currents. The vectors of the surface currents were decomposed into along-plateau and cross-plateau components pointing respectively outward and inward with respect to plateau bathymetric contours. The computed outflow water flux Φ_{out} averaged over the period 2006-2013 was $60.1 \pm 4.510^3 m^2 s^{-1}$. This flow can be partitioned into 45% coming from the northern part of the plateau (north of 49.5° N, i.e. a north of the Polar Front), and 55% coming from the southern part of the plateau. The integrated concentration of iron (Q_{source}) in the outflow (top 150m of the water column) was derived from direct measurements of iron concentrations at stations located on the plateau (Queroué et al., this issue). The

source from the northern part of the plateau (i.e., Kerguelen plateau) was estimated to be $153-236$ and $138-158 \mu molm^{-2}$ in winter and spring respectively, whereas the source in the south (Heard plateau) was estimated to be ~ 77 and $54 \mu molm^{-2}$ in winter and spring, respectively. It is likely that this difference results from shallower bathymetry and the proximity of the island in the north. Because the travel time to reach the downstream plume edge is circa 3 months, the horizontal flux in Nov-Dec was calculated using the winter time Q_{source} estimate (based on the remnant winter water temperature minimum Fe data) and the horizontal flux in Jan-Feb was calculated with the springtime Q_{source} estimate (based on the Oct-Nov surface water Fe data).

Using the altimetric mean velocities and these Q_{source} estimates, we obtained the total amount of DFe injected into the 0-150 m layer per day. To express this as an areal average flux, we derived the size of the plume from satellite ocean colour images. Using a threshold of 0.3-0.4 mg Chl m^{-3}, the area is 2.5-3.8 $10^{11} m^2$. This is in good agreement with the estimates based on altimetry (2.7-3.3 $10^{11} m^2$) assuming an age of the water parcel in the plume not older than 90 and 120 days, respectively. Thus the average supply flux for the whole plume is $2.4 \pm 0.6 10^{-6} molm^{-2} d^{-1}$ in Oct-Nov and $1.7 \pm 0.4 10^{-6} molm^{-2} d^{-1}$ in Jan-Feb. These values are obtained propagating the uncertainties on the iron estimation indicated above and have to be considered as orders of magnitudes. Indeed, if the calculation is repeated by including the uncertainties in the altimetry-derived water fluxes and plume extension, the uncertainty over the iron supply flux grows up to 60%. The calculation does consider different iron concentrations for the Kerguelen and for the Heard plateau, but it neglects possible smaller-scale iron variability along the shelf break of these two plateaux. Although the along-shelf jet associated to the meander of the Polar front east of Kerguelen plateau (dashed line in Fig. A.1) mitigate this issue providing a homogenization effect, we are not able to exclude that some contrasts in iron concentration still remain. Future campaigns aimed at pinpointing iron sources in will undoubtedly help in constraining this uncertainty.

Iron content and export

The idealized model Eq. A.4 also allows estimation of the vertical flux of iron that is exported below the plume into deeper waters. Substituting in Eq. A.4 a removal term F_{exp} which follows a first order law:

$$F_{exp} = \lambda Q, \tag{A.5}$$

the solution at equilibrium is:

$$Q_{eq} = H/\lambda. \tag{A.6}$$

The amount of iron that is exported (Q_{exp}) at 150m during the time t_s at each location of the plume is:

$$Q_{exp} = Q_{source} e^{-\lambda\tau}(1 - e^{-\lambda t_s}). \tag{A.7}$$

If $\lambda t_s << 1$ (i.e. for removal periods shorter than a month) , then the exponential can be expanded at first order:

$$Q_{exp} = Q_{source} e^{-\lambda\tau}(1 - 1 + \lambda t_s) = Q_{source} \lambda t_s e^{-\lambda\tau}. \tag{A.8}$$

Thus the vertically exported flux during t_s is:

$$F_{exp} = Q_{source} \lambda e^{-\lambda\tau}. \tag{A.9}$$

Acknowledgements

The authors would like to thank the Marion Dufresne crew and B. Queguiner. The altimeter and colour/temperature products for the Kerguelen area were produced by Ssalto/Duacs and CLS with support from Cnes. The authors would also like to acknowledge AVISO/CLS, Météo-France, and the Global Drifter Program/NOAA/AOML, Miami, Florida both the Drifter Operations Center and Data Assembly Centers for arranging drifter deployments and data assembly, quality control and distribution of the data. A. Della Penna was supported by a conjoint Frontières du Vivant (Paris 7) and CSIRO-UTAS Quantitative Marine Science PhD scholarship. This work was supported by the French Research program of INSU-CNRS LEFE-CYBER (Les Envéloppes Fluides et l'Environnement–CYcles Biogéochimiques, Environnement et Ressources), the French ANR (Agence Nationale de la Recherche, SIMI-6 program, ANR-10-BLAN-0614), the French Cnes (Centre National d'Etudes Spatiales), the French Polar Institute IPEV (Institut Polaire Paul-Emile Victor), the NASA/Cnes OSTST ALTIMECO project, and ANR MYCTO-3D-Map.

Appendix B

Appendix B. Autonomous profiling float observations of the high biomass plume downstream of the Kerguelen plateau in the Southern Ocean

This appendix is published as *Autonomous profiling float observations of the high biomass plume downstream of the Kerguelen plateau in the Southern Ocean* by M. Grenier, A. Della Penna and T. W. Trull in *Biogeosciences*, 2015.

Abstract

Natural iron fertilisation from Southern Ocean islands results in high primary production and phytoplankton biomass accumulations readily visible in satellite ocean colour observations. These images reveal great spatial complexity with highly varying concentrations of chlorophyll, presumably reflecting both variations in iron supply and conditions favouring phytoplankton accumulation. To examine the second aspect, in particular the influences of variations in temperature and mixed layer depth, we deployed four autonomous profiling floats in the Antarctic Circumpolar Current near the Kerguelen plateau in the Indian sector of the Southern Ocean. Each 'bio-profiler' measured more than 250 profiles of temperature (T), salinity (S), dissolved oxygen, chlorophyll-a (Chl-a) fluorescence, and particulate backscattering (bbp) in the top 300 meters of the water

column, sampling up to 5 profiles per day along meandering trajectories extending up to 1000 km. Comparison of surface Chl-a estimates (analogous to values from satellite images) with total water column inventories revealed largely linear relationships, suggesting that these images provide credible information on total and not just surface biomass accumulations. Regions of very high Chl-a accumulation (1.5-10 μg L-1) were associated predominantly with a narrow T-S class of surface waters. In contrast, waters with only moderate Chl-a enrichments (0.5-1.5 μg L-1) displayed no clear correlation with specific water properties, including no dependence on mixed layer depth or the intensity of stratification. Geostrophic trajectory analysis suggests that both these observations can be explained if the main determinant of biomass in a given water parcel is the time since leaving the Kerguelen plateau. One float became trapped in a cyclonic eddy, allowing temporal evaluation of the water column in early autumn. During this period, decreasing surface Chl-a inventories corresponded with decreases in oxygen inventories on sub-mixed layer density surfaces, consistent with significant export of organic matter ($\sim$ 35%) and its respiration and storage as dissolved inorganic carbon in the ocean interior. These results are encouraging for the expanded use of autonomous observing platforms to study biogeochemical, carbon cycle, and ecological problems, although the complex blend of Lagrangian and Eulerian sampling achieved by the floats suggests that arrays rather than single floats will often be required, and that frequent profiling offers important benefits in terms of resolving the role of mesoscale structures on biomass accumulation.

Introduction

The productivity of the Southern Ocean is important for many reasons. It supports fisheries and high conservation value marine mammal and bird populations [Constable et al., 2003, Nicol et al., 2000], influences the carbon dioxide content of the atmosphere [Sarmiento and Le Quere, 1996, Sigman and Boyle, 2000, Watson et al., 2000], and affects the magnitude of nutrient supply to large portions of the global surface ocean [Sarmiento et al., 2004]. This productivity is limited by the scarce availability of iron (Fe) as an essential micro-nutrient [Boyd and Ellwood, 2010, Boyd et al., 2007, Martin et al., 1990]. Island sources of Fe elevate productivity and produce downstream 'plumes' of elevated phytoplankton biomass that contrasts with the general HNLC (High Nutrients, Low Chlorophyll) nature of the Southern Ocean [Blain et al., 2007, De Baar et al., 1995, Mongin et al., 2009, Pollard et al., 2009, Nielsdóttir et al., 2012]. Ship based studies of several of these regions, focused on the influence of Fe on carbon (C) transfer to the ocean interior [Blain et al., 2008, Salter et al., 2007], have revealed

a diversity of responses in terms of intensity of enhanced productivity, biomass accumulation, and ecosystem structures. This diversity derives from interactions between the supply and bio-availability of iron with other drivers of productivity such as temperature, water column stratification and stability, light levels, and the possibility of co-limitation by other nutrients [Assmy et al., 2013, Boyd et al., 2001, Boyd et al., 1999, Quéguiner, 2013]. Assessing influences on productivity, biomass accumulation, carbon export, and carbon dioxide (CO_2) uptake in the Southern Ocean is challenging because of variations across many scales, including weather, seasonal, and interannual time-scales, and sub-mesoscale, mesoscale, and circumpolar frontal space scales [Joubert et al., 2014, Le Quéré et al., 2010, Lenton et al., 2013, Lévy, 2003, Nicol et al., 2000, Shadwick et al., 2015, Sokolov and Rintoul, 2007, Swart et al., 2014, Thomalla et al., 2011, Weeding and Trull, 2014]. Satellite observations offer extensive space-time coverage [Martinez et al., 2009, Moore and Abbott, 2000], but may provide a biased view if surface distributions are not representative of water column inventories. Important ways that bias could arise include lack of direct correlations of surface values with their vertical extents (e.g. high surface chlorophyll values might be predominantly associated with shallow accumulations, through the promotion of production by higher light levels in shallow mixed layers; [Sverdrup, 1953]), the presence of unobserved subsurface chlorophyll maxima [car, , Schlitzer, 2002], or the variation of phytoplankton to chlorophyll ratios with growth conditions [Cloern et al., 1995, Fennel and Boss, 2003, Goericke and Montoya, 1998]. These difficulties of observation become even more acute for carbon export estimates, which require either flux measurements (e.g. from moored or free-drifting sediment traps or radionuclide activities [Planchon et al., 2014, Savoye et al., 2004] or the partitioning of changes in state variables across biogeochemical versus oceanographic causes (e.g. nitrate depletions in surface waters or oxygen consumption at mesopelagic depth; [Trull et al., 2014, Matear et al., 2000]). Obtaining estimates of carbon export and the depth of its penetration into the ocean interior are important to determining impacts on the climate system, because variations in these two factors have similar influence to variations in total primary production in terms of the sequestration of CO_2 from the atmosphere [Boyd and Trull, 2007]. Notably, export estimates expressed as 'e-ratio' fractions of primary production [Maiti et al., 2013], or as 'f-ratio' fractions of production derived from 'new' nitrate supply [Savoye et al., 2004] vary widely in the Southern Ocean, with the possibility that these efficiencies are increased by natural iron fertilisation [Jouandet et al., 2011, Trull et al., 2008]. This space-time complexity is abundantly demonstrated by the 'mosaic of blooms' (i.e. patchiness pattern) encountered in waters downstream from the Kerguelen plateau during the KEOPS2 field program in austral spring (October-November 2011), as detailed in many papers in a special volume of Biogeosciences [d'Ovidio et al., 2015, Trull et al., 2014, Lasbleiz et al., 2014, Laurenceau et al., 2014, Cavagna et al., 2014]. Much of the meso-scale spatial

variations in biomass accumulation, as seen in satellite images and animations [Mongin et al., 2009, d'Ovidio et al., 2015, Trull et al., 2014], appears to result from the interleaving of iron-enriched water parcels that have transited the Kerguelen plateau with surrounding iron poor waters, as demonstrated by analysis of satellite altimetry based circulation estimates and surface drifter trajectories [d'Ovidio et al., 2015, Park et al., 2014]. However, shipboard studies close to the plateau [Mosseri et al., 2008, d'Ovidio et al., 2015, Blain et al., 2015, Trull et al., 2014, Lasbleiz et al., 2014, Laurenceau et al., 2014] suggest that other factors are also likely to play a role, including mixed layer depth and upper water column stratification. To explore the influence of variations in these water column properties on bloom structure at larger scale, in particular further from the plateau than could be surveyed by ship, we deployed autonomous profiling drifters. The first one was successfully launched during the KEOPS2 field program in late October 2011, and the other three during the MyctO-3D-MAP (referred to as MYCTO, from now on in this text) interdisciplinary survey between late January and early February 2014. Given the extent of the Kerguelen biomass plume ($>$ 1000 km; [Mongin et al., 2009]), the remoteness from ports, and the generally rough sea states, the use of autonomous platforms is arguably the only affordable way to survey this region. As shown in Figure B.1, these deployments returned data from a large proportion of the enriched biomass plume downstream of the Kerguelen plateau.

In this paper, we use the bio-profiler observations to address three questions:

- Do satellite images of surface chlorophyll provide an unbiased guide to the spatial distribution of total water column chlorophyll, or are they biased by lack of knowledge of variations in the vertical extent of chlorophyll distributions or the presence of subsurface chlorophyll maxima?
- Do regions of high biomass correlate with particular oceanographic properties, such as warmer or fresher waters, or the intensity of stratification? If so, are these properties determined locally or by the upstream origins of the different water parcels?
- Can the fate of surface enrichments in biomass be determined (and eventually quantified) from along-trajectory temporal variations in biogeochemical properties, for example by progressive downward movement of fluorescence or particulate backscattering signals or decreases of oxygen in subsurface waters?

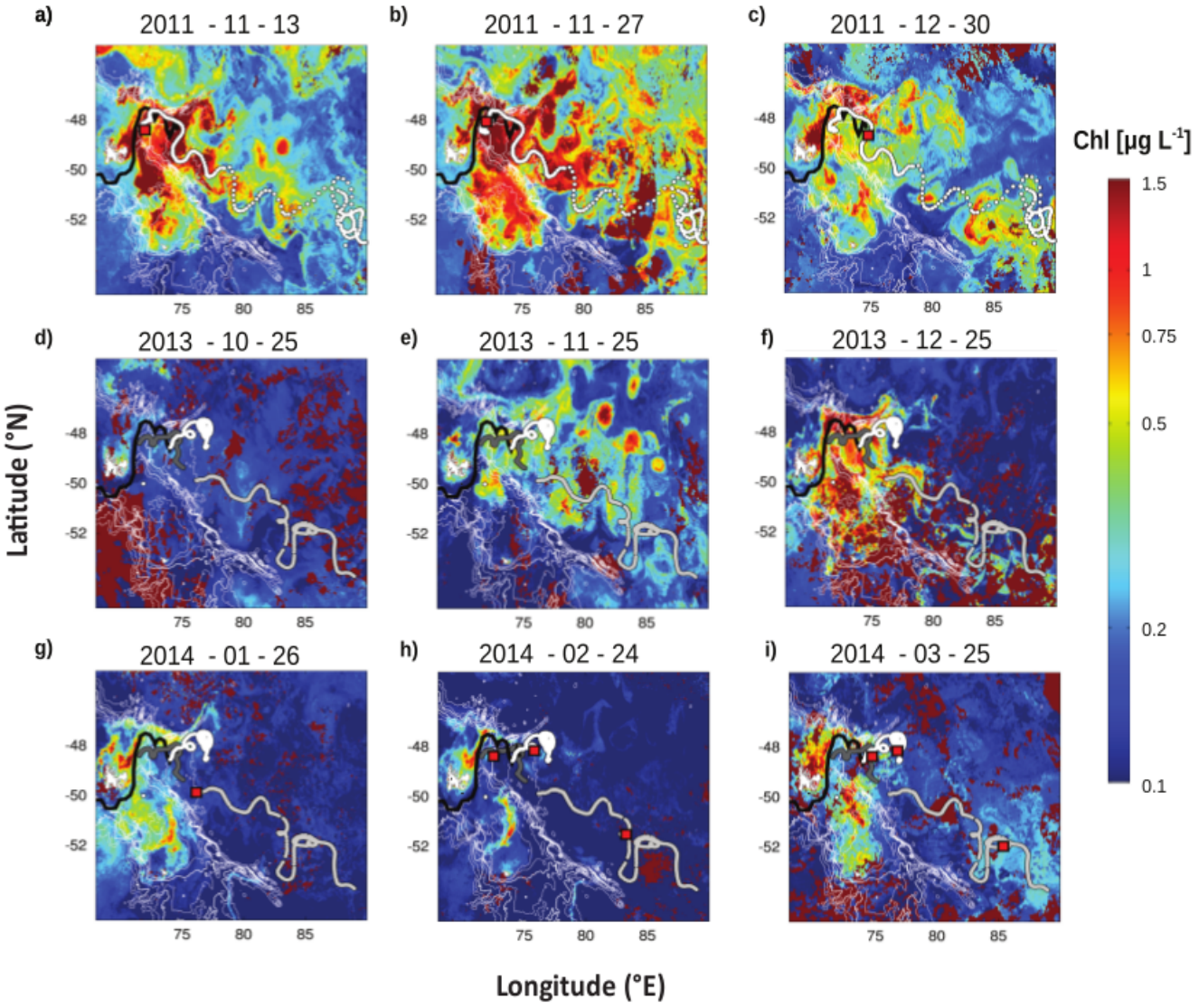

FIGURE B.1: Maps of bio-profiler trajectories (white and grey lines) over remotely sensed chlorophyll-a distributions (a-h: daily, 4 km CLS/CNES product; i: weekly composite from GlobColour 4 km product). Top row: 2011 bloom season for bio-profiler #1. Middle and bottom rows: 2013/2014 bloom and beginning of post-bloom season for bio-profilers #2 (light grey trajectory), #3 (dark grey trajectory) and #4 (white trajectory). Red squares indicate the bio-profiler locations corresponding to the day of the image. The black thick line refers to the position of the Polar Front measured from hydrographic samples by Park et al. [Park et al., 2014].

Methods

Float sensor and mission configurations

The float deployment locations are provided in Table B.1, along with their identification numbers which provide access to their full data sets via the Australian Integrated Marine Observing System (www.imos.org.au). Float deployment was done in 2011 by manual transfer to a small boat and then the sea, and in 2014 by deploying the floats from the ship deck inside cardboard boxes designed to readily disintegrate after release. The autonomous profiling floats were all of the same design (Model APF9I, Teledyne-Webb, Inc.). Each was equipped with pumped, poisoned, thermosalinographs (Model SBE 41CP-2.0, Seabird, Inc.), end-cap mounted un-pumped oxygen optodes (Model 3830, Aanderaa, Inc.), and two-channel bio-optical sensors (Model FLBBAP2, Wetlabs, Inc.) strapped onto the lower third of the float hull with their optical ports facing horizontally to minimize possible interferences from particle accumulation. Owing to the structure of the firmware for the floats and the varying power requirements for the sensors, the sampling rates differed for the physical and biogeochemical parameters. Temperature and salinity were sampled at the highest rates, yielding values at 2 decibar intervals (used in this work as equivalent to 2 meter depth intervals without density corrections), whereas oxygen, fluorescence and backscatter were sampled at 10 decibar intervals, except for bio-profiler #1 where they were sampled at 5 decibar intervals in the first 150 m. Temperature and salinity calibrations were performed by Seabird, Inc., with estimated accuracy and precision of better than 0.005 ° C and 0.01, respectively [Oka and Ando, 2004]. These variables, used as water mass proxies and to estimate mixed layer depths and stratification intensity (expressed as the Brunt-Väisälä frequency), helped to determine if dissolved oxygen evolutions were mainly due to physical processes or to biological production or respiration processes. The oxygen optodes were calibrated at CSIRO prior to mounting on the floats against a 20 point matrix of 4 temperatures (0.5 - 30) and 5 oxygen saturations (0 - 129%) using the methods detailed in Weeding and Trull [Weeding and Trull, 2014]. Similar sensors exhibited drift during a 6 month mooring deployment in the Southern Ocean of less than 1.7 μmol kg-1 over 6 months [Weeding and Trull, 2014]. The bio-optical sensors measured chlorophyll-a fluorescence via stimulation/emission at 470/695 nm) and particulate backscattering at 700 nm. Chlorophyll-a fluorescence is a useful proxy for chlorophyll-a concentration and standing stocks of phytoplankton biomass [Falkowski and Kiefer, 1985, Huot et al., 2007]. Particulate backscattering provides a good proxy for particulate organic carbon [Stramski et al., 2008, Cetinić et al., 2012]. The bio-optical fluorescence sensors were calibrated (by the manufacturer, Wetlabs, Inc.) against fluorescent uranine solutions as working standards, and cross- referenced to prior measurements of a laboratory culture (25 mg

m-3 chlorophyll) of the diatom *Thallassiosira weissflogii* to yield chlorophyll estimates. These calibrations are warranted to yield linear responses with precisions among multiple sensors of better than 10%, and (after one cycle of testing and replacement with the manufacturer) we obtained reproducibility for the set of three floats deployed in 2014 of better than 4% based on measurements with fluorescent and non-reflective plastics [Earp et al., 2011]. Accordingly, calculation of the chlorophyll fluorescence from the float data was done by removal of the background dark signals measured prior to deployment and scaling to chlorophyll using the manufacturer's calibrations. Similarly, the retrieval of particulate backscattering, bbp (m-1), at 700 nm from the backscatter raw transmitted measurement (counts) was done by applying the manufacturer-provided scaling factor after correction for dark counts (i.e. measured signal output of the backscatterometer in clean water with black tape over the detector), with the additional steps of removal of the pure seawater backscattering contribution [Zhang et al., 2009], and scaling from the limited solid angle sensor measurement to the total backscattered hemisphere based on relations estimated from observations for a wide range of marine particles [Boss and Pegau, 2001, Sullivan et al., 2013]. In contrast to typical Argo program float missions for climate studies (www.argo.org), which consist of deep (2000 m) profiles every 10 days, the bio-profilers were programmed to focus on the upper water column and carried out continuous profiling between the surface and 300 m depth, achieving 4 to 6 profiles per day, depending on the stratification. This temporal resolution was intended to allow examination of daily cycles related to insolation, photosynthesis, and respiration. In practice, it proved difficult to extract clear cycles because of aliasing from spatial variations. Consequently, after several weeks for the 2011 KEOPS2 deployment of bio-profiler #1, the frequency of profiles was reduced to twice daily, to provide extended battery life while still obtaining night and day observations to allow insolation quenching of the fluorescence response to be evaluated and corrected, and thus to avoid inappropriate inference of subsurface chlorophyll maxima from the fluorescence signal [Sackmann et al., 2008, Xing et al., 2012]. For bio-profilers #2, #3, and #4 deployed in 2014, the missions were further refined, via automated telemetric switching of mission configuration files, to carry out a deep profile to ∼1500 m every 3 days to provide deep reference points for temperature, salinity, and oxygen observations, and also with the intention to slow the development of bio-fouling of the bio-optical sensors by exposing surface organisms to high pressures.

Float data quality control

Extensive experience by the Argo program with profiling float measurements for temperature (T) and salinity (S), including recovery of floats for post deployment tests [Oka

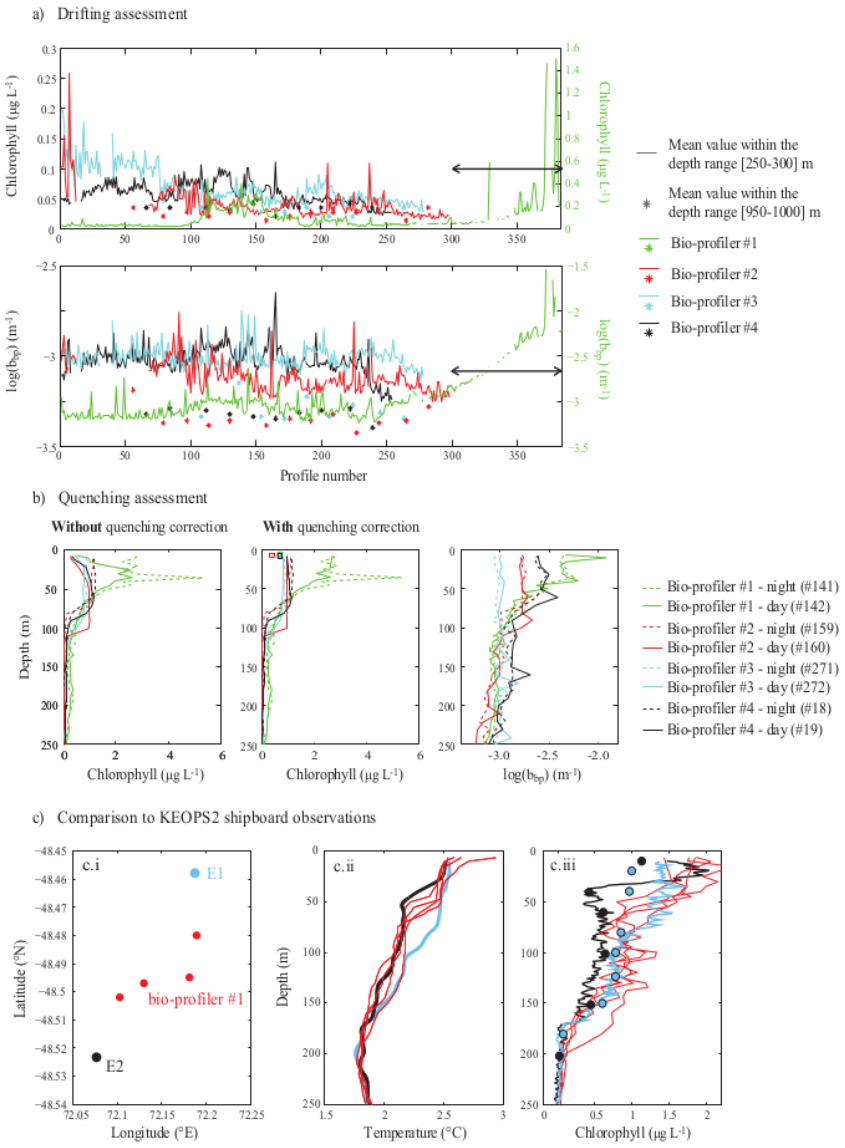

FIGURE B.2: a) Assessment of bio-optical sensor stability from temporal evolution of chlorophyll and particulate backscattering values averaged over two depth ranges, 250-300 m (lines) and 950-1000 m (stars). Arrows indicate profiles considered to be affected by bio-fouling, which were not used in further analysis. b) Illustration of quenching corrections, showing pairs of successive night/day profiles (day: continuous lines; night: dashed lines). For each bio-profiler, the panel shows: chlorophyll profiles without quenching correction (left), chlorophyll profiles with quenching correction (middle), and associated particulate backscattering profiles (right). Squares in the middle panel represent threshold values of the lowest surface chlorophyll concentration for the night profiles of each bio-profiler (#1: 0.7 μg L-1; #2: 0.4 μg L-1; #3: 0.65 μg L-1; #4: 0.7 μg L-1). These threshold were used to flag day profiles having surface chlorophyll concentration still below this threshold after the quenching correction (see Table B.3, Figures B.7 (squares), 5 (red circles) and 7 (squares)), for which quenching might have been under-corrected. c) Comparison of bio-profiler #1 fluorescence Chl-a estimates to shipboard results obtained by the KEOPS2 project:, c.i. Location of KEOPS2 stations E1 (blue symbols) and E2 (black symbols) along a quasi-Lagrangian track followed by bio-profiler#1 (red symbols); c.ii Temperature profiles showing similar structures of the ship and bio-profiler sampled water columns; c.iii Fluorescence profiles (lines) showing that the bio-profiler provided similar fluorescence results to the ship CTD mounted sensor, and that both exhibited complex relationships to Niskin bottle total chlorophyll-a sample values (dots; see text for further discussion).

TABLE B.1: Bio-profiler deployments. Hull #: serial number for the bio-profiler body. WMO #: World Meteorological Organization identification number for the bio-profiler data stream.

#	Hull #	WMO #	UTC date	Lat. (° N)	Long. (° E)	Campaign	Last profile (UTC date)
1	5122	1901329	29 October 211	-48.5	72.2	KEOPS2	22 April 2012
2	6684	5904882	26 January 2014	-49.9	76.2	MYCTO	14 April 2014
3	6682	1901338	28 January 2014	-48.4	71.5	MYCTO	14 April 2014
4	6683	1901339	4 February 2014	-48.6	74.0	MYCTO	14 April 2014

and Ando, 2004], suggests that these sensors reliably deliver accurate and precise observations (to better than 0.005 °C and 0.01 salinity) over multi-annual deployments. Given our much shorter bio-profiler deployments (3 to 6 months) and their observed T-S relationships which fall within those of the ship-based KEOPS2 observations, we assume these variables are correct and make no further assessment or correction. We similarly accept the oxygen observations, given our careful attention to their pre-deployment calibration, their reasonable range of surface water oxygen super-saturations (96-103% for low chlorophyll waters and extending up to 108% in correlation with very high chlorophyll waters, as discussed further below), and their deep ocean values (950-1000 m depths) which fall within the range of nearby ship observations and showed no temporal trends and standard deviations of less than 4 μmol kg-1 over the deployment periods (ranging from 1 to 3.9 μmol kg-1 for the four bio-profilers). To evaluate the possibility of temporal sensor drifts in bio-optical variables, we examined the variations of the bio-optical variables in mesopelagic (250-300 m) and deep water (950-1000 m) values, i.e. at depths where little signal was anticipated and most profiles reached steady background values (Figure B.2 a). The particulate backscattering and, to a lesser extent, the Chl-a fluorescence signals showed spikes which presumably reflect larger particles such as aggregates and zooplankton, motivating our examination of average values over 50 m ranges (250-300 m and 950-1000 m depth layers) for the assessment of temporal drifts. As shown in Figure B.2a and quantified in Table B.2, for most of their deployment periods all four bio-profilers exhibited no significant temporal drift of these deep values except for bio-profiler #1, for which high and erratic values of Chl-a and bbp began to occur after profile #300 both at depth (Figure B.2a) and throughout the water column (Figure B.3c and e). We consider this to be caused by bio-fouling and do not use this data in any subsequent analysis (this loss of signal fidelity was one of the motivations for including periodic deep profiles in the subsequent three bio-profiler deployments, as a means of retarding fouling). In contrast, the high fluorescence chlorophyll values found in mesopelagic waters from profiles ~#100 to ~#170 along the bio-profiler #1 trajectory appear to be real and to reflect the deep extension of high biomass occurrence at this time, as discussed further below (see also Figure B.3c). Consequently, this range of profile was not taken into account for the drift calculation in Table B.2. Overall, except for the bio-profiler #1, most of the bio-optical sensors showed a slight loss of sensitivity

with time, as indicated by the negative slopes of the trend of their responses in the two considered depth layers (Table B.2). Over the time course of the bio-optical sensor observations, these sensor drifts were small in comparison to the changes observed for surface bio-optical values, contributing less than 7% to either fluorescence or particulate backscattering. The only exception was the drift for the bio-profiler #2 bbp sensor in the 250-300 m layer, where drift appeared to have been larger (though of course changes at this depth range may also be oceanic) and reached up to 19 % of the low surface bbp values for this bio-profiler. Fluorescence signals were also corrected for daytime quenching. This effect, which derives from the photo-inhibition of phytoplankton by an excess of light (maximum at midday), decreases surface fluorescence [Falkowski and Kolber, 1995, Kiefer, 1973] and, if uncorrected, can produce a false impression of subsurface maxima in fluorescence derived chlorophyll profiles. We explain this correction and its evaluation in considerable detail in the following paragraphs, but note that none of the conclusions of the paper depend on these corrections because the same overall results are obtained if we use only Chl-a fluorescence signals collected at night. Our purpose in detailing the correction is to contribute to active discussion of the best way to use daylight Chl-a fluorescence data obtained from platforms which may not have as good night time coverage as our floats (such as sensors deployed on seals, on standard ARGO 10- day profile interval missions, or on float missions that target co-measurement with daytime satellite ocean colour observations). We defined the daytime profiles, potentially affected by quenching, as profiles acquired between one hour after local sunrise time and one hour after local sunset time, to allow for dark acclimation since quenching effect could still persist after sunset [Sackmann et al., 2008]. Daytime profiles from the four bio-profilers are shown to illustrate this effect (continuous lines in Figure B.2b, left panel). To correct this bias, we applied the method of Sackmann et al. ([Sackmann et al., 2008], which uses the particulate backscattering signal as a relative reference. For the sake of consistency with the other studies of this issue, we defined the mixed layer depth, MLD, as the depth where density increased by 0.02 kg m-3 relative to the density at 10 m [Park et al., 1998]. Within the deeper half of the mixed layer (targeted to be below the depth of daytime quenching), we determined a mean value of the (relatively constant, see below) Chl-a fluorescence to bbp ratio (at depth defined as dF/bbp) and multiplied this ratio by the bbp signal at this depth to retrieve the Chl-a fluorescence. Then, we multiplied this same ratio by the surface bbp value to estimate unquenched surface Chl-a fluorescence, and interpolated between these two depths to obtain the unquenched Chl-a fluorescence profile. This assumes that phytoplankton populations were not stratified within the density defined mixed layer. This works particularly well for deep mixed layers (>50 m) which exhibit relatively constant Chl-a fluorescence/bbp ratios (to within ∼10%) in their deeper half. In less than 3% of the daytime profiles, in average, we could not identify a region of uniform Chl-a fluorescence/bbp and apply the

quenching correction; consequently, these profiles were not used further. The greater spikiness of the bbp profiles in comparison to those of fluorescence (as illustrated in Figure B.2b, right panels) means that this quenching correction introduces some noise into the daytime chlorophyll estimates. In principle, this could be filtered or smoothed, but the low 10 m vertical resolution of the observations made this rather uncertain and so we have used the unfiltered observations throughout this paper (except in Figure B.12f below where we show median-filtered particulate backscattering profiles for the sake of visual clarity). Note that to avoid to correct the surface Chl-a fluorescence with a spiked surface bbp value and create a "bbp spiked" interpolation, we verified before that the bbp surface value did not seem to be spiked, assuming that surface value should not exceed more than ±50% of the bbp value at the depth dF/bbp, since within the mixed layer. This threshold was defined after assessing the backscatterometer precision (using the coefficient of variation of bbp, i.e. the ratio of the standard deviation to the mean) between 500 and 1000 m depth of 14 ± 4% in average. If the surface bbp value was considered as spiked (less than 4% of the daytime bbp profiles, except for bio-profiler #4 for which it reached 9%), the test was done with the second depth value, until a "non-spiked" value was found, and the value was then extrapolated to the surface. The effects of the quenching correction on our selected chlorophyll profiles are shown in Figure B.2b (middle panels, continuous lines), and summary statistics for all the profiles are provided in Table B.3. Without the correction, on average, more than 70% of the daytime profiles exhibited a subsurface maximum exceeding 60% of the surface value –defined after assessing the fluorometer error (coefficient of variation of Chl-a concentration) between 250 and 300 m depth and between 500 and 1000 m depth of 22 ± 10% in average. After applying the quenching correction method, the number of daytime profiles exhibiting a subsurface maximum exceeding 60% of the surface value was reduced to very similar levels to those observed in the night time profiles, although slightly higher (of 21% in average), indicating, with the fact that these daytime subsurface maxima occurred mostly below the MLD, that the correction was largely successful. Notably, for the total data set, after quenching correction, less than 11% of the profiles exhibited a deep maximum exceeding 100% of the surface value (Table B.3), and these profiles were primarily located in a restricted region near the Gallieni Spur, as discussed further in the Results section. Even after our quenching correction, 10% of the corrected daytime profiles (in average for all 4 bio-profilers) still exhibited significant decrease of the Chl-a fluorescence in the surface layer. We were not able to conclude if these decreases were due to an incomplete quenching correction or if they were true features, given that ∼ 14% of the night profiles in average exhibited subsurface values at least 60% higher than the surface values. Consequently, we defined a threshold surface value for each bio-profiler, defined as a slightly lower value than the minimum surface value reached during night profiles (see squares in Figure B.2b, middle panel, and caption)

and we flagged all the corrected daytime profiles that had a surface value lower than this threshold as potentially arising from incomplete correction of quenching. These distinctions between night, daytime and flagged profiles are illustrated in Figures B.7, B.8 and B.10, and further discussed in the Results and Discussion sections below. Note that, using a different quenching correction method, Biermann et al. [Biermann et al., 2015] recently observed similar features and statistics in fluorescence profiles collected by southern elephant seals during austral summer in the vicinity of Kerguelen Island.

Finally, we emphasize that the bio-optical measures of chlorophyll and particulate backscattering are based on laboratory calibrations that are not specific to Southern Ocean phytoplankton or particle properties. This means that while interpretation of local variations is reasonably straightforward, quantitative comparisons to other observations much more uncertain (except perhaps in the future for other serial numbers of these sensors, calibrated in the same limited way). For the 3 bio-profilers deployed in 2014, no ancillary shipboard measurements are available to evaluate this issue, but in 2011 some chlorophyll samples were collected by the KEOPS2 science team that allow for limited evaluation of the bio-profiler #1 calibration. Bioprofiler #1 was deployed into a semi-permanent meander of the Polar Front, which the KEOP2 program examined as a Lagrangian time series following surface drifters. As shown in Figure B.2c, the first and second stations in the meander (E1 CTD-27 on 29 October 2011 at 22:46 local time and E2 CTD-43 on 1 November 2011 at 12:00 local time) bracketed the locations of the first 11 autonomous bio-profiler #1 profiles (Figure B.2c.i). The bio-profiler #1 temperature profiles are intermediate between the ship results (Figure B.2c.ii), with the variations in temperature profiles mainly driven by vertical motions associated with internal waves (Park et al., 2014b). In Figure B.2c.iii, the KEOPS2 shipboard fluorescence results are displayed after linear calibration to high pressure liquid chromatography (HPLC) total chlorophyll-a results from below 40 meters depth (below the depth of non-photochemical quenching). The data reveal two important features: i) good fits achieved below 40 meters do not extend to the surface – where fluorescence/chlorophyll-a ratios were higher than at depth, apparently as a result of community composition variations with depth (see also Lasbleiz et al. [Lasbleiz et al., 2014]), and ii) the bio-profiler #1 fluorescence data displayed similar characteristics and good accord with the shipboard results. In light of the limited available data, a non-linear calibration of fluorescence to chlorophyll-a was not pursued, and no adjustments were made to the laboratory bio-profiler calibration. These variations in fluorescence/chlorophyll-a ratios within individual CTD casts in the shipboard observations serve as a strong reminder that fluorescence is an imperfect proxy for chlorophyll-a concentrations, owing to variations with phytoplankton community structure, physiology, and other effects (e.g. References [Babin et al., 1996, Cullen, 1982, Suggett et al., 2011]. Thus, interpretation of our sensor records, as

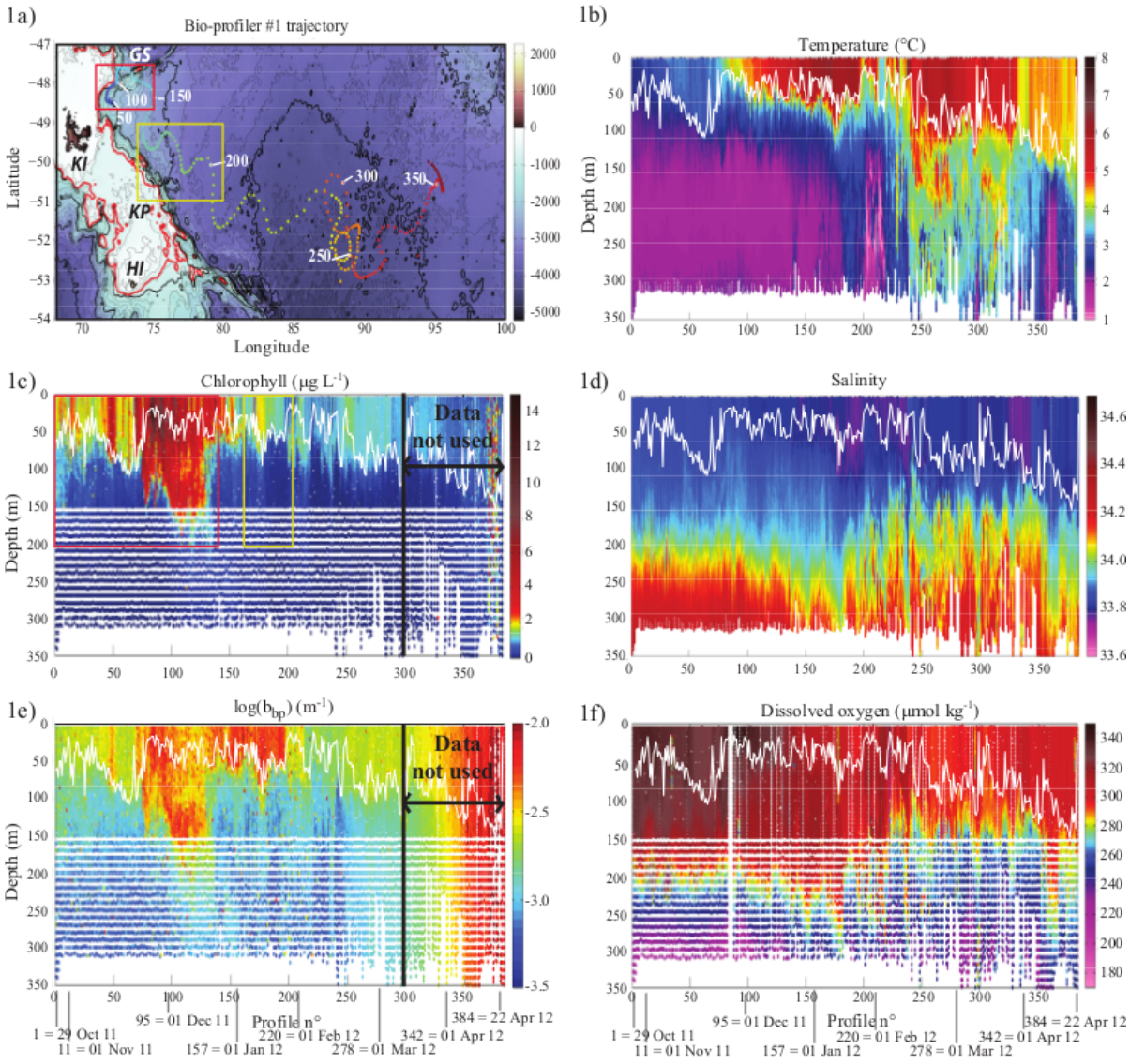

FIGURE B.3: Bio-profiler #1 observations a) bio-profiler #1 trajectory over the bathymetry, with each point representing a depth profile and the colour of the points changing from blue to red over time (dates are shown below the bottom plots). The 700 m isobath is represented by the red line contour. KI = Kerguelen Island; KP = Kerguelen Plateau; HI = Heard Island; GS = Gallieni Spur. b-f) Evolution of hydrological parameters along the float trajectory: b) temperature (°C), c) chlorophyll (μg L-1), d) salinity (unitless), e) particulate backscattering (bbp; log scale; m-1), and f) dissolved oxygen (μmol kg-1). The white line represents the mixed layer depth. Red and yellow rectangles refer to rich and moderate chlorophyll areas used in Figure B.10 and discussed in Section 4.2.

with any bio-optical sensor results, must keep this in mind and avoid over-interpreting small variations in fluorescence as necessarily resulting from variations in chlorophyll or phytoplankton biomass.

TABLE B.2: Drift assessment of the bio-profiler over their lifetime within the [250-300] m and [950-1000] m depth layers. (Mean absolute drift = Mean slope x no. of profiles. Mean drift relative to Chlorophyll concentration = Mean slope x no. of profiles / mean Chl concentration. For bio-profiler 1 the Chl drift was calculated between profiles #1 and #300 and excluding the deep biomass production profiles (range [100-171]). Mean drift relative to mean surface b_{bp} = Mean slope x no. profiles / mean particulate backscattering.)

Chlorophyll concentration drift within the [250-300] m depth layer			
#	Mean slope (μ g L $^{-1}$ profile $^{-1}$)	Mean absolute drift (μ g L $^{-1}$)	Mean drift relative to the mean surface Chl a concentration
1	8.4050 E-5	0.0252	+1%
2	-1.7832 E-4	-0.0531	-5%
3	-2.8722 E-4	-0.0798	-6%
4	-1.1976 E-4	-0.0304	-3%
Chlorophyll concentration drift within the [950-1000] m depth layer			
#	Mean slope (μ g L $^{-1}$ profile $^{-1}$)	Mean absolute drift (μ g L $^{-1}$)	Mean drift relative to the mean surface Chl a concentration
1	-	-	-
2	-2.1917 E-6	-0.0007	<-1%
3	-9.0120 E-5	-0.0251	-2%
4	1.2438 E-5	0.0032	<+1%
Particulate backscattering drift within the [250-300] m depth layer			
#	Mean slope (m $^{-1}$)	Mean absolute drift (m $^{-1}$)	Mean drift relative to the mean surface b_{bp}
1	1.1625 E-6	3.4876 E-04	+11%
2	-1.1613 E-6	-3.4608 E-04	-19%
3	-1.9682 E-7	-5.4716 E-05	-2%
4	-6.7301 E-7	-1.7094 E-04	-10%
Particulate backscattering drift within the [950-1000] m depth layer			
#	Mean slope (m $^{-1}$)	Mean absolute drift (m $^{-1}$)	Mean drift relative to the mean surface b_{bp}
1	-	-	-
2	-2.2931 E-7	-6.8335 E-05	-4%
3	-4.4734 E-7	-1.2436 E-04	-6%
4	-2.0227 E-7	-5.1378 E-05	-3%

Satellite data sources

We used satellite products to provide physical and biological context for the bio-profiler trajectories, including the effectiveness of their sampling of high biomass waters downstream of Kerguelen. The images of surface chlorophyll concentrations shown in Figure 1 to provide context for the plume sampling achieved by the bio-profilers are the CLS SSALTO/DUACS 4 km daily product derived from NASA MODIS-Aqua observations (Figure B.1), without modification for recent suggestions that this algorithm may underestimate chlorophyll in low chlorophyll waters south of Australia [Johnson et al., 2013].

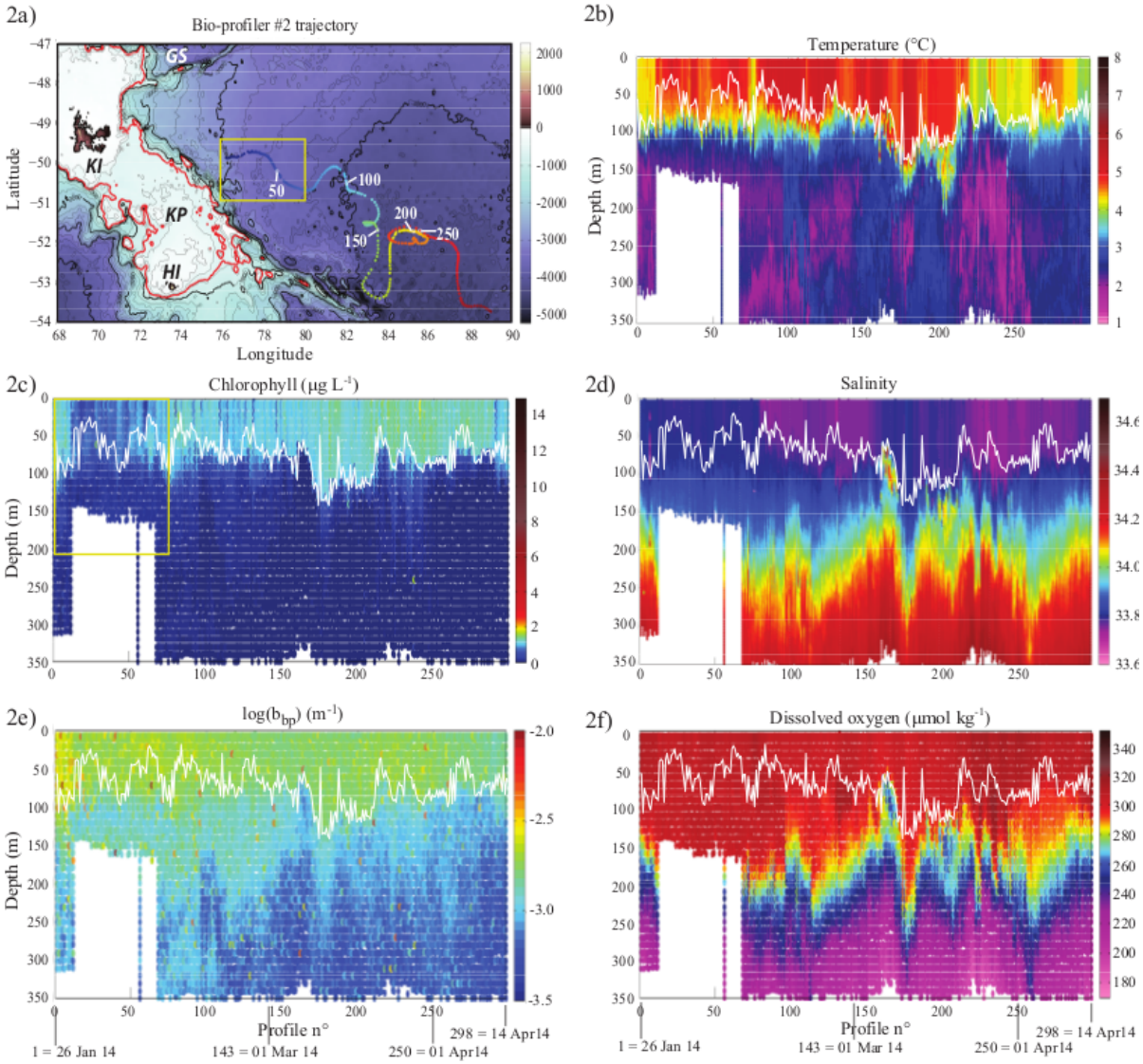

FIGURE B.4: Bio-profiler #2 observations (see Figure B.3 caption for details).

To better understand the observed bio-profiler trajectories, we calculated expected movements based on geostrophic currents estimated from satellite altimetry using the multi-satellite global product Delayed Time Maps of Absolute Dynamic Heights (DT-MADT) developed by the CNES/CLS Aviso project (www.aviso.oceanobs.com). This product has 1 week temporal and 1/3° spatial resolutions, and was used to compute Lagrangian trajectories to produce a diagnostic for eddy retention ([d'Ovidio et al., 2013]; Figure B.12b) and water origin and age ([d'Ovidio et al., 2015]; Figure B.11). Eddy retention is a measure of how much time a synthetic water parcel has been recirculating within an eddy core. Long-lived and coherent eddies are characterised by water parcels with high values of retention (measured in days since a water parcel has been entrained by

an eddy), whereas recently formed eddies or eddies that exchange strongly with surrounding regions have low retention values. Following d'Ovidio et al. [d'Ovidio et al., 2015] and Sanial et al. [Sanial et al., 2014a], we used back-tracking of virtual water parcels (from the bio-profiler profile locations) to compute how long ago (water age) and at which latitude (water origin) the sampled parcels had been in contact with the Kerguelen Plateau (defined as the 700 m isobath, as shown in red in Figure B.3). Figure B.11 a) and c), adapted from d'Ovidio et al. [d'Ovidio et al., 2015] , display example maps of the calculated daily snapshots of these water ages and water origins. For each pixel in these maps, virtual water parcels were back tracked for 90 days. They are shown as white pixels on the maps if during that time they never touched the Kerguelen Plateau (shown in grey on the map), and otherwise are coloured for the time between the contact with the plateau and the day of the map computation (water age, Figure B.11a) and the latitude of the last contact with the plateau stored (water origin, Figure B.11c). These same computations were performed for each location sampled by the bio-profilers, in order to compare the water ages and origins with their measured chlorophyll inventories.

Results

Coverage of the plume

The drifts of the bio-profilers provided coverage of a large portion of the elevated biomass plume (Figure B.1), from near the Kerguelen plateau to more than 700 miles downstream (71 to 95 ° E) and nearly 400 miles from north to south (47.5 to 54° S), thereby spanning waters of the Polar Frontal and Antarctic Zones [Orsi et al., 1995, Park et al., 2008, Sokolov and Rintoul, 2009]. Unfortunately, this breadth of spatial coverage of the plume did not extend to full temporal seasonal coverage, and this is important to keep in mind given the strong seasonal cycle of biomass accumulation [Trull et al., 2014, Blain et al., 2007, Mongin et al., 2008]. As shown in these images, the 2011 bio-profiler covered the period of highest biomass accumulation, while the 2014 deployments occurred after this seasonal peak, and thus sampled the system during its senescence (to illustrate these prior conditions, Figure B.1 also includes biomass distribution images from late 2013, before the launch of the three bio-profilers in early 2014). Thus, the profilers obtained some seasonal context for the central portion of the plume (which was sampled well in 2011 by bio-profiler #1 in spring and summer and again by bio-profilers #2 and #3 in summer and autumn). However, sampling of the north-eastern portion of the downstream plume (north of the Polar Front) was achieved only in late summer and autumn (by bio-profiler #4). Bio-profiler #1 in spring 2011 and bio-profiler #3 in 2014

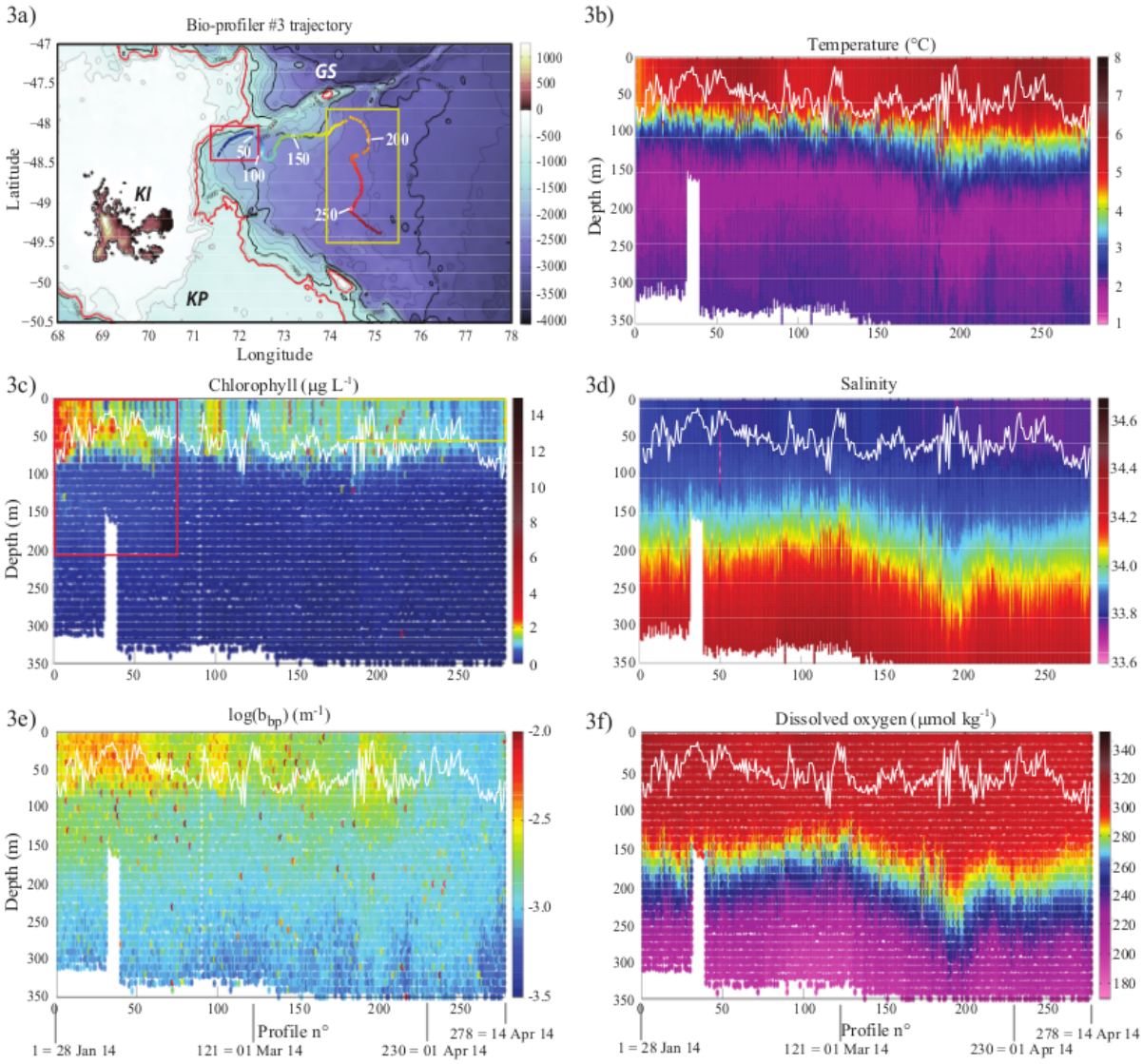

FIGURE B.5: Bio-profiler #3 observations (see Figure B.3 caption for details).

were deployed in the centre of the quasi-stationary cyclonic recirculation just east of the northern Kerguelen plateau [d'Ovidio et al., 2015, Park et al., 2014]. Both bio-profilers exited this region to the northeast, tracking towards the Gallieni Spur, before transiting strongly southward near 74° E. This southward transport has also been observed for surface drifters and appears to be associated with a persistent meander of the Polar Front [d'Ovidio et al., 2015, Park et al., 2014]. Thus bio-profilers #1 and #3 provide spring and summer perspectives respectively for these portions of the biomass plume (albeit in different years). Bio-profiler #2 was deployed further south, close to the region where the strong north to south transport portions of the bio-profilers #1 and #3 trajectories finished. Thus bio-profiler #2 provided some overlap with the southern portion of the bio-profiler #1 trajectory, before being carried the furthest south, where it explored cold waters close to the Williams Ridge that extends to the southeast of Heard Island and

terminates near the Fawn Trough (a gap in the plateau which permits the passage of much of the deep water eastward transport [Park et al., 2008, Park et al., 2014]). Waters in this region tend to exhibit archetypical high-nutrient, low-chlorophyll characteristics, and were used as a reference station for iron non-fertilised waters during the KEOPS field program in 2005 (Blain et al., 2007; 2008) [Blain et al., 2007, Blain et al., 2008]. In contrast, bio-profiler #4 was deployed at similar latitude to bio-profilers #1 and #3, but further east, in particular east of the southward meander of the Polar Front which carried these others to the south. Bio-profiler #4 remained in the northern portion of the plume throughout its deployment, drifting to the northeast roughly parallel to the shallow Eastern Kerguelen Ridge before becoming trapped in a cyclonic eddy in which it obtained a time series of ∼100 profiles (as discussed in detail below).

Overview of observed oceanographic properties

The bio-profilers return a large number of water column observations making visualisation at the scale of individual profiles only possible for targeted issues. The simplest first-order assessment is most easily done by presenting the results as along-trajectory sections. These are shown for all the observed variables for each bio-profiler in Figures B.3, B.4, B.5 and B.6, and briefly described in the following paragraphs. Bio-profiler #1, launched in late October 2011 in the centre of the deep water recirculation just east of Kerguelen Island, initially encountered cold, well oxygenated waters with moderate biomass (T $\sim$ 3 $^\circ$ C, $O_2 \sim 330$ μmol kg^{-1}, 0.5 μg L^{-1} < Chl-a < 2μg L^{-1}; profiles 1-90, Nov.). It was then carried north-eastward across the Gallieni Spur where it encountered warmer waters with extremely high biomass (T $\sim$ 5 $^\circ$ C, chlorophyll up to nearly 10 μg L^{-1}), which satellite ocean colour animations suggest was being swept northward as a mix of waters from the northern and central regions of the Kerguelen plateau (see the animation "bloom 2011" in supplementary material; [Trull et al., 2014]). During the subsequent southward transport, it crossed the Polar Front near 51.5° S, as shown by the presence of a temperature minimum near 150 m depth (T $\sim$ 1 °C; profiles $\sim$ 200-220, end of Jan.). The shoaling of low dissolved oxygen layers in this region provides another indication of their Antarctic Zone oceanographic classification. Surface waters above this remnant winter water were relatively warm despite deep mixed layer depths ($\sim$ 100 m, T > 6°C; profiles ∼240-330, Feb.-Mar.). Much of this warming is probably seasonal, as these waters were encountered in late summer, but the co-occurrence of somewhat elevated salinity ($\sim$ 33.8) suggests that flow of Polar Frontal Zone surface waters over the Antarctic waters was also involved. During the February bio-profiler transit, these waters exhibited only low to moderate chlorophyll biomass (∼1.5 μg L-1), although satellite images suggest higher concentrations (∼3 μg L^{-1}) were present earlier

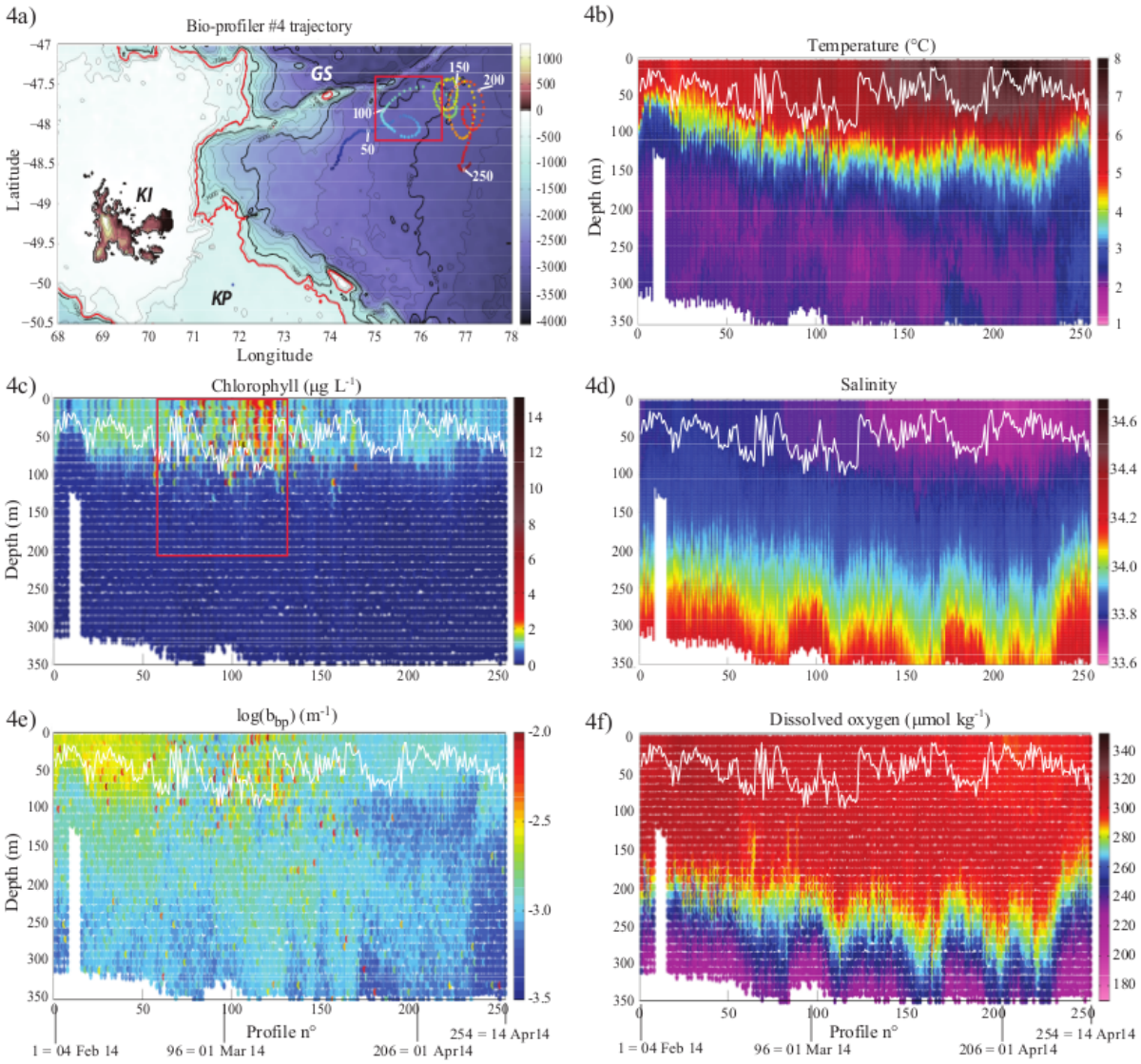

FIGURE B.6: Bio-profiler #4 observations (see FigureB.3 caption for details).

in December and January (see Figures B.1b and B.1c and the animation "bloom 2011" in supplementary material; [Trull et al., 2014]). The particulate backscattering signal reflected the chlorophyll evolution along most of the trajectory, except in January when, as the chlorophyll levels decreased (from >3 μg L^{-1} to $\leq$ 2 μg L^{-1}), bbp remained high and constant (-2.5 m^{-1} $\leq$ log(bbp) $\geq$ -2.0 m^{-1}), suggesting detrital particles developed from the high chlorophyll biomass, or possibly a (relatively large) change in chlorophyll/particulate organic carbon ratio (Chl/POC) due to phytoplankton community composition. Finally, after 300 shallow profiles, bio-fouling of the fluorescence and particulate backscattering sensors marked the end of their utility, as shown by the occurrence of elevated and highly noisy values throughout the water column (see Figure B.3c and e).

Bio-profiler #2, launched in late January 2014 south and east of the recirculation feature, initially encountered Polar Frontal Zone waters which were present further south in this region than during the 2011 year sampled by bio-profiler #1. For approximately the first 150 profiles, these waters displayed relatively homogenous, moderately warm temperatures (4-5 ° C) that continued to warm to ∼6 ° C through February. The bio-profiler then transited much further south, briefly encountering waters with strong shoaling of subsurface salty, low oxygen characteristics around profiles 160-170 (S ∼ 34.0-34.2, $O_2 \sim 260$ μmol kg^{-1}), and entered colder Antarctic waters where it remained through profile ∼220, at which time its return north brought it back into Polar Frontal Zone waters showing autumn cooling. Throughout its life, in comparison to bio-profiler #1, only low-to-moderate biomass waters were encountered (<1.5 μg L^{-1}), though these values were persistently above Southern Ocean HNLC background values (< 0.5 μg L-1). Within this range, the higher biomass values, which also extended over greater vertical extents (∼ 100 m), were found in the Antarctic waters (profiles 170-250, Mar.-Apr.). In contrast, the higher bbp values were found at the beginning of the trajectory (log(bbp) ∼ -2.5 m^{-1}), and their deep extent and high values compared to chlorophyll levels suggest the existence of higher chlorophyll concentrations prior to the bio-profiler deployment. This is in agreement with satellite ocean colour animations on which high biomass development is observed in December 2013 in the area of the bio-profiler deployment (see Figures B.1e and B.1f and the animation "bloom 2013" in supplementary material). After this initial difference, the bbp variations followed those of chlorophyll along the rest of the trajectory. Bio-profiler #3, launched in late January 2014 in the northern portion of the recirculation feature, followed a similar trajectory to that of bio-profiler #1 launched in October 2011 and encountered much warmer waters with similar mixed layer depths, between 40 and 70 m (Figure B.5). Presumably this represents seasonal warming as salinities were similar to those encountered in spring (∼ 33.85), and the warming from ∼3 ° C to nearly 6 °C is consistent with seasonal warming amplitudes observed in satellite surface temperature records for unfertilized open ocean Polar Frontal Zone waters [Trull et al., 2001]. Persistent high chlorophyll levels were also observed initially in the recirculation region (up to ∼4 versus ∼1 μg L^{-1}), but the float did not cross the Gallieni Spur (GS in maps of Figure B.3) where bio-profiler #1 encountered values up to nearly 10 μg L^{-1}. During its transit south near 75 ° E, only Polar Frontal Zone waters were encountered, and chlorophyll levels remained moderately high (between 1 and 2 μg L^{-1}). At the beginning of the trajectory, the particulate backscattering bbp signal evolved in concert with the chlorophyll signal, but with a ∼ 7-10 day delay. Another difference between the two biomass parameter evolutions was the large increase of bbp compared to chlorophyll between the surface and 100 m, right after the profiler turned southward in the vicinity of the Gallieni Spur (∼ profiles 190-205, end of March). Bio-profiler #4, deployed well east of the recirculation feature in early February, was

initially in warm, quite salty and well oxygenated waters, characterized by moderate biomass (first 80 profiles: T $\sim$ 5.5 $^\circ$ C, S $\sim$ 33.8, O_2 $\sim$ 310 μmol kg^{-1}, Chl-a $<$ 1.5 μg L^{-1}, log(bbp) $\sim$ 3.35 m^{-1}). As its trajectory approached the Gallieni Spur, surface waters became progressively warmer, fresher and less oxygenated (profiles 80-250: T $\sim$ 7 $^\circ$ C, S $\sim$ 33.7, O_2 $\sim$ 290 μmol kg-1). During this time, the bio-profiler recorded high chlorophyll and particle concentrations (chlorophyll values reaching up to 3 μg L^{-1} for profiles 80-130). This high biomass could be a remnant of the rich filament that transited in this area a month prior to the visit of the bio-profiler (see the animation "bloom 2013" in supplementary material). As the bio-profiler drifted further east, it was entrained in a relatively stationary cyclonic eddy where it performed several loops before exiting to the south (profiles $\sim$ 130-240, mid-March – mid-April). This eddy can be identified from altimetry as retentive – i.e. capable of entraining Lagrangian particles for, in this case, a few weeks to one month ([d'Ovidio et al., 2013]; Figure B.11b). While retained by this mesoscale eddy, the bio-profiler measured a relatively constant profile of temperature and salinity, with slowly decreasing Chl-a concentrations and bbp (Figure B.11). Relatively constant hydrological properties throughout this period and the repeated looping suggest a largely Lagrangian trajectory within a single water parcel at this time. Of all the observations, this region displayed surface waters with the highest temperatures and lowest salinities (T $\sim$ 8.0 $^\circ$ C, S $\sim$ 33.6).

Discussion

With this overview of the spatial and temporal characteristics of our observations in hand, we proceed to evaluate our research questions.

Do the satellite images of surface chlorophyll reflect water column contents?

As discussed in the Introduction, it is important to determine whether the water column information provided by the bio-profilers changes perspectives on the mesoscale distributions of chlorophyll as seen in satellite images (Figure B.1) This is a larger issue than whether our in-situ measurements of surface values differ from satellite values. We did not evaluate that question owing to extensive cloud cover greatly limiting match-ups between bio-profiler and satellite observations, and because we know that both our sensor calibrations and the satellite algorithms have large uncertainties (see the Methods). Instead, we examined the bio-profiler water column observations to determine what biases might be expected from observing only their upper portions, i.e. as a satellite would.

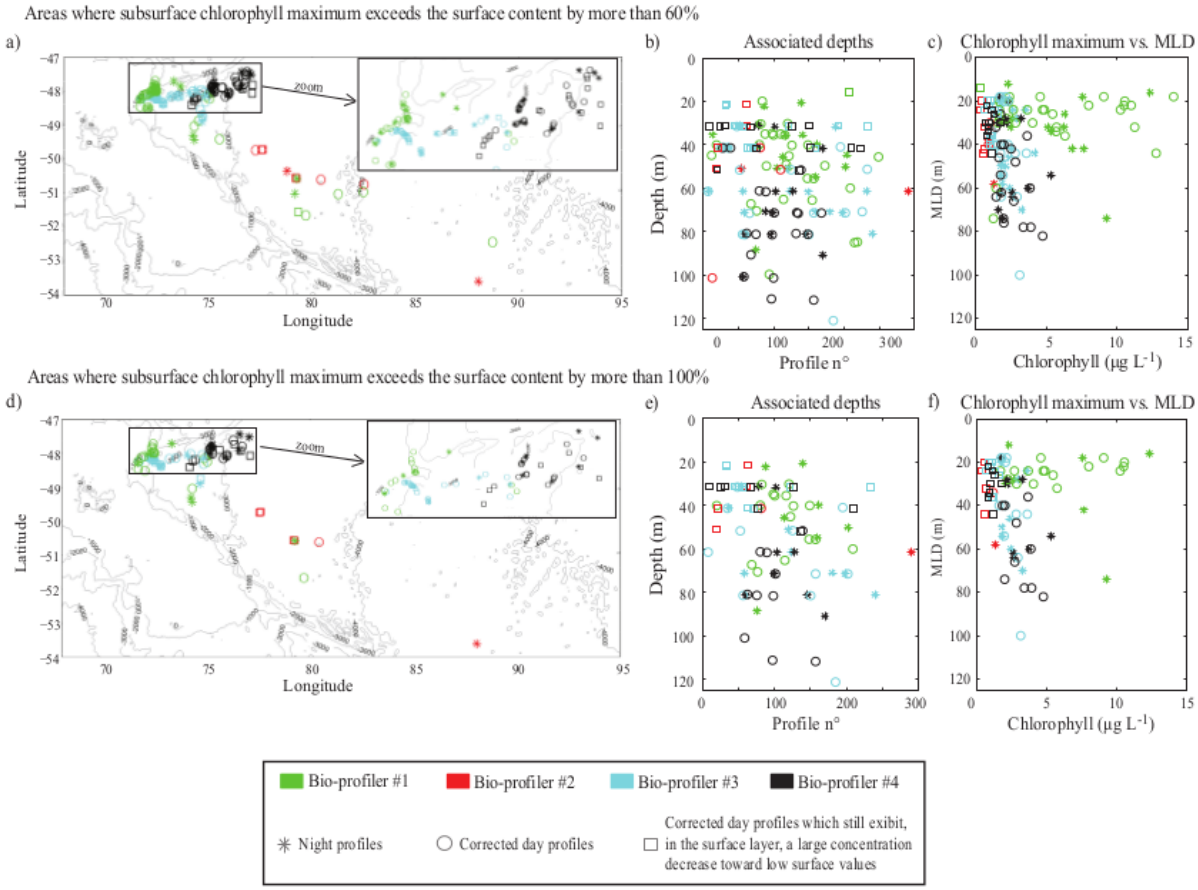

FIGURE B.7: Characteristics of subsurface chlorophyll maxima occurring at depths greater than the mixed layer depth and exceeding the surface content by more than 60% (top) and 100% (bottom). a) and d): geographical areas where these subsurface Chl-a maxima occur with an expanded view for the Gallieni Spur region; b) and e): associated depths of these subsurface Chl-a maxima along the bio-profiler trajectories (i.e. versus profile numbers); c) and f): relationship between the amplitude of these Chl-a maxima (in μg L^{-1}) and the mixed layer depth (MLD, in m). Symbols: stars refer to night profiles, circles to day profiles and squares to flagged day profiles (i.e. which still exhibit, in the surface layer, a large concentration decrease toward low surface values that indicates the possibility of incomplete quenching correction; see definition in the caption of Figure B.2b).

There are two aspects of this issue that we could readily address: i) were subsurface chlorophyll maxima commonly present below the depth of satellite observation, and did they vary spatially or temporally? ii) were surface chlorophyll values linearly and tightly correlated with water column inventories with similar dynamic ranges, or were surface values poor guides to water column inventories? We address these issues in this order in the following paragraphs. Our statistics on the occurrence of subsurface chlorophyll maxima (Table B.3) show that these features were present in a significant fraction of the profiles (up to 14% of the night profiles and up to 21% of the quenching-corrected day profiles). They mostly occurred at depths greater than the MLD (Table B.3) and,

thus, too deep to be taken into account in the satellite observations. Without radiation sensors on the bio-profilers, the first penetration depth (zpd, light attenuation by 1/e) that characterizes satellite observations could not be directly estimated, but based on the model of Morel and Maritorena (2001; their figure B.9), and using the relationship zpd= zeu/4.6 for the euphotic zone definition of the 1% photosynthetically active radiation level [Gordon and McCluney, 1975], it was at most 10-15 meters, and thus always within the mixed layer. Thus, we focused on these subsurface maxima occurring below the MLD (hereafter $SubMax_{>MLD}$) and we examined the location of the profiles exhibiting these features as well as their associated depth (see Figures B.7a, B.7b, B.7d and B.7e).

These $SubMax_{>MLD}$ were quite localized. They occurred primarily near the plateau or close to the location of the Polar Front. Specifically, most of the profiles exhibiting this feature were found in the vicinity of the steep slope between the Northern Kerguelen Plateau and the Gallieni Spur, between 40 and 80 m depth (Figures B.7a, B.7b, B.7d and B.7e). Occurrences of $SubMax_{>MLD}$ were much more sporadic south of 50 ° S, on the south-eastward trajectories of bio-profilers #1 and #2. These conclusions about the locations of subsurface chlorophyll maxima are similar for both night and day occurrences (stars and open circles in Figure B.7, respectively), although $SubMax_{>MLD}$ of day flagged profiles occurred mostly at shallow depths ($<$ 50 m, Figures B.7b and B.7d) and may result from an under-correction of the surface quenched Chl-a concentrations (see Methods). It seems that light limitation may not be a major driver of subsurface Chl-a maxima via the mechanism of increased Chl-a production per cell, at least under a certain threshold of Chl-a content, since $SubMax_{>MLD}$ observed by bio-profilers #3 and #4 occurred more frequently when the mixed layer was deep (for 2.5 μg L^{-1} $\leq$ Chl-a $\geq$ 5 μg L^{-1}; Figures B.7c and B.7f). However, the quasi-ubiquitous concomitance of $SubMax_{>MLD}$ for bio-profiler #1 with shallow mixed layers, less than 50 m, suggests that above a certain threshold of Chl-a content, self-shading may promote pigment production by phytoplankton at depth. Subsurface chlorophyll maxima beyond the reach of satellite imagery can be thought of as a specific class of the wide range of possible chlorophyll distributions (such as varying thicknesses of relatively constant near-surface biomass layers, or changes in the rate of decrease of biomass with depth) that could introduce bias between surface concentration and water column inventory perspectives. To gain perspective on the overall importance of these possibilities, we compared surface chlorophyll concentrations measured by the profilers (using the shallowest $\sim$10 m depth observation since this was reliably within both the 1/e satellite ocean colour penetration depth and the mixed layer) with their column inventories calculated from all observations in the top 200 m (since chlorophyll distributions generally reduced to background values below this depth). These comparisons, shown in Figure

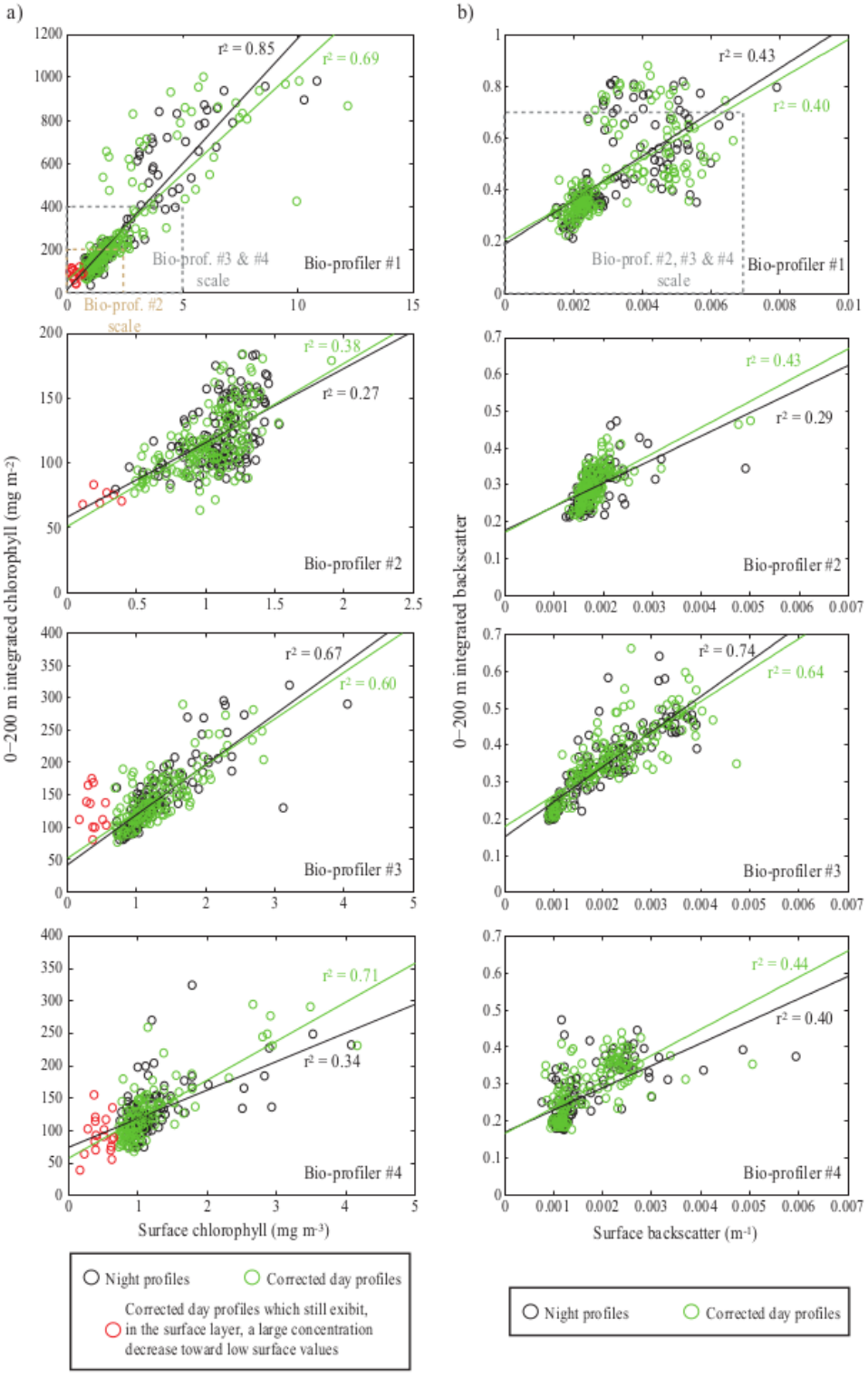

FIGURE B.8: a) Surface chlorophyll concentrations (in mg m^{-3}) compared to chlorophyll inventories (0-200 m; in mg m^{-2}), for each bio-profiler. b) Surface particulate backscattering (m^{-1}) compared to particulate backscattering inventories (0-200 m), for each bio-profiler. Note that scales are slightly larger for bio-profiler #1 than for the others; the dashed rectangles in upper plots indicate the scales used for the other bio-profilers. Night profiles (black circles), day profiles (green circles) and potentially quenching under-corrected day profiles (red circles, flagged as defined in the caption of Figure 2b) are distinguished. Correspondingly, the green and black lines refer to the linear regression of day and night profiles, and their associated correlation coefficients.

B.8a (left column), display reasonably linear relationships over almost the entire range of both night and daytime observations. This was especially true for bio-profilers #1 and #3 (correlation coefficientsr^2=[0.60-0.85]), which include high chlorophyll values (greater than 2 mg m^{-3} for the surface concentration and greater than 160 mg m^{-2} for the 0-200 m inventory). Most of the flagged daytime profiles (red circles in Figure B.8a) seem to be shifted slightly left of the linear regression lines, suggesting that they may well represent under-corrected quenched chlorophyll rather than true features. Overall, qualitatively, these quite linear relationship between surface Chl-a concentration and 0-200 m integrated Chl-a content suggests that satellite observations are reasonably good indicators of the spatial distributions water column chlorophyll inventories. Concerning the particulate backscattering signal, the linear correlations between surface values and inventories were generally not as strong as for Chl-a, except for bio-profiler #3, as shown in Figure B.8b (right column: r^2 = [0.29-0.74]. It appears that surface bbp values lower than ~2 x 10-3 m^{-1} vary similarly to the 0-200 m bbp inventories, whereas higher surface values exhibit noisier correlations when compared to the 0-200 m integrated bbp contents (see the slope breaks in the relationship between surface and 0-200 m integrated bbp in Figure B.8b). The origin of this non-linearity is not clear, and its evaluation is potentially compromised by the spikiness of the bbp records and their poor vertical resolution. The particulate backscatter profiles (Figures B.2b, B.3 B.4,B.5,B.6e and B.12e) suggest that spikes may be particularly common at the base of the mixed layer and below, and thus might reflect differential control of phytoplankton and total particle populations. Future deployments with improved firmware to yield higher resolution may be able to advance the interesting possibility that backscatter information can provide ecosystem perspectives beyond phytoplankton biomass alone. Because our qualitative assessment indicated that surface Chl-a concentrations provide a relatively unbiased indication of the water column Chl-a inventory, we now try to go a little bit further towards a quantitative assessment of possible biases between satellite and in-situ Chl-a perspectives. First, we compared the coefficients of variation (i.e. the ratio of the standard deviation to the mean) of the surface chlorophyll concentrations and of the water column inventories. Using only the night data to avoid quenching correction uncertainties, surface distribution coefficients of variation (#1: 82%; #2: 20%; #3: 39%; #4: 43%) revealed very similar relative dispersions to the water column (0-200 m) inventory coefficients of variation (#1: 84%; #2: 20%; #3: 34%; #4: 31%). Thus, satellite images reasonably reflect the relative range of mesoscale variability in water column phytoplankton biomass accumulations. Surprisingly, surface chlorophyll values (i.e. satellite images) would tend to slightly overestimate the relative dispersion of Chl-a data for bio-profilers #3 and #4, despite those profiles exhibiting the largest numbers of night subsurface maxima (in %, Table B.3). This means that the association of high surface chlorophyll concentrations with shallow chlorophyll layers was more important

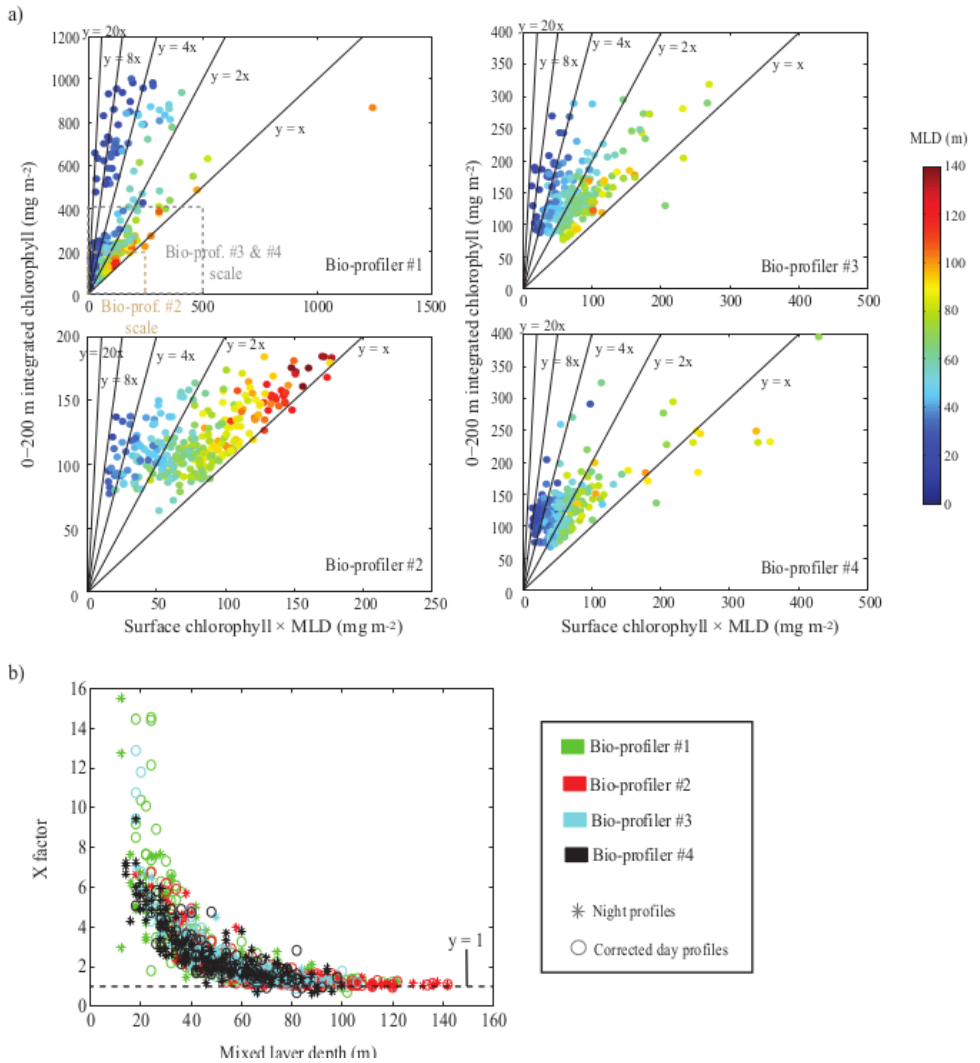

FIGURE B.9: a) Chlorophyll water column inventories (in mg m-2), estimated by multiplying surface chlorophyll concentrations by the mixed layer depth, compared to chlorophyll inventories (0-200 m; in mg m^{-2}) recorded by the bio-profilers. Only night and unflagged day profiles are represented. The colour code shows the associated depth of the mixed layer (in m). The 5 lines y = x, y = 2x, y = 4x, y = 8x and y = 20x are given as indicators to quantify the ratio between the "surface Chl-a × MLD" product and the 0-200 m integrated Chl-a. b) Representation of the X factor (X = (0-200 m integrated Chl-a)/(surface Chl-a × MLD)) as a function of the mixed layer depth (in m), for the total data set. Symbols and colours are defined in the legend.

than the presence of subsurface chlorophyll maxima in determining the relationships between surface and water column inventories.

To further explore this issue, we calculated expected water column inventories for chlorophyll layers confined to the physical mixed layer depths at the time of observation (by multiplying each surface concentration by its associated mixed layer depth, MLD). This is akin to trying to improve satellite assessments using mixed layer depth information from, for example, standard ARGO floats that measure only temperature and salinity.

These comparisons are shown in Figure 6a and reveal that this approach badly underestimates water column inventories (at least with our MLD definition) and that this underestimation is very common. Most of the "0-200 m integrated Chl-a/(surface Chl-a × MLD)" ratios range from 1/1 to 4/1, with a few profiles of bio-profilers #1 and #3, at the time when they recorded the highest bio-optical values, reaching ratios of 20/1 (profiles ∼ 70-130 for bio-profiler #1 and profiles ∼ 0-70 for bio-profiler #3). Moreover, the colour coding in Figure 6a shows that this bias is strongest for shallow mixed layers in general. In other words, the presence of significant amounts of chlorophyll below the mixed layer is very common (though generally not as local vertical chlorophyll maxima, for which our statistics confine the occurrence of those exceeding 60% of surface to 17% of the sampled locations and those exceeding 100% of surface to 11% of the sampled locations). Notably, this bias still persists strongly if we change our MLD definition to the much larger criterion of Levitus ([Levitus, 1982]; density increase of 0.125 kg m^{-3} relative to the density at 0 m). For this criterion, the (surface Chl-a × MLD) estimation ranged between half and twice the 0-200 m integrated Chl-a content for MLD deeper than 60 m (close to half for MLD ∼ [60-90] m and surface Chl-a < 2 μg L^{-1} to close to twice for MLD > 120 m and surface Chl-a > 2 μg L^{-1}). However, (surface Chl-a × MLD) estimations were still twice to four times lower than the 0-200 m integrated Chl-a content recorded by the bio-profilers when the MLD ranges between 40 and 60 m (not shown). The most probable explanation for these observations is that the mixed layer at the time of observation was shallower than at the time of generation of the biomass. This is of course expected as a result of seasonal shallowing of the mixed layer, but the magnitude of the effect is important to recognize (as we have shown above) it is well above what could be corrected using some other mixed layer depth criterion. Interestingly, there appears to be a relatively simple hyperbolic relationship between the ratio "0-200 m integrated Chl-a" / "surface Chl-a × MLD" (hereafter designated as X) and MLD, as shown in Figure B.9b for the MLD definition of Park et al. [Park et al., 1998]. It also holds for the MLD definition of Levitus [Levitus, 1982]. This X vs MLD hyperbola reaches an asymptote of X ∼ 1 for MLD values close to the 150-200 m depths of regional winter mixed layers (visible as temperature minima remnant signatures of winter cooling in profiles south of the Polar Front in Figure B.3b). Moreover, the curve is reasonably well parameterized by X ∼ MLDt/MLDw, in which the superscripts t and w indicate mixed layer depths at the time of observation and the end of winter, respectively. This relationship could arise if most biomass accumulation occurred in early deep mixed layers with subsequent stratification adding little additional biomass, or if mixed layers shallowed and deepened episodically as biomass accumulation developed throughout the season. Overall, these results emphasize the major challenges that are present for connecting surface chlorophyll distributions to total water column biomass and primary productivity, since they reveal that physical mixed layer depths are often

not a reliable guide to biomass distributions. These physical and biological responses seem to be modulated differently on diel, weather, and seasonal timescales, and are also affected by the mesoscale and sub-mesoscale interleaving of water parcels. The quantification of near surface mixing (i.e. going beyond the limited mixed layer depth concept) is currently under very active exploration and debate in the context of seasonal drivers of production [Behrenfeld, 2010, Taylor and Ferrari, 2011b], and these data reveal the need to extend those perspectives to shorter time and space scales. The presence of significant amounts of chlorophyll below the mixed layer is also important to its ultimate fate if this biomass is not re-entrained then it may well contribute preferentially to export and to mesopelagic oxygen consumption (issues which we revisit in Discussion section below).

Do regions of high biomass correlate with (local) oceanographic properties?

To evaluate this issue, we examined bivariate regressions of Chl-a inventories (0-200 m) with physical water column characteristics, after having separated the observations into two groups: 1) Chl-a inventories $>$ 200 mg m^{-2} in rich biomass regions close to the plateau, and 2) Chl-a inventories $\leq$ 200 mg m^{-2} in moderate biomass regions far from the plateau (the rich and moderate biomass regions considered here are identified by red and yellow rectangles in Figures B.3c, B.4c, B.5c and B.6c). As shown in Figure B.10 (a, b and c), the richest biomass regions encountered by bio-profiler #1 in 2011 and bio-profiler #3 in 2014 were associated with waters with very similar properties, specifically moderate temperatures (3.5-5 $^\circ$ C), high salinities (33.82-33.85), and thus relatively high densities (sigma-theta values of 26.7-26.9 kg m^{-3}). The bio-profiler #1 distributions of chlorophyll with these properties showed linear decreases on either side of these values, suggestive of mixing with surrounding waters much poorer in Chl-a. This characteristic is also observed between integrated Chl-a and mean surface oxygen saturation (O_2 sat, Figure B.10f), for which the high O_2 sat states (reaching 10% supersaturation) indicate oxygen production in these high biomass waters (since these values exceeding expected from processes such as warming or bubble injection; [Shadwick et al., 2014]). Relatively high biomass was also encountered in waters with extreme T-S properties (the warmest and freshest observed) in the vicinity of the Gallieni Spur by bio-profiler #4 (black symbols in Figure B.10). Thus, there was not a unique class of waters with high biomass. This perspective is further reinforced by the lack of any clear relationships between chlorophyll inventories and local water column properties for regions of moderate biomass, including versus mixed layer depth and the intensity of stratification as represented by the Brunt-Väisälä frequency (Figure B.10, right column). These low biomass

waters also exhibited lower O_2 sat states (95-103%) than those of rich biomass areas. The under-saturated oxygen levels reflect either strong local respiration or the supply of low oxygen waters from below, with these processes difficult to distinguish (except for specific portions of the bio-profiler #4 trajectory where time series within constant physical property layers were obtained, as discussed in section 4.3). Linking local water parcel properties to past water trajectories with respect to the Kerguelen Plateau, as a known natural source of iron fertilization, provides an additional view of the role of water mass properties in the control of chlorophyll inventories. For the richest Chl-a waters (T ~ 4 ° C, S ~ 33.83, $\sigma \sim 26.8$ kg m^{-3}) encountered by bio-profiler#1, surface drifters released during the KEOPS2 voyage [d'Ovidio et al., 2015] suggest these waters derive from the northern Kerguelen plateau. The computation of trajectories based on satellite altimetry (see Methods) for all the bio-profilers confirms this perspective and also indicates that the time since a water mass left the plateau (Figure 8b) is another important determinant of chlorophyll levels (presumably as a result loss of Fe over time after its addition from the plateau; [d'Ovidio et al., 2015]). These results are shown in Figure B.11. Figure B.11 b) and d) compares water age and origin with the 0-200 m Chl-a inventories for spring (bio-profiler #1, in blue in the plots) and summer (bio-profilers #2, #3, #4, in black in the plots). Beside a strong seasonal difference: spring values range from up to 1000 mg m^{-2}, whereas in the summer few measurements exceed 300 mg m^{-2}- water parcels corresponding to high Chl-a inventories appear to be waters that have recently left the Kerguelen Plateau (20-40 days of water age; Figure B.11a) and come generally from its northern part ([-49; -47] ° S; Figure B.11c). Bio-profilers locations that correspond to water parcels that have not touched the Plateau in the last 100 days (points shown in white for water age = 100 in Figure B.11b) do not present any high integrated Chl-a values, suggesting that the main source of iron fertilization for the explored water masses is horizontal advection from the Kerguelen Plateau. This correlation of high Chl-a inventories with age since leaving the plateau is unlikely to be biased by the lower frequency of sampling (shown in the Figure B.11b inset) of older waters, given that a statistical test based a 104 samplings of a uniform distribution of integrated Chl-a at the sampling frequency of each water age yielded a probability (p) of not-sampling integrated Chl-a value greater than 200 mg m^{-2} for water parcels with water ages greater than 40 days of $p < 10^{-4}$.

These results suggest that the northern Kerguelen Plateau is an important target region for future studies of iron delivery mechanisms into the plume downstream. In terms of the secondary influences of mixed layer depth and stratification, the bio-profiler #1 profiles with integrated Chl-a greater than 600 mg m^{-2} were mainly characterized by a shallow mixed layer, lower than 60 m (Figure 7d), and a low stratification (-0.01 s^{-2} <

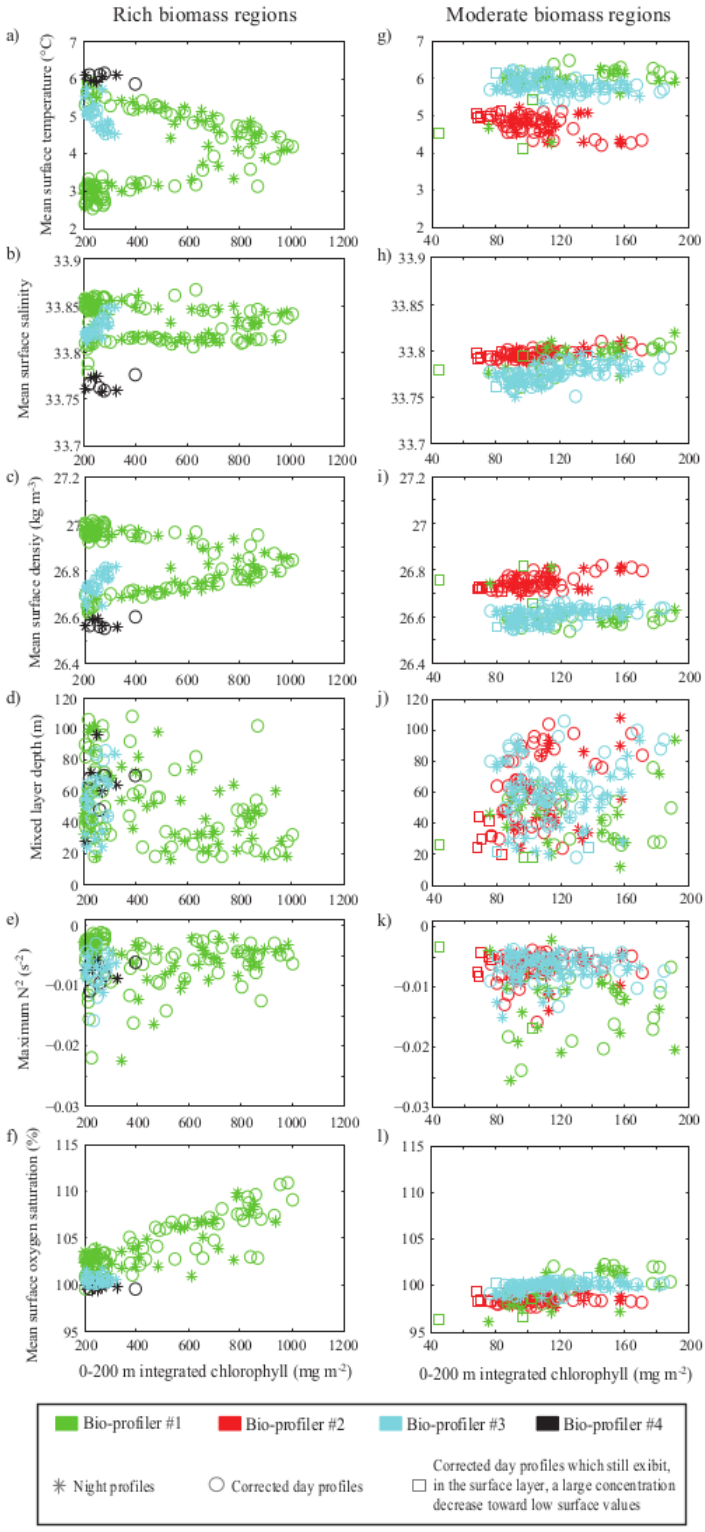

FIGURE B.10: Relationship between 0-200 m integrated chlorophyll a concentration and various water properties for a-f) high biomass regions close to the plateau (bio-profilers #1 and #3) or entrapped in eddies (bio-profilers #2 and #4; red rectangles in Figures B.3, B.4, B.5 and B.6) and g-l) moderate biomass regions far from the plateau (yellow rectangles in Figures B.3,B.4, B.5 and B.6). a) and g): surface temperature (in ° C); b) and h): surface salinity (unitless); c) and i): surface density (in kg m^{-3}); d) and j) mixed layer depth (MLD; in m); e) and k) maximum Brunt-Väisälä frequency squared (N^2; in s-2) f) and l) oxygen saturation state (in %). Symbols and colours are defined in the legend.

max $N^2 < 0$ s^{-2}; Figure B.10e). Below this Chl-a inventory threshold, no clear relationships emerged between MLD or N^2 and 0-200 m integrated chlorophyll (Figures B.10d and B.10e). In a steady state perspective, this lack of correlation could arise because mixed layers were shallow enough that light limitation was not sufficient to halt phytoplankton accumulation, yet not so shallow that mean mixed layer light levels allowed light promoted growth to reach accumulations that became self-shading (viewpoints that have been developed previously, based on relationships between fluorescence and mixed layer depth observations in this region using sensors on elephant seals; [Blain et al., 2013]). Importantly, our observations emphasize that chlorophyll distributions do not track the shoaling of mixed layer depth on seasonal or weather timescales, and thus that MLD variability is unlikely to show simple relationships to biomass accumulation. This point has also been emphasized in terms of competing effects of light and Fe limitation responses to MLD variability [Joubert et al., 2014], for waters where vertical Fe supply is dominant (rather than the horizontal dominance of supply studied here).

Can the fate of surface enrichments in biomass be determined, and if so, what is the percentage of biological production exported?

Evaluating this question requires the extraction of a temporal perspective from the bio-profiler records, and is thus only possible for portions of their trajectories which appear to be essentially Lagrangian. The best record for this approach is for bio-profiler #4 during the period when it carried out several clockwise loops in late autumn, i.e. for profiles 150-240 (Figure B.6a). During this time, its trajectory was very similar to that expected based on surface currents estimated from satellite altimetry, the density stratification of the water column was relatively steady, and the T-S profiles were tightly grouped (Figures B.12b, B.12c and B.12d). These observations suggest that the profiler remained within a single water parcel, that was entrained by a retentive eddy and underwent only small exchanges with surrounding waters, as shown by slightly warmer (profiles 165-170 and 200-220) and cooler (profiles 175-195) conditions along the trajectory (these are discussed further below). At the start of this period (blue lines subset in Figure B.12e), chlorophyll profiles showed moderate to high surface and subsurface layer levels, well above HNLC background values, with some profiles exhibiting subsurface maxima reaching up to 1.5 μg L^{-1} between 50-70 m depth and up to 1 μg L^{-1} around 120 m depth. Both the surface constant Chl-a layer and the subsurface "chlorocline" layer (by analogy to thermocline or halocline, "chlorocline" is defined here as the depth range with the highest chlorophyll concentration gradient) were thick, equal to $\sim$ 80 m and $\sim$50 m, respectively. The origin of the smaller and variable subsurface maxima seen in some profiles in Figure B.12e is uncertain. One possibility is that they are remnants of

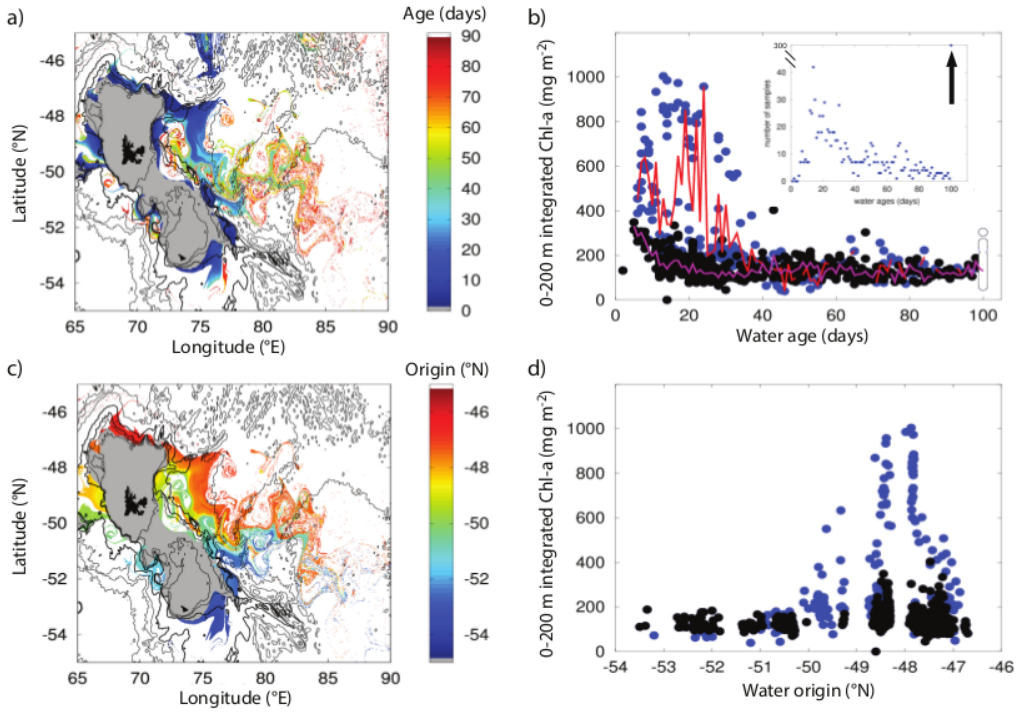

FIGURE B.11: Lagrangian diagnostics computed from altimetry. Maps of age and origins of the water parcels shown in plots (a) and (c) are from Figure 4 of d'Ovidio et al. [d'Ovidio et al., 2015]. White pixels represent water parcels that have not touched in the past 100 days the Kerguelen Plateau (defined by the 700 m isobath and shown in grey). Comparison of these age and origin metrics with the bio-profiler total integrated Chlorophyll-a values are shown in plots (b) and (d). Blue dots correspond to data collected during spring (bio-profiler #1, mean values in red) and black dots to data collected during summer (bio-profilers #2, #3, #4, mean values in magenta). White dots correspond to water parcels that have not touched the Kerguelen Plateau. The inset in plot b) shows the number of measurements for each water age. The black arrow highlights the fact that low Chl-a levels associated with water parcels that have not touched the Kerguelen Plateau within the last 100 days is supported by a large number of samples and, thus, seems to be a robust feature.

the high surface chlorophyll biomass observed just prior to the eddy entrapment (visible in Figure B.6c and the "bloom 2013" animation in the supplementary material), that had been carried to depth by particle settling or by subduction of the denser, saltier, and slightly cooler water associated with that high biomass. Associated bbp profiles showed similar large variations with strong local maxima correlated to local Chl-a maxima (blue lines subset in Figure B.12f). The strong variability of the Chl-a/bbp profiles over the first 100 m suggests possible changes in the composition of the particulate assemblage (blue lines subset in Figure B.12g).

During the Lagrangian eddy entrapment period, the surface mixed layer chlorophyll levels declined further from 1.5 μg L^{-1} to $\sim$1 μg L^{-1} (Figure B.6c and B.12e). Since the constant chlorophyll surface layer shallowed progressively with time, this Chl-a decrease

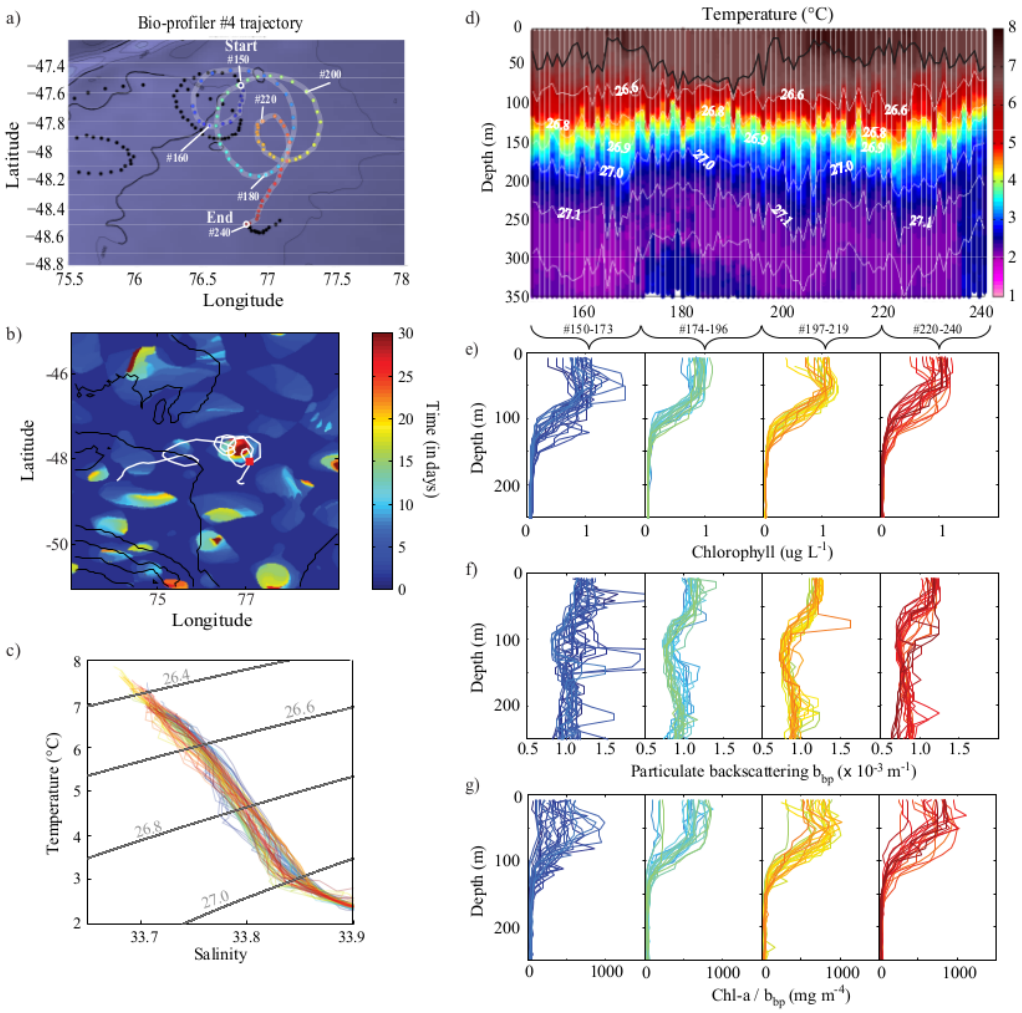

FIGURE B.12: Eddy entrapment of bio-profiler #4. a) Identification of entrapment along the bio-profiler trajectory, with the colour of the points changing, from blue to red over time, from profile 150 to profile 240. b) Overlay of bio-profiler trajectory (white line) and eddy retention indices, showing the portion of the trajectory within a long-lasting (more than 30 days) retentive structure. The red square marks the temporal reference (profile 177) from which the Lagrangian trajectories were computed for the retention statistic, as described in Methods section 2.3. c) Temperature-salinity diagram. Colours correspond to location on the map in a). d) Temperature versus depth section with mixed layer depth (black line) and isopycnals indicated (white lines). e) Chlorophyll profiles, coloured as on the map and separated, for the sake of clarity, in 4 subsets of ∼23 profiles (equivalent to ∼2 weeks of data acquisition). f) As e), but for particulate backscattering (bbp) profiles. g) As e), but for the chlorophyll/bbp ratio. Note that chlorophyll and bbp signals were filtered for visual clarity, using a 3 point running median.

did not result from the possible effect of dilution by mixed layer deepening (i.e. entrainment). Furthermore, the chlorocline content decreased briefly before re-increasing progressively in its upper part, and then its deeper part. In parallel, bbp and Chl-a/bbp profiles became tighter and tighter (light blue to orange profiles in Figures B.12f and B.12g) before re-exhibiting larger variations (red profiles). These results suggest the possibility of some chlorophyll conversion to non-fluorescent material, or its removal by export to depth or by local respiration or both, throughout the eddy entrapment. They may also of course partly reflect small spatial variations in the structure of the biomass distributions. To evaluate these possibilities we examined changes in three layers, the surface layer (labelled layer 1 and defined as the surface down to the 26.6 isopycnal surface), and two density layers immediately below it (layers 2 and 3, respectively for density ranges 26.6-26.8 and 26.8-26.9). In order to characterize the existence of vertical or horizontal mixing during the eddy entrapment, mean temperature, salinity, depth of the density layers, as well as their thickness and their stratification state, are shown in Figure B.13 (a, b, and c). The thickness and mean depth of the surface density layer were relatively constant in the first half of the eddy entrapment, then slightly increased as some warmer and fresher - thus lighter - water entered into the eddy structure (profiles 200-220). Contrastingly, the physical properties of the two deeper underlying density layers showed insignificant temporal trends and smaller variability over the period of interest, and thus changes in their biogeochemical properties can be attributed to local processes rather than exchanges. The evolution of chlorophyll, particulate backscattering and dissolved oxygen inventories also exhibited different trends and variability for each layer (as shown in Figure B.13d, e and f). In surface layer 1, mean chlorophyll and bbp showed no overall temporal trend (green and grey curves in Figure B.13d, respectively), although characterized by two maxima, one at the beginning of the eddy and one coinciding with the fresher warmer water occurrence described above. The oxygen content continuously decreased steadily until after profile 200, when larger variations were observed, with a minimum content coinciding with the fresher warmer waters. Within the underlying layer 2, chlorophyll, bbp and oxygen inventories showed similar evolutions: all had maximums at the beginning of the eddy and then decreased with time until the bio-profiler exited the eddy (Figure B.13e). These characteristics were also present in the deepest layer 3, although with significant differences in the magnitudes of change, specifically the oxygen decrease was similar to that of layer 2, but the chlorophyll level and its absolute magnitude of decrease were much smaller, and the bbp levels remained relatively high for a longer portion of the record. To verify that these changes were oceanographic, we again evaluated fluorometer and oxygen sensor drifts, but this time only over the range of profiles considered for the eddy entrapment investigation (following the approach used in Table B.2, of examining the evolution of the mean values within the depth layer 950-1000 m). Chl-a and O_2 drifts were respectively estimated

to be +0.017 μ g L $^{-1}$ and +1.05 μ mol kg^{-1}.Thus, the temporal drifts probably lead to underestimations of the observed decrease of Chl-a (of ∼7% in layer 2 and of ∼ 20% in layer 3) and of O_2 (∼30% in layers 2 and 3). Knowing that excluding the contribution of the drifts would only reinforce the trends described above, we can now suggest the following overall interpretation to explain these variations of Chl-a, bbp and O_2 in these 3 density layers during the eddy entrapment of bio-profiler #4. In the surface layer 1, the chlorophyll inventory seems to result from the combination of local biological processes with weak horizontal resupply from warmer, fresher, and less oxygenated water (Figures B.12a and B.12d). In the middle density layer 2, where mixing is considered insignificant because of the tightly grouped T-S properties, the chlorophyll decrease does not seem to be due to local transformation to non-fluorescent detritus since no corresponding increase in the bbp signal was observed (Figure B.13e). This leaves loss by settling or respiration as possible explanations. Loss by settling is certainly possible on this timeframe (rates of only a few meters per day are required), and the high bbp values found in the lower density layer 3 around profiles 160-180 could reflect transfer from the overlying layer 2. Biomass loss by respiration and remineralization to dissolved inorganic carbon is almost certainly also occurring given the decreasing oxygen inventories of the middle layer 2 and deep layer 3. For both these layers the rate of chlorophyll loss is too small (by factors of 2-3, assuming a moderately high phytoplankton C/Chl-a ratio of 50) to explain all the oxygen decrease, implying that degradation of detritus (represented by the decreasing particulate backscattering signal) and dissolved organic matter probably also contributes (this remains true even if we use a very high phytoplankton C/Chl-a ratio of 100; [Cloern et al., 1995]). For the deepest layer 3, remineralization of settling particles coming from above with a minor remineralization of local chlorophyll may best explain the slower decrease of chlorophyll in comparison to that of oxygen. In combination, these results suggest that not all of the accumulated biomass was respired in the surface layer, with the CO_2 then returned to the atmosphere, and thus that there was some export. Quantifying this export amount is difficult and merits a modelling and sensitivity assessment that is beyond the scope of this paper. Here we simply provide an indication of its possible magnitude by comparison of the rates of mean oxygen loss in the surface layer 1 (representing carbon likely to be returned to the atmosphere) versus the subsurface layers 2 and 3 (representing carbon which may be exported in the ocean interior). The linear fits to the oxygen decreases for layers 1, 2, and 3 (as shown in Figure B.13) imply oxygen consumption rates of approximately 5, 4, and 4 μmol m$^{-3}d^{-1}$, respectively. These values lie towards the lower end of estimates for annual rates at mesopelagic depths [Sarmiento et al., 1990]. Comparing O_2 consumption of layers 2 and 3 (by multiplying the O_2 consumption rate by the thickness and the average density of the layer) relative to the total mean consumption among the three layers, we estimate that 35% of the CO_2 produced during this autumn period of bloom decline was exported

from the surface layer (with 20% respired within layer 2 and 15% within layer 3). An analogous area of low-to-moderate production and relatively high export was observed during the KEOPS2 field cruise just south of Polar Front, in a meander area around 72.5° E – 49° S where the flow – considered as Lagrangian – was sampled in few stations as a time series [Planchon et al., 2014, Laurenceau et al., 2014]. This area coincides with the location of the anti-cyclonic trajectory of bio-profiler #3, around profile #110, where moderate biomass production was observed (Figure B.5c), although spatial variations in this region unfortunately precluded estimation of biologically driven oxygen consumption from the bio-profiler.

Conclusions

The bio-profilers revealed several interesting aspects of the enriched biomass plume downstream from the Kerguelen plateau, by providing observations of its vertical dimension. First of all, the observations show that surface and total water column chlorophyll inventories are generally well correlated, which suggests that satellite perspectives on bloom spatial dynamics (e.g. References [Mongin et al., 2009, Mongin et al., 2008]) are unlikely to be strongly biased. This result holds true despite the presence of moderate (60% above surface values) subsurface chlorophyll maxima in up to ∼20% of all the profiles, and strong (100% above surface values) in ∼10% of all the profiles (Table B.3 and Figure B.7). Furthermore, satellite surface observations seem to well reflect the water column relative range of mesoscale variability in biomass accumulations. However, the retrieval of water column Chl-a inventory from satellite surface observations is not simple. The bio-profilers often recorded significant quantities of biomass below the diel mixed layer, potentially correlated to the degree of shallowing of the mixed layer from deep winter values. The mixed layer at the time of the observations may not be the best parameter to quantify the chlorophyll inventories, especially when stratification by advection of lighter water mass or by seasonal warming creates strong density variations in the upper layer and, thus, shallow mixed layers, and considering that chlorophyll production may have occurred much earlier than at the time of the observations. And of course, our work does not imply that satellite chlorophyll estimates are necessarily accurate. That is an issue which our data cannot address owing to the imprecision of the bio-optical sensors and the absence of calibration against local chlorophyll observations, an approach which recent work has shown to be necessary for satellite estimates as well [Johnson et al., 2013]. The occurrence of moderate subsurface chlorophyll maxima in our data (17%) was higher than for results obtained with fluorescence sensors deployed on elephant seals around the Kerguelen plateau (∼9% using a criterion of 30% excess over surface values to define the maxima; [Guinet et al., 2013]). This may reflect the

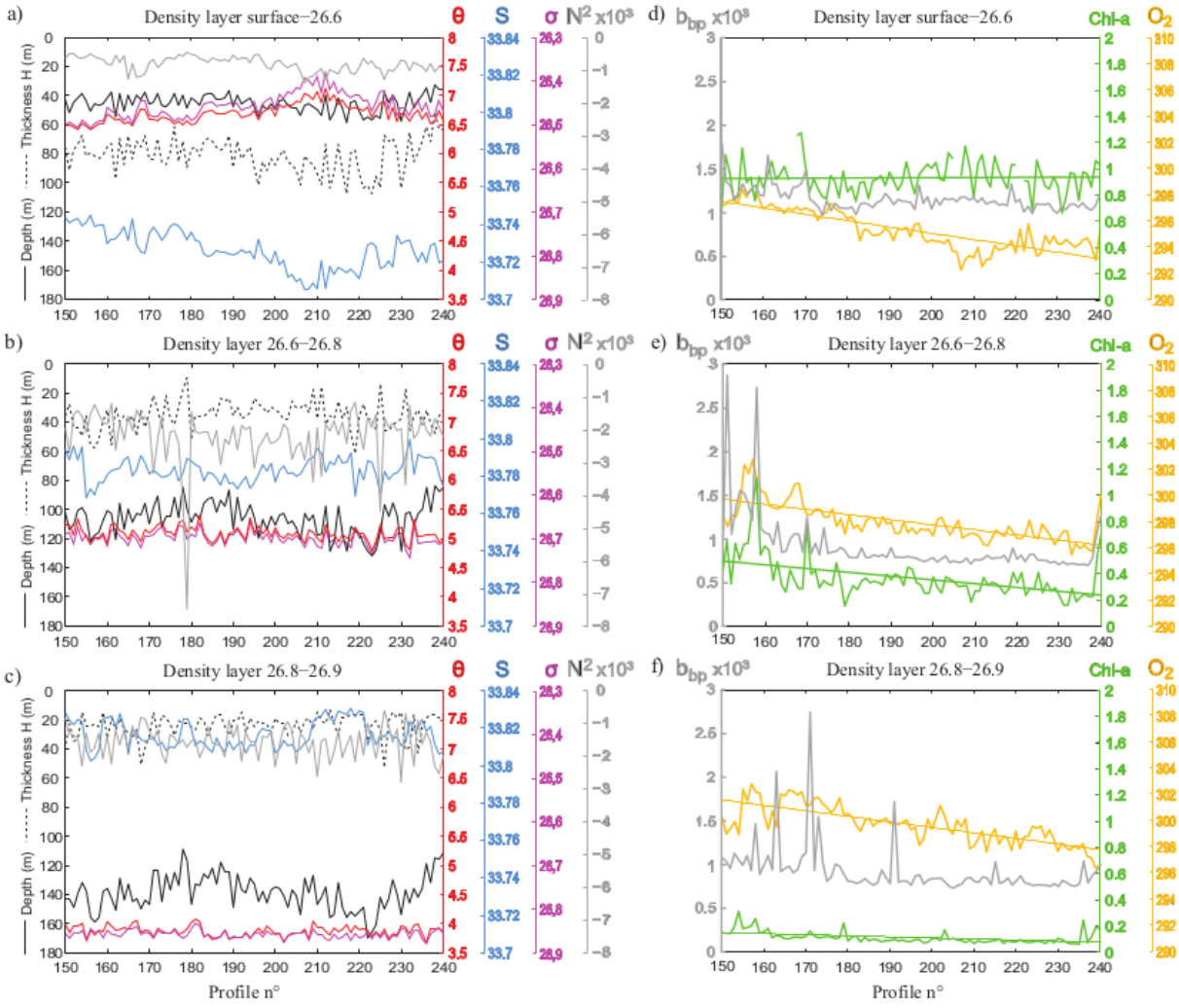

FIGURE B.13: Temporal evolution of physical and biological properties during the eddy entrapment of bio-profiler #4 for three density layers: with sigma-theta ranges of surface-26.6; 26.6-26.8; 26.8-26.9. Left column plots a-c) show physical properties: mean depth (in m; black line and scale), thickness (in m, dashed black line and black scale), temperature (θ , in °C; red line and scale), salinity (S, unitless; blue line and scale), density (, in kg m $^{-3}$; purple line and scale) and Brunt-Väisälä frequency squared (N^2, in s $^{-2}$; gray line and scale). Right column plots d-f) show biogeochemical properties: mean chlorophyll (Chl-a, in μ g L $^{-1}$; green line and scale), particulate backscattering (bbp, in m $^{-1}$; gray line and scale), and oxygen concentrations (O_2, in μ mol kg $^{-1}$; orange line and scale).

greater proportion of observations in the southern portion of the plume in the Guinet et al. [Guinet et al., 2013] study, a region where we also found that subsurface maxima were less common (∼4% of profiles for bio-profiler #2 for our moderate criterion of 60% excess, Table B.3, and ∼6% using their 30% criterion, data not shown). Subsurface maxima were also uncommon well downstream to the east of the Kerguelen plateau. This is interesting in that it suggests that subsurface iron levels supplied by upwelling or vertical mixing were insufficient to drive biomass accumulations at the base of the mixed layer, or at least were less important than horizontal supply of Fe in surface waters. This is in contrast to Polar Frontal Zone waters much further to the east south of Australia where persistent subsurface maxima have been observed [Parslow et al., 2001], and with observations from other autonomous profiling floats elsewhere in the Southern Ocean in which small subsurface maxima were found to be common in summer below the mixed layer [car,]. Variations in the relative intensities of surface and deep iron supplies is a possible cause of these variations, but other processes may also be involved. As an example, the origin of the relatively more common and stronger subsurface chlorophyll maxima near the Gallieni Spur is not clear. Settling of surface biomass generated earlier in the season (Figure B.1) and/or seasonal depletion of iron in surface waters which reduces phytoplankton growth rates are possibilities, but they cannot be assessed given our lack of early seasonal observations. A third possibility of the overlaying of low density waters southward across the Polar Front appears less likely, given that shipboard observations during KEOPS2 found that this process generated shallow high biomass layers (at the Polar Frontal stations F-L, TEW-7, and TEW-8; [Trull et al., 2014, Lasbleiz et al., 2014]. Our initial research goals included looking for oxygen supersaturations in deep chlorophyll maxima to estimate net community production [Spitzer and Jenkins, 1989], but this could not be achieved owing to confounding effects on super-saturations from strong mixing with higher productivity overlying waters, and on aliasing of daily cycles by internal waves [Park et al., 2008]. Thus our results cannot address the issues of whether productivity in subsurface layers may partly explain offsets between satellite and in-situ estimates of the Southern Ocean biological pump [Schlitzer, 2002] or whether the phytoplankton that grow in deep chlorophyll maxima are preferential contributors to carbon export [Kemp et al., 2000, Quéguiner, 2013]. We were able to make a first simple assessment of subsurface autumn oxygen consumption during the portion of the bio-profiler #4 trajectory that delivered a quasi-Lagrangian time series, and this provided the very useful result that approximately 35% of the biomass respiration in that period occurred beneath the mixed layer, and thus at depths favouring CO_2 export toward the ocean interior. This 35% can be approximately equated to an export/production "e-ratio" of 0.4, which is relatively high by global standards, but in the middle of the large range of values observed in cold Southern Ocean waters [Maiti et al., 2013], and similar to f-ratios estimated for high biomass waters over the central Kerguelen

plateau in autumn during the KEOPS1 campaign [Trull et al., 2008]. Of course the subsequent fate of the exported CO_2 inferred from the bio-profiler #4 observations is uncertain, in that these waters were still within the depth range of possible exposure to the atmosphere during later deeper winter mixing, although the larger scale circulation in this region suggests it is a region dominated by subduction [Sallée et al., 2010]. Our simple correlative evaluation of the bio-profiler observations of biomass variations revealed that the highest chlorophyll levels were observed in surface waters with a narrow range of densities and moderate temperatures (σ ~26.9 ±.05 kg m^{-3}, T ~4 ±.5°C; Figure B.10). This occurrence of maximum biomass at moderate temperatures, along with the lack of correlation with mixed layer depth (Figure B.10) suggests that local controls on growth rates were less important than the history of the levels of iron supplied in this water type. Notably, water with these properties was found preferentially near the northern Kerguelen plateau and Gallieni Spur suggesting iron supply from this region. This is consistent with geostrophic circulation estimates and a favourable wind regime for upwelling in this region during the 2011 KEOPS2 period when bio-profiler #1 was deployed [d'Ovidio et al., 2015, Gille et al., 2014] and with Lagrangian analyses that backtrack water parcels to identify their origin. Further observations and analyses are of course necessary to determine the generality of this inference that the northern Kerguelen plateau provides the major source of iron to the downstream biomass plume. This is especially true given the limited seasonal and inter-annual scope of our bio-profiler observations.

Acknowledgements

This work was supported by the Australian Commonwealth Cooperative Research Program via the ACE CRC. M. Grenier was supported by a conjoint LEGOS and ACE CRC postdoctoral appointment and a CAMPUS FRANCE grant (FASIC award # 30418QG; campusfrance.org). A. Della Penna was supported by a conjoint Frontières du Vivant (Paris 7) and CSIRO-UTAS Quantitative Marine Science PhD scholarship. We thank Ann Thresher (CSIRO) for the harvesting and processing of the data from the bio-profilers, as supported by the Australian Integrated Marine Observing Argo and Southern Ocean Time Series facilities. We thank Cedric Cotté and Francesco d'Ovidio (LOCEAN, Universite de Paris VI) and the crew of the RV Marion Dufresne for bio-profiler deployments, and Stephane Blain and Bernard Quéguiner for KEOPS2 voyage leadership. Thanks to Vito Dirita, Alan Poole, and Craig Hanstein (CSIRO) for bio-profiler preparation, and Craig Neill and Kelly Brown (CSIRO) for oxygen optode calibrations. Thanks to Helen Phillips (IMAS) for fruitful discussions and advice concerning physical analyses of the hydrological variables, and Francesco d'Ovidio (LOCEAN, CNRS) for

insights into Lagrangian perspectives on water parcel trajectories and their evolution. Finally, we gratefully acknowledge Dr S. Thomalla and an anonymous reviewer for their valuable comments on an earlier version of the paper that allowed us to improve it significantly.

TABLE B.3: Fluorescence quenching corrections and subsurface chlorophyll maxima statistics. (Subsurface maxima (moderate) are defined as values exceeding surface ones of more than 60 %. Large ones are the ones exceeding the surface ones of more than 100 %. For some corrected profiles, a large decrease in the chlorophyll concentration still occurred in the surface layer. These profiles are flagged in Figs. B.2 b) (squares), B.10 (squares) and B.11 (red circles).))

Individual bio-profiler statistics	#1	#2	#3	#4
Fluorescence profiles collected	384	298	278	254
Fluorescence profiles usable	300	298	277	254
Night-time profiles	129	143	133	119
Daytime profiles	171	155	144	135
Night-time profiles with subsurface maxima total/within the ML/below the ML (% of night-time profiles)	17/5/12 (13/4/9) %	3/1/2 (2/1/1) %	24/9/15 (18/7/11) %	25/14/11 (21/12/9) %
Daytime profiles with subsurface maxima total/within the ML/below the ML (% of daytime profiles)	142/62/80 (83/36/47) %	93/55/38 (60/35/25) %	105/48/57 (73/33/40) %	95/40/55 (70/30/40) %
Quenching corrected profiles (and among them, number of corrected profiles which still exhibit low surface values)	170 (22)	155 (6)	139 (12)	127 (18)
Daytime profiles with subsurface maxima after correction total/within the ML/below the ML (% of corrected day prorfiles)	40/0/40 (24/0/24) %	10/1/9 (6/0/6) %	32/3/29 (23/2/21) %	40/9/31 (31/7/24) %
Total night and corrected day profiles with moderate subsurface maxima total/within the ML/below the ML (% of night and corrected day profiles)	57/2/52 (19/2/17) %	13/2/11 (4/1/3) %	56/12/44 (20/4/16) %	65/23/42 (26/9/17) %
Total night and corrected day profiles with large subsurface maxima total/within the ML/below the ML (% of night and corrected day profiles)	32/1/31 (10/0/10) %	6/0/6 (2/0/2) %	36/5/31 (13/2/11) %	45/15/30 (18/6/12) %

Appendix C

Appendix C: Lagrangian analysis of multi-satellite data in support of open ocean Marine Protected Area design

This appendix has been submitted to *Deep Sea Research II* as *Lagrangian analysis of multi-satellite data in support of open ocean Marine Protected Area design* by A. Della Penna, P. Koubbi, C. Cotte', C. Bon, C-A. Bost and F. d'Ovidio.

Abstract

Compared to the ecosystem conservation in territorial seas, protecting the open ocean has peculiar geopolitical, economic and scientific challenges. One of the major obstacle lies in defining the boundary itself of an open ocean Marine Protected Area (MPA). In contrast to coastal ecosystems, which are constrained by topographic structures fixed in time, life of marine organisms in the open ocean is entrained by fluid dynamical structures like eddies and fronts, whose lifetime occurs on ecologically-relevant timescales. Invisible to our terrestrial eyes, the position of these highly dynamical structures can appear one year after the other hundreds of km apart, challenging the use of animal tracking data beyond the year in which they have been collected. Here we explore the potential of Lagrangian tools applied to multisatellite data as a support tool for MPA proposal by focusing on the Crozet archipelago oceanic area (Indian Sector of the Southern Ocean). By combining remote sensing with bio-logging information from a

top predator (Eudyptes Chrysolophus, or Macaroni penguin), we identify a highly dynamical branch of the subantarctic front as a foraging hotspot. By tracking this feature in historical satellite data (1993-2012) we are able to extrapolate the position of this foraging ground beyond the years in which tracking data is available. An interannual analysis allows us to estimate the area which encloses the spatial variability of the foraging hotspot, and to compare its internal variability in respect go its dependence on a regional mode of climatic variability which is expected to follow a trend under plausible scenarios of climate change.

Introduction

The open ocean environment represents the largest realm on Earth (99% of the biosphere) [Game et al., 2009] and plays a key role in our economy with $> 80\%$ of the fish consumed by humans coming from open ocean fisheries [Game et al., 2009, Pauly et al., 2002]. Under pressure for an increasing resource exploitation, pollution, and maritime traffic, it is one of the least protected ecosystems on Earth. Open ocean regions present difficulties in their spatial management and enforcement [Hobday and Hartog, 2014]. Juridically encompassing both national exclusive economic zones (EEZ) and "high seas" -i.e. not part of any country's exclusive economic zone (EEZ), beyond 200 nautical miles from any nation's territory- open ocean regions present difficulties in their spatial management and enforcement [Hobday and Hartog, 2014]. Only 3% of the marine environment is protected, and of this fraction, high seas protected areas constitute a minority [Game et al., 2009](in 2013, the U.N. Millennium Goal Report states that less than 1% of the high seas are protected).

At the scale of 1000s of km, Longhurst [Longhurst, 2010] described world oceans' biogeographical provinces according to abiotic and biotic pelagic factors. He identified four biogeographical provinces within the polar biome in the Southern Ocean: the South Subtropical Convergence province (SSTC), the Sub-Antarctic water ring Province (SANT), the Antarctic province (ANTA) and the Polar Southern Province (APLR). Each of these provinces theoretically delimits the particular types of environmental or hydrological forcing that can be encountered. Raymond (2014) [De Broyer et al., 2014] used a bioregionalisation multivariate procedure to delineate regions according to seasurface temperature, depth and sea-ice. In both approaches, these oceanic regions are important to determine priority areas for protecting the pelagic environment. They are proxies of ecoregions which are "assemblages of flora, fauna and the supporting geophysical environment contained within distinct but dynamic spatial boundaries" [Vierros et al., 2009]. Depending on the availability of data, the approach can be based on species lists

by regions or mapping of species distributions (either observed data or prediction of species or community presence/abundance based on environmental factors). For example, Koubbi et al. (2011) [Koubbi et al., 2011]determined ecoregions based on modelling mesopelagic fish assemblages in the Indian part of the Southern Ocean.

How to identify key ecological areas 100s of km wide (the typical manageable size of a pelagic Marine Protected Areas) inside these basin-wide biogeographical provinces however is not trivial. In particular, the practical and juridical need of defining fixed boundaries for a Marine Protected Area clashes with the intrinsically dynamical nature of ecological relevant pelagic features, whose position is not fixed in time. Unlike terrestrial and benthic systems – from which most management approaches are borrowed- the ecosystems of the open ocean upper layer are only weakly constrained by a bottom topography, often thousands of meters below. Life of pelagic marine organisms depends on oceanographic features like eddies – the ocean equivalent of atmospheric cyclones and anticyclones - and fronts - highly dynamical boundaries between distinct water masses. Such features belong to the so-called (sub-)mesoscale regime, which spans spatial scales of 1-100 km, and temporal ones of few days to months. Eddies and fronts create a dynamical "seascape" characterised by strong gradients in physical and biogeochemical properties including temperature, salinity and nutrient availability [Mahadevan and Campbell, 2002, Gaube et al., 2013, Klein and Lapeyre, 2009b, Pérez-Muñuzuri and Huhn, 2010, Lévy et al., 2012b]. These features have been observed to structure the distribution of ocean life from phytoplankton (both in terms of primary production [Strass et al., 2002, Abraham, 1998, Martin, 2003, Lehahn et al., 2007, Lévy et al., 2015], community structure [d'Ovidio et al., 2010] and biodiversity [Sunagawa et al., 2015, De Monte et al., 2013]) to zoo-plankton [Labat et al., 2009], bacteria [Baltar et al., 2010b], micronekton [Sabarros et al., 2009, Godø et al., 2012] and top predators [Bailleul et al., 2010b, Cotté et al., 2011, Waluda et al., 2001a, Polovina et al., 2006, Nel et al., 2001, De Monte et al., 2012, Cotté et al., 2007, Scales et al., 2014]. Identifying which of these dynamical features are of relevance for marine organisms, finding the boundaries of the ecoregion in which they evolve, and anticipating their drift in response to scenarios of climate change are therefore issues of primary concern in the definition of open ocean MPAs. Due to the chaotic nature of the ocean dynamics and to the temporal dependence of their external forcings, mesoscale features present a high degree of inter-annual variability. Much like atmospheric weather patterns, oceanic fronts and eddies may show some recurrency, but their position and trajectory can vary of hundreds of km from one year to another. This characteristic poses a problem when biologging data have to be extrapolated in time for the establishment of an MPA. An oceanographic feature that has been targeted by some tagged animals during some years may appear at a different location in the future, possibly falling outside the perimeter of an MPA

established with previous information. In order to address this issue, multisatellite data which nowadays span several decades offer a potentially powerful tool, because once an ecologically relevant physical feature has been identified, its interannual variability, drift, and statistical relation to mode of climate variability can be identified. This way, the perimeter of an MPA can be designed so to include this spatial range of variability, encompassing possible trends under scenarios of climate change.

The ecological potential of combining satellite data and biologging is still however in large part to explore. Only relatively recently data from remote-sensing (Surface Chlorophyll concentration, Sea Surface Temperature, ocean currents, etc.), bio-logging [Rutz and Hays, 2009], in situ measurement networks and high resolution models have converged together to a spatial and temporal resolution capable to resolve (sub-)mesoscale dynamical mechanisms. Remotely sensed sea surface temperature has been used to infer location and frequency of thermal fronts as proxies for biodiversity in the planning of marine protected areas (MPA) [Miller and Christodoulou, 2014, Miller et al., 2015]. Because of the lack of data on the prey distribution (macrozooplankton, nekton, information from bio-logging (in particular animal tracking data) is regularly used in habitat modelling of large marine animals to predict the spatial distribution of top predators [Torres et al., 2008, Hazen et al., 2013]. All these studies have used the environmental field measured from satellite (like Sea Surface Temperature or Sea Surface Height). However, in the recent years advanced analytical tools have been developed, which allow to extract dynamical information of the oceanic environment. Adapted to satellite observations of the ocean a few decades ago ([Abraham, 1998, d'Ovidio et al., 2009, Waugh and Abraham, 2008, Hernandez-Garcia et al., 2002, Hernández-Carrasco et al., 2011, Beron-Vera et al., 2008, Olascoaga et al., 2006], Lagrangian tools in particular provide now a mature and powerful technique for exploring the (sub)mesoscale regime, yielding useful ecological properties like stirring pathways, retentive regions, and frontal systems. More recently, these tools have been shown to be particularly adapted to complement biologging observations, helping to interpret the environmental context which shapes the habitat and behavior of various marine vertebrates, including seabirds, whales, and seals [Kai et al., 2009a, De Monte et al., 2012, Della Penna et al., 2015, Cotté et al., 2015, Cotté et al., 2011, Bon et al., 2015]. Nevertheless, in our knowledge Lagrangian tools have not been considered yet as a tool for conservation. This work aims to bridge this gap, adapting the Lagrangian approach to a specific conservation context (the definition of an MPA in the Southern Ocean) and exploring its potential.

In this study we combine Lagrangian analysis of remote sensing and bio-logging to identify which open ocean transport structures are regularly targeted by Macaroni penguin - *Eudyptes chrysolophus* which has important colonies on the Crozet Island (Indian Sector of the Southern Ocean). The Macaroni penguins are listed by IUCN as a vulnerable

species [Crossin et al., 2013]. Due to their diet and long range capabilities observing their trajectories reveals pelagic hotspots where crustaceans congregate. Our study focuses on the incubating phase of their life cycles and identifies a dynamical branch of the subantarctic front as a foraging ground for these penguins. Once this oceanographic feature targeted by penguins has been identified in terms of remote sensing data, we map its position also for years in which biologging data are not available,. In particular, we employ the decadal-long temporal availability of altimetry information constructing an interannual density kernel. Studying its correlation with a climatic mode, we finally estimate internal vs. climatic variability, thus inferring possible trends in its position in the wake of climate change.

Regional context

The Crozet ecosystem

The Crozet archipelago is located in the Indian sector of the Southern Ocean and represents a region of high productivity in the otherwise High Nutrient Low Chlorophyll environment of the Southern Ocean(see [Sanial et al., 2014a, Pollard et al., 2007a, Pollard et al., 2002, Pollard et al., 2007b] for more details). The re-suspension of iron-enriched sediments from the Crozet Plateau is thought to naturally fertilize the iron depleted waters downstream triggering in springtime a diatom dominated phytoplanktonic bloom. The chlorophyll-rich plume flows initially north toward - and then disperses eastward through - the Antarctic Circumpolar Current (ACC). Crozet bloom's spatial distribution is largely constrained by the dynamical landscape of (sub)mesoscale fronts and eddies induced by the interaction of two of the Antarctic Circumpolar large-scale fronts, the Sub-Antarctic and Polar fronts, with the shallow bathymetry of the Crozet Plateau and the Del Caño Rise located upstream in respect to the plateau . References [Pollard et al., 2007a, Pollard et al., 2007b] described the circulation around Crozet C.1. They indicate that a major branch of the Antarctic Circumpolar Current, the SubAntarctic Front (SAF), flows anticyclonically round the Del Caño Rise west of the Crozet Plateau. The region's circulation is also affected by the Agulhas Return Current (ARC) which flows east along 40°S with major meanders and gradually turns to the southeast to cross 60°E at about 44°S. The confluence of ARC, STF and SAF is also named Crozet Triple Front [Belkin and Gordon, 1996]. The ARC and the SAF north of Crozet show that they remain separate, usually about 200 km apart, coming closest to the north of Crozet, where the ARC turns sharply south and meets the SAF at its northernmost excursion. This S-bend in the SAF seems to be a permanent feature, controlled by the bathymetry [Pollard and Read, 2001]. It is the area of weakest circulation where

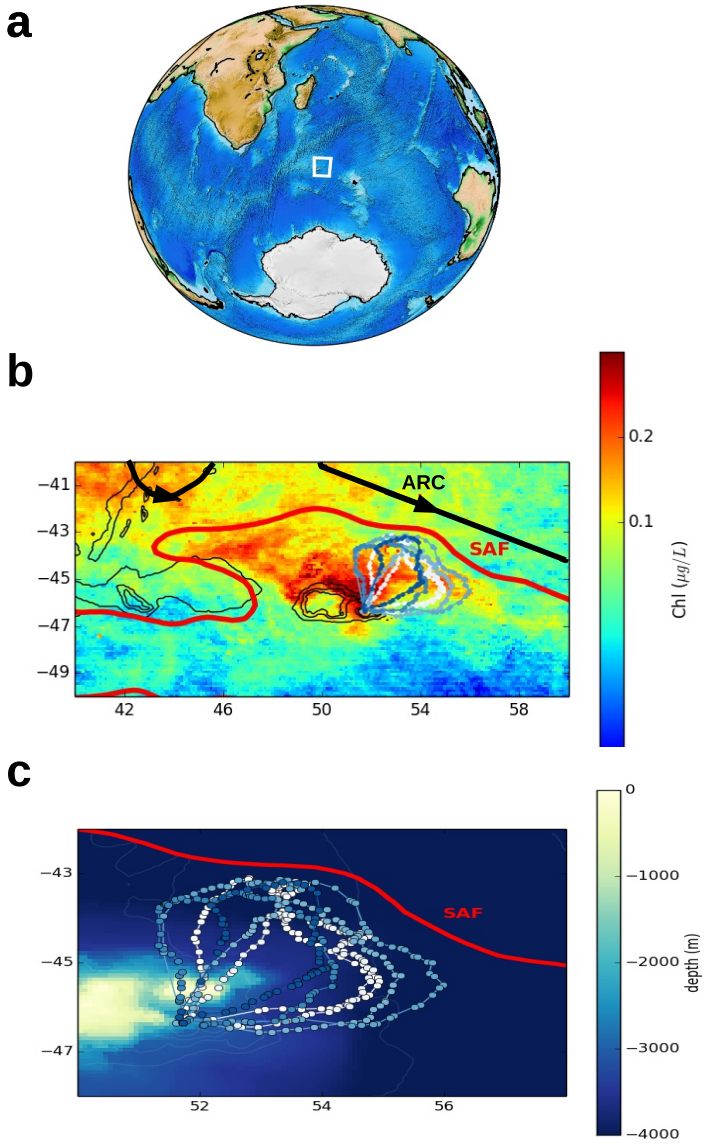

FIGURE C.1: a) Location of the study region, the Crozet Archipelago, in the Indian Sector of the Souther Ocean. b) Chlorophyll climatology between the 15 November to 15 December (years 2000-2012, colorscale) overlapped by the main large scale dynamical structures, the Sub-Antarctic Front (SAF, red line) and the Algulhas Retroflection Current (ARC, black line) and the Macaroni penguin trajectories (shades of blue). c) Zoom on the penguins trajectories and the local bathymetry (colorscale).

water entering resides for about 2 months. Mesoscale structures such as meanders in the S-bend are responsible for the spatial patchiness of plankton bloom [Read et al., 2007]. The CROZEX experiment (CROZet natural iron bloom and Export) described the broad-scale distribution of macro-nutrients and phytoplankton

The national marine and terrestrial nature reserve of Crozet

The national marine and terrestrial nature reserve of the French southern territories was created in October 2006. This MPA is managed by Terres Australes et Antarctiques Françaises (TAAF) which has established a management plan in 2011. Covering 22 700 km^2 of land and sea, it is France's largest national reserve which encompasses 6651 km^2 of the territorial sea (12 nautical miles from the coast) of the Crozet Archipelago. Islands are rare in the southern Indian Ocean, but those that are present are essential for land-breeding marine species. Four islands of the Crozet Archipelago (Apostles Island, Hogs island, Penguins island and East Island) are integrally protected; their territorial seas are "no take areas" for fisheries, and access to these islands is strictly controlled. A fifth island, Possession Island, is also within the terrestrial reserve and human activity is authorized for scientific purposes. The territorial sea of Possession Island is not included within the marine reserve but TAAF regulations forbid fisheries activities in adjacent waters. It is the aim of the TAAF administration to seek for scientific advises to extend geographically the marine reserve by adopting an ecoregionalisation approach and spatial planning including rational use of marine resources such as toothfish (*Dissostichus elegenoides*).

Study species

In this study we used 6 trajectories of Macaroni penguins, a pelagic diving predator that forages within the mixed layer to mean depths of 50 m [Bon et al., 2015, Green et al., 1998b]. The birds were tracked during the incubation season (end of the austral spring) of 2012 . Macaroni penguins are most abundant penguin species and have been estimated to be the largest biomass consumer among seabird [Brooke, 2004], yet their world population is currently decreasing [Crossin et al., 2013, Reid and Croxall, 2001] and they are rated as "vulnerable" by the IUCN. This study focused on male Macaroni penguins during the incubation phase that is particularly critical in the penguins' breeding cycle. First, when foraging at sea, penguins during the incubating phase have a strong time constrain to go back to the colony in order to allow their partner to forage and restore her body condition. Second, the foraging time at sea occurs between two

fasting periods while they are incubating at the colony [Bon et al., 2015]. The combination of these two constrains is likely to have shaped the adaptation of Macaroni penguins to their environment: they have been observed to slow down their swimming velocities in presence of strong currents (probably to optimize their energetics) and to limit the upstream swimming [Bon et al., 2015]. The diet of Macaroni penguins mainly consist in crustaceans (krill and amphipods). Considering that Macaroni penguins can swim hundreds of kms in search of food, tracking their foraging grounds is a way for identifying open oean hotspots of large biomasses of their prey.

Previous studies [Bon et al., 2015, Thiebot et al., 2011, Barlow and Croxall, 2002] suggest that Macaroni penguin tend to exploit frontal regions and shelf areas to forage. In particular, the trajectories discussed in this study refers to individuals who went foraging in the dynamical area of the SAF , presenting a foraging behaviour that is similar to the one of Crozet's King penguins targeting the Polar Front [Bost et al., 2015]. King penguins have been observed to increase their foraging success when they reach the front and to be affected strongly and immediately by its displacement due to large scale climatic anomalies of the subtropical Indian Ocean.

Climate change scenarios

The effect of climate change of the Crozet region are difficult to assess, since only recently observations time series allow to study appropriately the inter-annual variability of physical and biological ocean landscape. Yet, studies in Crozet [Weimerskirch et al., 2003, Inchausti et al., 2003] and in other sub-Antarctic islands (e.g. Marion Island, at approximately the same latitude of the Crozet archipelago) [Smith, 2002] show that since the 1950s (and in particularly after the 1970s) simultaneous increases in air and sea temperatures have been registered. Such changes are coherent with the observed and predicted changes for the entire Southern Ocean: Argo floats and hydrographic surveys registered a warming and freshening over all the basin [Böning et al., 2008, Gille, 2008].

The observed Southern Ocean warming and freshening associated to a shift in the fronts of the ACC. The ACC is strongly wind-forced and in turn it has been observed to respond readily to variations in the Southern Annular Mode (SAM), the dominant mode of extra-tropical variability of the Southern Hemisphere [Sallée et al., 2008, Lovenduski and Gruber, 2005].

Climate projections suggest a further (although slower) positive change of the SAM [Cai et al., 2005, Mayewski et al., 2009, Miller et al., 2006]with a consequent enhancement of westerly winds and an increased equatorial Ekman transport [Sallée et al., 2008]. A major consequence of this shift is a poleward movement of the ACC fronts, including

the branches of the SAF, one of the dominant structures of the ocean circulation around Crozet.

Method

In this analysis we integrated different datasets to locate putative key foraging regions for Macaroni penguins and study their inter-annual variability. First, we combined the animal tracking with multi-satellite observations (chlorophyll, SST) and their re-analysis (FSLE, water age and water origin) to identify the properties of the front targeted by Macaroni penguins in 2012. Consistently with what recently found for elephant seals, which can swim even faster we we assumed that, when reaching a profitable area, Macaroni penguins focus their movements into diving and chasing preys and not into searching new foraging grounds and therefore tend to be transported by the horizontal ocean dynamics [Della Penna et al., 2015]. Coherently with this hypothesis, we used the altimetry-derived horizontal velocity field to advect a patch of simulated passive tracer and we compared the temporal evolution of its location with the penguins trajectories. Then, we gathered the same, when possible, information from previous years and we estimated the location of the "entry point" of penguins on the front and the evolution of the patch. The inter-annual variability of the patch location and its distance from the colony was then related to the Southern Annular Mode, the main atmospheric mode influencing the inter-annual climate variability of the region.

Tracking data

The trajectories used in this study refer to male Macaroni penguins during the incubation seasons and they are the sameones studied by Bon and co-authors [Bon et al., 2015]. The dataset underwent the process of filtering mentioned in Reference [Bon et al., 2015] consisting in deleting location implying speeds larger than $10km/h$, the maximum travel speed recorded for Macaroni penguins [Brown, 1987].

Multi-satellite data

Altimetry-derived geostrophic velocities were provided by AVISO (SSALTO/Duacs products, version April 2014). The products has nominal spatial and temporal resolutions of 1/4 degree and 1 day respectively [Handbook, 2014] and is available for all the years considered in this study (1993-2012). To quantify the chlorophyll spatial distribution we

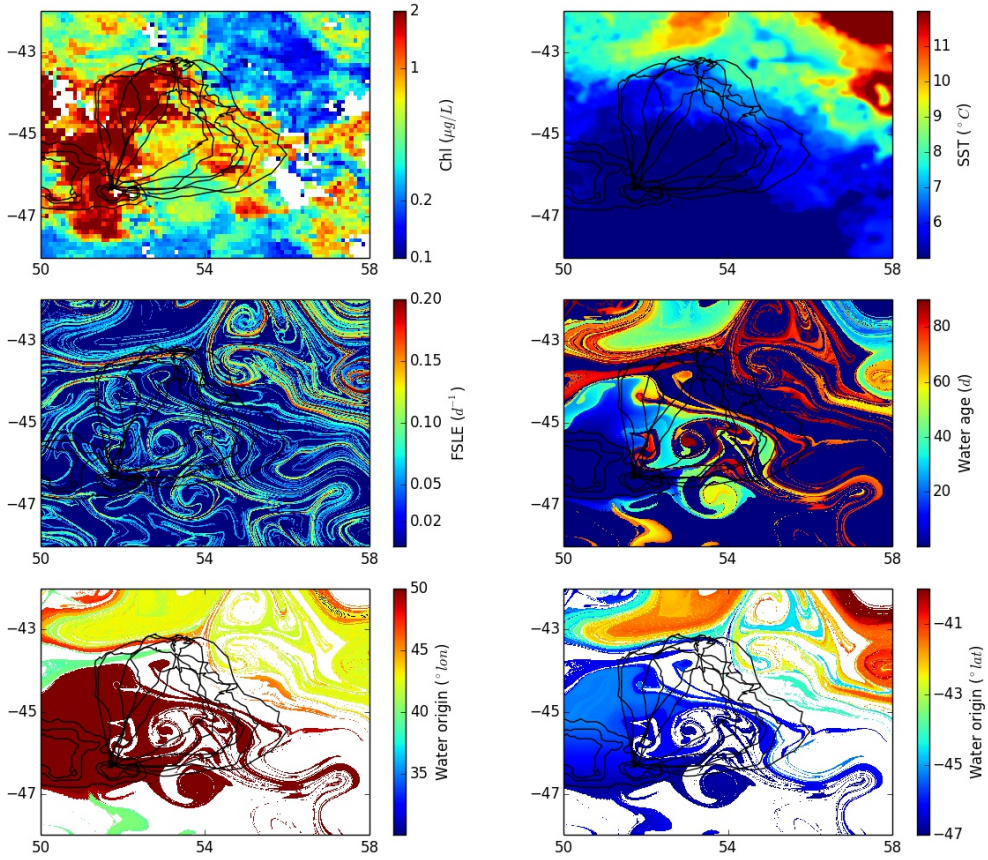

FIGURE C.2: Multi-satellite observations and re-analysis for November 2012 (period referring to the Macaroni penguins foraging trajectories, black lines). a) Chlorophyll climatology (15 Nov-15 Dec), b) Sea Surface Temperature (daily image, referring to the 27/11/2012), c) Finite Size Lyapunov Exponent, d) water age, water origin (e), longitude, (f), latitude), reffering to 27/11/2012.

used the GlobColour [glo,] gridded chlorophyll (Chl) product for case 1 waters (adapt for open ocean waters). The resolution of this product is 4 km/ 1 day, however, it is not available for all the study period, but only after 2002. For the Sea Surface Temperature (SST) we used the GHRSST web portal to identify the product with the highest spatial resolution available for the different years of the study. Concretely, we used, AVHRR (resolution: 25 km) for the years 1993-2001, AVHRR-AMSR-01 (25 km) for the years 2002-2004, mw-ir-O1 (9 km) for years 2005-2009 and the L4 product G1SST (1 km, integrating also in-situ observations and model output) for the years 2010-2012. More details about the products can be found in Reference [ghr,].

Lagrangian approaches

We used Lagrangian approaches to locate transport fronts (i.e. regions where waters having different origins and properties converge) in the regions explored by the tracked

penguins and to identify favourable foraging areas. In fluid dynamics, Lagrangian approaches are based on following individual fluid parcels (water parcels) through time as they move in a velocity field. In the case of this study the velocity field consists in horizontal geostrophic velocities measured from altimetry, as detailed in the previous section. To calculate the trajectories of water parcels we integrated the geostrophic velocity field using a Runge-Kutta algorithm of 4th order.

In this study we mainly use three Lagrangian diagnostics: the Finite Size Lyapunov Exponents and water ages and origin from bathymetric features.

We used ridges of Finite Size Lyapunov Exponents (FSLE) to locate fine-scale transport fronts[d'Ovidio et al., 2009]. The FSLE measures the rate of separation between particles initialised nearby. Maxima (ridges) of Lyapunov exponents computed backward in time are used to identify fronts defined as regions of water masses' confluence, that is, where properties of water parcels originally far away are advected in close proximity. Technically they are computed as:

$$FSLE(lon, lat, t, \delta_0, \delta) = \frac{1}{\tau} log(\frac{\delta}{\delta_0}) \tag{C.1}$$

where δ_0 represents the initial separation of water parcels, and τ the time taken for the water parcels to reach a separation δ. For this study the values of delta and δ_0 were of 0.01 deg and 0.6 respectively. (lon,lat) refer to the location in time and space of the region where the FSLE is computed.

Besides identifying frontal areas, we also discriminated water parcels coming from different regions. In order to do that, we used two Lagrangian diagnostics defined in References [Sanial et al., 2014a, d'Ovidio et al., 2015]: the water age and the water origin. The water age quantifies how long before a specific water parcel has been in contact with a specific bathymetric line and the water origin the location (in terms of longitude and latitude) where the water parcel has left such bathymetric line (for this study, following Sanial and co-authors [Sanial et al., 2014a] we used the -2000 m isobath). In these studies such diagnostics have been to validate the hypothesis that iron (the limiting factor for phytoplankton growth in the Southern Ocean) advection from shallow bathymetries is largely responsible for chlorophyll plumes in the proximity of islands. In particular, they were used to predict the extent and the structure of the Crozet [Sanial et al., 2014a] and Kerguelen [d'Ovidio et al., 2015] plumes during the KEOPS2 voyage and interpret the observations of high chlorophyll concentrations sampled with bio-argo autonomous profilers [Grenier et al., 2015]. The altimetry-derived water age computed from the -2000m isobath that we use in this study has been shown to be in quantitative agreement with the same quantity estimated from lythogenic isotopes and from the trajectory of a drifter $sanial_2014_study$.

To predict areas of interest for the studied penguins we started from the observation detailed in Bon et al. [Bon et al., 2015] and Bost et al. [Bost et al., 2015]. Bon and co-authors studied trajectories of Macaroni penguins that went foraging in the dynamical region located near the Sub-Antarctic Front (SAF). A comparison with geostrophic ocean currents showed that the studied trajectories presented a recurring pattern of active swimming from the colony to a frontal area, followed by few days when the difference between the penguin velocities and the currents ones were very low and concluded by active swimming from the frontal area to the colony. During the second phase of this patterns the penguins are largely transported by the fast currents of the front on the horizontal, while they are likely to concentrate their movements in diving and chasing myctophids, small mesopelagic fish constituting the largest proportion of their diet. After the intensive-foraging phase, the tracked penguins swam actively back to the colony. Following these observations, we identify regions of interest for tracked animals by advecting a simulated passive tracer using an altimetry-derived velocity field.

Inter-annual variability data

The spatial evolution of the patch was computed for years 1993-2012 by initialising a 50 km radius circular patch around the closer location to Possession Island having the properties detailed in the results. An isotropic Gaussian kernel was computed (with a grid space of 10 km) to quantify the density of the passive tracers through the years.

To compare the location of the estimated region of interested for Macaroni penguins with climate inter-annual variability we used the "Southern Annular Mode / Antarctic Oscillations" dataset from NOAA/CPC (CF-1.0). SAM is measured as pressure gradient between the polar and subpolar regions of the Southern Hemisphere. The used dataset contains monthly estimates of the SAM values from 1979 to 2015. The value of the SAM was compared with three diagnostics (the initial latitude of the center of the patch, the mean latitude of the patch after one week and the mean distance from the colony after one week) by using a correlation matrix.

Results

Putative foraging regions for Macaroni penguins

The comparison between the trajectories of Macaroni penguins from the colony in Possession Island and multi-satellite observations suggests that, as detailed in Reference [Bon et al., 2015], once the penguins reach a strong transport front (within the envelope

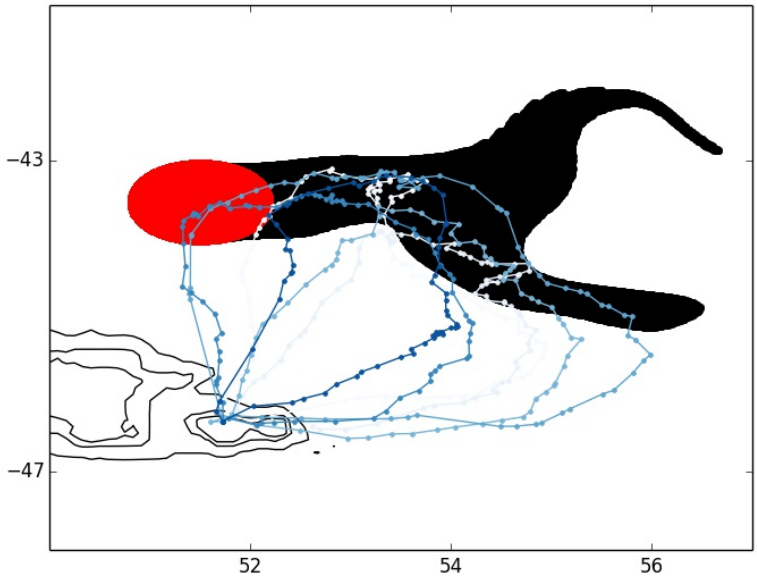

FIGURE C.3: Example of patch advection for year 2012. The simulated passive tracer is initialised North of the Possession Island colony (red patch) and advected for 15 days by altimetry-derived geostrophic currents (black patch). The trajectories of the penguins are represented in blue and the black contours represent the bathymetry.

of the SAF), their movements tend to be entrained by the currents. The front where the penguins change directions (and swimming behaviour) presents a strong gradient in Chl concentration and SST and separates waters having a strong difference in origin and age as shown in Figure C.2). The change in penguins' swimming behaviour occurs in a location of strong transport (FSLE $> 0.2d-1$), between water parcels closer to the colony and likely to be enriched on the Crozet plateau having very high Chl content and less productive ones that have been enriched in waters from a much northerner latitude.

A patch of simulated passive tracer initialised at the latitude where these conditions are satisfied and at the longitude of Possession Island is transported East by the strong transport of the front, with a considerable overlap with the penguins' trajectories (see Figure C.3).

Inter annual variability of the key structures

To study the inter-annual variability of the dynamical structure identified in the previous section, a 50 km radius circular patch of simulated passive tracer was initialised in yearly identified locations satisfying the following criteria:

1. a longitude within 50 km from the one of Possession Island;

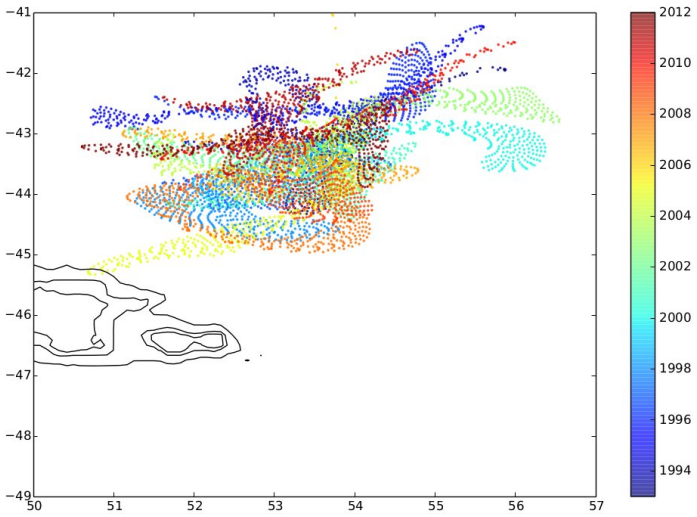

FIGURE C.4: Inter-annual variability of the patch spatial distribution after 7 days of advection.

2. a transport front is present (FSLE $> 0.1d^{-1}$, after [Lehahn et al., 2007]);

3. a water origin (latitude) gradient is between origin ~ -44 deg and ~ -41 deg

4. SST in the range 7-8 deg C

5. Chl gradient, when available.

The location of the patch presents a strong spatial variability between the years 1993-2012. Figure C.4 a) shows the location of the patch after 7 days of advection calculated for years 1992-2012. The patch's shape is stretched by the strong velocities on the front and the latitudes ranges from -45 deg to -42 deg. The Gaussian kernel of the spatial distribution of the passive tracer, that takes into account of the location of the patch during 15 days of advection , shows very high concentration of the tracer between 52-54 deg E and 43 deg S (see Figure C.5 b)). Other recurring patches occur around 52 deg E, 44 deg S and 54 deg E, 44 deg S. However, the inter-annual spatial variability is particularly evident, when looking at the spread of the patch East of 55 deg E.

The initial latitude of the patch (i.e. the "entry point" of the penguins on the front), the mean latitude after one week and its distance from the colony calculated for several years did not show any significant relationship with the SAM ($p > 0.05$ for all the three variables).

Discussion

Many marine predators are known to congregate over specific regions of oceanic fronts [Bost et al., 2009]. In contrast to terrestrial landscapes, the pelagic physical context is dynamic both spatially and temporally and its changes occur on a scale that is comparable with the one at which marine predators forage. The position of fronts in the open ocean may move substantially from one year to another, creating a challenge for the definition of the boundaries for a Marine Protected Area, especially in the wake of climate change. This problem is typically addressed by pooling together observations of animal location from different years. If MPAs are often spatially defined with the core of ecoregions where environmental factors are more stable, this concept cannot be used for highly dynamic areas or borders of ecoregions. Fronts and transitions between ecoregions can be important for conservation as they can be highly productive or marking sharp biogeographic transitions as observed by Koubbi et al.(2011) [Koubbi et al., 2011] on mesopelagic fish or by Koubbi et al. [De Broyer et al., 2014] . It is obvious that in such dynamic systems, potential MPAs have to integrate spatial variations of dynamic features such as meanders of frontal zones.

Adaptive and dynamical forms of management are especially relevant in the wake of climate change. Ocean warming and changes in the currents patterns have been observed to have important biological consequences from the species to the community level [Hughes, 2000, Walther et al., 2002, Parmesan, 2006, Hunt et al., 2011, Baier and Napp, 2003, Hazen et al., 2013, Forcada and Trathan, 2009, Bost et al., 2015].

Here we propose a supporting tool, based on the multi-annual tracking of the fine-scale congregation region over the physical front itself. The congregation region is firstly identified by comparing satellite data to animals' positions within a Lagrangian scheme; then its position is tracked in historical satellite data. A possible relation of its position with a mode of climatic variability (in our case, the Southern Annular Mode) is considered. This approach is obviously not intended in alternative to habitat modelling with animal telemetry, but as a complementary support. Indeed, in this study instead of calculating probability of spatial distributions using the animal trajectories themselves, we consider the variability of the physical structure on which animals appear to congregate.

Furthermore the Lagrangian diagnostics used in this study could be relevant in the context of dynamical ocean management strategies [Hobday and Hartmann, 2006, Hobday and Hartog, 2014, Lewison et al., 2015, Maxwell et al., 2015] that aims at changing protection (and generally management) measures according to the changes in ocean

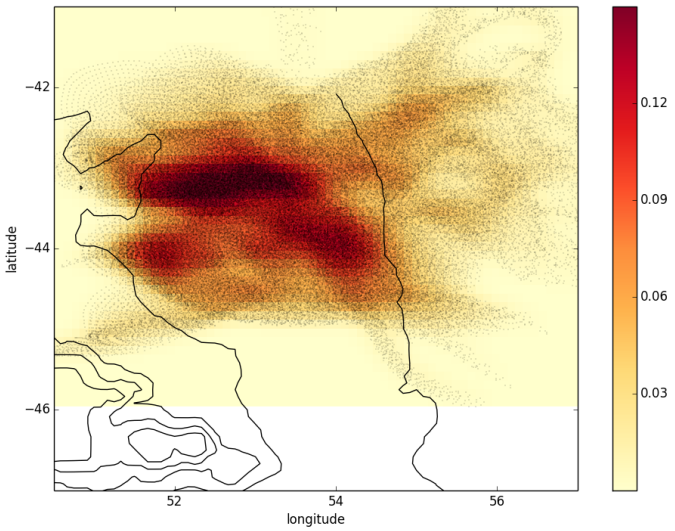

FIGURE C.5: Density plot of the spatial distribution of the simulated passive tracer. The grey dots represent the locations of the simulated passive tracer (from day =1 to day = 15 of advection). In color, the Gaussian kernel of their spatial distribution.

conditions complementing the use of near-real time Sea Surface Temperature and animal tracking data with Lagrangian diagnostics as indicators of transport fronts and converging waters.

The results of this study rely on a number of assumptions. First of all, we assume that Macaroni penguins target each year an equivalent dynamical structure during their foraging trips. Further animal tracking observations are necessary in order to evaluate this assumptions. Secondly, we assume that, once the penguins encountered a profitable foraging ground, the are horizontally transported by the currents. This assumption relies on the findings from Bon et al. [Bon et al., 2015] that in the middle of their trajectories, when they are expected to forage more intensively, penguins tend to decrease their horizontal swimming velocity. This change in the swimming behaviour results in an overall transport caused by the surrounding flowing medium. A similar result has been found for other diving predators, such as southern elephant seals moving in highly dynamic oceanic regimes [Della Penna et al., 2015] and sea turtles [Gaspar et al., 2006]. Finally, our projections are based on the reliability and the appropriateness of the altimetry-derived velocity field. Macaroni penguins are diving predators, diving on average to 50m (ranging 10-154m) depth [Bon et al., 2015, Green et al., 1998b]. Altimetry velocities are considered to be representative of the horizontal currents in the mixed layer, that in the region of Crozet ranges between 40 m and 100m for the season considered in this study (November-December) as detailed in [Sallée et al., 2010, Venables et al., 2007]. Although altimetry-derived currents neglect ageostrophic and fine scale (<70km) features, altimetry-derived stirring patterns in the Crozet region benefits of an excellent

validation study, which showed agreement with drifters' trajectory, chlorophyll patterns, and isotope measurements sanial$_2$014$_s$*tudy*.

The inter-annual variability analysis presented in this study (see Figure C.4) suggests that the region's mesoscale turbulence influences heavily the dispersion of the patch. In particular for years where mesoscale eddies are present, it is difficult to infer how the penguins will respond to such a change in the structuring of their prey field. Also, the spatial distribution of Chl (not shown) presents a high spatial variability that makes it harder to predict how it will affect the penguins' movements. Such high variability may be responsible for the non-significant relationship between the patch location and the SAM. Another possible reason behind it, could be the, even if generally the SAF are expected to shift southward, the SAF location in the Crozet area is strongly constrained by the bathymetry, so the trend may be more difficult to detect, if it occurs.

Conclusions

This study presents a proof of concept for the use of Lagrangian approaches as a support tool for the design of MPAs. Lagrangian diagnostics have been successfully used to identify regions of ecological interest like foraging grounds [Cotté et al., 2015, Bon et al., 2015, Della Penna et al., 2015], yet our preliminary results suggest that they can also be a valuable tool for tracking dynamical ecological key regions. Future field studies are necessary in order to improve the presented method and evaluate its feasibility as a tool to constantly monitor and protect Macaroni penguins. In particular, a time series of trajectories from several year will be essential to validate and refine the algorithm. It would be also very important to gather data about this specie's prey – myctophids, euphausiids and amphipods – concentration and availability in respect to the tracked region of interest.

Acknowledgments

The altimeter products were produced by Ssalto/Duacs and distributed by Aviso with support from Cnes. ADP thanks the Fondation Bettencourt-Schueller (through the program Frontières du Vivant) for its financial support. The authors would like to thank the ANR MYCTO-3D MAP and OSTS Altimeco projects.

Bibliography

[glo,] GlobColour. http://www.globcolour.info.

[ghr,] Group for High Resolution Sea Surface Temperature. http://www.ghrsst.org.

[car,] Mixed-layer depth and Chl a variability in the Southern Ocean.

[r$_s$,] The R Foundation for Statistical Computing 2013. www.r-project.org.

[sun,] Sun or Moon Rise/Set Table for One Year. http://aa.usno.navy.mil/data/docs/RS_OneYear.php.

[cca, 2008] CCAMLR, 2008. XXVII Annual Meeting, Final Report.

[Abraham, 1998] Abraham, E. R. The generation of plankton patchiness by turbulent stirring. *Nature*, 391:577–580.

[Abrams, 1985] Abrams, R. Environmental determinants of pelagic seabird distribution in the African sector of the Southern Ocean. *Journal of Biogeography*, pages 473–492.

[Åkesson and Alerstam, 1998] Åkesson, S. and Alerstam, T. Oceanic navigation: are there any feasible geomagnetic bi-coordinate combinations for albatrosses? *Journal of avian biology*, pages 618–625.

[Allen et al., 2005] Allen, J. T., Brown, L., Sanders, R., Moore, C. M., Mustard, A., Fielding, S., Lucas, M., Rixen, M., Savidge, G., Henson, S., et al. Diatom carbon export enhanced by silicate upwelling in the northeast Atlantic. *Nature*, 437:728–732.

[Alvain et al., 2005] Alvain, S., Moulin, C., Dandonneau, Y., and Bréon, F. M. Remote sensing of phytoplankton groups in case 1 waters from global SeaWiFS imagery. *Deep Sea Research Part I: Oceanographic Research Papers*, 52:1989–2004.

[Alvain et al., 2008] Alvain, S., Moulin, C., Dandonneau, Y., and Loisel, H. Seasonal distribution and succession of dominant phytoplankton groups in the global ocean: A satellite view. *Global Biogeochemical Cycles*, 22(3).

[Amores et al., 2013] Amores, A., Monserrat, S., and Marcos, M. Vertical structure and temporal evolution of an anticyclonic eddy in the Balearic Sea (western Mediterranean). *Journal of Geophysical Research: Oceans*, 118(4):2097–2106.

[Armand et al., 2008] Armand, L. K., Cornet-Barthaux, V., Mosseri, J., and Quéguiner, B. Late summer diatom biomass and community structure on and around the naturally iron-fertilised Kerguelen Plateau in the Southern Ocean. *Deep Sea Research Part II: Topical Studies in Oceanography*, 55:653–676.

[Arrigo, 2005] Arrigo, K. R. Marine microorganisms and global nutrient cycles. *Nature*, 437(7057):349–355.

[Assmy et al., 2013] Assmy, P., Smetacek, V., Montresor, M., Klaas, C., Henjes, J., Strass, V. H., Arrieta, J. M., Bathmann, U., Berg, G. M., Breitbarth, E., et al. Thick-shelled, grazer-protected diatoms decouple ocean carbon and silicon cycles in the iron-limited Antarctic Circumpolar Current. *Proceedings of the National Academy of Sciences*, 110(51):20633–20638.

[Aurell et al., 1997] Aurell, E., Boffetta, G., Crisanti, A., Paladin, G., and Vulpiani, A. Predictability in the large: an extension of the concept of Lyapunov exponent. *Journal of Physics A: Mathematical and General*, 30:1.

[Babin et al., 1996] Babin, M., Morel, A., and Gentili, B. Remote sensing of sea surface sun-induced chlorophyll fluorescence: consequences of natural variations in the optical characteristics of phytoplankton and the quantum yield of chlorophyll a fluorescence. *International Journal of Remote Sensing*, 17(12):2417–2448.

[Baier and Napp, 2003] Baier, C. T. and Napp, J. M. Climate-induced variability in Calanus marshallae populations. *Journal of Plankton Research*, 25(7):771–782.

[Bailey and Thompson, 2009] Bailey, H. and Thompson, P. M. Using marine mammal habitat modelling to identify priority conservation zones within a marine protected area. *Marine Ecology Progress Series*, 378:279–287.

[Bailleul et al., 2010a] Bailleul, F., Authier, M., Ducatez, S., Roquet, F., Charrassin, J.-B., Cherel, Y., and Guinet, C. Looking at the unseen: combining animal bio-logging and stable isotopes to reveal a shift in the ecological niche of a deep diving predator. *Ecography*, 33:709–719.

[Bailleul et al., 2007] Bailleul, F., Charrassin, J.-B., Monestiez, P., Roquet, F., Biuw, M., and Guinet, C. Successful foraging zones of southern elephant seals from the Kerguelen Islands in relation to oceanographic conditions. *Philosophical Transactions of the Royal Society B: Biological Sciences*, 362:2169–2181.

[Bailleul et al., 2010b] Bailleul, F., Cotté, C., Guinet, C., et al. Mesoscale eddies as foraging area of a deep-diving predator, the southern elephant seal. *Marine Ecology Progress Series*, 408:251–264.

[Bailleul et al., 2008] Bailleul, F., Pinaud, D., Hindell, M., Charrassin, J.-B., and Guinet, C. Assessment of scale-dependent foraging behaviour in southern elephant seals incorporating the vertical dimension: a development of the First Passage Time method. *Journal of Animal Ecology*, 77(5):948–957.

[Bakun, 2006] Bakun, A. Fronts and eddies as key structures in the habitat of marine fish larvae: opportunity, adaptive response and competitive advantage. *Scientia Marina*, 70(S2):105–122.

[Ballard et al., 2012] Ballard, G., Jongsomjit, D., Veloz, S. D., and Ainley, D. G. Co-existence of mesopredators in an intact polar ocean ecosystem: the basis for defining a Ross Sea marine protected area. *Biological Conservation*, 156:72–82.

[Baltar et al., 2010a] Baltar, F., Arístegui, J., Gasol, J. M., Lekunberri, I., and Herndl, G. J. Mesoscale eddies: hotspots of prokaryotic activity and differential community structure in the ocean. *ISME J*, 4:975–988.

[Baltar et al., 2010b] Baltar, F., Arístegui, J., Gasol, J. M., Lekunberri, I., and Herndl, G. J. Mesoscale eddies: hotspots of prokaryotic activity and differential community structure in the ocean. *The ISME journal*, 4(8):975–988.

[Bannasch et al., 1994] Bannasch, R., Wilson, R. P., and Culik, B. Hydrodynamic aspects of design and attachment of a back-mounted device in penguins. *The Journal of experimental biology*, 194(1):83–96.

[Barlow and Croxall, 2002] Barlow, K. and Croxall, J. P. Seasonal and interannual variation in foraging range and habitat of macaroni penguins Eudyptes chrysolophus at South Georgia. *Marine Ecology Progress Series*, 232(291-304).

[Barton et al., 2013] Barton, A. D., Pershing, A. J., Litchman, E., Record, N. R., Edwards, K. F., Finkel, Z. V., Kiørboe, T., and Ward, B. A. The biogeography of marine plankton traits. *Ecol Lett*, 16:522–534.

[Baum and Worm, 2009] Baum, J. K. and Worm, B. Cascading top-down effects of changing oceanic predator abundances. *J Anim Ecol*, 78:699–714.

[Begon et al., 1996] Begon, M., Harper., J., and Townsend Ecology: Individuals, Populations and Communities. *3rd.–Blackwell Science oxford.*

[Béhagle et al., 2015] Béhagle, N., Cotté, C., Ryan, T. E., Gauthier, O., Roudaut, G., Brehmer, P., Josse, E., and Cherel, Y. Acoustic micronektonic distribution is structured by macroscale oceanographic processes across 20–50° S latitudes in the South-Western Indian Ocean. *Deep Sea Research Part I: Oceanographic Research Papers*.

[Behrenfeld, 2010] Behrenfeld, M. J. Abandoning Sverdrup's critical depth hypothesis on phytoplankton blooms. *Ecology*, 91(4):977–989.

[Belkin et al., 2009] Belkin, I. M., Cornillon, P. C., and Sherman, K. Fronts in large marine ecosystems. *Progress in Oceanography*, 81(1):223–236.

[Belkin and Gordon, 1996] Belkin, I. M. and Gordon, A. L. Southern Ocean fronts from the Greenwich meridian to Tasmania. *Journal of Geophysical Research: Oceans*, 101(C2):3675–3696.

[Beron-Vera et al., 2008] Beron-Vera, F. J., Olascoaga, M. J., and Goni, G. J. Oceanic mesoscale eddies as revealed by Lagrangian coherent structures. *Geophysical Research Letters*, 35.

[Bestley et al., 2009] Bestley, S., Gunn, J. S., and Hindell, M. A. Plasticity in vertical behaviour of migrating juvenile southern bluefin tuna (Thunnus maccoyii) in relation to oceanography of the south Indian Ocean. *Fisheries Oceanography*, 18:237–254.

[Biermann et al., 2015] Biermann, L., Guinet, C., Bester, M., Brierley, A. S., and Boehme, L. An alternative method for correcting fluorescence quenching. *Ocean Science*.

[Biuw et al., 2007] Biuw, M., Boehme, L., Guinet, C., Hindell, M., Costa, D., Charrassin, J.-B., Roquet, F., Bailleul, F., Meredith, M., Thorpe, S., et al. Variations in behavior and condition of a Southern Ocean top predator in relation to in situ oceanographic conditions. *Proceedings of the National Academy of Sciences*, 104:13705–13710.

[Blain et al., 2015] Blain, S., Capparos, J., Guéneuguès, A., Obernosterer, I., and Oriol, L. Distributions and stoichiometry of dissolved nitrogen and phosphorus in the iron-fertilized region near Kerguelen (Southern Ocean). *Biogeosciences*, 12(2):623–635.

[Blain et al., 2007] Blain, S., Quéguiner, B., Armand, L., Belviso, S., Bombled, B., Bopp, L., Bowie, A., Brunet, C., Brussaard, C., Carlotti, F., et al. Effect of natural iron fertilization on carbon sequestration in the Southern Ocean. *Nature*, 446:1070–1074.

[Blain et al., 2008] Blain, S., Quéguiner, B., and Trull, T. The natural iron fertilization experiment KEOPS (KErguelen Ocean and Plateau compared Study): An overview. *Deep Sea Research Part II: Topical Studies in Oceanography*, 55:559–565.

[Blain et al., 2013] Blain, S., Renaut, S., Xing, X., Claustre, H., and Guinet, C. Instrumented elephant seals reveal the seasonality in chlorophyll and light-mixing regime in the iron-fertilized Southern Ocean. *Geophysical Research Letters*, 40(24):6368–6372.

[Blain et al., 2001] Blain, S., Tréguer, P., Belviso, S., Bucciarelli, E., Denis, M., Desabre, S., Fiala, M., Martin Jézéquel, V., Le Fèvre, J., Mayzaud, P., et al. A biogeochemical study of the island mass effect in the context of the iron hypothesis: Kerguelen Islands, Southern Ocean. *Deep Sea Research Part I: Oceanographic Research Papers*, 48:163–187.

[Block et al., 2002] Block, B. A., Costa, D. P., Boehlert, G. W., and Kochevar, R. E. Revealing pelagic habitat use: the tagging of Pacific pelagics program. *Oceanologica Acta*, 25:255–266.

[Block et al., 2011] Block, B. A., Jonsen, I. D., Jorgensen, S. J., Winship, A. J., Shaffer, S. A., Bograd, S. J., Hazen, E. L., Foley, D. G., Breed, G. A., Harrison, A.-L., Ganong, J. E., Swithenbank, A., Castleton, M., Dewar, H., Mate, B. R., Shillinger, G. L., Schaefer, K. M., Benson, S. R., Weise, M. J., Henry, R. W., and Costa, D. P. Tracking apex marine predator movements in a dynamic ocean. *Nature*, 475:86–90.

[Bocher et al., 2001] Bocher, P., Cherel, Y., Labat, J.-P., Mayzaud, P., Razouls, S., Jouventin, P., et al. Amphipod-based food web: Themisto gaudichaudii caught in nets and by seabirds in Kerguelen waters, southern Indian Ocean. *Marine Ecology Progress Series*, 223:251–260.

[Boero, 2014] Boero, F. The future of the Mediterranean Sea ecosystem: towards a different tomorrow. *Rendiconti Lincei*, 26(1):3–12.

[Boffetta et al., 2001] Boffetta, G., Lacorata, G., Redaelli, G., and Vulpiani, A. Detecting barriers to transport: a review of different techniques. *Physica D: Nonlinear Phenomena*, 159:58–70.

[Bon et al., 2015] Bon, C., Della Penna, A., d'Ovidio, F., Arnould, J. Y., Poupart, T., and Bost, C.-A. Influence of oceanographic structures on foraging strategies: Macaroni penguins at Crozet Islands. *Movement ecology*, 3(1):1–11.

[Böning et al., 2008] Böning, C. W., Dispert, A., Visbeck, M., Rintoul, S., and Schwarzkopf, F. U. The response of the Antarctic Circumpolar Current to recent climate change. *Nature Geoscience*, 1(12):864–869.

[Borrione et al., 2014] Borrione, I., Aumont, O., Nielsdóttir, M., and Schlitzer, R. Sedimentary and atmospheric sources of iron around South Georgia, Southern Ocean: a modelling perspective. *Biogeosciences*, 11:1981–2001.

[Boss and Pegau, 2001] Boss, E. and Pegau, W. S. Relationship of light scattering at an angle in the backward direction to the backscattering coefficient. *Applied Optics*, 40(30):5503–5507.

[Bost et al., 2009] Bost, C. A., Cotté, C., Bailleul, F., Cherel, Y., Charrassin, J. B., Guinet, C., Ainley, D. G., and Weimerskirch, H. The importance of oceanographic fronts to marine birds and mammals of the southern oceans. *Journal of Marine Systems*, 78:363–376.

[Bost et al., 2015] Bost, C. A., Cotté, C., Terray, P., Barbraud, C., Bon, C., Delord, K., Gimenez, O., Handrich, Y., Naito, Y., Guinet, C., et al. Large-scale climatic anomalies affect marine predator foraging behaviour and demography. *Nature communications*, 6.

[Bost et al., 1997] Bost, C. A., Georges, J. Y., Guinet, C., Cherel, Y., Pütz, K., Charrassin, J. B., Handrich, Y., Zorn, T., Lage, J., and Le Maho, Y. Foraging habitat and food intake of satellite-tracked king penguins during the austral summer at Crozet Archipelago. *Marine Ecology Progress Series*, 150:21–33.

[Bowie et al., 2014] Bowie, A., van der Merwe, P., Quéroué, F., Trull, T., Fourquez, M., Planchon, F., Sarthou, G., Chever, F., Townsend, A., Obernosterer, I., et al. Iron budgets for three distinct biogeochemical sites around the Kerguelen archipelago (Southern Ocean) during the natural fertilisation experiment KEOPS-2. *Biogeosciences Discussions*, 11(12):17861–17923.

[Boyd et al., 2004] Boyd, I. L., Kato, A., and Ropert-Coudert, Y. Bio-logging science: sensing beyond the boundaries. *Memoirs of the National Institute of Polar Research*, 58:1.

[Boyd et al., 2001] Boyd, P., Crossley, A., DiTullio, G., Griffiths, F., Hutchins, D., Queguiner, B., Sedwick, P., and Trull, T. Control of phytoplankton growth by iron supply and irradiance in the subantarctic Southern Ocean: Experimental results from the SAZ Project. *J. Geophys. Res*, 106(31):573–31.

[Boyd and Ellwood, 2010] Boyd, P. and Ellwood, M. The biogeochemical cycle of iron in the ocean. *Nature Geoscience*, 3(10):675–682.

[Boyd et al., 1999] Boyd, P., LaRoche, J., Gall, M., Frew, R., and McKay, R. M. L. Role of iron, light, and silicate in controlling algal biomass in subantarctic waters SE of New Zealand. *Journal of Geophysical Research: Oceans*, 104(C6):13395–13408.

[Boyd et al., 2005] Boyd, P., Law, C., Hutchins, D., Abraham, E., Croot, P. L., Ellwood, M., Frew, R., Hadfield, M., Hall, J., Handy, S., et al. FeCycle: Attempting an iron

biogeochemical budget from a mesoscale SF6 tracer experiment in unperturbed low iron waters. *Global Biogeochemical Cycles*, 19(4).

[Boyd et al., 2015] Boyd, P., Strzepek, R., Ellwood, M., Hutchins, D., Nodder, S., Twining, B., and Wilhelm, S. Why are biotic iron pools uniform across high-and low-iron pelagic ecosystems? *Global Biogeochemical Cycles*, 29(7):1028–1043.

[Boyd and Trull, 2007] Boyd, P. and Trull, T. Understanding the export of biogenic particles in oceanic waters: is there consensus? *Progress in Oceanography*, 72(4):276–312.

[Boyd et al., 2012a] Boyd, P. W., Arrigo, K. R., Strzepek, R., and Dijken, G. L. Mapping phytoplankton iron utilization: Insights into Southern Ocean supply mechanisms. *Journal of Geophysical Research: Oceans (1978–2012)*, 117.

[Boyd et al., 2007] Boyd, P. W., Jickells, T., Law, C. S., Blain, S., Boyle, E. A., Buesseler, K. O., Coale, K. H., Cullen, J. J., de Baar, H. J. W., Follows, M., Harvey, M., Lancelot, C., Levasseur, M., Owens, N. P. J., Pollard, R., Rivkin, R. B., Sarmiento, J., Schoemann, V., Smetacek, V., Takeda, S., Tsuda, A., Turner, S., and Watson, A. J. Mesoscale iron enrichment experiments 1993-2005: synthesis and future directions. *Science*, 315:612–617.

[Boyd et al., 2012b] Boyd, P. W., Strzepek, R., Chiswell, S., Chang, H., DeBruyn, J. M., Ellwood, M., Keenan, S., King, A. L., Maas, E. W., Nodder, S., et al. Microbial control of diatom bloom dynamics in the open ocean. *Geophysical Research Letters*, 39(18).

[Bracco et al., 2000] Bracco, A., Provenzale, A., and Scheuring, I. Mesoscale vortices and the paradox of the plankton. *Proceedings of the Royal Society B: Biological Sciences*, 267:1795–1800.

[Bradshaw et al., 2004] Bradshaw, C. J., Higgins, J., Michael, K. J., Wotherspoon, S. J., and Hindell, M. A. At-sea distribution of female southern elephant seals relative to variation in ocean surface properties. *ICES Journal of Marine Science: Journal du Conseil*, 61(6):1014–1027.

[Brewin et al., 2011] Brewin, R. J., Hardman-Mountford, N. J., Lavender, S. J., Raitsos, D. E., Hirata, T., Uitz, J., Devred, E., Bricaud, A., Ciotti, A., and Gentili, B. An intercomparison of bio-optical techniques for detecting dominant phytoplankton size class from satellite remote sensing. *Remote Sensing of Environment*, 115:325–339.

[Brooke, 2004] Brooke, M. d. L. The food consumption of the world's seabirds. *Proceedings of the Royal Society of London B: Biological Sciences*, 271(Suppl 4):S246–S248.

[Brown, 1987] Brown, C. R. Traveling Speed and Foraging Range of Macaroni and Rockhopper Penguins at Marion Island (Velocidad de Movimiento y Extensión de las Áreas de Forrajeo de los Pingüinos Eudyptes chrysolophus y E. chrysocome). *Journal of field ornithology*, pages 118–125.

[Brussaard et al., 2008] Brussaard, C., Timmermans, K., Uitz, J., and Veldhuis, M. Virioplankton dynamics and virally induced phytoplankton lysis versus microzooplankton grazing southeast of the Kerguelen (Southern Ocean). *Deep Sea Research Part II: Topical Studies in Oceanography*, 55(5):752–765.

[Burger and Gochfeld, 2004] Burger, J. and Gochfeld, M. Marine birds as sentinels of environmental pollution. *EcoHealth*, 1:263–274.

[Burnham and Anderson, 2004] Burnham, K. P. and Anderson, D. R. Multimodel inference understanding AIC and BIC in model selection. *Sociological methods & research*, 33(2):261–304.

[Cai et al., 2005] Cai, W., Shi, G., Cowan, T., Bi, D., and Ribbe, J. The response of the Southern Annular Mode, the East Australian Current, and the southern mid-latitude ocean circulation to global warming. *Geophysical Research Letters*, 32(23).

[Campagna and Lewis, 1992] Campagna, C. and Lewis, M. Growth and distribution of a southern elephant seal colony. *Marine Mammal Science*, 8:387–396.

[Campagna et al., 2006] Campagna, C., Piola, A. R., Rosa Marin, M., Lewis, M., and Fernández, T. Southern elephant seal trajectories, fronts and eddies in the Brazil/-Malvinas Confluence. *Deep Sea Research Part I: Oceanographic Research Papers*, 53:1907–1924.

[Camphuysen, 2006] Camphuysen, C. J. (2006). *Top Predators in Marine Ecosystems: Their Role in Monitoring and Management*.

[Carlotti et al., 2015] Carlotti, F., Jouandet, M.-P., Nowaczyk, A., Harmelin-Vivien, M., Lefèvre, D., Guillou, G., Zhu, Y., and Zhou, M. Mesozooplankton structure and functioning during the onset of the Kerguelen phytoplankton bloom during the Keops2 survey. *Biogeosciences Discussions*, 12:2381–2427.

[Carlson et al., 2010] Carlson, J. K., Ribera, M. M., Conrath, C. L., Heupel, M. R., and Burgess, G. H. Habitat use and movement patterns of bull sharks Carcharhinus leucas determined using pop-up satellite archival tags. *Journal of Fish Biology*, 77:661–675.

[Carpenter et al., 1985] Carpenter, S. R., Kitchell, J. F., and Hodgson, J. R. Cascading trophic interactions and lake productivity. *BioScience*, pages 634–639.

[Catry et al., 2004] Catry, P., Phillips, R. A., Phalan, B., Silk, J. R., and Croxall, J. P. Foraging strategies of grey-headed albatrosses Thalassarche chrysostoma: integration of movements, activity and feeding events.

[Cavagna et al., 2014] Cavagna, A., Fripiat, F., Elskens, M., Dehairs, F., Mangion, P., Chirurgien, L., Closset, I., Lasbleiz, M., Flores-Leiva, L., Cardinal, D., et al. Biological productivity regime and associated N cycling in the vicinity of Kerguelen Island area, Southern Ocean. *Biogeosciences Discussions*, 11(12):18073–18104.

[Cetinić et al., 2012] Cetinić, I., Perry, M. J., Briggs, N. T., Kallin, E., D'Asaro, E. A., and Lee, C. M. Particulate organic carbon and inherent optical properties during 2008 North Atlantic Bloom Experiment. *Journal of Geophysical Research: Oceans (1978–2012)*, 117(C6).

[Charrassin et al., 2008] Charrassin, J.-B., Hindell, M., Rintoul, S. R., Roquet, F. and-Sokolov, S., Biuw, M., Costa, D., Boehme, L., Lovell, P., Coleman, R., et al. Southern Ocean frontal structure and sea-ice formation rates revealed by elephant seals. *Proceedings of the National Academy of Sciences*, 105:11634–11639.

[Chelton, 2001] Chelton, D. B. Report of the High-Resolution Ocean Topography Science Working Group Meeting. *College of Oceanic and Atmospheric Sciences*.

[Chelton et al., 2011] Chelton, D. B., Schlax, M. G., and Samelson, R. M. Global observations of nonlinear mesoscale eddies. *Progress in Oceanography*, 91:167–216.

[Chelton et al., 2007] Chelton, D. B., Schlax, M. G., Samelson, R. M., and Szoeke, R. A. d. Global observations of large oceanic eddies. *Geophysical Research Letters*, 34:15606.

[Cheney et al., 1983] Cheney, R. E., Marsh, J. G., and Beckley, B. D. Global mesoscale variability from collinear tracks of Seasat altimeter data. *Journal of Geophysical Research: Oceans*, 88(C7):4343–4354.

[Cherel et al., 2008] Cherel, Y., Ducatez, S., Fontaine, C., Richard, P., and Guinet, C. Stable isotopes reveal the trophic position and mesopelagic fish diet of female southern elephant seals breeding on the Kerguelen Islands. *Marine Ecology Progress Series*, 370:239–247.

[Cherel et al., 2010] Cherel, Y., Fontaine, C., Richard, P., and Labatc, J.-P. Isotopic niches and trophic levels of myctophid fishes and their predators in the Southern Ocean. *Limnology and oceanography*, 55(1):324–332.

[Cherel and Weimerskirch, 1995] Cherel, Y. and Weimerskirch, H. Seabirds as indicators of marine resources: black-browed albatrosses feeding on ommastrephid squids in Kerguelen waters. *Marine Ecology Progress Series*, 129:295–300.

[Cloern et al., 1995] Cloern, J. E., Grenz, C., and Vidergar-Lucas, L. An empirical model of the phytoplankton chlorophyll: carbon ratio-the conversion factor between productivity and growth rate. *Limnology and Oceanography*, 40(7):1313–1321.

[Coale et al., 1996] Coale, K. H., Johnson, K. S., Fitzwater, S. E., Gordon, R. M., Tanner, S., Chavez, F. P., Ferioli, L., Nightingale, P., Cooper511, D., Cochlan11, W. P., et al. A massive phytoplakton bloom induced by an ecosystem-scale iron fertilization experiment in the equatorial Pacific Ocean. *Nature*, 383:495–501.

[Coles et al., 2016] Coles, V., Stukel, M., Hood, R., and Brroks, M. Top-down, bottom-up and physical controls on diatom-diazotroph assemblage growth in the Amazon River plume. *Biogeosciences*, 11(12).

[Collie et al., 2004] Collie, J. S., Richardson, K., and Steele, J. H. Regime shifts: can ecological theory illuminate the mechanisms? *Progress in Oceanography*, 60:281–302.

[Connan et al., 2007] Connan, M., Cherel, Y., and Mayzaud, P. Lipids from stomach oil of procellariiform seabirds document the importance of myctophid fish in the Southern Ocean. *Limnology and Oceanography*, 52(6):2445–2455.

[Constable et al., 2003] Constable, A. J., Nicol, S., and Strutton, P. G. Southern Ocean productivity in relation to spatial and temporal variation in the physical environment. *Journal of Geophysical Research: Oceans (1978–2012)*, 108(C4).

[Cotté et al., 2011] Cotté, C., d'Ovidio, F., Chaigneau, A., Lévy, M., Taupier-Letage, I., Mate, B., and Guinet, C. Scale-dependent interactions of Mediterranean whales with marine dynamics. *Limnology and Oceanography*, 56:219.

[Cotté et al., 2015] Cotté, C., d'Ovidio, F., Dragon, A.-C., Guinet, C., and Lévy, M. Flexible preference of southern elephant seals for distinct mesoscale features within the Antarctic Circumpolar Current. *Progress in Oceanography*, 131:46–58.

[Cotté et al., 2007] Cotté, C., Park, Y.-H., Guinet, C., and Bost, C.-A. Movements of foraging king penguins through marine mesoscale eddies. *Proceedings of the Royal Society B: Biological Sciences*, 274:2385–2391.

[Cracknell, 2007] Cracknell, A. P. (2007). *Introduction to remote sensing*.

[Crossin et al., 2013] Crossin, G. T., Trathan, P. N., and Crawford, R. J. Macaroni penguin (Eudyptes chrysolophus) and royal penguin (Eudyptes schlegeli).

[Croxall et al., 1993] Croxall, J., Briggs, D., Kato, A., Naito, Y., Watanuki, Y., and Williams, T. Diving pattern and performance in the macaroni penguin Eudptes chrysolophus. *Journal of Zoology*, 230(1):31–47.

[Cruz et al., 2001] Cruz, J., Lalas, C., Jillett, J., Kitson, J., Lyver, P. O., Imber, M., Newman, J., and Moller, H. Prey spectrum of breeding sooty shearwaters (Puffinus griseus) in New Zealand. *New Zealand Journal of Marine and Freshwater Research*, 35(4):817–829.

[Cullen, 1982] Cullen, J. J. The deep chlorophyll maximum: comparing vertical profiles of chlorophyll a. *Canadian Journal of Fisheries and Aquatic Sciences*, 39(5):791–803.

[Cushing, 1989] Cushing, D. A difference in structure between ecosystems in strongly stratified waters and in those that are only weakly stratified. *Journal of Plankton Research*, 11(1):1–13.

[De Baar et al., 2005] De Baar, H. J., Boyd, P. W., Coale, K. H., Landry, M. R., Tsuda, A., Assmy, P., Bakker, D. C., Bozec, Y., Barber, R. T., Brzezinski, M. A., et al. Synthesis of iron fertilization experiments: from the iron age in the age of enlightenment. *Journal of Geophysical Research: Oceans (1978–2012)*, 110.

[De Baar et al., 1995] De Baar, H. J., De Jong, J. T., Bakker, D. C., Löscher, B. M., Veth, C., Bathmann, U., and Smetacek, V. Importance of iron for plankton blooms and carbon dioxide drawdown in the Southern Ocean.

[De Broyer et al., 2014] De Broyer, C., Koubbi, P., Griffiths, H., and Grant, S. (2014). *Biogeographic Atlas of the Southern Ocean*. Scientific Committee on Antarctic Research Cambridge.

[De Monte et al., 2012] De Monte, S., Cotté, C., d'Ovidio, F., Lévy, M., Le Corre, M., and Weimerskirch, H. Frigatebird behaviour at the ocean–atmosphere interface: integrating animal behaviour with multi-satellite data. *Journal of The Royal Society Interface*, 9:3351–3358.

[De Monte et al., 2013] De Monte, S., Soccodato, A., Alvain, S., and d'Ovidio, F. Can we detect oceanic biodiversity hotspots from space&quest. *The ISME journal*, 7(10):2054–2056.

[Deagle et al., 2007] Deagle, B. E., Gales, N. J., Evans, K., Jarman, S. N., Robinson, S., Trebilco, R., and Hindell, M. A. Studying seabird diet through genetic analysis of faeces: a case study on macaroni penguins (Eudyptes chrysolophus). *PLoS One*, 2:831.

[Della Penna et al., 2015] Della Penna, A., De Monte, S., Kestenare, E., Guinet, C., and d'Ovidio, F. Quasi-planktonic behavior of foraging top marine predators. *Scientific reports*, 5.

[Di Lorenzo and Ohman, 2013] Di Lorenzo, E. and Ohman, M. D. A double-integration hypothesis to explain ocean ecosystem response to climate forcing. *Proc Natl Acad Sci U S A*, 110:2496–2499.

[Doney et al., 2012] Doney, S. C., Ruckelshaus, M., Duffy, J. E., Barry, J. P., Chan, F., English, C. A., Galindo, H. M., Grebmeier, J. M., Hollowed, A. B., Knowlton, N., et al. Climate change impacts on marine ecosystems. *Marine Science*, 4.

[Dong et al., 2008] Dong, S., Sprintall, J., Gille, S. T., and Lynney, T. Southern Ocean mixed-layer depth from Argo float profiles. *Journal of Geophysical Research*, 113.

[d'Ovidio et al., 2013] d'Ovidio, F., De Monte, S., Della Penna, A., Cotte', C., and Guinet, C. Ecological implications of eddy retention in the open ocean: a Lagrangian approach. *Journal of Physics A*.

[d'Ovidio et al., 2015] d'Ovidio, F., Della Penna, A., Trull, T. W., Nencioli, F., Pujol, I., Rio, M. H., Park, Y.-H., Cotté, C., Zhou, M., and Blain, S. The biogeochemical structuring role of horizontal stirring: Lagrangian perspectives on iron delivery downstream of the Kerguelen plateau. *Biogeosciences*, 12(1):779–814.

[d'Ovidio et al., 2004] d'Ovidio, F., Fernández, V., Hernández-García, E., and López, C. Mixing structures in the Mediterranean Sea from finite-size Lyapunov exponents. *Geophysical Research Letters*, 31:4.

[d'Ovidio et al., 2009] d'Ovidio, F., Isern-Fontanet, J., López, C., Hernández-García, E., and García-Ladona, E. Comparison between Eulerian diagnostics and finite-size Lyapunov exponents computed from altimetry in the Algerian basin. *Deep Sea Research Part I: Oceanographic Research Papers*, 56:15–31.

[d'Ovidio et al., 2010] d'Ovidio, F., Monte, S. D., Alvain, S., Dandonneau, Y., and Lévy, M. Fluid dynamical niches of phytoplankton types. *Proceedings of the National Academy of Sciences*, 107:18366–18370.

[Dragon et al., 2012a] Dragon, A.-C., Bar-Hen, A., Monestiez, P., Guinet, C., et al. Comparative analysis of methods for inferring successful foraging areas from Argos and GPS tracking data. *Marine Ecology Progress Series*, 452:253–267.

[Dragon et al., 2012b] Dragon, A.-C., Bar-Hen, A., Monestiez, P. P., Guinet, C., et al. Horizontal and vertical movements as predictors of foraging success in a marine predator. *Marine Ecology Progress Series*, 447:243–257.

[Dragon et al., 2010] Dragon, A.-C., Monestiez, P., Bar-Hen, A., and Guinet, C. Linking foraging behaviour to physical oceanographic structures: Southern elephant seals and mesoscale eddies east of Kerguelen Islands. *Progress In Oceanography*, 87:61–71.

[Dubischar and Bathmann, 1997] Dubischar, C. D. and Bathmann, U. V. Grazing impact of copepods and salps on phytoplankton in the Atlantic sector of the Southern Ocean. *Deep Sea Research Part II: Topical Studies in Oceanography*, 44(1):415–433.

[Dubischar et al., 2006] Dubischar, C. D., Pakhomov, E., and Bathmann, U. The tunicate Salpa thompsoni ecology in the Southern Ocean. II. Proximate and elemental composition. *Marine biology*, 149(3):625–632.

[Ducklow et al., 2007] Ducklow, H. W., Baker, K., Martinson, D. G., Quetin, L. B., Ross, R. M., Smith, R. C., Stammerjohn, S. E., Vernet, M., and Fraser, W. Marine pelagic ecosystems: the west Antarctic Peninsula. *Philosophical Transactions of the Royal Society B: Biological Sciences*, 362(1477):67–94.

[Durham et al., 2013] Durham, W. M., Climent, E., Barry, M., De Lillo, F., Boffetta, G., Cencini, M., and Stocker, R. Turbulence drives microscale patches of motile phytoplankton. *Nature communications*, 4.

[Dutkiewicz et al., 2009] Dutkiewicz, S., Follows, M. J., and Bragg, J. G. Modeling the coupling of ocean ecology and biogeochemistry. *Global Biogeochemical Cycles*, 23.

[D'Asaro et al., 2011] D'Asaro, E., Lee, C., Rainville, L., Harcourt, R., and Thomas, L. Enhanced turbulence and energy dissipation at ocean fronts. *science*, 332(6027):318–322.

[Earp et al., 2011] Earp, A., Hanson, C. E., Ralph, P. J., Brando, V. E., Allen, S., Baird, M., Clementson, L., Daniel, P., Dekker, A. G., Fearns, P. R., et al. Review of fluorescent standards for calibration of in situ fluorometers: Recommendations applied in coastal and ocean observing programs. *Optics express*, 19(27):26768–26782.

[Estes and Duggins, 1995] Estes, J. A. and Duggins, D. O. Sea otters and kelp forests in Alaska: generality and variation in a community ecological paradigm. *Ecological Monographs*, 65(1):75–100.

[Estes et al., 2011] Estes, J. A., Terborgh, J., Brashares, J. S., Power, M. E., Berger, J., Bond, W. J., Carpenter, S. R., Essington, T. E., Holt, R. D., Jackson, J. B., et al. Trophic downgrading of planet earth. *science*, 333:301–306.

[Estes et al., 1998] Estes, J. A., Tinker, M. T., Williams, T. M., and Doak, D. F. Killer Whale Predation on Sea Otters Linking Oceanic and Nearshore Ecosystems. 282:473.

[Evans et al., 2015] Evans, K., Brown, J. N., Sen Gupta, A., Nicol, S. J., Hoyle, S., Matear, R., and Arrizabalaga, H. When 1+ 1 can be¿ 2: Uncertainties compound when simulating climate, fisheries and marine ecosystems. *Deep Sea Research Part II: Topical Studies in Oceanography*, 113:312–322.

[Evans et al., 2013] Evans, K., Lea, M.-A., and Patterson, T. A. Recent advances in bio-logging science: Technologies and methods for understanding animal behaviour and physiology and their environments. *Deep Sea Research Part II: Topical Studies in Oceanography*, 88:1–6.

[Falkowski and Kiefer, 1985] Falkowski, P. and Kiefer, D. A. Chlorophyll a fluorescence in phytoplankton: relationship to photosynthesis and biomass. *Journal of Plankton Research*, 7(5):715–731.

[Falkowski and Kolber, 1995] Falkowski, P. and Kolber, Z. Variations in chlorophyll fluorescence yields in phytoplankton in the world oceans. *Functional Plant Biology*, 22(2):341–355.

[Falkowski et al., 1998] Falkowski, P. G., Barber, R. T., and Smetacek, V. Biogeochemical controls and feedbacks on ocean primary production. *Science*, 281:200–206.

[Fauchald and Tveraa, 2003] Fauchald, P. and Tveraa, T. USING FIRST-PASSAGE TIME IN THE ANALYSIS OF AREA-RESTRICTED SEARCH AND HABITAT SELECTION. *Ecology*, 84:282–288.

[Fawcett, 2004] Fawcett, T. ROC graphs: Notes and practical considerations for researchers. *Machine learning*, 31:1.

[Fennel and Boss, 2003] Fennel, K. and Boss, E. Subsurface maxima of phytoplankton and chlorophyll: Steady-state solutions from a simple model. *Limnology and Oceanography*, 48(4):1521–1534.

[Fernandez et al., 1992] Fernandez, E., Serret, P., De Madariaga, I., Harbour, D., and Davies, A. Photosynthetic Carbon Metabolism and Biochemical Composition of Spring Phytoplankton Assemblages Enclosed in Microcosms: The Diatom–Phaeocystis sp. Succession. *Marine Ecology Progress Series MESEDT,*, 90(1).

[Field et al., 1998] Field, C. B., Behrenfeld, M. J., Randerson, J. T., and Falkowski, P. Primary production of the biosphere: integrating terrestrial and oceanic components. *Science*, 281(5374):237–240.

[Finkel et al., 2009] Finkel, Z. V., Beardall, J., Flynn, K. J., Quigg, A., Rees, T. A. V., and Raven, J. A. Phytoplankton in a changing world: cell size and elemental stoichiometry. *Journal of plankton research*, page fbp098.

[Flemming et al., 2006] Flemming, J. E., Field, C. A., James, M. C., Jonsen, I. D., and Myers, R. A. How well can animals navigate?: Estimating the circle of confusion from tracking data. *Environmetrics*, 17:351–362.

[Follows et al., 2007] Follows, M. J., Dutkiewicz, S., Grant, S., and Chisholm, S. W. Emergent biogeography of microbial communities in a model ocean. *Science*, 315:1843–1846.

[Forcada and Trathan, 2009] Forcada, J. and Trathan, P. N. Penguin responses to climate change in the Southern Ocean. *Global Change Biology*, 15(7):1618–1630.

[Fossette et al., 2015] Fossette, S., Gleiss, A. C., Chalumeau, J., Bastian, T., Armstrong, C. D., Vandenabeele, S., Karpytchev, M., and Hays, G. C. Current-oriented swimming by jellyfish and its role in bloom maintenance. *Current Biology*, 25(3):342–347.

[Fossi et al., 2012] Fossi, M. C., Casini, S., Caliani, I., Panti, C., Marsili, L., Viarengo, A., Giangreco, R., Notarbartolo di Sciara, G., Serena, F., Ouerghi, A., and Depledge, M. H. The role of large marine vertebrates in the assessment of the quality of pelagic marine ecosystems. *Mar Environ Res*, 77:156–158.

[Frank et al., 2005] Frank, K. T., Petrie, B., Choi, J. S., and Leggett, W. C. Trophic cascades in a formerly cod-dominated ecosystem. *Science*, 308(5728):1621–1623.

[Frank et al., 2007] Frank, K. T., Petrie, B., and Shackell, N. L. The ups and downs of trophic control in continental shelf ecosystems. *Trends Ecol Evol*, 22:236–242.

[Fraser and Hofmann, 2003] Fraser, W. R. and Hofmann, E. E. A predator's perspective on causal links between climate change, physical forcing and ecosystem. *Marine Ecology Progress Series*, 265:1.

[Frederiksen et al., 2006] Frederiksen, M., Edwards, M., Richardson, A. J., Halliday, N. C., and Wanless, S. From plankton to top predators: bottom-up control of a marine food web across four trophic levels. *Journal of Animal Ecology*, 75(6):1259–1268.

[Fulton, 2010] Fulton, E. A. Approaches to end-to-end ecosystem models. *Journal of Marine Systems*, 81(1):171–183.

[Fulton et al., 2011] Fulton, E. A., Link, J. S., Kaplan, I. C., Savina-Rolland, M., Johnson, P., Ainsworth, C., Horne, P., Gorton, R., Gamble, R. J., Smith, A. D., et al. Lessons in modelling and management of marine ecosystems: the Atlantis experience. *Fish and Fisheries*, 12(2):171–188.

[Fung et al., 2011] Fung, T., Seymour, R. M., and Johnson, C. R. Alternative stable states and phase shifts in coral reefs under anthropogenic stress. *Ecology*, 92(4):967–982.

[Gallon et al., 2012] Gallon, S., Bailleul, F., Charrassin, J.-B., Guinet, C., Bost, C.-A., Handrich, Y., and Hindell, M. Identifying foraging events in deep diving southern elephant seals, Mirounga leonina, using acceleration data loggers. *Deep Sea Research Part II: Topical Studies in Oceanography*.

[Game et al., 2009] Game, E. T., Grantham, H. S., Hobday, A. J., Pressey, R. L., Lombard, A. T., Beckley, L. E., Gjerde, K., Bustamante, R., Possingham, H. P., and Richardson, A. J. Pelagic protected areas: the missing dimension in ocean conservation. *Trends in ecology & evolution*, 24:360–369.

[Gaspar et al., 2006] Gaspar, P., Georges, J.-Y., Fossette, S., Lenoble, A., Ferraroli, S., and Le Maho, Y. Marine animal behaviour: neglecting ocean currents can lead us up the wrong track. *Proceedings of the Royal Society B: Biological Sciences*, 273:2697–2702.

[Gaube et al., 2013] Gaube, P., Chelton, D. B., Strutton, P. G., and Behrenfeld, M. J. Satellite observations of chlorophyll, phytoplankton biomass, and Ekman pumping in nonlinear mesoscale eddies. *Journal of Geophysical Research: Oceans*.

[Gille et al., 2014] Gille, S., Carranza, M., Cambra, R., and Morrow, R. Wind-induced upwelling in the Kerguelen Plateau Region. *Biogeosciences*, 11(22):6389–6400.

[Gille, 2008] Gille, S. T. Decadal-scale temperature trends in the Southern Hemisphere ocean. *Journal of Climate*, 21(18):4749–4765.

[Girard et al., 2006] Girard, C., Sudre, J., Benhamou, S., Roos, D., and Luschi, P. Homing in green turtles Chelonia mydas: oceanic currents act as a constraint rather than as an information source. *Marine Ecology Progress Series*, 322:281–289.

[Godø et al., 2012] Godø, O. R., Samuelsen, A., Macaulay, G. J., Patel, R., Hjøllo, S. S., Horne, J., Kaartvedt, S., and Johannessen, J. A. Mesoscale eddies are oases for higher trophic marine life. *PloS one*, 7:30161.

[Goericke and Montoya, 1998] Goericke, R. and Montoya, J. P. Estimating the contribution of microalgal taxa to chlorophyll a in the field-variations of pigment ratios under nutrient-and light-limited growth.

[Goldsworthy et al., 2001] Goldsworthy, S., He, X., Tuck, G., Lewis, M., and Williams, R. Trophic interactions between the Patagonian toothfish, its fishery, and seals and seabirds around Macquarie Island. *Marine Ecology Progress Series*, 218:283–302.

[Gordon and McCluney, 1975] Gordon, H. R. and McCluney, W. Estimation of the depth of sunlight penetration in the sea for remote sensing. *Applied optics*, 14(2):413–416.

[Green et al., 2009] Green, J. A., Boyd, I. L., Woakes, A. J., Warren, N. L., and Butler, P. J. Evaluating the prudence of parents: daily energy expenditure throughout the annual cycle of a free-ranging bird, the macaroni penguin Eudyptes chrysolophus. *Journal of Avian Biology*, 40(5):529–538.

[Green et al., 1998a] Green, K., Williams, R., and Green, M. Foraging ecology and diving behaviour of macaroni penguins Eudyptes chrysolophus at Heard Island. *Mar Ornithol*, 26:27–34.

[Green et al., 1998b] Green, K., Williams, R., and Green, M. Foraging ecology and diving behaviour of macaroni penguins Eudyptes chrysolophus at Heard Island. *Mar Ornithol*, 26:27–34.

[Grenier et al., 2015] Grenier, M., Della Penna, A., and Trull, T. Autonomous profiling float observations of the high biomass plume downstream of the Kerguelen plateau in the Southern Ocean. *Biogeosciences*, 11(12):17413–17462.

[Guinet et al., 1996] Guinet, C., Cherel, Y., Ridoux, V., and Jouventin, P. Consumption of marine resources by seabirds and seals in Crozet and Kerguelen waters: changes in relation to consumer biomass 1962–85. *Antarctic Science*, 8:23–30.

[Guinet et al., 2001] Guinet, C., Dubroca, L., Lea, M., Goldsworthy, S., Cherel, Y., Duhamel, G., Bonadonna, F., and Donnay, J. Spatial distribution of foraging in female Antarctic fur seals Arctocephalus gazella in relation to oceanographic variables: a scale-dependent approach using geographic information systems. *Marine Ecology Progress Series*, 219:251–264.

[Guinet et al., 1992] Guinet, C., Jouventin, P., and Weimerskirch, H. Population changes, movements of southern elephant seals on Crozet and Kerguelen Archipelagos in the last decades. *Polar Biology*, 12:349–356.

[Guinet et al., 1999] Guinet, C., Jouventin, P. I. E. R. R. E., and Weimerskirch, H. E. N. R. I. Recent population change of the southern elephant seal at lies Crozer and Iles Kerguelen: the end of the decrease? *Antarctic Science*, 11:193–197.

[Guinet et al., 2014] Guinet, C., Vacquié-Garcia, J., Picard, B., Bessigneul, G., Lebras, Y., Dragon, A.-C., Viviant, M., Arnould, J. P., Bailleul, F., et al. Southern elephant seal foraging success in relation to temperature and light conditions: insight into prey distribution. *Marine Ecology Progress Series*, 499:285–301.

[Guinet et al., 2013] Guinet, C., Xing, X., Walker, E., Monestiez, P., Marchand, S., Picard, B., Jaud, T., Authier, M., Cotté, C., Dragon, A., et al. Calibration procedures and first dataset of Southern Ocean chlorophyll a profiles collected by elephant seals

equipped with a newly developed CTD-fluorescence tags. *Earth System Science Data*, 5:15–29.

[Haller and Yuan, 2000] Haller, G. and Yuan, G. Lagrangian coherent structures and mixing in two-dimensional turbulence. *Phys. D*, 147:352–370.

[Handbook, 2010] Handbook, S. U. (2010). *(M)SLA and (M)ADT Near-Real Time and Delayed Time Products*.

[Handbook, 2014] Handbook, S. U. (2014). *(M)SLA and (M)ADT Near-Real Time and Delayed Time Products*.

[Hardin et al., 1960] Hardin, G. et al. The competitive exclusion principle. *science*, 131:1292–1297.

[Harvey et al., 2011] Harvey, M. J., Law, C. S., Smith, M. J., Hall, J. A., Abraham, E. R., Stevens, C. L., Hadfield, M. G., Ho, D. T., Ward, B., Archer, S. D., et al. The SOLAS air–sea gas exchange experiment (SAGE) 2004. *Deep Sea Research Part II: Topical Studies in Oceanography*, 58(6):753–763.

[Hays et al., 2001] Hays, G. C., Dray, M., Quaife, T., Smyth, T. J., Mironnet, N. C., Luschi, P., Papi, F., and Barnsley, M. J. Movements of migrating green turtles in relation to AVHRR derived sea surface temperature. *International Journal of Remote Sensing*, 22:1403–1411.

[Hazen et al., 2013] Hazen, E. L., Jorgensen, S., Rykaczewski, R. R., Bograd, S. J., Foley, D. G., Jonsen, I. D., Shaffer, S. A., Dunne, J. P., Costa, D. P., Crowder, L. B., et al. Predicted habitat shifts of Pacific top predators in a changing climate. *Nature Climate Change*, 3(3):234–238.

[Heithaus et al., 2008] Heithaus, M. R., Frid, A., Wirsing, A. J., and Worm, B. Predicting ecological consequences of marine top predator declines. *Trends Ecol Evol*, 23:202–210.

[Hengeveld, 2007] Hengeveld, G. M. (2007). *Moving to eat: animal foraging movements in a heterogeneous environment*.

[Hernández-Carrasco,] Hernández-Carrasco, I. *Scaling properties and robustness of finite-size Lyapunov exponents in surface marine flows*. PhD thesis.

[Hernández-Carrasco et al., 2011] Hernández-Carrasco, I., López, C., Hernández-García, E., and Turiel, A. How reliable are finite-size Lyapunov exponents for the assessment of ocean dynamics? *Ocean Modelling*, 36:208–218.

[Hernandez-Garcia et al., 2002] Hernandez-Garcia, E., Lopez, C., and Neufeld, Z. Spatial Patterns in Chemically and Biologically Reacting Flows. *arXiv:nlin/0205009*.

[Hindell et al., 1991] Hindell, M., Slip, D., and Burton, H. The diving behavior of adult male and female southern elephant seals, Mirounga-Leonina (Pinnipedia, Phocidae). *Australian Journal of Zoology*, 39(5):595–619.

[Hindell et al., 2011] Hindell, M. A., Lea, M., Bost, C.-A., Charrassin, J.-B., Gales, N., Goldsworthy, S., Page, B., Robertson, G., Wienecke, B., O'Toole, M., et al. Foraging habitats of top predators, and areas of ecological significance, on the Kerguelen Plateau. *The Kerguelen Plateau: marine ecosystem and fisheries. Société Française d'Ichtyologie, Paris*, pages 203–215.

[Hirata et al., 2011] Hirata, T., Hardman-Mountford, N., Brewin, R., Aiken, J., Barlow, R., Suzuki, K., Isada, T., Howell, E., Hashioka, T., Noguchi-Aita, M., et al. Synoptic relationships between surface Chlorophyll-a and diagnostic pigments specific to phytoplankton functional types. *Biogeosciences*, 8(2):311–327.

[Hobday and Hartmann, 2006] Hobday, A. and Hartmann, K. Near real-time spatial management based on habitat predictions for a longline bycatch species. *Fisheries Management and Ecology*, 13(6):365–380.

[Hobday et al., 2015] Hobday, A. J., Arrizabalaga, H., Evans, K., Nicol, S., Young, J. W., and Weng, K. C. Impacts of climate change on marine top predators: advances and future challenges. *Deep Sea Research Part II: Topical Studies in Oceanography*, 113:1–8.

[Hobday and Hartog, 2014] Hobday, A. J. and Hartog, J. R. Derived ocean features for dynamic ocean management. *Oceanography*, 27(4):134–145.

[Hoegh-Guldberg and Bruno, 2010] Hoegh-Guldberg, O. and Bruno, J. F. The impact of climate change on the world's marine ecosystems. *Science*, 328:1523–1528.

[Horsburgh et al., 2008] Horsburgh, J. M., Morrice, M., Lea, M.-a., and Hindell, M. A. Determining feeding events and prey encounter rates in a southern elephant seal: a method using swim speed and stomach temperature. *Marine mammal science*, 24:207–217.

[Huggett, 2014] Huggett, J. A. Mesoscale distribution and community composition of zooplankton in the Mozambique Channel. *Deep Sea Research Part II: Topical Studies in Oceanography*, 100:119–135.

[Hughes, 2000] Hughes, L. Biological consequences of global warming: is the signal already apparent? *Trends in ecology & evolution*, 15(2):56–61.

[Hughes et al., 2013] Hughes, T. P., Linares, C., Dakos, V., van de Leemput, I. A., and van Nes, E. H. Living dangerously on borrowed time during slow, unrecognized regime shifts. *Trends in ecology & evolution*, 28(3):149–155.

[Hunt et al., 1999] Hunt, G., Mehlum, F., Russell, R. W., Irons, D., Decker, M. B., and Becker, P. H. Physical processes, prey abundance, and the foraging ecology of seabirds. *Proc 22 Int Ornithol Congr, Durban,20–22 Aug,1998. BirdLife South Africa, Johannesburg, p 2040– 2056*.

[Hunt et al., 2011] Hunt, G. L., Coyle, K. O., Eisner, L. B., Farley, E. V., Heintz, R. A., Mueter, F., Napp, J. M., Overland, J. E., Ressler, P. H., Salo, S., et al. Climate impacts on eastern Bering Sea foodwebs: a synthesis of new data and an assessment of the Oscillating Control Hypothesis. *ICES Journal of Marine Science: Journal du Conseil*, page fsr036.

[Hunt and McKinnell, 2006] Hunt, G. L. and McKinnell, S. Interplay between top-down, bottom-up, and wasp-waist control in marine ecosystems. *Progress in Oceanography*, 68(2):115–124.

[Huot et al., 2007] Huot, Y., Babin, M., Bruyant, F., Grob, C., Twardowski, M., and Claustre, H. Relationship between photosynthetic parameters and different proxies of phytoplankton biomass in the subtropical ocean. *Biogeosciences*, 4(5):853–868.

[Hussey et al., 2015] Hussey, N. E., Kessel, S. T., Aarestrup, K., Cooke, S. J., Cowley, P. D., Fisk, A. T., Harcourt, R. G., Holland, K. N., Iverson, S. J., Kocik, J. F., et al. Aquatic animal telemetry: a panoramic window into the underwater world. *Science*, 348(6240):1255642.

[Hyrenbach et al., 2002] Hyrenbach, K. D., Fernández, P., Anderson, D. J., et al. Oceanographic habitats of two sympatric North Pacific albatrosses during the breeding season. *Marine Ecology Progress Series*, 233:283–301.

[Inchausti et al., 2003] Inchausti, P., Guinet, C., Koudil, M., Durbec, J.-P., Barbraud, C., Weimerskirch, H., Cherel, Y., and Jouventin, P. Inter-annual variability in the breeding performance of seabirds in relation to oceanographic anomalies that affect the Crozet and the Kerguelen sectors of the Southern Ocean. *Journal of Avian Biology*, 34(2):170–176.

[Irigoien et al., 2002] Irigoien, X., Harris, R. P., Verheye, H. M., Joly, P., Runge, J., Starr, M., Pond, D., Campbell, R., Shreeve, R., Ward, P., et al. Copepod hatching success in marine ecosystems with high diatom concentrations. *Nature*, 419(6905):387–389.

[Isern-Fontanet et al., 2008] Isern-Fontanet, J., Lapeyre, G., Klein, P., Chapron, B., and Hecht, M. W. Three-dimensional reconstruction of oceanic mesoscale currents from surface information. *Journal of Geophysical Research: Oceans (1978–2012)*, 113(C9).

[Jaccard, 1912] Jaccard, P. The distribution of the flora in the alpine zone. *New phytologist*, 11(2):37–50.

[Jaine et al., 2012] Jaine, F. R., Couturier, L. I., Weeks, S. J., Townsend, K. A., Bennett, M. B., Fiora, K., and Richardson, A. J. When giants turn up: sighting trends, environmental influences and habitat use of the manta ray Manta alfredi at a coral reef.

[Jaud et al., 2016] Jaud, T., Riviere, P., Klein, P., Cotte', C., d'Ovidio, F., Guinet, C., Le Sommer, J., and Dencausse, G. The life of female Elephant Seals in a field of submesoscale front regions. *In preparation*.

[Jeandel et al., 1998] Jeandel, C., Ruiz-Pino, D., Gjata, E., Poisson, A., Brunet, C., Charriaud, E., Dehairs, F., Delille, D., Fiala, M., Fravalo, C., et al. KERFIX, a time-series station in the Southern Ocean: a presentation. *Journal of Marine Systems*, 17:555–569.

[Johnson et al., 2013] Johnson, R., Strutton, P. G., Wright, S. W., McMinn, A., and Meiners, K. M. Three improved satellite chlorophyll algorithms for the Southern Ocean. *Journal of Geophysical Research: Oceans*, 118(7):3694–3703.

[Jouandet et al., 2011] Jouandet, M.-P., Trull, T. W., Guidi, L., Picheral, M., Ebersbach, F., Stemmann, L., and Blain, S. Optical imaging of mesopelagic particles indicates deep carbon flux beneath a natural iron-fertilized bloom in the Southern Ocean. *Limnology and Oceanography*, 56(3):1130–1140.

[Joubert et al., 2014] Joubert, W., Swart, S., Tagliabue, A., Thomalla, S., and Monteiro, P. The sensitivity of primary productivity to intra-seasonal mixed layer variability in the sub-Antarctic Zone of the Atlantic Ocean. *Biogeosciences Discussions*, 11(3):4335–4358.

[Kai et al., 2009a] Kai, E. T., Rossi, V., Sudre, J., Weimerskirch, H., Lopez, C., Hernandez-Garcia, E., Marsac, F., and Garcon, V. Top marine predators track Lagrangian coherent structures. *Proceedings of the National Academy of Sciences of the United States of America*, 106:8245–8250.

[Kai et al., 2009b] Kai, E. T., Rossi, V., Sudre, J., Weimerskirch, H., Lopez, C., Hernandez-Garcia, E., Marsac, F., and Garçon, V. Top marine predators track Lagrangian coherent structures. *Proceedings of the National Academy of Sciences*, 106:8245–8250.

[Karl and Trenberth, 2003] Karl, T. R. and Trenberth, K. E. Modern global climate change. *science*, 302(5651):1719–1723.

[Kemp et al., 2000] Kemp, A. E., Pike, J., Pearce, R. B., and Lange, C. B. The "Fall dump"—a new perspective on the role of a "shade flora" in the annual cycle of diatom production and export flux. *Deep Sea Research Part II: Topical Studies in Oceanography*, 47(9):2129–2154.

[Kiefer, 1973] Kiefer, D. Fluorescence properties of natural phytoplankton populations. *Marine Biology*, 22(3):263–269.

[Klein et al., 2005] Klein, P., Hua, B.-L., Le Gentil, S., and Sasaki, H. The Vertical Pump Organized by the Mesoscale Oceanic Eddies. *Annual Report of the Earth Simulator Center*, pages 331–334.

[Klein and Lapeyre, 2009a] Klein, P. and Lapeyre, G. The Oceanic Vertical Pump Induced by Mesoscale and Submesoscale Turbulence. *Annual Review of Marine Science*, 1:351–375.

[Klein and Lapeyre, 2009b] Klein, P. and Lapeyre, G. The oceanic vertical pump induced by mesoscale and submesoscale turbulence. *Annual review of marine science*, 1:351–375.

[Klocker et al., ress] Klocker, A., Maddison, J., Marshall, D., and Naveira Garbato, A. Wave-turbulence-mean flow interaction in the Antarctic Circumpolar Current.

[Kopczynska, 1992] Kopczynska, E. E. Dominance of microflagellates over diatoms in the Antarctic areas of deep vertical mixing and krill concentrations. *Journal of Plankton Research*, 14:1031–1054.

[Kostianoy et al., 2003] Kostianoy, A. G., Ginzburg, A. I., Lebedev, S. A., Frankignoulle, M., and Delille, B. Fronts and mesoscale variability in the southern Indian Ocean as inferred from the TOPEX/POSEIDON and ERS-2 altimetry data. *OCEANOLOGY C/C OF OKEANOLOGIIA*, 43(5):632–642.

[Koubbi, 1993] Koubbi, P. Influence of the frontal zones on ichthyoplankton and mesopelagic fish assemblages in the Crozet Basin (Indian sector of the Southern Ocean). *Polar Biology*, 13(8):557–564.

[Koubbi et al., 2011] Koubbi, P., Moteki, M., Duhamel, G., Goarant, A., Hulley, P.-A., O'Driscoll, R., Ishimaru, T., Pruvost, P., Tavernier, E., and Hosie, G. Ecoregionalization of myctophid fish in the Indian sector of the Southern Ocean: results from generalized dissimilarity models. *Deep Sea Research Part II: Topical Studies in Oceanography*, 58(1):170–180.

[Kowalewsky et al., 2006] Kowalewsky, S., Dambach, M., Mauck, B., and Dehnhardt, G. High olfactory sensitivity for dimethyl sulphide in harbour seals. *Biology Letters*, 2(1):106–109.

[Koz, 1995] Koz, A. A review of the trophic role of mesopelagic fish of the family Myctophidae in the Southern Ocean ecosystem. *CCAMLR Science*, 2:71–77.

[Kubryakov et al., 2016] Kubryakov, A., Stanichny, S., and Zatsepin, A. River plume dynamics in the Kara Sea from altimetry-based lagrangian model, satellite salinity and chlorophyll data. *Remote Sensing of Environment*, 176:177–187.

[Labat et al., 2009] Labat, J.-P., Gasparini, S., Mousseau, L., Prieur, L., Boutoute, M., and Mayzaud, P. Mesoscale distribution of zooplankton biomass in the northeast Atlantic Ocean determined with an Optical Plankton Counter: Relationships with environmental structures. *Deep Sea Research Part I: Oceanographic Research Papers*, 56:1742–1756.

[Laird et al., 1982] Laird, N. M., Ware, J. H., Team, R. D. C., et al. Random-effects models for longitudinal data: A language and environment for statistical computing.

[Landry et al., 2008] Landry, M. R., Decima, M., Simmons, M. P., Hannides, C. C., and Daniels, E. Mesozooplankton biomass and grazing responses to Cyclone Opal, a subtropical mesoscale eddy. *Deep Sea Research Part II: Topical Studies in Oceanography*, 55(10):1378–1388.

[Lapeyre and Klein, 2006a] Lapeyre, G. and Klein, P. Dynamics of the Upper Oceanic Layers in Terms of Surface Quasigeostrophy Theory. *Journal of Physical Oceanography*, 36:165–176.

[Lapeyre and Klein, 2006b] Lapeyre, G. and Klein, P. Impact of the small-scale elongated filaments on the oceanic vertical pump. *Journal of Marine Research*, 64(6):835–851.

[Lasbleiz et al., 2014] Lasbleiz, M., Leblanc, K., Blain, S., Ras, J., Cornet-Barthaux, V., Hélias Nunige, S., and Quéguiner, B. Pigments, elemental composition (C, N, P, and Si), and stoichiometry of particulate matter in the naturally iron fertilized region of Kerguelen in the Southern Ocean. *Biogeosciences*, 11(20):5931–5955.

[Laurenceau et al., 2014] Laurenceau, E. C., Trull, T. W., Davies, D. M., Bray, S. G., Doran, J., Planchon, F., Carlotti, F., Jouandet, M.-P., Cavagna, A.-J., Waite, A. M., and Blain, S. The relative importance of phytoplankton aggregates and zooplankton fecal pellets to carbon export: insights from free-drifting sediment trap deployments in naturally iron-fertilised waters near the Kerguelen plateau. 11:13623–13673.

[Le Boeuf et al., 2000] Le Boeuf, B. J., Crocker, D. E., Costa, D. P., Blackwell, S. B., Webb, P. M., and Houser, D. S. Foraging ecology of northern elephant seals. *Ecological monographs*, 70:353–382.

[Le Quéré et al., 2010] Le Quéré, C., Takahashi, T., Buitenhuis, E. T., Rödenbeck, C., and Sutherland, S. C. Impact of climate change and variability on the global oceanic sink of CO2. *Global Biogeochemical Cycles*, 24(4).

[Le Traon et al., 1998] Le Traon, P. Y., Nadal, F., and Ducet, N. An improved mapping method of multisatellite altimeter data. *Journal of Atmospheric and Oceanic Technology*, 15:522–534.

[Lea et al., 2006] Lea, M.-A., Guinet, C., Cherel, Y., Duhamel, G., Dubroca, L., Pruvost, P., Hindell, M., et al. Impacts of climatic anomalies on provisioning strategies of a Southern Ocean predator. *Marine Ecology Progress Series*, 310:77–94.

[Lea et al., 2008] Lea, M.-A., Guinet, C., Cherel, Y., Hindell, M., Dubroca, L., and Thalmann, S. Colony-based foraging segregation by Antarctic fur seals at the Kerguelen Archipelago. *MARINE ECOLOGY-PROGRESS SERIES-*, 358:273.

[Lea et al., 2009] Lea, M.-A., Johnson, D., Ream, R., Sterling, J., Melin, S., and Gelatt, T. Extreme weather events influence dispersal of naive northern fur seals. *Biology letters*, 5(2):252–257.

[Lebourges-Dhaussy et al., 2014] Lebourges-Dhaussy, A., Huggett, J., Ockhuis, S., Roudaut, G., Josse, E., and Verheye, H. Zooplankton size and distribution within mesoscale structures in the Mozambique Channel: a comparative approach using the TAPS acoustic profiler, a multiple net sampler and ZooScan image analysis. *Deep Sea Research Part II: Topical Studies in Oceanography*, 100:136–152.

[Lehahn et al., 2007] Lehahn, Y., d'Ovidio, F., Lévy, M., and Heifetz, E. Stirring of the northeast Atlantic spring bloom: A Lagrangian analysis based on multisatellite data. *Journal of Geophysical Research*, 112:15.

[Lehodey et al., 2008] Lehodey, P., Senina, I., and Murtugudde, R. A spatial ecosystem and populations dynamics model (SEAPODYM)–Modeling of tuna and tuna-like populations. *Progress in Oceanography*, 78(4):304–318.

[Leis, 2006] Leis, J. M. Are larvae of demersal fishes plankton or nekton? *Advances in marine biology*, 51:57–141.

[Lenton et al., 2013] Lenton, A., Tilbrook, B., Law, R., Bakker, D., Doney, S. C., Gruber, N., Hoppema, M., Ishii, M., Lovenduski, N. S., Matear, R. J., et al. Sea-air CO2

fluxes in the Southern Ocean for the period 1990–2009. *Biogeosciences Discussions*, 10:285–333.

[Lenton, 2013] Lenton, T. M. Environmental tipping points. *Annual Review of Environment and Resources*, 38:1–29.

[Levitus, 1982] Levitus, S. Climatological atlas of the world ocean. *NOAA Prof. Pap.*, 13.

[Lévy, 2003] Lévy, M. Mesoscale variability of phytoplankton and of new production: Impact of the large-scale nutrient distribution. *Journal of Geophysical Research*, 108:3358.

[Lévy, 2008] Lévy, M. (2008). chapter The modulation of biological production by oceanic mesoscale turbulence, pages 219–261.

[Lévy et al., 2012a] Lévy, M., Ferrari, R., Franks, P. J. S., Martin, A. P., and Rivière, P. Bringing physics to life at the submesoscale. *Geophysical Research Letters*, 39.

[Lévy et al., 2012b] Lévy, M., Iovino, D., Resplandy, L., Klein, P., Madec, G., Tréguier, A.-M., Masson, S., and Takahashi, K. Large-scale impacts of submesoscale dynamics on phytoplankton: Local and remote effects. *Ocean Modelling*, 43:77–93.

[Lévy et al., 2015] Lévy, M., Jahn, O., Dutkiewicz, S., Follows, M. J., and d'Ovidio, F. The dynamical landscape of marine phytoplankton diversity. *Journal of The Royal Society Interface*, 12(111):20150481.

[Levy et al., 2001] Levy, M., Klein, P., and Treguier, A.-M. Impact of sub-mesoscale physics on production and subduction of phytoplankton in an oligotrophic regime. *Journal of Marine Research*, 59:535–565.

[Lewison et al., 2015] Lewison, R., Hobday, A. J., Maxwell, S., Hazen, E., Hartog, J. R., Dunn, D. C., Briscoe, D., Fossette, S., O'Keefe, C. E., Barnes, M., et al. Dynamic ocean management: identifying the critical ingredients of dynamic approaches to ocean resource management. *BioScience*, 65(5):486–498.

[Ling and Johnson, 2009] Ling, S. and Johnson, C. Population dynamics of an ecologically important range-extender: kelp beds versus sea urchin barrens. *Marine Ecology Progress Series*, 374:113–125.

[Ling et al., 2015] Ling, S., Scheibling, R., Rassweiler, A., Johnson, C., Shears, N., Connell, S., Salomon, A., Norderhaug, K., Pérez-Matus, A., Hernández, J., et al. Global regime shift dynamics of catastrophic sea urchin overgrazing. *Philosophical Transactions of the Royal Society of London B: Biological Sciences*, 370(1659):20130269.

[Liu et al., 2012] Liu, Y., Dong, C., Guan, Y., Chen, D., McWilliams, J., and Nencioli, F. Eddy analysis in the subtropical zonal band of the North Pacific Ocean. *Deep Sea Research Part I: Oceanographic Research Papers*, 68:54–67.

[Lochte et al., 1993] Lochte, K., Ducklow, H., Fasham, M., and Stienen, C. Plankton succession and carbon cycling at 47 N 20 W during the JGOFS North Atlantic Bloom Experiment. *Deep Sea Research Part II: Topical Studies in Oceanography*, 40(1):91–114.

[Loeb et al., 1997] Loeb, V., Siegel, V., Holm-Hansen, O., Hewitt, R., Fraser, W., Trivelplece, W., and Trivelplece, S. Effects of sea-ice extent and krill or salp dominance on the Antarctic food web. *Nature*, 387(6636):897–900.

[Longhurst, 2010] Longhurst, A. R. (2010). *Ecological geography of the sea*.

[Lovenduski and Gruber, 2005] Lovenduski, N. S. and Gruber, N. Impact of the Southern Annular Mode on Southern Ocean circulation and biology. *Geophysical Research Letters*, 32(11).

[Lowther et al., 2014] Lowther, A. D., Lydersen, C., Biuw, M., De Bruyn, P., Hofmeyr, G. J., and Kovacs, K. M. Post-breeding at-sea movements of three central-place foragers in relation to submesoscale fronts in the Southern Ocean around Bouvetøya. *Antarctic Science*, 26(05):533–544.

[Luo et al., 2014] Luo, J. Y., Grassian, B., Tang, D., Irisson, J.-O., Greer, A. T., Guigand, C. M., McClatchie, S., and Cowen, R. K. Environmental drivers of the fine-scale distribution of a gelatinous zooplankton community across a mesoscale front.

[Luschi et al., 2003] Luschi, P., Hays, G. C., and Papi, F. A review of long-distance movements by marine turtles, and the possible role of ocean currents. *Oikos*, 103:293–302.

[Mackey et al., 2015] Mackey, K. R., Post, A. F., McIlvin, M. R., Cutter, G. A., John, S. G., and Saito, M. A. Divergent responses of Atlantic coastal and oceanic Synechococcus to iron limitation. *Proceedings of the National Academy of Sciences*, 112(32):9944–9949.

[Mahadevan and Campbell, 2002] Mahadevan, A. and Campbell, J. W. Biogeochemical patchiness at the sea surface. *Geophysical Research Letters*, 29:4.

[Mahadevan et al., 2012] Mahadevan, A., D'Asaro, E., Lee, C., and Perry, M. J. Eddy-driven stratification initiates North Atlantic spring phytoplankton blooms. *Science*, 337:54–58.

[Maiti et al., 2013] Maiti, K., Charette, M. A., Buesseler, K. O., and Kahru, M. An inverse relationship between production and export efficiency in the Southern Ocean. *Geophysical Research Letters*, 40(8):1557–1561.

[Martin, 2003] Martin, A. P. Phytoplankton patchiness: the role of lateral stirring and mixing. *Progress In Oceanography*, 57:125–174.

[Martin, 1990] Martin, J. H. Glacial-interglacial CO2 change: The iron hypothesis. *Paleoceanography*, 5:1.

[Martin et al., 1990] Martin, J. H., Fitzwater, S. E., and Gordon, R. M. Iron deficiency limits phytoplankton growth in Antarctic waters. *Global Biogeochemical Cycles*, 4(1):5–12.

[Martin et al., 2013] Martin, P., Loeff, M. R., Cassar, N., Vandromme, P., d'Ovidio, F., Stemmann, L., Rengarajan, R., Soares, M., González, H. E., Ebersbach, F., et al. Iron fertilization enhanced net community production but not downward particle flux during the Southern Ocean iron fertilization experiment LOHAFEX. *Global Biogeochemical Cycles*, 27(3):871–881.

[Martinez et al., 2009] Martinez, E., Antoine, D., D'Ortenzio, F., and Gentili, B. Climate-driven basin-scale decadal oscillations of oceanic phytoplankton. *Science*, 326(5957):1253–1256.

[Marzloff et al., 2011] Marzloff, M. P., Dambacher, J. M., Johnson, C. R., Little, L. R., and Frusher, S. D. Exploring alternative states in ecological systems with a qualitative analysis of community feedback. *Ecological Modelling*, 222(15):2651–2662.

[Marzloff et al., 2013] Marzloff, M. P., Johnson, C. R., Little, L. R., Soulié, J.-C., Ling, S. D., and Frusher, S. D. Sensitivity analysis and pattern-oriented validation of TRITON, a model with alternative community states: insights on temperate rocky reefs dynamics. *Ecological modelling*, 258:16–32.

[Matear et al., 2000] Matear, R., Hirst, A., and McNeil, B. Changes in dissolved oxygen in the Southern Ocean with climate change. *Geochemistry, Geophysics, Geosystems*, 1(11).

[Maxwell et al., 2015] Maxwell, S. M., Hazen, E. L., Lewison, R. L., Dunn, D. C., Bailey, H., Bograd, S. J., Briscoe, D. K., Fossette, S., Hobday, A. J., Bennett, M., et al. Dynamic ocean management: Defining and conceptualizing real-time management of the ocean. *Marine Policy*, 58:42–50.

[May, 1977] May, R. M. Thresholds and breakpoints in ecosystems with a multiplicity of stable states. *Nature*, 269:471–477.

[Mayewski et al., 2009] Mayewski, P. A., Meredith, M., Summerhayes, C., Turner, J., Worby, A., Barrett, P., Casassa, G., Bertler, N. A., Bracegirdle, T., Naveira Garabato, A., et al. State of the Antarctic and Southern Ocean climate system. *Reviews of Geophysics*, 47(1).

[McGillicuddy et al., 2007] McGillicuddy, D. J., Anderson, L. A., Bates, N. R., Bibby, T., Buesseler, K. O., Carlson, C. A., Davis, C. S., Ewart, C., Falkowski, P. G., Goldthwait, S. A., Hansell, D. A., Jenkins, W. J., Johnson, R., Kosnyrev, V. K., Ledwell, J. R., Li, Q. P., Siegel, D. A., and Steinberg, D. K. Eddy/Wind Interactions Stimulate Extraordinary Mid-Ocean Plankton Blooms. *Science*, 316:1021–1026.

[McGillicuddy et al., 1998] McGillicuddy, D. J., Robinson, A. R., Siegel, D. A., Jannasch, H. W., Johnson, R., Dickey, T. D., McNeil, J., Michaels, A. F., and Knap, A. H. Influence of mesoscale eddies on new production in the Sargasso Sea. *Nature*, 394:263–266.

[McIntyre et al., 2010] McIntyre, T., De Bruyn, P. J. N., Ansorge, I. J., Bester, M. N., Bornemann, H., Plötz, J., and Tosh, C. A. A lifetime at depth: vertical distribution of southern elephant seals in the water column. *Polar biology*, 33:1037–1048.

[McMahon et al., 2005] McMahon, C. R., Autret, E., Houghton, J. D., Lovell, P., Myers, A. E., and Hays, G. C. Animal-borne sensors successfully capture the real-time thermal properties of ocean basins. *Limnology and Oceanography: Methods*, 3(9):392–398.

[Mcmahon et al., 2003] Mcmahon, C. R., Burton, H. R., and Bester, M. N. A demographic comparison of two southern elephant seal populations. *Journal of Animal Ecology*, 72(1):61–74.

[McMahon et al., 2008] McMahon, C. R., Field, I. C., Bradshaw, C. J., White, G. C., and Hindell, M. A. Tracking and data–logging devices attached to elephant seals do not affect individual mass gain or survival. *Journal of Experimental Marine Biology and Ecology*, 360(2):71–77.

[Miller and Christodoulou, 2014] Miller, P. I. and Christodoulou, S. Frequent locations of oceanic fronts as an indicator of pelagic diversity: application to marine protected areas and renewables. *Marine Policy*, 45:318–329.

[Miller et al., 2015] Miller, P. I., Xu, W., and Carruthers, M. Seasonal shelf-sea front mapping using satellite ocean colour and temperature to support development of a marine protected area network. *Deep Sea Research Part II: Topical Studies in Oceanography*, 119:3–19.

[Miller et al., 2006] Miller, R., Schmidt, G., and Shindell, D. Forced annular variations in the 20th century intergovernmental panel on climate change fourth assessment report models. *Journal of Geophysical Research: Atmospheres*, 111(D18).

[Moline et al., 2004] Moline, M. A., Claustre, H., Frazer, T. K., Schofield, O., and Vernet, M. Alteration of the food web along the Antarctic Peninsula in response to a regional warming trend. 10:1973–1980.

[Mongin et al., 2008] Mongin, M., Molina, E., and Trull, T. W. Seasonality and scale of the Kerguelen plateau phytoplankton bloom: A remote sensing and modeling analysis of the influence of natural iron fertilization in the Southern Ocean. *Deep Sea Research Part II: Topical Studies in Oceanography*, 55:880–892.

[Mongin et al., 2009] Mongin, M. M., Abraham, E. R., and Trull, T. W. Winter advection of iron can explain the summer phytoplankton bloom that extends 1000 km downstream of the Kerguelen Plateau in the Southern Ocean. *Journal of Marine Research*, 67:225–237.

[Montes-Hugo et al., 2009] Montes-Hugo, M., Doney, S. C., Ducklow, H. W., Fraser, W., Martinson, D., Stammerjohn, S. E., and Schofield, O. Recent changes in phytoplankton communities associated with rapid regional climate change along the western Antarctic Peninsula. *Science*, 323(5920):1470–1473.

[Moore and Abbott, 2000] Moore, J. K. and Abbott, M. R. Phytoplankton chlorophyll distributions and primary production in the Southern Ocean. *Journal of Geophysical Research: Oceans (1978–2012)*, 105(C12):28709–28722.

[Mosseri et al., 2008] Mosseri, J., Quéguiner, B., Armand, L., and Cornet-Barthaux, V. Impact of iron on silicon utilization by diatoms in the Southern Ocean: A case study of Si/N cycle decoupling in a naturally iron-enriched area. *Deep Sea Research Part II: Topical Studies in Oceanography*, 55:801–819.

[Mumby, 2009] Mumby, P. J. Phase shifts and the stability of macroalgal communities on Caribbean coral reefs. *Coral Reefs*, 28(3):761–773.

[Mumby et al., 2007] Mumby, P. J., Hastings, A., and Edwards, H. J. Thresholds and the resilience of Caribbean coral reefs. *Nature*, 450(7166):98–101.

[Myers et al., 2007] Myers, R. A., Baum, J. K., Shepherd, T. D., Powers, S. P., and Peterson, C. H. Cascading effects of the loss of apex predatory sharks from a coastal ocean. *Science*, 315:1846–1850.

[Nel et al., 2001] Nel, D. C., Lutjeharms, J. R. E., Pakhomov, E. A., Ansorge, I. J., Ryan, P. G., and Klages, N. T. W. Exploitation of mesoscale oceanographic features

by grey-headed albatross Thalassarche chrysostoma in the southern Indian Ocean. *Marine Ecology Progress Series*, 217:15–26.

[Nencioli et al., 2010] Nencioli, F., Dong, C., Dickey, T., Washburn, L., and McWilliams, J. C. A vector geometry-based eddy detection algorithm and its application to a high-resolution numerical model product and high-frequency radar surface velocities in the Southern California Bight. *Journal of Atmospheric and Oceanic Technology*, 27(3):564–579.

[Nencioli et al., 2011] Nencioli, F., d'Ovidio, F., Doglioli, A. M., and Petrenko, A. A. Surface coastal circulation patterns by in-situ detection of Lagrangian coherent structures. *Geophysical Research Letters*, 38:17604.

[Nevitt and Bonadonna, 2005] Nevitt, G. A. and Bonadonna, F. Sensitivity to dimethyl sulphide suggests a mechanism for olfactory navigation by seabirds. *Biology Letters*, 1(3):303–305.

[Nevitt et al., 1995] Nevitt, G. A., Veit, R. R., and Kareiva, P. Dimethyl sulphide as a foraging cue for Antarctic Procellariiform seabirds. *Published online: 24 August 1995; doi:10.1038/376680ao*, 376:680–682.

[Nicol et al., 2000] Nicol, S., Pauly, T., Bindoff, N. L., Wright, S., Thiele, D., Hosie, G. W., Strutton, P. G., and Woehler, E. Ocean circulation off east Antarctica affects ecosystem structure and sea-ice extent. *Nature*, 406(6795):504–507.

[Nielsdóttir et al., 2012] Nielsdóttir, M. C., Bibby, T. S., Moore, C. M., Hinz, D. J., Sanders, R., Whitehouse, M., Korb, R., and Achterberg, E. P. Seasonal and spatial dynamics of iron availability in the Scotia Sea. *Marine Chemistry*, 130:62–72.

[Nordstrom et al., 2012] Nordstrom, C. A., Battaile, B. C., Cotte, C., and Trites, A. W. Foraging habitats of lactating northern fur seals are structured by thermocline depths and submesoscale fronts in the eastern Bering Sea. *Deep Sea Research Part II: Topical Studies in Oceanography*.

[Nyström et al., 2000] Nyström, M., Folke, C., and Moberg, F. Coral reef disturbance and resilience in a human-dominated environment. *Trends in Ecology & Evolution*, 15(10):413–417.

[Oka and Ando, 2004] Oka, E. and Ando, K. Stability of temperature and conductivity sensors of Argo profiling floats. *Journal of oceanography*, 60(2):253–258.

[Okubo, 1970] Okubo, A. Horizontal dispersion of floatable particles in the vicinity of velocity singularities such as convergences. *Deep Sea Research and Oceanographic Abstracts*, 17:445–454.

[Olascoaga et al., 2006] Olascoaga, M. J., Rypina, I. I., Brown, M. G., Beron-Vera, F. J., Kocak, H., Brand, L. E., Halliwell, G. R., and Shay, L. K. Persistent transport barrier on the West Florida Shelf. *Geophys. Res. Lett.*, 33.

[Oliver and Irwin, 2008] Oliver, M. J. and Irwin, A. J. Objective global ocean biogeographic provinces. *Geophysical research letters*, 35.

[Olson, 1991] Olson, D. B. Rings in the ocean. *Annual Review of Earth and Planetary Sciences*, 19:283.

[Orsi et al., 1995] Orsi, A. H., Whitworth, T., and Nowlin, W. D. On the meridional extent and fronts of the Antarctic Circumpolar Current. *Deep Sea Research Part I: Oceanographic Research Papers*, 42:641–673.

[Özgökmen et al., 2000] Özgökmen, T. M., Griffa, A., Mariano, A. J., and Piterbarg, L. I. On the predictability of Lagrangian trajectories in the ocean. *Journal of Atmospheric and Oceanic Technology*, 17(3):366–383.

[O'Toole et al., 2014] O'Toole, M., Hindell, M. A., Charrassin, J.-B., and Guinet, C. Foraging behaviour of southern elephant seals over the Kerguelen Plateau. *Marine Ecology Progress Series*, 502:281.

[Padman et al., 2010] Padman, L., Costa, D. P., Bolmer, S. T., Goebel, M. E., Huckstadt, L. A., Jenkins, A., McDonald, B. I., and Shoosmith, D. R. Seals map bathymetry of the Antarctic continental shelf. *Geophysical Research Letters*, 37.

[Pail et al., 2011] Pail, R., Bruinsma, S., Migliaccio, F., Förste, C., Goiginger, H., Schuh, W.-D., Höck, E., Reguzzoni, M., Brockmann, J. M., Abrikosov, O., et al. First GOCE gravity field models derived by three different approaches. *Journal of Geodesy*, 85(11):819–843.

[Pakhomov and Froneman, 1999a] Pakhomov, E. and Froneman, P. Macroplankton/micronekton dynamics in the vicinity of the Prince Edward Islands (Southern Ocean). *Marine Biology*, 134(3):501–515.

[Pakhomov and Froneman, 1999b] Pakhomov, E. and Froneman, P. Macroplankton/micronekton dynamics in the vicinity of the Prince Edward Islands (Southern Ocean). *Marine Biology*, 134(3):501–515.

[Pakhomov et al., 2002] Pakhomov, E., Froneman, P., and Perissinotto, R. Salp/krill interactions in the Southern Ocean: spatial segregation and implications for the carbon flux. *Deep Sea Research Part II: Topical Studies in Oceanography*, 49(9):1881–1907.

[Pakhomov and McQuaid, 1996] Pakhomov, E. and McQuaid, C. Distribution of surface zooplankton and seabirds across the Southern Ocean. *Polar Biology*, 16(4):271–286.

[Pakhomov et al., 1996] Pakhomov, E. A., Perissinotto, R., and McQuaid, C. D. Prey composition and daily rations of myctophid fishes in the Southern Ocean. *Marine ecology progress series. Oldendorf*, 134:1.

[Park et al., 1998] Park, Y.-H., Charriaud, E., Pino, D. R., and Jeandel, C. Seasonal and interannual variability of the mixed layer properties and steric height at station KERFIX, southwest of Kerguelen. *Journal of Marine Systems*, 17(1):571–586.

[Park et al., 2014] Park, Y.-H., Durand, I., Kestenare, E., Rougier, G., Zhou, M., d'Ovidio, F., Cotté, C., and Lee, J.-H. Polar Front around the Kerguelen Islands: An up-to-date determination and associated circulation of surface/subsurface waters. *Journal of Geophysical Research: Oceans*.

[Park et al., 1993] Park, Y.-H., Gamberoni, L., and Charriaud, E. Frontal structure, water masses, and circulation in the Crozet Basin. *Journal of Geophysical Research: Oceans (1978–2012)*, 98(C7):12361–12385.

[Park et al., 2008] Park, Y.-H., Roquet, F., Durand, I., and Fuda, J.-L. Large-scale circulation over and around the Northern Kerguelen Plateau. *Deep Sea Research Part II: Topical Studies in Oceanography*, 55:566–581.

[Parmesan, 2006] Parmesan, C. Ecological and evolutionary responses to recent climate change. *Annual Review of Ecology, Evolution, and Systematics*, pages 637–669.

[Parslow et al., 2001] Parslow, J. S., Boyd, P. W., Rintoul, S. R., and Griffiths, F. B. A persistent subsurface chlorophyll maximum in the Interpolar Frontal Zone south of Australia: Seasonal progression and implications for phytoplankton-light-nutrient interactions. *Journal of Geophysical Research: Oceans (1978–2012)*, 106(C12):31543–31557.

[Pauly et al., 2002] Pauly, D., Christensen, V., Guénette, S., Pitcher, T. J., Sumaila, U. R., Walters, C. J., Watson, R., and Zeller, D. Towards sustainability in world fisheries. *Nature*, 418:689–695.

[Pedlosky, 1987] Pedlosky, J. An inertial theory of the equatorial undercurrent. *Journal of physical oceanography*, 17(11):1978–1985.

[Pérez-Muñuzuri and Huhn, 2010] Pérez-Muñuzuri, V. and Huhn, F. The role of mesoscale eddies time and length scales on phytoplankton production. *Nonlin. Processes Geophys.*, 17:177–186.

[Perissinotto and Pakhomov, 1997] Perissinotto, R. and Pakhomov, E. Feeding association of the copepod Rhincalanus gigas with the tunicate salp Salpa thompsoni in the southern ocean. *Marine Biology*, 127(3):479–483.

[Perruche et al., 2011] Perruche, C., Rivière, P., Lapeyre, G., Carton, X., and Pondaven, P. Effects of surface quasi-geostrophic turbulence on phytoplankton competition and coexistence. *Journal of Marine Research*, 69:105–135.

[Petraitis and Dudgeon, 2004] Petraitis, P. S. and Dudgeon, S. R. Detection of alternative stable states in marine communities. *Journal of Experimental Marine Biology and Ecology*, 300(1):343–371.

[Pichegru et al., 2011] Pichegru, L., Ropert-Coudert, Y., Kato, A., Takahashi, A., Dyer, B. M., and Ryan, P. G. Diving patterns of female macaroni penguins breeding on Marion Island, South Africa. *Polar biology*, 34(7):945–954.

[Planchon et al., 2014] Planchon, F., Ballas, D., Cavagna, A.-J., Bowie, A., Davies, D., Trull, T., Laurenceau, E., Van Der Merwe, P., and Dehairs, F. Carbon export in the naturally iron-fertilized Kerguelen area of the Southern Ocean based on the 234 Th approach. *Biogeosciences Discussions*, 11(11):15991–16032.

[Planquette et al., 2007] Planquette, H., Statham, P. J., Fones, G. R., Charette, M. A., Moore, C. M., Salter, I., Nedelec, F. H., Taylor, S. L., French, M., Baker, A. R., et al. Dissolved iron in the vicinity of the Crozet Islands, Southern Ocean. *Deep Sea Research Part II: Topical Studies in Oceanography*, 54(18):1999–2019.

[Pollard and Read, 2001] Pollard, R. and Read, J. Circulation pathways and transports of the Southern Ocean in the vicinity of the Southwest Indian Ridge. *Journal of Geophysical Research: Oceans (1978–2012)*, 106(C2):2881–2898.

[Pollard et al., 2007a] Pollard, R., Sanders, R., Lucas, M., and Statham, P. The Crozet natural iron bloom and export experiment (CROZEX). *Deep Sea Research Part II: Topical Studies in Oceanography*, 54(18):1905–1914.

[Pollard et al., 2007b] Pollard, R., Venables, H., Read, J., and Allen, J. Large-scale circulation around the Crozet Plateau controls an annual phytoplankton bloom in the Crozet Basin. *Deep Sea Research Part II: Topical Studies in Oceanography*, 54(18):1915–1929.

[Pollard et al., 2002] Pollard, R. T., Lucas, M. I., and Read, J. F. Physical controls on biogeochemical zonation in the Southern Ocean. *Deep Sea Research Part II: Topical Studies in Oceanography*, 49:3289–3305.

[Pollard et al., 2009] Pollard, R. T., Salter, I., Sanders, R. J., Lucas, M. I., Moore, C. M., Mills, R. A., Statham, P. J., Allen, J. T., Baker, A. R., Bakker, D. C., et al. Southern Ocean deep-water carbon export enhanced by natural iron fertilization. *Nature*, 457(7229):577–580.

[Polovina et al., 2006] Polovina, J., Uchida, I., Balazs, G., Howell, E. A., Parker, D., and Dutton, P. The Kuroshio Extension Bifurcation Region: A pelagic hotspot for juvenile loggerhead sea turtles. *Deep Sea Research Part II: Topical Studies in Oceanography*, 53:326–339.

[Potier et al., 2014] Potier, M., Bach, P., Ménard, F., and Marsac, F. Influence of mesoscale features on micronekton and large pelagic fish communities in the Mozambique Channel. *Deep Sea Research Part II: Topical Studies in Oceanography*, 100:184–199.

[Price et al., 1994] Price, N., Ahner, B., and Morel, F. The equatorial Pacific Ocean: Grazer-controlled phytoplankton populations in an iron-limited ecosystem. *Limnology and Oceanography*, 39(3):520–534.

[Pütz et al., 1999] Pütz, K., Ropert-Coudert, Y., Charrassin, J., and Wilson, R. Foraging areas of King penguins Aptenodytes patagonicus breeding at Possession Island, southern Indian Ocean. *Marine Ornithology*, 27:77–84.

[Quéguiner, 2013] Quéguiner, B. Iron fertilization and the structure of planktonic communities in high nutrient regions of the Southern Ocean. 90:43–54.

[Quéroué et al., 2015] Quéroué, F., Sarthou, G., Planquette, H., Bucciarelli, E., Chever, F., Van Der Merwe, P., Lannuzel, D., Townsend, A., Cheize, M., Blain, S., et al. High variability in dissolved iron concentrations in the vicinity of the Kerguelen Islands (Southern Ocean). *Biogeosciences*, 12(12):3869–3883.

[Raclot et al., 1998] Raclot, T., Groscolas, R., and Cherel, Y. Fatty acid evidence for the importance of myctophid fishes in the diet of king penguins, Aptenodytes patagonicus. *Marine Biology*, 132(3):523–533.

[Read et al., 2007] Read, J., Pollard, R., and Allen, J. Sub-mesoscale structure and the development of an eddy in the Subantarctic Front north of the Crozet Islands. *Deep Sea Research Part II: Topical Studies in Oceanography*, 54(18):1930–1948.

[Reid and Croxall, 2001] Reid, K. and Croxall, J. P. Environmental response of upper trophic-level predators reveals a system change in an Antarctic marine ecosystem. *Proceedings of the Royal Society of London B: Biological Sciences*, 268(1465):377–384.

[Reisinger et al., 2011] Reisinger, R. R., de Bruyn, P. N., and Bester, M. N. Predatory impact of killer whales on pinniped and penguin populations at the Subantarctic Prince Edward Islands: fact and fiction. *Journal of Zoology*, 285(1):1–10.

[Rey et al., 2010] Rey, A. R., Bost, C.-A., Schiavini, A., and Pütz, K. Foraging movements of Magellanic Penguins Spheniscus magellanicus in the Beagle Channel, Argentina, related to tide and tidal currents. *Journal of Ornithology*, 151(4):933–943.

[Riandey et al., 2005] Riandey, V., Champalbert, G., Carlotti, F., Taupier-Letage, I., and Thibault-Botha, D. Zooplankton distribution related to the hydrodynamic features in the Algerian Basin (western Mediterranean Sea) in summer 1997. *Deep Sea Research Part I: Oceanographic Research Papers*, 52(11):2029–2048.

[Rio, 2012] Rio, M.-H. Use of altimeter and wind data to detect the anomalous loss of SVP-type drifter's drogue. *Journal of Atmospheric and Oceanic Technology*, 29(11):1663–1674.

[Rio et al., 2012] Rio, M.-H., Mulet, S., Schaeffer, P., and Picot, N. *Proceedings of the 20 Years Progress in Radar Altimetry Symposium.*

[Rio et al., 2007] Rio, M. H., Poulain, P. M., Pascual, A., Mauri, E., Larnicol, G., and Santoleri, R. A mean dynamic topography of the Mediterranean Sea computed from altimetric data, in-situ measurements and a general circulation model. *Journal of Marine Systems*, 65:484–508.

[Ripple and Beschta, 2007] Ripple, W. J. and Beschta, R. L. Restoring Yellowstone's aspen with wolves. 138:514–519.

[Roach et al., 2015] Roach, C. J., Phillips, H. E., Bindoff, N. L., and Rintoul, S. R. Detecting and Characterizing Ekman Currents in the Southern Ocean. *Journal of Physical Oceanography*, 45(5):1205–1223.

[Robinson et al., 2015] Robinson, L., Hobday, A., Possingham, H., and Richardson, A. Trailing edges projected to move faster than leading edges for large pelagic fish habitats under climate change. *Deep Sea Research Part II: Topical Studies in Oceanography*, 113:225–234.

[Ropert-Coudert et al., 2009] Ropert-Coudert, Y., Beaulieu, M., Hanuise, N., and Kato, A. Diving into the world of biologging. 10:21–27.

[Ropert-Coudert and Wilson, 2004] Ropert-Coudert, Y. and Wilson, R. P. Subjectivity in bio-logging science: do logged data mislead. *Mem Natl Inst Polar Res*, 58:23–33.

[Ropert-Coudert and Wilson, 2005] Ropert-Coudert, Y. and Wilson, R. P. Trends and perspectives in animal-attached remote sensing. *Frontiers in Ecology and the Environment*, 3:437–444.

[Roquet et al., 2009] Roquet, F., Park, Y.-H., Guinet, C., Bailleul, F., and Charrassin, J.-B. Observations of the Fawn Trough Current over the Kerguelen Plateau from instrumented elephant seals. *Journal of Marine Systems*, 78:377–393.

[Rose et al., 2010] Rose, K. A., Allen, J. I., Artioli, Y., Barange, M., Blackford, J., Carlotti, F., Cropp, R., Daewel, U., Edwards, K., Flynn, K., et al. End-to-end models for the analysis of marine ecosystems: challenges, issues, and next steps. *Marine and Coastal Fisheries*, 2(1):115–130.

[Rosso et al., 2014] Rosso, I., Hogg, A. M., Strutton, P. G., Kiss, A. E., Matear, R., Klocker, A., and van Sebille, E. Vertical transport in the ocean due to sub-mesoscale structures: Impacts in the Kerguelen region. *Ocean Modelling*.

[Rousseau et al., 2002] Rousseau, V., Leynaert, A., Daoud, N., Lancelot, C., et al. Diatom succession, silicification and silicic acid availability in Belgian coastal waters (Southern North Sea). *Marine Ecology Progress Series*, 236:61–73.

[Rutz and Hays, 2009] Rutz, C. and Hays, G. C. New frontiers in biologging science. *Biology letters*, 5:289–292.

[Sabarros et al., 2009] Sabarros, P. S., Mnard, F., Lvnez, J., TewKai, E., and Ternon, J. Mesoscale eddies influence distribution and aggregation patterns of micronekton in the Mozambique Channel. *Marine Ecology Progress Series*, 395:101–107.

[Sackmann et al., 2008] Sackmann, B., Perry, M., and Eriksen, C. Seaglider observations of variability in daytime fluorescence quenching of chlorophyll-a in Northeastern Pacific coastal waters. *Biogeosciences Discussions*, 5(4):2839–2865.

[Sala, 2006] Sala, E. Top predators provide insurance against climate change. *Trends in ecology & evolution*, 21:479–480.

[Sallée et al., 2008] Sallée, J., Speer, K., and Morrow, R. Response of the Antarctic Circumpolar Current to atmospheric variability. *Journal of Climate*, 21(12):3020–3039.

[Sallée et al., 2010] Sallée, J., Speer, K., and Rintoul, S. Zonally asymmetric response of the Southern Ocean mixed-layer depth to the Southern Annular Mode. *Nature Geoscience*, 3(4):273–279.

[Salter et al., 2007] Salter, I., Lampitt, R. S., Sanders, R., Poulton, A., Kemp, A. E., Boorman, B., Saw, K., and Pearce, R. Estimating carbon, silica and diatom export from a naturally fertilised phytoplankton bloom in the Southern Ocean using PELAGRA: a novel drifting sediment trap. *Deep Sea Research Part II: Topical Studies in Oceanography*, 54(18):2233–2259.

[Sanial et al., 2014a] Sanial, V., van Beek, P., Lansard, B., d'Ovidio, F., Kestenare, E., Souhaut, M., Zhou, M., and Blain, S. Study of the phytoplankton plume dynamics off the Crozet Islands (Southern Ocean): A geochemical-physical coupled approach. *Journal of Geophysical Research: Oceans*, 119(4):2227–2237.

[Sanial et al., 2014b] Sanial, V., van Beek, P., Lansard, B., Souhaut, M., Kestenare, E., d'Ovidio, F., Zhou, M., and Blain, S. Use of Ra isotopes to deduce rapid transfer of sediment-derived inputs off Kerguelen. *Biogeosciences Discussions*, 11:14023–14061.

[Sarmiento et al., 2004] Sarmiento, J., Gruber, N., Brzezinski, M., and Dunne, J. High-latitude controls of thermocline nutrients and low latitude biological productivity. *Nature*, 427(6969):56–60.

[Sarmiento and Le Quere, 1996] Sarmiento, J. L. and Le Quere, C. Oceanic carbon dioxide uptake in a model of century-scale global warming. *Science*, 274(5291):1346–1350.

[Sarmiento et al., 1990] Sarmiento, J. L., Thiele, G., Key, R. M., and Moore, W. S. Oxygen and nitrate new production and remineralization in the North Atlantic subtropical gyre. *J. Geophys. Res*, 95(18):303–18.

[Sarthou et al., 2008] Sarthou, G., Vincent, D., Christaki, U., Obernosterer, I., Timmermans, K. R., and Brussaard, C. P. The fate of biogenic iron during a phytoplankton bloom induced by natural fertilisation: Impact of copepod grazing. *Deep Sea Research Part II: Topical Studies in Oceanography*, 55(5):734–751.

[Savoca and Nevitt, 2014] Savoca, M. S. and Nevitt, G. A. Evidence that dimethyl sulfide facilitates a tritrophic mutualism between marine primary producers and top predators. *Proceedings of the National Academy of Sciences*, 111(11):4157–4161.

[Savoye et al., 2004] Savoye, N., Dehairs, F., Elskens, M., Cardinal, D., Kopczyńska, E. E., Trull, T. W., Wright, S., Baeyens, W., and Griffiths, F. B. Regional variation of spring N-uptake and new production in the Southern Ocean. *Geophysical Research Letters*, 31(3).

[Scales et al., 2014] Scales, K. L., Miller, P. I., Embling, C. B., Ingram, S. N., Pirotta, E., and Votier, S. C. Mesoscale fronts as foraging habitats: composite front mapping reveals oceanographic drivers of habitat use for a pelagic seabird. *Journal of the Royal Society Interface*, 11(100):20140679.

[Schaeffer et al., 2012] Schaeffer, P., Faugere, Y., Legeais, J., Ollivier, A., Guinle, T., and Picot, N. The CNES_CLS11 global mean sea surface computed from 16 years of satellite altimeter data. *Marine Geodesy*, 35(sup1):3–19.

[Scheffer et al., 2001] Scheffer, M., Carpenter, S., Foley, J. A., Folke, C., and Walker, B. Catastrophic shifts in ecosystems. *Nature*, 413(6856):591–596.

[Scheffer and van Nes, 2007] Scheffer, M. and van Nes, E. H. Shallow lakes theory revisited: various alternative regimes driven by climate, nutrients, depth and lake size. *Hydrobiologia*, 584(1):455–466.

[Schlitzer, 2002] Schlitzer, R. Carbon export fluxes in the Southern Ocean: results from inverse modeling and comparison with satellite-based estimates. *Deep Sea Research Part II: Topical Studies in Oceanography*, 49(9):1623–1644.

[Sen Gupta et al., 2009] Sen Gupta, A., Santoso, A., Taschetto, A. S., Ummenhofer, C. C., Trevena, J., and England, M. H. Projected changes to the Southern Hemisphere ocean and sea ice in the IPCC AR4 climate models. *Journal of Climate*, 22(11):3047–3078.

[Seuront et al., 2004] Seuront, L., Brewer, M. C., and Strickler, J. R. Quantifying zooplankton swimming behavior: the question of scale. *Handbook of scaling methods in aquatic ecology: measurement, analysis, simulation. CRC Press, Boca Raton*, 333:359.

[Shadden, 2005] Shadden, S. C. Lagrangian coherent structures. *Transport and Mixing in Laminar Flows: From Microfluidics to Oceanic Currents*, pages 59–89.

[Shadden et al., 2005] Shadden, S. C., Lekien, F., and Marsden, J. E. Definition and properties of Lagrangian coherent structures from finite-time Lyapunov exponents in two-dimensional aperiodic flows. *Physica D: Nonlinear Phenomena*, 212:271–304.

[Shadwick et al., 2014] Shadwick, E., Tilbrook, B., Cassar, N., Trull, T., and Rintoul, S. Summertime physical and biological controls on O 2 and CO 2 in the Australian Sector of the Southern Ocean. *Journal of Marine Systems*.

[Shadwick et al., 2015] Shadwick, E., Trull, T., Tilbrook, B., Sutton, A., Schulz, E., and Sabine, C. Seasonality of biological and physical controls on surface ocean CO2 from hourly observations at the Southern Ocean Time Series site south of Australia. *Global Biogeochemical Cycles*, 29(2):223–238.

[Shin and Cury, 2001] Shin, Y.-J. and Cury, P. Exploring fish community dynamics through size-dependent trophic interactions using a spatialized individual-based model. *Aquatic Living Resources*, 14(02):65–80.

[Sigman and Boyle, 2000] Sigman, D. M. and Boyle, E. A. Glacial/interglacial variations in atmospheric carbon dioxide. *Nature*, 407(6806):859–869.

[Sims et al., 2012] Sims, D. W., Humphries, N. E., Bradford, R. W., and Bruce, B. D. Lévy flight and Brownian search patterns of a free-ranging predator reflect different prey field characteristics. *J Anim Ecol*, 81:432–442.

[Sims et al., 2009] Sims, D. W., Queiroz, N., Doyle, T. K., Houghton, J. D., and Hays, G. C. Satellite tracking of the World's largest bony fish, the ocean sunfish (Mola mola L.) in the North East Atlantic. *Journal of Experimental Marine Biology and Ecology*, 370(1):127–133.

[Sleeman et al., 2010] Sleeman, J. C., Meekan, M. G., Wilson, S. G., Polovina, J. J., Stevens, J. D., Boggs, G. S., and Bradshaw, C. J. To go or not to go with the flow: environmental influences on whale shark movement patterns. *Journal of experimental marine biology and ecology*, 390:84–98.

[Slip and Burton, 1999] Slip, D. J. and Burton, H. R. Population status and seasonal haulout patterns of the southern elephant seal (Mirounga leonina) at Heard Island. *Antarctic Science*, 11:38–47.

[Smetacek et al., 2004] Smetacek, V., Assmy, P., and Henjes, J. The role of grazing in structuring Southern Ocean pelagic ecosystems and biogeochemical cycles. *Antarctic Science*, 16:541–558.

[Smetacek et al., 2012] Smetacek, V., Klaas, C., Strass, V. H., Assmy, P., Montresor, M., Cisewski, B., Savoye, N., Webb, A., d'Ovidio, F., Arrieta, J. M., Bathmann, U., Bellerby, R., Berg, G. M., Croot, P., Gonzalez, S., Henjes, J., Herndl, G. J., Hoffmann, L. J., Leach, H., Losch, M., Mills, M. M., Neill, C., Peeken, I., Röttgers, R., Sachs, O., Sauter, E., Schmidt, M. M., Schwarz, J., Terbrüggen, A., and Wolf-Gladrow, D. Deep carbon export from a Southern Ocean iron-fertilized diatom bloom. *Nature*, 487:313–319.

[Smith, 2002] Smith, V. Climate change in the sub-Antarctic: an illustration from Marion Island. *Climatic Change*, 52(3):345–357.

[Sokolov and Rintoul, 2007] Sokolov, S. and Rintoul, S. R. On the relationship between fronts of the Antarctic Circumpolar Current and surface chlorophyll concentrations in the Southern Ocean. *Journal of Geophysical Research: Oceans (1978–2012)*, 112(C7).

[Sokolov and Rintoul, 2009] Sokolov, S. and Rintoul, S. R. Circumpolar structure and distribution of the Antarctic Circumpolar Current fronts: 1. Mean circumpolar paths. *Journal of Geophysical Research: Oceans (1978–2012)*, 114(C11).

[Spitzer and Jenkins, 1989] Spitzer, W. S. and Jenkins, W. J. Rates of vertical mixing, gas exchange and new production: Estimates from seasonal gas cycles in the upper ocean near Bermuda. *Journal of Marine Research*, 47(1):169–196.

[Stahl et al., 1985] Stahl, J.-C., Derenne, P., Jouventin, P., Mougin, J.-L., Teulieres, L., and Weimerskirch, H. Le cycle reproducteur des gorfous de l'archipel Crozet: Eudyptes chrysolophus, le gorfou macaroni et Eudyptes chrysocome, le gorfou sauteur. *Oiseau et la Revue Francaise d'Ornithologie*, 55(1):27–43.

[Steneck et al., 2002] Steneck, R. S., Graham, M. H., Bourque, B. J., Corbett, D., Erlandson, J. M., Estes, J. A., and Tegner, M. J. Kelp forest ecosystems: biodiversity, stability, resilience and future. *Environmental conservation*, 29(04):436–459.

[Sterling et al., 2014] Sterling, J. T., Springer, A. M., Iverson, S. J., Johnson, S. P., Pelland, N. A., Johnson, D. S., Lea, M.-A., and Bond, N. A. The sun, moon, wind, and biological imperative–shaping contrasting wintertime migration and foraging strategies of adult male and female northern fur seals (Callorhinus ursinus). *PloS one*, 9(4).

[Stramski et al., 2008] Stramski, D., Reynolds, R., Babin, M., Kaczmarek, S., Lewis, M., Röttgers, R., Sciandra, A., Stramska, M., Twardowski, M., Franz, B., et al. Relationships between the surface concentration of particulate organic carbon and optical properties in the eastern South Pacific and eastern Atlantic Oceans. *Biogeosciences*, 5(1):171–201.

[Strass et al., 2002] Strass, V. H., Naveira Garabato, A. C., Pollard, R. T., Fischer, H. I., Hense, I., Allen, J. T., Read, J. F., Leach, H., and Smetacek, V. Mesoscale frontal dynamics: shaping the environment of primary production in the Antarctic Circumpolar Current. *Deep Sea Research Part II: Topical Studies in Oceanography*, 49:3735–3769.

[Strzepek et al., 2005] Strzepek, R., Maldonado, M., Higgins, J., Hall, J., Safi, K., Wilhelm, S., and Boyd, P. Spinning the "Ferrous Wheel": The importance of the microbial community in an iron budget during the FeCycle experiment. *Global biogeochemical cycles*, 19(4).

[Suggett et al., 2011] Suggett, D. J., Prášil, O., and Borowitzka, M. A. (2011). *Chlorophyll a fluorescence in aquatic sciences: methods and applications*. Springer.

[Sullivan et al., 1993] Sullivan, C. W., Arrigo, K. R., McClain, C. R., Comiso, J. C., and Firestone, J. Distributions of phytoplankton blooms in the Southern Ocean. *Science*, 262:1832–1837.

[Sullivan et al., 2013] Sullivan, J. M., Twardowski, M. S., Ronald, J., Zaneveld, V., and Moore, C. C. Measuring optical backscattering in water. In *Light Scattering Reviews 7*, pages 189–224. Springer.

[Sunagawa et al., 2015] Sunagawa, S., Coelho, L. P., Chaffron, S., Kultima, J. R., Labadie, K., Salazar, G., Djahanschiri, B., Zeller, G., Mende, D. R., Alberti, A., et al. Structure and function of the global ocean microbiome. *Science*, 348(6237):1261359.

[Sverdrup, 1953] Sverdrup, H. On conditions for the vernal blooming of phytoplankton. *Journal du Conseil*, 18(3):287–295.

[Swart et al., 2014] Swart, S., Thomalla, S., and Monteiro, P. The seasonal cycle of mixed layer dynamics and phytoplankton biomass in the sub-antarctic zone: a high-resolution glider experiment. *Journal of Marine Systems*.

[Takahashi et al., 2003] Takahashi, A., Dunn, M., Trathan, P., Sato, K., Naito, Y., and Croxall, J. Foraging strategies of chinstrap penguins at Signy Island, Antarctica: importance of benthic feeding on Antarctic krill. *Marine Ecology Progress Series*, 250:279–289.

[Taylor and Ferrari, 2011a] Taylor, J. R. and Ferrari, R. Ocean fronts trigger high latitude phytoplankton blooms. *Geophysical Research Letters*, 38(23).

[Taylor and Ferrari, 2011b] Taylor, J. R. and Ferrari, R. Shutdown of turbulent convection as a new criterion for the onset of spring phytoplankton blooms. *Limnology and Oceanography*, 56(6):2293–2307.

[Tew Kai and Marsac, 2010] Tew Kai, E. and Marsac, F. Influence of mesoscale eddies on spatial structuring of top predators' communities in the Mozambique Channel. *Progress In Oceanography*, 86:214–223.

[Thiebot et al., 2011] Thiebot, J.-B., Cherel, Y., Trathan, P. N., and Bost, C.-A. Inter-population segregation in the wintering areas of macaroni penguins. *Marine Ecology Progress Series*, 421:279–290.

[Thomalla et al., 2011] Thomalla, S., Fauchereau, N., Swart, S., and Monteiro, P. Regional scale characteristics of the seasonal cycle of chlorophyll in the Southern Ocean. *Biogeosciences*, 8(10):2849–2866.

[Thomalla et al., 2015] Thomalla, S. J., Racault, M.-F., Swart, S., and Monteiro, P. M. High-resolution view of the spring bloom initiation and net community production in the Subantarctic Southern Ocean using glider data. *ICES Journal of Marine Science: Journal du Conseil*, page fsv105.

[Timmermans et al., 2001] Timmermans, K. R., Gerringa, L. J., De Baar, H. J., Van Der Wagt, B., Veldhuis, M. J., De Jong, J. T., Croot, P. L., and Boye, M. Growth rates of large and small Southern Ocean diatoms in relation to availability of iron in natural seawater. *Limnology and Oceanography*, 46(2):260–266.

[Timmermans et al., 2004] Timmermans, K. R., Van Der Wagt, B., and De Baar, H. J. Growth rates, half-saturation constants, and silicate, nitrate, and phosphate depletion in relation to iron availability of four large, open-ocean diatoms from the Southern Ocean. *Limnology and Oceanography*, 49(6):2141–2151.

[Timmermans et al., 2008] Timmermans, K. R., Veldhuis, M. J., Laan, P., and Brussaard, C. P. Probing natural iron fertilization near the Kerguelen (Southern Ocean) using natural phytoplankton assemblages and diatom cultures. *Deep Sea Research Part II: Topical Studies in Oceanography*, 55(5):693–705.

[Torres et al., 2008] Torres, L. G., Read, A. J., and Halpin, P. Fine-scale habitat modeling of a top marine predator: do prey data improve predictive capacity. *Ecological Applications*, 18(7):1702–1717.

[Trull et al., 2001] Trull, T., Bray, S., Manganini, S., Honjo, S., and Francois, R. Moored sediment trap measurements of carbon export in the Subantarctic and Polar Frontal Zones of the Southern Ocean, south of Australia. *Journal of Geophysical Research: Oceans (1978–2012)*, 106(C12):31489–31509.

[Trull et al., 2008] Trull, T. W., Davies, D., and Casciotti, K. Insights into nutrient assimilation and export in naturally iron-fertilized waters of the Southern Ocean from nitrogen, carbon and oxygen isotopes. *Deep Sea Research Part II: Topical Studies in Oceanography*, 55(5):820–840.

[Trull et al., 2014] Trull, T. W., Davies, D. M., Dehairs, F., Cavagna, A.-J., Lasbleiz, M., Laurenceau, E. C., d'Ovidio, F., Planchon, F., Leblanc, K., Quéguiner, B., and Blain, S. Chemometric perspectives on plankton community responses to natural iron fertilization over and downstream of the Kerguelen Plateau in the Southern Ocean. 11:13841–13903.

[Tynan, 1997] Tynan, C. T. Cetacean distributions and oceanographic features near the Kerguelen Plateau. *Geophysical Research Letters*, 24(22):2793–2796.

[Uitz et al., 2009] Uitz, J., Claustre, H., Griffiths, F. B., Ras, J., Garcia, N., and Sandroni, V. A phytoplankton class-specific primary production model applied to the Kerguelen Islands region (Southern Ocean). *Deep Sea Research Part I: Oceanographic Research Papers*, 56:541–560.

[Van Der Merwe et al., 2015] Van Der Merwe, P., Bowie, A., Quéroué, F., Armand, L., Blain, S., Chever, F., Davies, D., Dehairs, F., Planchon, F., Sarthou, G., et al. Sourcing the iron in the naturally fertilised bloom around the Kerguelen Plateau: particulate trace metal dynamics. *Biogeosciences*, 12(3):739–755.

[Van Nes et al., 2007] Van Nes, E. H., Amaro, T., Scheffer, M., and Duineveld, G. C. Possible mechanisms for a marine benthic regime shift in the North Sea. *Marine Ecology Progress Series*, 330:39–47.

[Vandromme et al., 2010] Vandromme, P., Schmitt, F. G., Souissi, S., Buskey, E. J., Strickler, J. R., Wu, C.-H., and Hwang, J.-S. Symbolic analysis of plankton swimming trajectories: case study of Strobilidium sp.(Protista) helical walking under various food conditions. *Zoological Studies*, 49:289–303.

[Venables et al., 2007] Venables, H. J., Pollard, R. T., and Popova, E. E. Physical conditions controlling the development of a regular phytoplankton bloom north of the Crozet Plateau, Southern Ocean. *Deep Sea Research Part II: Topical Studies in Oceanography*, 54(18):1949–1965.

[Vergassola et al., 2007] Vergassola, M., Villermaux, E., and Shraiman, B. I. 'Infotaxis' as a strategy for searching without gradients. *Nature*, 445:406–409.

[Vidussi et al., 2001] Vidussi, F., Claustre, H., Manca, B. B., Luchetta, A., and Marty, J.-C. Phytoplankton pigment distribution in relation to upper thermocline circulation in the eastern Mediterranean Sea during winter. *Journal of Geophysical Research: Oceans (1978–2012)*, 106:19939–19956.

[Vierros et al., 2009] Vierros, M., Commission, I. O., et al. (2009). *Global open oceans and deep seabed (GOODS): biogeographic classification*. UNESCO.

[Viviant et al., 2010] Viviant, M., Trites, A. W., Rosen, D. A., Monestiez, P., and Guinet, C. Prey capture attempts can be detected in Steller sea lions and other marine predators using accelerometers. *Polar biology*, 33:713–719.

[Vivier et al., 2014] Vivier, F., Park, Y.-H., Sekma, H., and Le Sommer, J. Variability of the Antarctic Circumpolar Current transport through the Fawn Trough, Kerguelen Plateau.

[V.Ridoux, 1995] V.Ridoux The diets and dietary segreagation of seabirds at the sub-antarctic Crozet Islands. *Oceanography Lit. Reviews*, 12:1128.

[Walther et al., 2002] Walther, G.-R., Post, E., Convey, P., Menzel, A., Parmesan, C., Beebee, T. J., Fromentin, J.-M., Hoegh-Guldberg, O., and Bairlein, F. Ecological responses to recent climate change. *Nature*, 416(6879):389–395.

[Waluda et al., 2001a] Waluda, C. M., Rodhouse, P. G., Trathan, P. N., and Pierce, G. J. Remotely sensed mesoscale oceanography and the distribution of Illex argentinus in the South Atlantic. *Fisheries Oceanography*, 10:207–216.

[Waluda et al., 2001b] Waluda, C. M., Rodhouse, P. G., Trathan, P. N., and Pierce, G. J. (2001b). *Remotely sensed mesoscale oceanography and the distribution of Illex argentinus in the South Atlantic.*

[Watson et al., 2000] Watson, A., Bakker, D., Ridgwell, A., Boyd, P., and Law, C. Effect of iron supply on Southern Ocean CO2 uptake and implications for glacial atmospheric CO2. *Nature*, 407(6805):730–733.

[Watson et al., 1991] Watson, A. J., Robinson, C., Robinson, J. E., Williams, P. l. B., and Fasham, M. J. R. Spatial variability in the sink for atmospheric carbon dioxide in the North Atlantic.

[Waugh and Abraham, 2008] Waugh, D. W. and Abraham, E. R. Stirring in the global surface ocean. *Geophys. Res. Lett.*, 35.

[Weeding and Trull, 2014] Weeding, B. and Trull, T. W. Hourly oxygen and total gas tension measurements at the Southern Ocean Time Series site reveal winter ventilation and spring net community production. *Journal of Geophysical Research: Oceans*, 119(1):348–358.

[Weimerskirch, 2007] Weimerskirch, H. Are seabirds foraging for unpredictable resources? *Deep Sea Research Part II: Topical Studies in Oceanography*, 54(3):211–223.

[Weimerskirch et al., 2003] Weimerskirch, H., Inchausti, P., Guinet, C., and Barbraud, C. Trends in bird and seal populations as indicators of a system shift in the Southern Ocean. *Antarctic Science*, 15(02):249–256.

[Weiss and Knobloch, 1989] Weiss and Knobloch Mass transport and mixing by modulated traveling waves. *Physical review. A*, 40:2579–2589.

[Weiss, 1991] Weiss, J. The dynamics of enstrophy transfer in two-dimensional hydrodynamics. *Physica D: Nonlinear Phenomena*, 48:273–294.

[Williams et al., 1990] Williams, A., Dyer, B., Randall, R., and Komen, J. Killer whales Orcinus orca and seabirds:" Play", predation and association. *Marine Ornithology*, 18(1):37–41.

[Williams and Croxall, 1991] Williams, T. and Croxall, J. Annual variation in breeding biology of macaroni penguins, Eudyptes chvysolophus, at Bird Island, South Georgia. *Journal of Zoology*, 223(2):189–202.

[Wilson and McMahon, 2006] Wilson, R. P. and McMahon, C. R. Measuring devices on wild animals: what constitutes acceptable practice? *Frontiers in Ecology and the Environment*, 4(3):147–154.

[Worm and Myers, 2003] Worm, B. and Myers, R. A. Meta-analysis of cod-shrimp interactions reveals top-down control in oceanic food webs. *Ecology*, 84:162–173.

[Wunsch, 1997] Wunsch, C. The vertical partition of oceanic horizontal kinetic energy. *Journal of Physical Oceanography*, 27:1770–1794.

[Xing et al., 2012] Xing, X., Claustre, H., Blain, S., D'Ortenzio, F., Antoine, D., Ras, J., and Guinet, C. Quenching correction for in vivo chlorophyll fluorescence acquired by autonomous platforms: A case study with instrumented elephant seals in the Kerguelen region (Southern Ocean). *Limnology and Oceanography: Methods*, 10(7):483–495.

[Zeldis et al., 1996] Zeldis, J., Davis, C., James, M., Ballara, S., Booth, W., et al. Salp grazing: effects on phytoplankton abundance, vertical distribution and taxonomic composition in a coastal habitat. *Oceanographic Literature Review*, 5(43):475–476.

[Zhang et al., 2009] Zhang, X., Hu, L., and He, M.-X. Scattering by pure seawater: effect of salinity. *Optics Express*, 17(7):5698–5710.

[Zhang et al., 2008] Zhang, Y., Lacan, F., and Jeandel, C. Dissolved rare earth elements tracing lithogenic inputs over the Kerguelen Plateau (Southern Ocean). *Deep Sea Research Part II: Topical Studies in Oceanography*, 55(5):638–652.

[Zhou et al., 2014] Zhou, M., Zhu, Y., d'Ovidio, F., Park, Y.-H., Durand, I., Kestenare, E., Sanial, V., Van-Beek, P., Queguiner, B., Carlotti, F., et al. Surface currents and upwelling in Kerguelen Plateau regions. *Biogeosciences Discussions*, 11:6845–6876.